

Development of a Lab-Scale, Rechargeable, Aqueous Coin Cell and Methods for  
Measuring the Self-Discharge Rate of Zinc Electrodes

by

Patrick Bonnick

Submitted in partial fulfilment of the requirements  
for the degree of Doctor of Philosophy

at

Dalhousie University  
Halifax, Nova Scotia  
August 2015

© Copyright by Patrick Bonnick, 2015

## **Dedication**

*This thesis is dedicated to my grandmother, Dr. Beatrice Bonnicks, who found herself widowed and jobless at age 38 with 3 children. Through sheer determination she put herself through school to become Dr. Bonnicks. She was strong willed, resourceful, proper and kind. It is because of her that I came to respect the title of Dr. and the responsibility that comes with it. I will always strive to live up to that title.*

## Table of Contents

List of Tables.....	ix
List of Figures .....	x
Abstract.....	xv
List of Abbreviations Used .....	xvi
Acknowledgements.....	xvii
Chapter 1: Introduction.....	1
1.1 Zinc Air (Zn-air) Cells .....	5
1.1.1 Benefits of Zn-Air Cells .....	5
1.1.2 Introduction to Zinc Electrodes .....	6
1.1.3 Introduction to Air Electrodes.....	7
1.1.4 Introduction to KOH Electrolyte.....	8
1.1.5 Zn-air Total Cell Reaction.....	10
1.2 Nickel Zinc (Ni-Zn) Cells.....	11
1.2.1 Purpose of Researching Ni-Zn Cells.....	11
1.2.2 Introduction to Nickel Electrodes .....	12
1.2.3 Ni-Zn Total Cell Reaction.....	15
1.3 A Note on Terminology .....	15
1.4 Introduction to Butler-Volmer .....	17
1.5 Overcharging Ni-Zn and Zn-air Cells.....	19
1.5.1 Electrolysis of the Electrolyte due to Overcharging.....	19
1.5.2 Other Consequences of Overcharging .....	21
1.6 Overdischarging Ni-Zn and Zn-air Cells .....	22

1.6.1	Electrolysis of the Electrolyte Due to Overdischarging.....	23
1.6.2	Other Consequences of Overdischarging.....	23
1.7	Self-Discharge Reactions in Ni-Zn and Zn-Air Cells.....	24
1.7.1	Zn Electrode Self-Discharge .....	24
1.7.2	Air Electrode Self-Discharge .....	25
1.7.3	Ni Electrode Self-Discharge.....	25
1.8	Rechargeable Zn Electrode Challenges .....	26
1.8.1	Dendrites.....	26
1.8.2	Passivation.....	27
1.8.3	Shape Change.....	29
1.9	Bi-functional (Rechargeable) Air Electrode Challenges .....	30
1.9.1	Destruction of the Support Structure.....	30
1.9.2	Manganese (Mn) Dissolution .....	31
1.9.3	Carbon Corrosion .....	33
1.9.4	Water Management.....	33
1.10	Rechargeable Ni Electrode Challenges.....	34
1.10.1	Stack Pressure .....	34
1.10.2	Conductivity .....	35
1.10.3	Water Loss.....	35
1.11	Construction of Typical Ni-Zn and Zn-Air Cells .....	36
1.11.1	Commercial Non-Rechargeable Zn-Air Coin Cell.....	36
1.11.2	Commercial Rechargeable Ni-Zn Cell.....	37

1.11.3 Historical Laboratory Rechargeable Ni-Zn and Zn-Air Cells.....	39
1.11.4 Historical Laboratory Rechargeable Li-ion Coin Cell.....	43
Chapter 2: Laboratory Nickel-Zinc (Ni-Zn) Coin Cells.....	45
2.1 Motivation.....	45
2.2 Experimental Methods.....	47
2.2.1 Electrode Manufacture .....	47
2.2.2 ZnO Purity.....	48
2.2.3 Ni-Zn Coin Cell Design.....	49
2.2.4 Cell Cycling Procedure .....	51
2.2.5 Cyclic Voltammogram Measurement Procedure.....	52
2.2.6 Cell Thickness Measurement Procedure .....	52
2.2.7 Stack Pressure Measurement Procedure .....	52
2.3 Ni-Zn Coin Cell Results and Discussion.....	53
2.3.1 Electrode Capacity Determination .....	53
2.3.2 Formation Cycling of Ni Electrodes .....	54
2.3.3 Reproducibility of the Coin Cells .....	58
2.3.4 Effect of Stainless Steel Coin Cell Parts on Ni-Zn Cell Performance .....	61
2.3.5 Zinc Electrode Current Collector and Cell Casing Materials.....	68
2.3.6 Nickel-Side Component Materials, Cell Orientation and Separator Effects..	72
2.3.7 Effect of Stack Pressure on Cell Performance.....	77
2.3.8 Effect of Gas Evolution in Coin Cells.....	79
2.3.9 Comparison of Coin Cells with Commercial Ni-Zn AA Cells .....	82
2.4 Coin Cell Design Conclusions.....	87

2.5	Aspects of the Coin Cell Design to be Mindful of .....	90
2.5.1	Primitive Pressure Release Valve .....	90
2.5.2	High Surface Area of Exposed Metal Surfaces.....	91
2.5.3	Microporous Separator Encasement of the Zn Electrode.....	91
2.5.4	Alignment of Cell Components.....	92
Chapter 3:	Further Applications of the Coin Cell Design .....	93
3.1	3-Electrode Ni-Zn Coin Cells .....	93
3.1.1	3-Electrode Coin Cell Design.....	93
3.1.2	Ideal Cycling of a Ni-Zn Coin Cell.....	94
3.1.3	Overcharging a Ni-Zn Coin Cell .....	96
3.1.4	Overdischarging a Ni-Zn Coin Cell.....	97
3.1.5	Concerns with the 3-Electrode Coin Cell Design.....	101
3.1.6	3-Electrode Coin Cell Conclusions and Future Work .....	102
3.2	Zn-Air Coin Cells.....	104
3.2.1	Zn-air Coin Cell Design.....	104
3.2.2	Zn-air Coin Cell Cycling .....	106
3.2.3	Zn-air Coin Cell Conclusions and Future Work .....	109
3.3	Aqueous Lithium Manganese Oxide Zinc (LiMn <sub>2</sub> O <sub>4</sub> -Zn) Coin Cells.....	109
3.3.1	LiMn <sub>2</sub> O <sub>4</sub> -Zn Coin Cell Design.....	110
3.3.2	LiMn <sub>2</sub> O <sub>4</sub> -Zn Coin Cell Cycling .....	112
3.3.3	LiMn <sub>2</sub> O <sub>4</sub> -Zn Coin Cell Conclusions and Future Work .....	115
Chapter 4:	Self-Discharge Experiments Using Metal Foil.....	117

4.1	Motivation.....	117
4.2	Experimental Methods.....	121
4.2.1	3-Electrode Cell Design.....	121
4.2.2	Cycling Method.....	123
4.2.3	Calculation of the Self-Discharge and Parasitic Reaction Currents.....	124
4.3	Electrolyte Wicking Along Conducting Surfaces.....	126
4.4	Results and Discussion.....	129
4.4.1	Time Dependence of Self-Discharge.....	129
4.4.2	KOH Concentration.....	131
4.4.3	Foil (Current Collector) Material.....	133
4.4.4	Electroplating (Charging) Current.....	137
4.4.5	Effect of Electrolyte Additives.....	140
4.5	Foil Experiment Conclusions.....	147
Chapter 5: Self-Discharge Experiments Using Coin Cells.....		151
5.1	Motivation.....	151
5.2	Self-Discharge of Ni Electrodes in Coin Cells and Commercial Ni-Zn Cells.....	152
5.3	Experimental Methods.....	156
5.3.1	The “Race to the Bottom” Between Self-Discharging Ni and Zn Electrodes.....	156
5.3.2	Preparation Procedure for the Ni-Zn Coin Cells.....	157
5.4	Effect of Time and Electrolyte Additives on the Self-Discharge of Ni-Zn Coin Cells.....	161
5.5	Coin Cell Self-Discharge Conclusions and Future Work.....	164

Chapter 6: Conclusions.....	167
6.1 Regarding Coin Cells.....	167
6.1.1 Chapter 2 Conclusions.....	167
6.1.2 Chapter 3 Conclusions.....	169
6.2 Coin Cell Future Work.....	172
6.3 Regarding Self-Discharge Measurements.....	173
6.3.1 Chapter 4 Conclusions.....	173
6.3.2 Chapter 5 Conclusions.....	174
6.4 Self-Discharge Measurement Future Work.....	176
6.5 A Note on World Resources.....	176
References.....	180
Appendix A: Simple and Intermediate Modeling of a Cell.....	191
A.1 Simple Zn-Air Cell.....	191
A.2 Intermediate Zn-Air Cell.....	193
A.3 Simple Ni-Zn Cell.....	195
A.4 Intermediate Ni-Zn Cell.....	196
A.5 Simple Aqueous Lithium Manganese Oxide Zinc (LiMn <sub>2</sub> O <sub>4</sub> -Zn) Cell.....	198
A.6 Intermediate LiMn <sub>2</sub> O <sub>4</sub> -Zn Cell.....	199
A.7 Simple Non-Aqueous Lithium Air (Li-Air) Cell.....	201
A.8 Intermediate Non-Aqueous Li-Air Cell.....	202
Appendix B: Permissions to Reprint Material from the Literature.....	206



## List of Tables

Table 1-1:	Crystal structure parameters for the four forms of nickel hydroxide. ....	12
Table 1-2:	Thickness of various components in commercial, rechargeable AA Ni-Zn cells. ....	37
Table 2-1:	Elemental analysis of the two ZnO powders used in this thesis and the typical concentrations found in primary alkaline battery Zn active material. ....	49
Table 2-2:	Error in $Q_T$ associated with assuming all foil disks have equal mass. ....	53
Table 2-3:	The grades and composition of various types of stainless steel. ....	61
Table 5-1:	Summary of storage preparation procedures. ....	158
Table 6-1:	Calculated years of peak resource production for five metals that are important to cell technologies. ....	178
Table A-1:	Theoretical capacity and energy densities of various cell chemistries mentioned in this thesis. ....	192

## List of Figures

Figure 1-1: Modeled volumetric energy densities of various promising cell chemistries. ....	1
Figure 1-2: Schematic of the reactions inside a Zn-air cell. ....	10
Figure 1-3: A diagram illustrating the different polymorphs of Ni(OH) <sub>2</sub> and NiOOH, and the possible phase transitions between them. ....	13
Figure 1-4: Example of Butler-Volmer curves. ....	17
Figure 1-5: Vapour pressure of the electrolyte ( $P_{\text{electrolyte}}$ ) as a function of KOH concentration at room temperature. ....	34
Figure 1-6: Cross section of a Zn-air button cell for a hearing aid.....	36
Figure 1-7: Dismantled PowerGenix and PKCell AA rechargeable Ni-Zn cells. ....	38
Figure 1-8: A Li-ion coin cell designed for laboratory R&D.....	43
Figure 2-1: Coin cell components and their order of assembly. ....	50
Figure 2-2: Formation cycles of Ni-Zn coin cells.....	54
Figure 2-3: Differential capacity plots for the first 2 cycles of the two cells shown in Figure 2-2. ....	55
Figure 2-4: Differential capacity plots for the 5 <sup>th</sup> and 30 <sup>th</sup> cycle of the two cells shown in Figure 2-2. ....	56
Figure 2-5: Demonstration of reproducibility in coin cells, part 1.....	59
Figure 2-6: Demonstration of reproducibility in coin cells, part 2.....	60
Figure 2-7: The effect of Stainless Steel (SS) coin cell components on cycling behaviour. ....	62
Figure 2-8: A simple Pourbaix diagram showing the potentials of fully charged Ni and Zn electrodes in 3.2 M KOH, and fully charged LiMn <sub>2</sub> O <sub>4</sub> and Zn electrodes in pH 4 electrolyte.....	63

Figure 2-9: Cyclic voltammograms of nickel as well as stainless steel 304 and 316 in 3.2 M KOH.....	65
Figure 2-10: Cyclic voltammogram sweeps to progressively lower potentials on stainless steel 304 foil in 3.2 M KOH.....	66
Figure 2-11: Effects of different can and current collector (CC) materials on cycle behaviour.....	70
Figure 2-12: Effects of cell orientation, Ti and separators on cell behaviour. ....	73
Figure 2-13: Extended cycling to cycle 50 of the best cell designs. ....	75
Figure 2-14: Example stack pressure distributions from the two shapes of spacers tested in this work.....	78
Figure 2-15: Ballooning of a sealed Ni-Zn coin cell during cycling.....	79
Figure 2-16: PowerGenix AA cell tested in the same manner as the coin cells (also shown).....	82
Figure 2-17: Cycling behaviour of PowerGenix AA cells using various charging regimes. ....	83
Figure 2-18: Comparison between the best PowerGenix AA cell and the best coin cells produced in this work.....	85
Figure 2-19: Comparison between PKCell AA cells cycled in two different ways and the best coin cell produced in this work.....	86
Figure 3-1: A schematic of a 3-electrode Ni-Zn coin cell. ....	93
Figure 3-2: The typical charge and discharge curves of well-behaved Ni and Zn electrodes as well as the total cell potential ( $V_{Ni} - V_{Zn}$ ) in a 3-electrode Ni-Zn coin cell. ....	95
Figure 3-3: Overcharge behaviour of 3-electrode Ni-Zn coin cells.....	96
Figure 3-4: Demonstration of overdischarge of the Ni electrode in a 3-electrode Ni-Zn coin cell.....	98

Figure 3-5: Demonstration of overdischarge of the Zn electrode in a 3-electrode Ni-Zn coin cell.....	100
Figure 3-6: The Zn-air coin cell designs used for this thesis.....	105
Figure 3-7: The cycling of a Zn-air coin cell.....	107
Figure 3-8: Current drawn by oxide layer formation and O <sub>2</sub> evolution on coin cell components within the potential range of the LiMn <sub>2</sub> O <sub>4</sub> – Zn system.....	110
Figure 3-9: The cycling of an example LiMn <sub>2</sub> O <sub>4</sub> – Zn coin cell.....	113
Figure 3-10: Discharge capacity of LiMn <sub>2</sub> O <sub>4</sub> – Zn coin cells that are overcharged each cycle to ensure that the Zn electrode has more capacity than the LiMn <sub>2</sub> O <sub>4</sub> electrode.....	114
Figure 4-1: Experimental apparatus for the foil experiments.....	121
Figure 4-2: Demonstration of the typical OCV self-discharge experimental method.....	123
Figure 4-3: Example data extracted from OCV self-discharge experiments.....	124
Figure 4-4: Demonstration of electrolyte wicking up conducting surfaces.....	126
Figure 4-5: Schematic of the mechanism of electrolyte wicking (electroosmosis).....	128
Figure 4-6: Example of self-discharge at long OCV times.....	129
Figure 4-7: Self-discharge and hydrogen evolution rates in increasing concentrations of KOH.....	132
Figure 4-8: Self-discharge and hydrogen evolution rates on various current collector materials.....	134
Figure 4-9: Self-discharge and H <sub>2</sub> evolution rates of Ni and graphite current collectors.....	135
Figure 4-10: SEM pictures of Zn deposits on various current collector materials.....	136
Figure 4-11: Self-discharge and hydrogen evolution rates with increasing plating current densities.....	139

Figure 4-12: Self-discharge current in the presence of electrolyte additives. ....	141
Figure 4-13: Scanning Electron Microscopy (SEM) pictures of Zn deposits on Sn foil from electrolytes with different additives. ....	143
Figure 4-14: Parasitic H <sub>2</sub> evolution current in the presence of electrolyte additives. ....	144
Figure 4-15: Schematic of the proposed mechanism for self-discharge in rechargeable Zn electrodes. ....	148
Figure 5-1: Self discharge of a Ni-Zn coin cell and commercial AA cell (PKCell). ....	152
Figure 5-2: dQ/dV curves for a typical Ni-Zn coin cell and commercial AA cell (PKCell). ....	153
Figure 5-3: dV/dt curves calculated from the V vs t data in Figure 3-1. ....	154
Figure 5-4: Normalized self-discharge current of the Ni electrodes of a coin cell and a commercial AA cell (PKCell). ....	155
Figure 5-5: Example self-discharge data for coin cells. ....	156
Figure 5-6: Formation of Ni electrodes for storage experiments. ....	158
Figure 5-7: Preparation cycling of a pre-formed Ni electrode and a small capacity Zn electrode in a Ni-Zn coin cell before placing the cell on the long term storage system. ....	159
Figure 5-8: Self-discharge rates of Ni-Zn coin cells with various electrolyte additives. ....	162
Figure 6-1: The predicted world production rates of five metals that are important to battery technologies. ....	177
Figure 6-2: Year of peak production of Zn as a function of the year used to generate the Gaussian fit. ....	178
Figure A-1: Example of three different simple cell models. ....	191
Figure A-2: Schematic of the stack for the intermediate model of a Zn-air battery. ....	193
Figure A-3: Volumetric energy density of a Ni-Zn 18650 cell using the intermediate model. ...	195

Figure A-4: Schematic of the stack for the intermediate model of a Ni-Zn battery. .... 197

Figure A-5: Volumetric energy density of a Ni-Zn 18650 cell using the intermediate model... 197

Figure A-6: Schematic of the stack for the intermediate model of a  $\text{LiMn}_2\text{O}_4$ -Zn cell. .... 199

Figure A-7: Volumetric energy density of a  $\text{LiMn}_2\text{O}_4$  – Zn cell in the charged state using an  
intermediate model..... 200

Figure A-8: Schematic of the stack for the intermediate model of a Li-air cell..... 203

Figure A-9:  $\text{VED}_{\text{Cell}}$  of a non-aqueous Li-air cell as the thickness of the Li electrode ( $t_{\text{Li}}$ ) is  
increased..... 204

## Abstract

Zinc-air cells are promising as a cheap, safe and sustainable energy storage technology, but few publicly funded institutions currently research them. One reason for this is a lack of a simple, standardized cell design to facilitate the comparison of data sets between labs. In the Li-ion battery research community, a coin cell format is one of the accepted standard cell designs and any researcher attempting to shift from Li-ion to Zn-air research will want to use their existing coin cell infrastructure. Coin cells require small amounts of material, can have good reproducibility, are easily fabricated in large quantities and have small space requirements that allow many cells to be tested simultaneously under controlled conditions. If thin electrodes are used, concerns over bulk electrode issues can be alleviated, making coin cells a good research tool for testing new active materials, electrode material recipes, electrolytes and separators.

Due to identical reactions at the zinc electrode, nickel-zinc (Ni-Zn) cells could potentially be used to study zinc electrodes without the complications of an air electrode. It was shown that to adapt coin cells for use with Ni-Zn, nickel should be used for all positive-side components, including the current collector, while tin should be used for all negative-side components. Additionally, a pressure-release valve, non-woven separator and microporous separator are required for long cycle life. Ni-Zn coin cells created in this work achieved Ni active material utilizations over 100% and cycle lives of over 300 cycles with un-optimized electrode materials. The procedures and equipment developed for Ni-Zn coin cells were also used to create a 3-electrode Ni-Zn coin cell, which demonstrated that future cycle life experiments on rechargeable Zn electrodes should not use Ni electrodes as a counter electrode as was done in this work. A Zn-air coin cell was created to demonstrate that Zn-air coin cells can be made when durable bi-functional air electrodes are acquired in the future. A promising alternative technology, aqueous  $\text{LiMn}_2\text{O}_4\text{-Zn}$ , was also tested in coin cells and showed to require overcharging every cycle to achieve a long cycle life.

The self-discharge rate of rechargeable Zn electrodes is an issue that is poorly measured in the literature. A new experimental method for directly measuring the self-discharge rate of rechargeable Zn electrodes in any cell format is presented here. The rate determining step for (galvanic) Zn corrosion was determined to be  $\text{H}_2\text{O}$  adsorption onto the current collector during  $\text{H}_2$  evolution.

## List of Abbreviations Used

AM	Active Material (material that stores charge)
CC	Current Collector (Electrode Substrate)
CE	Coulombic Efficiency ( $Q_{\text{Discharge}} / Q_{\text{Charge}}$ )
EDS	Energy-Dispersive X-ray Spectroscopy
Hg/HgO	Mercury/Mercury Oxide Reference Electrode (0.098 V vs SHE)
ICP-OES	Inductively Coupled Plasma Optical Emission Spectroscopy
$i_{\text{H}_2}$	Parasitic H <sub>2</sub> Evolution Current Density (or Rate/cm <sup>2</sup> )
$i_{\text{SD}}$	Self-Discharge Current Density (or Rate/cm <sup>2</sup> )
O1	Octahedral Structure, Repeats Every 1 Layer
OCV	Open Circuit Voltage (i.e. the cell is disconnected)
P3	Prismatic Structure, Repeats Every 3 Layers
PTFE	Polytetrafluoroethylene (Teflon)
rds	Rate Determining Step (i.e. the slowest step)
SEM	Scanning Electron Microscopy
SHE	Standard Hydrogen Electrode
SS	Stainless Steel
$\text{Zn}(\text{OH})_4^{-2}$	Zincate Ion



## **Acknowledgements**

First and foremost, this work would not have been possible without the support of my supervisor, Jeff Dahn, who never lost faith in me.

Much of the equipment I used was built and designed with the help of Simon Trussler. His jovial nature was always appreciated and I will miss our talks.

The lab was sometimes a chaotic and confusing place, and navigating it was made all the more easier by Robbie Sanderson and David Stevens who maintained equipment, located missing things and provided general technical advice (usually paired with a joke).

Similarly, Dalhousie's bureaucracy was sometimes difficult to navigate and so I extend my sincere thanks to Tanya Timmins, Krista Cullymore, Barbara Gauvin and Anne Murphy for smoothing over the many bumps along the way.

I wish to heartily thank my good friend and colleague, Aaron Rowe, for his support and loyalty throughout this degree. I could not have done it without him.

Several of my friends provided invaluable moral support along the way: Kathryn Duffy, Chantalle Briggs, Dorian Lang, Mathew Tufts, Ted Campbell and Gray O'Byrne. I owe you all a great debt of gratitude.

But above all, I must express my deepest thanks to my family, Teresa, Phil, Silver and Elaine Bonnick, and my beloved partner, Eszter Horvath, whose patience and compassion kept me going through the toughest of times.

## Chapter 1: Introduction

As both electric vehicles and grid scale energy storage become more popular, the demand for cheap, high energy density and long lasting batteries will continue to increase.<sup>1</sup> Figure 1-1 shows the average volumetric energy densities of a few of the potential cell chemistry alternatives to the ubiquitous sealed Li-ion cells that dominate the cell phone and laptop markets today. The details of these volumetric energy density calculations are covered in Appendix A. The success of each of these technologies will depend in part on the number of people researching them.<sup>2</sup>

Central in Figure 1-1 is the LiCoO<sub>2</sub>-Carbon cell, which is the most common positive and negative electrode combination used in Li-ion batteries. Li-ion batteries are currently the most universally favoured rechargeable battery technology due to their combination of relatively high energy densities (about 240 Wh/kg and 640 Wh/L) and a long cycle life of

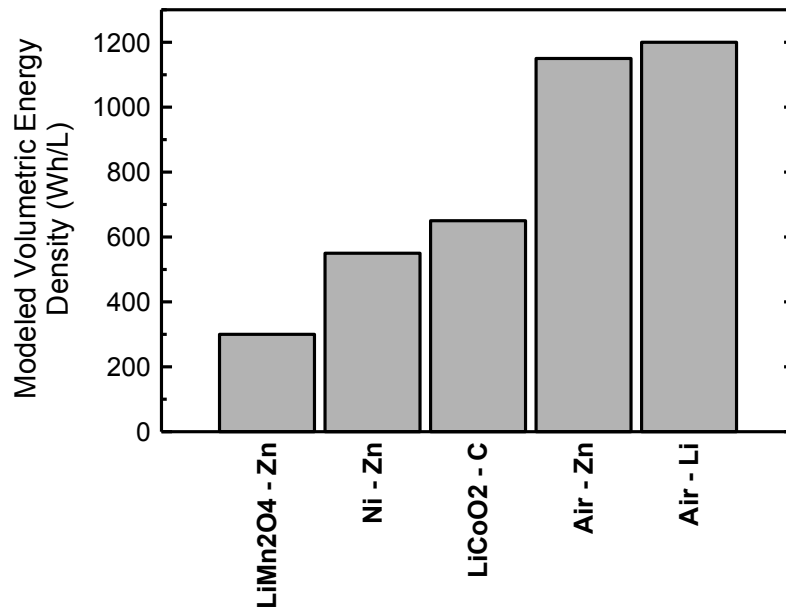


Figure 1-1: Modeled volumetric energy densities of various promising cell chemistries. All cells in this figure are listed in the “Positive electrode active material – Negative electrode active material” format. The LiCoO<sub>2</sub>-Carbon cell is the most commonly encountered Li-ion battery. The calculation method is discussed in Appendix A, where the values shown here are the averages of the range presented in the leftmost column of Table A-1.

3,000+ cycles, but they are also toxic, flammable and relatively expensive.<sup>2-6</sup> Since the introduction of Sony's Li-ion cell to the market in 1991, research efforts into this technology have increased dramatically worldwide, which has in turn increased our understanding of Li-ion systems, and improved the technology.<sup>6</sup> A search for "lithium ion battery" as the topic on the Web of Science website yielded 39,236 papers, 7,928 of which were in 2014 alone.

Figure 1-1 shows that the Li-air cell has the highest theoretical energy density but unfortunately it is also plagued with monumental technical challenges that are unlikely to be solved within the next decade, and might never be solved.<sup>7-9</sup> Additionally, Appendix A demonstrates that fantastically high theoretical volumetric energy density of Li-air (> 5,000 Wh/L) is unattainable in a realistic system. Instead, the calculations in Appendix A suggest that the high volumetric energy density of non-aqueous Li-air batteries is likely to be close to that of Zn-air batteries, which face far fewer challenges to reach commercialization.<sup>9</sup> Regardless, the promise of an energy density rivaling gasoline has driven many research labs to devote significant amounts of effort to researching Li-air.<sup>10</sup> A search for "lithium air battery" as the topic on the Web of Science website yielded 2,574 papers, 574 of which were from 2014.

The electrically rechargeable Zn-air battery (as opposed to the so-called mechanically rechargeable or flow cell designs) is non-toxic, non-flammable, inexpensive, and has large attainable gravimetric and volumetric energy densities.<sup>11-15</sup> For example, a Duracell 675 primary (non-rechargeable) Zn-air cell designed for a hearing aid was discharged and measured to contain 440 Wh/kg and 1,800 Wh/L. Furthermore, recycling zinc electrodes is neither as difficult nor as energy intensive as Li-ion positive electrode materials.<sup>16,17</sup> The drawbacks to Zn-air batteries appear to be their approximately 60% energy efficiency,<sup>9</sup> low cycle life of less than 500 cycles<sup>18</sup> and high self-discharge rate.<sup>19</sup>

These issues are a subset of those that Li-air batteries face, and the cycle life of Zn-air cells in the mid 1990's was already superior to that of current-day Li-air. For instance, Muller *et al.* created a Zn-air cell in 1995 that cycled nearly 500 times before the air electrode failed, and Cairns *et al.* created a Ni-Zn cell in 1993 that cycled over 800 times before the Zn electrode failed.<sup>18, 20</sup> As a rough guideline for comparison, about 1,000 cycles are required for commercialization. In order to extend the cycle life of their Zn-air cell design, the EDF (Electricité de France) research group has sacrificed energy density, as modeled in Appendix A.2, by adding space between the air electrode and zinc electrode to prevent the O<sub>2</sub> bubbles evolved during charging from affecting the Zn electrode.<sup>21, 22</sup> The fact that the low energy efficiency, low cycle life and high self-discharge issues are the only barriers to a commercial Zn-air cell<sup>9</sup> suggest that a concentrated research effort to bring rechargeable Zn-air cells to the market is more sensible than the efforts currently being focused on Li-air. However, the research community is not investing nearly as much effort into Zn-air as it is Li-air. A search for “zinc air battery” as the topic on the Web of Science website yielded only 544 papers, 55 from 2014. The low publication rate is not due to Zn-air being a new technology: several papers published in 1968 specifically discuss using Zn-air batteries to power electric vehicles, suggesting that the topic of Zn-air batteries has been relevant for the past 47 years.<sup>23-26</sup> So why are so few researchers working on Zn-air systems in comparison to Li-air? Likely, the answer will contain political, financial, personal and technological reasons. Although the political, personal and financial reasons are beyond the scope of this thesis, there appear to be no technological barriers that would favour Li-air over Zn-air.

Perhaps a better question is: What might help inspire more researchers to study Zn-air systems? Many existing battery research labs focus on non-aqueous cells like Li-ion and Li-air, and might lack the knowledge and/or experience to feel confident beginning work on

an alkaline, aqueous battery system. So how then would a lab begin to do quality research on Zn-air cells without previous expertise? A logical first step is to create a cell to conduct reliable experiments with. Countless cell designs exist, but two, in particular, seem to be the most prominent in the Li-ion community: Swagelok cells and coin cells. If a means of adapting coin cells to work with alkaline electrolyte were developed, it would help more researchers begin their own research on Zn-air.

Due to the fact that this lab (the Dahn lab at Dalhousie University) uses coin cells for Li-ion research, this project set out to convert the typical coin cell design to work with aqueous, alkaline electrolyte. This task would both build expertise within the lab with alkaline systems and create a needed test vehicle for future Zn-air electrode research. Since this lab also did not have any previous experience making battery air electrodes, and since the air electrode appeared to be the component limiting cycle life, it was decided that the  $\text{Ni(OH)}_2$  electrode, commonly used in Ni-Cd and Ni-MH batteries, would be used as the positive electrode opposite the rechargeable zinc (Zn) electrode intended to be studied. Using a  $\text{Ni(OH)}_2$  electrode (referred to from here onwards as simply a Ni electrode) made sense for three main reasons. First, a pasted Ni electrode can be made in the same manner as the Li-ion electrodes that the lab already had experience making. Second, as already mentioned Cairns *et al.* demonstrated that Ni electrodes had a longer cycle life than Zn electrodes. Third, a rechargeable Ni-Zn cell uses the same electrolyte (2 to 8 M KOH) as a Zn-air cell, which means the reactions at the Zn electrode are identical in both systems. Hopefully, this thesis will serve as a starting point for academic, government and industrial researchers who want to expand their research to include Zn-air or other aqueous battery systems. To this end, Chapter 1 explains the reactions that occur in both Ni-Zn and Zn-air systems. Chapter 2 explores the adaptation of coin cells for use with alkaline electrolyte

systems, namely Ni-Zn, and Chapter 3 demonstrates that the design can be adapted for use with a reference electrode, an air electrode and a different aqueous electrolyte.

As will be discussed in Chapter 4, the self-discharge rate of rechargeable Zn electrodes are currently studied in either difficult or possibly inaccurate ways. Chapter 4 covers a novel cycling procedure to directly measure Zn self-discharge rates that can be used in a variety of experimental set-ups. Chapter 5 demonstrates how to measure the self-discharge rate of an intercalation electrode such as Ni. Then, a method of measuring the self-discharge rate of a plating/stripping electrode, such as Zn, is described in situations where the opposing electrode is likely to finish discharging first. Finally, the results of using Ni-Zn coin cells to test the effectiveness of additives on Zn electrode self-discharge rates are presented.

## **1.1 Zinc Air (Zn-air) Cells**

Zinc air (Zn-air) cells are half battery (the zinc electrode) and half fuel cell (the air electrode). The Zn electrode is the negative electrode while the air electrode is the positive electrode. These two electrodes are usually separated by one or more polyolefin separators to prevent electrical contact. The separators and Zn electrode are soaked with electrolyte, which is an aqueous KOH solution with concentrations typically ranging from 3 – 8 M (15 weight percent (wt%) to 34 wt%). Pictures of Zn-air cells are shown later in Figure 1-6 (pg. 36) and Figure 3-6 (pg. 105).

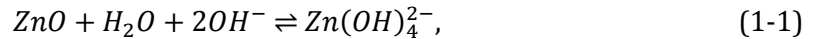
### **1.1.1 Benefits of Zn-Air Cells**

According to Appendix A, rechargeable Zn-air cells could have a volumetric energy density of up to 1,400 Wh/L, or nearly double that of Li-ion cells today, and a gravimetric energy density that could also be up to double that of Li-ion, which would allow cell phones

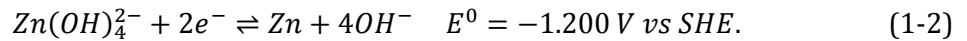
to last longer and electric vehicles to drive further without increasing the size of the battery pack. They are safe since they contain no lead (Pb), mercury (Hg) or cadmium (Cd),<sup>3</sup> are non-flammable because Zn and water do not burn, and are non-explosive because the cell is open to the atmosphere. Since they can be overcharged (described in Section 1.5) without the risks of starting a fire, battery pack designers have the option to leave out volume-consuming cell monitoring circuitry, which would increase the volumetric energy density of a Zn-air battery pack in comparison to Li-ion battery packs that require such circuitry. Zn-air also has a nearly flat discharge potential curve, which eases electronic circuit design.<sup>27, 28</sup> Additionally, the active material is easily recyclable if Zn supplies become a concern.<sup>17</sup> Zn can be recovered from alkaline batteries by dissolving Zn in flowing alkaline electrolyte, which is less energy intensive than melting down cells, as in the case of Li-ion cells being recycled to recover Co and Ni.<sup>16, 17</sup>

### 1.1.2 Introduction to Zinc Electrodes

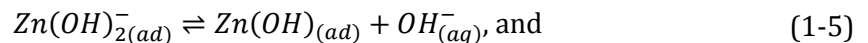
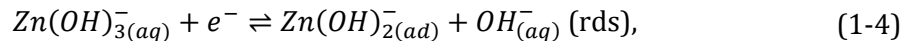
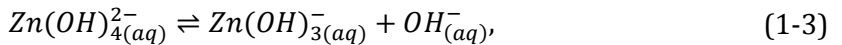
Zinc electrodes can be created in either the charged or discharged state. All zinc electrodes in this thesis were created in the discharged state and began their first cycle by being charged, which involved the dissolution of ZnO,<sup>29</sup>

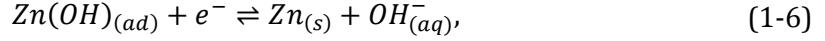


followed by the electrochemical reduction of zincate ( $\text{Zn}(\text{OH})_4^{2-}$ ):



The most likely mechanism for electroplating Zn (Reaction (1-2)) was proposed by Bockris *et al.* and consists of the following 4 steps:

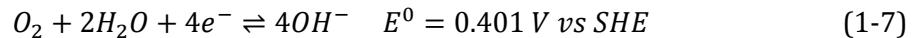




where Reaction (1-4) is the rate determining step (rds).<sup>29</sup> The first step, Reaction (1-3), likely occurs in the bulk electrolyte while Reactions (1-4), (1-5) and (1-6) occur at the surface. As charging (plating) continues, the hydroxide ion (OH<sup>-</sup>) concentration increases and the Zn(OH)<sub>4</sub><sup>2-</sup> concentration decreases, making ZnO dissolution favourable locally. Discharge, or “stripping”, follows the same mechanism as charging, except backward. In this direction the overall reaction is referred to as a dissolution/precipitation reaction since Zn is temporarily present in the electrolyte as Zn(OH)<sub>4</sub><sup>2-</sup> before precipitating out as ZnO.

### 1.1.3 Introduction to Air Electrodes

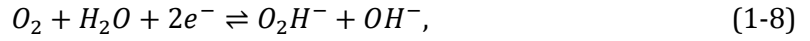
Air electrodes are created in many different ways, but generally consist of some form of carbon, binder and catalyst being pressed onto a Ni mesh.<sup>30</sup> In primary cells (non-rechargeable) the catalyst is usually MnO<sub>2</sub> because it is cheap and supports a respectable O<sub>2</sub> reduction rate of about 10 mA/cm<sup>2</sup> at a potential of 1.35 V vs Zn.<sup>27,30</sup> Over the years, many different catalyst materials have been used as bi-functional (rechargeable) catalysts that have respectable O<sub>2</sub> evolution and reduction rates,<sup>31</sup> but a comprehensive review of those catalysts is beyond the scope of this thesis. The side facing the electrolyte wicks a thin layer of the electrolyte over the high surface area of the electrode, thereby creating a 3-phase region on the surface consisting of gaseous O<sub>2</sub>, liquid electrolyte and solid carbon, which is the electron conductor. During discharge, O<sub>2</sub> drifts into the electrode and reacts at the 3-phase region via



to produce hydroxide ions (OH<sup>-</sup>) that flow through the liquid to the bulk electrolyte. The mechanism of this process is complex and the reader is directed to the Encyclopedia of Electrochemical Power Sources for an in depth discussion of the possible reaction



mechanisms.<sup>32</sup> A short explanation is that O<sub>2</sub> is reduced through one of two pathways depending on the surface on which it is being reduced. The pathway favoured on MnO<sub>2</sub>, a common catalyst used in air electrodes, first creates peroxide,



which is then chemically decomposed by the catalyst:



The decomposition of peroxide is the rate determining step (rds),<sup>27</sup> and is slow since breaking the oxygen-oxygen bond has a high activation energy. Evolving O<sub>2</sub> (Reaction (1-7) backward) follows a different pathway than reduction as described by Jöerissen.<sup>32</sup> In this direction, the rds is the initial adsorption of OH<sup>-</sup> onto the surface.<sup>32</sup>

#### 1.1.4 Introduction to KOH Electrolyte

The preferred electrolyte for Zn-air, Ni-Zn, and other cells is KOH dissolved in water and then saturated with ZnO, which dissolves in solutions with a pH > 14.<sup>33</sup> This is because KOH is cheap and has a higher conductivity and lower freezing point than NaOH above a concentration of about 12 weight percent (wt%) (2.4 M KOH).<sup>34</sup> The conductivity of KOH reaches a maximum of about 53 Ω<sup>-1</sup>cm<sup>-1</sup> at a concentration of about 27 wt% (6.0 M KOH), which has a freezing point of -44°C.<sup>34</sup> The diffusion constant of OH<sup>-</sup> is extremely high for its charge density and size due to its ability to accept a proton from an adjacent water molecule thereby recreating itself in a new position. The diffusion constant is about 5.27 × 10<sup>-5</sup> cm<sup>2</sup>/s for OH<sup>-</sup> as compared with 1.96 × 10<sup>-5</sup> cm<sup>2</sup>/s for K<sup>+</sup> or 1.33 × 10<sup>-5</sup> cm<sup>2</sup>/s for Na<sup>+</sup>.<sup>35</sup>

Unlike with some battery technologies, the electrolyte in alkaline cells is intimately involved in the electrode reactions since these reactions produce and consume OH<sup>-</sup> and H<sub>2</sub>O. Zinc electrodes operate via electrochemical dissolution and deposition and are thus dependent on the Zn(OH)<sub>4</sub><sup>2-</sup> concentration in the electrolyte, which itself is dependent on

$\text{OH}^-$  concentration.<sup>36-39</sup> Typical KOH concentrations vary from about 3.2 M to 8 M (16 wt% to 34 wt%). High KOH concentrations are detrimental to the long cycle life of Zn electrodes since the solubility of ZnO increases approximately with the square of the KOH concentration<sup>14</sup> and greater amounts of Zn dissolved in the electrolyte speeds up the rate of “shape change” (described in Section 1.8.3 on page 29), which decreases cycle life. Unfortunately, most positive electrodes operate more efficiently in high KOH concentrations, and as a result the best concentration to use is the lowest that the positive electrode will tolerate for the rates desired, with a supporting electrolyte salt to keep the conductivity at a maximum.<sup>15</sup> The KOH concentration used in this thesis is usually 3.2 M (16 wt%) since that was the lowest concentration proven to work well in Ni-Zn cells at the time this research began.<sup>20, 40</sup>

ZnO dissolves in alkaline electrolytes according to Reaction (1-1).  $\text{Zn}(\text{OH})_4^{2-}$  ions have a tetrahedral structure and have been shown to be the dominant  $\text{Zn}^{+2}$  complex in KOH solutions with a concentration greater than 1 M, although  $\text{Zn}(\text{OH})_4^{2-}$  might begin to aggregate at high concentrations.<sup>15, 41</sup> The dissolution rate of ZnO is slow, requiring days or weeks to reach saturation levels if ZnO is left to sit in KOH at room temperature.<sup>36</sup> Heating and stirring speeds up dissolution significantly; the quickest way to saturate KOH electrolyte with ZnO seems to be to add an excess of ZnO to the solution, greater than twice the amount needed to reach saturation, and then shake the solution at room temperature for at least 1 minute.<sup>36</sup> Finally, centrifuge the solution to remove the excess ZnO.<sup>36</sup>

Interestingly, Zn discharged off the electrode into solution in alkaline electrolytes can reach  $\text{Zn}(\text{OH})_4^{2-}$  concentrations of two to three times the ZnO saturation value attainable by mixing ZnO powder with a KOH solution. For instance, Liu *et al.* prepared a 7.3 M KOH (32 wt%) electrolyte that was saturated with ZnO at a concentration of 0.64 M  $\text{Zn}(\text{OH})_4^{2-}$ .<sup>37</sup> They then discharged Zn into solution and measured the conductivity, finding

that it dropped from  $0.54 \Omega^{-1}\text{cm}^{-1}$  at  $0.64 \text{ M Zn(OH)}_4^{2-}$  to  $0.39 \Omega^{-1}\text{cm}^{-1}$  at  $1.52 \text{ M Zn(OH)}_4^{2-}$ . This corresponds to a slope of about  $-0.16 \Omega^{-1}\text{cm}^{-1}\text{M}^{-1}$ .<sup>36,37</sup> Precipitating ZnO was evident above  $1.3 \text{ M Zn(OH)}_4^{2-}$ , but the maximum observed concentration was  $1.52 \text{ M}$ . This means that the conductivity of the electrolyte close to a discharging electrode drops when  $\text{Zn(OH)}_4^{2-}$  concentrations in the Nernst layer reach more than twice the equilibrium saturation concentration.

### 1.1.5 Zn-air Total Cell Reaction

By combining Zn electrodisolution and ZnO precipitation (Reactions (1-2) and (1-1) backward) with oxygen reduction (Reaction (1-7)), the result,



is the total cell reaction for Zn-air. Figure 1-2 shows a schematic of the flow of ions and molecules in a Zn-air cell during operation. It is evident that the electrolyte is intimately involved in the reactions of this cell chemistry since the solvent itself reacts at the air electrode during discharge and Zn electrode during charge. During cell operation an  $\text{OH}^-$  ion concentration gradient is set up, which in turn causes the electrolyte to slowly flow

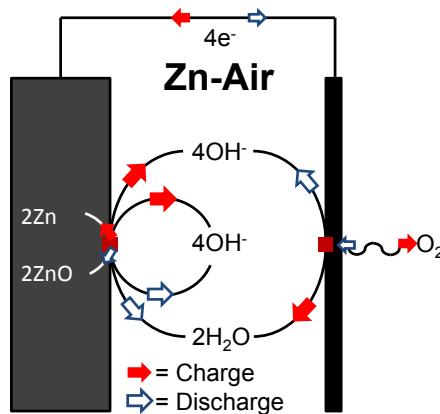


Figure 1-2: Schematic of the reactions inside a Zn-air cell. The reactions proceed in a clockwise direction during charging and counter clockwise during discharging. The oxygen atoms that drift into the cell are not the ones that end up in ZnO; rather, the ZnO oxygen atom is pulled from the closest  $\text{OH}^-$  atom.

around the cell.<sup>42</sup> This is the basis of the 'shape change' phenomenon discussed in Section 1.8.3 (pg. 29).<sup>43</sup>

## **1.2 Nickel Zinc (Ni-Zn) Cells**

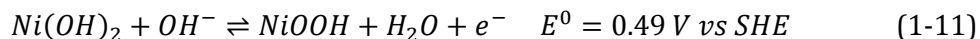
Unlike Zn-air cells, sealed, rechargeable nickel zinc (Ni-Zn) cells are produced commercially with some success, namely for high power applications like portable power tools. Ni-Zn batteries are capable of discharge rates of about 900 W/kg and have energy densities similar to that of Ni-MH batteries (about 170 Wh/L and 65 Wh/kg).<sup>44</sup> Ni-Zn cells charge at around 1.9 V and have an average discharge potential of about 1.65 V, which is higher than other alkaline cells and is the source of their superior power capabilities in comparison to Ni-MH and Ni-Cd cells.<sup>44</sup>

### *1.2.1 Purpose of Researching Ni-Zn Cells*

The purpose of this thesis is to develop a test vehicle for further aqueous, alkaline research and to highlight the trials and tribulations of developing such a system for the benefit of other researchers who also wish to work on these systems. Given that consumer sized, electrically rechargeable Zn-air cells are currently relegated to labs, while Ni-Zn cells are commercially successful, and that the Zn electrode reactions are identical in the Ni-Zn and Zn-air systems, the logical first step towards designing a test vehicle for rechargeable Zn electrodes seemed to be the development of a Ni-Zn system. It was assumed that the Ni-Zn system would be easier than Zn-air to get working properly since durable Ni electrodes were prevalent and external environment issues could be avoided by using a sealed system.

### 1.2.2 Introduction to Nickel Electrodes

So called ‘pasted’ nickel electrodes are usually created in the discharged state, Ni(OH)<sub>2</sub>, by mixing the active material (Ni(OH)<sub>2</sub> in this case) with acetylene black or cobalt to improve conductivity, and binder (PTFE) to hold the electrode together. More advanced Ni active material is coprecipitated with about 3 wt% Co(OH)<sub>2</sub> and 1 wt% Zn(OH)<sub>2</sub> to improve conductivity, increase the O<sub>2</sub> evolution reaction potential (Reaction (1-7) backward) and enhance the reversibility of Reaction (1-11), below.<sup>45-47</sup> It is also beneficial to coat the Ni(OH)<sub>2</sub> active material in Co(OH)<sub>2</sub>, which is converted to CoOOH during the first charge half-cycle. Co(OH)<sub>2</sub> is used in lieu of carbon to boost conductivity since the carbon promotes O<sub>2</sub> evolution and slowly corrodes at high potentials.<sup>48</sup> During charging, the Ni(OH)<sub>2</sub> is oxidized via<sup>44</sup>



to form nickel oxyhydroxide (NiOOH). It is important to note that Ni(OH)<sub>2</sub> and NiOOH both have two polymorphic forms found in electrodes: α-Ni(OH)<sub>2</sub>, β-Ni(OH)<sub>2</sub>, γ-NiOOH and β-NiOOH as shown in Figure 1-3. β-Ni(OH)<sub>2</sub> is historically the material sought after for use in electrodes since it cycles to and from β-NiOOH without changing crystallite size, making it less prone to detaching from the current collector.<sup>51</sup> This is slightly surprising when the pure crystallographic dimensions are considered, as shown in Table 1-1, since β-Ni(OH)<sub>2</sub> and β-NiOOH are not the same size.

Table 1-1: Crystal structure parameters for the four forms of nickel hydroxide. The volume was calculated using  $\frac{\sqrt{3}}{2}a_0^2c_0$  and the volume change is relative to that of β-Ni(OH)<sub>2</sub>.<sup>49</sup>

Ni Polymorph	a <sub>0</sub> (Å)	c <sub>0</sub> (Å)	Unit Cell Volume (Å <sup>3</sup> )	Volume Change
β-Ni(OH) <sub>2</sub>	3.126	4.605	38.97	0%
β-NiOOH	2.81	4.84	33.1	-15%
γ-NiOOH	2.82	6.9	48	22%
α-Ni(OH) <sub>2</sub>	3.08	7.6 - 8.5	62 - 70	60% - 79%

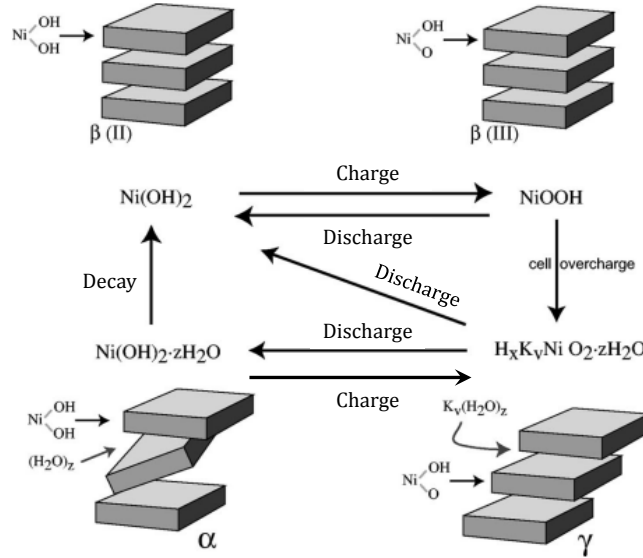
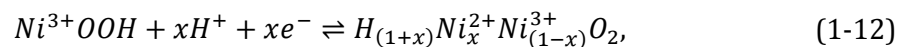


Figure 1-3: A diagram illustrating the different polymorphs of  $\text{Ni(OH)}_2$  and  $\text{NiOOH}$ , and the possible phase transitions between them. The prefix “ $\beta$ ” refers to the layered hydroxide structure that has no  $\text{H}_2\text{O}$  or  $\text{K}$  intercalated within it, while the “(II)” and “(III)” refer to the oxidation state of the  $\text{Ni}$  atom (i.e.  $\text{Ni}^{+2}$  and  $\text{Ni}^{+3}$ ). The  $\alpha$  and  $\gamma$  forms of nickel hydroxide have crystal planes that are shifted and tilted due to the incorporation of  $\text{H}_2\text{O}$  and  $\text{K}$  within the crystal structure. *Reproduced with permission from JES.*<sup>50</sup>

In practice,  $\beta\text{-Ni(OH)}_2$  with an O1 oxygen stacking sequence is converted to  $\beta\text{-NiOOH}$ , likely with a P3 oxygen stacking sequence,<sup>50</sup> during the first several charge cycles through a mixed-phase charging process known as “formation” (discussed in Section 2.3.2, pg. 54). Subsequently during discharge, any  $\beta\text{-NiOOH}$  present maintains its structure until it has accepted about 80% of the  $\text{H}^+$  ions and electrons that it could theoretically hold, depending on crystallinity and dopants.<sup>51</sup> This reaction is a single-phase reaction described by



where  $0 \leq x \lesssim 0.8$ . As long as  $x$  remains below about 0.8, the  $\text{H}_{(1+x)}\text{NiO}_2$  active material can cycle as a single-phase reaction without significantly changing in size. Forcing more  $\text{H}$  atoms into the P3 structure beyond this approximate limit (i.e.  $0.8 \lesssim x \leq 1$ ) requires more energy (i.e. a higher overpotential) and triggers a structural change back to the O1 oxygen stacking sequence of  $\beta\text{-Ni(OH)}_2$ .<sup>50, 51</sup> If the  $\beta\text{-Ni(OH)}_2$  is reformed like this, the next charge

half-cycle must once again progress through a mixed-phase process.<sup>51</sup> Thankfully, avoiding the structural change and associated increase in volume is easy. A discharging Ni electrode has two potential plateaus: The first has an average discharge potential of about 0.4 V vs Hg/HgO that contains about 80% of the theoretical capacity of the electrode.<sup>51</sup> The second has an average discharge potential about 0.5 V lower than the upper plateau and contains about 20% of the theoretical capacity.<sup>51</sup> To avoid the structural transition, Ni electrodes are usually only discharged to about 0.1 V vs Hg/HgO, which also means that practical Ni electrodes can only deliver about 80% of their theoretical capacity unless active material additives are used, like  $\text{Co}(\text{OH})_2$  and  $\text{Zn}(\text{OH})_2$ .<sup>51, 52</sup>

$\gamma$ -NiOOH is formed during overcharge, since the Ni atom can theoretically attain an oxidation state of about +3.66 when  $\text{K}^+$  and  $\text{H}_2\text{O}$  are intercalated into the structure.<sup>50</sup> Discharging  $\gamma$ -NiOOH usually produces  $\beta$ -Ni(OH)<sub>2</sub>, but under the right conditions it can instead discharge to  $\alpha$ -Ni(OH)<sub>2</sub>.<sup>53</sup>  $\alpha$ -Ni(OH)<sub>2</sub> is relatively unstable in highly alkaline electrolyte though and rapidly converts to  $\beta$ -Ni(OH)<sub>2</sub>, so it rarely gets a chance to be recharged into  $\gamma$ -NiOOH.<sup>54</sup> Consequently, stability issues prevent an  $\alpha/\gamma$  Ni electrode from being realized. Furthermore, the large volume expansion that accompanies  $\gamma$ -NiOOH and  $\alpha$ -Ni(OH)<sub>2</sub> formation detaches the active material from the current collector and absorbs a significant amount of water, which dries out the separator.<sup>49</sup> Both of these effects are deleterious to cycle life and as such most researchers avoid  $\gamma$  and  $\alpha$  polymorphs, but some have pursued stable versions nevertheless.<sup>53, 55-58</sup>

Prior to 1984, the surface of the active material was suspected to be a hydrogel when exposed to water since Ni(OH)<sub>2</sub> likely has water absorbed into and onto itself.<sup>59, 60</sup>  $\alpha$ -Ni(OH)<sub>2</sub> and  $\gamma$ -NiOOH are known to absorb water, and other electrolyte constituents, suggesting that this hydrogel would be made of  $\alpha$ -Ni(OH)<sub>2</sub> and  $\gamma$ -NiOOH. This gel was theorized to grow and crack with cycling, thereby increasing the electrode resistance over

time.<sup>60</sup> It should be noted that the idea of a hydrogel surface did not arise in the literature again after 1984, although it was not disproved either.

### 1.2.3 Ni-Zn Total Cell Reaction

As far as this thesis is concerned, the main benefit of the Ni-Zn cell is the fact that the Zn electrode reactions and environment are identical to that of a Zn-air cell and described by Reactions (1-1) and (1-2). When those reactions are combined with the Ni charge reaction (Reaction (1-11)), the total cell reaction results:



Note that the total cell reaction involves the production or consumption of water. As such, it is important to keep a small reservoir of extra electrolyte in the cell so that consumption of H<sub>2</sub>O during discharge does not dry out the separator. Reaction (1-13) consumes 0.336 μL H<sub>2</sub>O/mAh discharged. In a typical coin cell in this thesis, about 30 μL of electrolyte is used, which is about 30× larger than the H<sub>2</sub>O consumed considering the coin cells discharge about 3 mAh at most.

## 1.3 A Note on Terminology

The term “cell” in the context of batteries refers to an electrochemical cell, which is “a device capable of either generating electrical energy from chemical reactions [during discharge] or facilitating chemical reactions through the introduction of electrical energy [during charge]”.<sup>61</sup> In this thesis, a cell refers to any such system that has only a single positive electrode and negative electrode. The term “battery” actually refers to a collection of cells. For instance, a typical laptop battery in the early 2000’s had 6 Li-ion cells in it. However, the term “battery” has become associated with single cells in our society; take, for example, the ubiquitous “alkaline AA battery”, which is actually a cell with a single MnO<sub>2</sub>



positive electrode and a Zn negative electrode. In this thesis, the term “cell” is primarily used, but the term “battery” is used interchangeably with “cell” when the context calls for it, like when referring to the “battery research community”.

Also used in this thesis is the term “battery-like cell”, which is meant to conjure an image of a commercial cell, like an AA battery. A “battery-like cell” means the cell has stack pressure (i.e. the electrodes are being squished), a current collector and only enough electrolyte to fill the pores in the electrodes and separators.

The definition of “electrolyte” is a substance that dissolves as ions, or a solute. However, in the battery research community, the term electrolyte is instead used to refer to the entire solution or other substance that conducts ions between the two electrodes. For example, the entire solution of 3.2 M KOH, 1.8 M KF, 1.8 M K<sub>2</sub>CO<sub>3</sub> and 0.2 M ZnO (in water) is the electrolyte.

The “cycle life” of a cell is generally the number of times a rechargeable cell can be recharged and discharged. A charge followed by a discharge is one cycle, while the charge or discharge portions alone are sometimes referred to as half-cycles. Cycle life measurements are typically graphs of discharge capacity vs cycle number, but other forms such as average potential vs cycle number are sometimes employed.<sup>18, 20</sup> One aspect that is not often specifically addressed is the criterion for when a cell is considered to be at the end of its cycle life.<sup>18</sup> For instance, the arbitrarily chosen end of cycle life criterion within this thesis was chosen to be 50% of the discharge capacity of the first cycle. So a hypothetical cell that delivered 100 mAh during the first discharge has reached the end of its cycle life when it delivers less than 50 mAh during a subsequent discharge. If that happens during cycle 123, for example, then that cell will have had a cycle life of 123 cycles.

The “State of Charge” (SoC) of an electrode is the ratio of the charge currently stored in it to the maximum amount of charge that the electrode could store:  $Q_{\text{Present}}/Q_{\text{Possible}}$ .

Therefore, as an electrode is charged, the SoC increases until it reaches 1 when the electrode is fully charged. Likewise, the SoC decreases during discharge until it reaches 0.

#### 1.4 Introduction to Butler-Volmer

So far, there has been no mention of reaction rates and so a brief description of the Butler-Volmer equation, without derivation, will be described here to aid the understanding of concepts throughout the thesis. If the following effects are not important to a reaction: diffusion, layer growth that slows diffusion or layer growth that changes the rate of electron transfer from the surface to the reactants, then the Butler-Volmer equation describes the relationship between the current and potential for a given electrochemical reaction.

$$i_{Total} = i_0 \left( e^{(1-\beta)\left(\frac{nF}{RT}\right)\eta} - e^{-\beta\left(\frac{nF}{RT}\right)\eta} \right) \quad (1-14)$$

where  $i_{Total}$  is the current and  $i_0$  is called the “exchange current density” (mA/cm<sup>2</sup>) and is a property of the reaction and the surface on which the reaction is happening.  $\beta$  is a “symmetry” factor that is dependent on the mechanism of the reaction and lies between 0 and 1;  $\beta$  is commonly assumed to equal 0.5, as has been done for Zn.<sup>29</sup>  $n$  is the number of

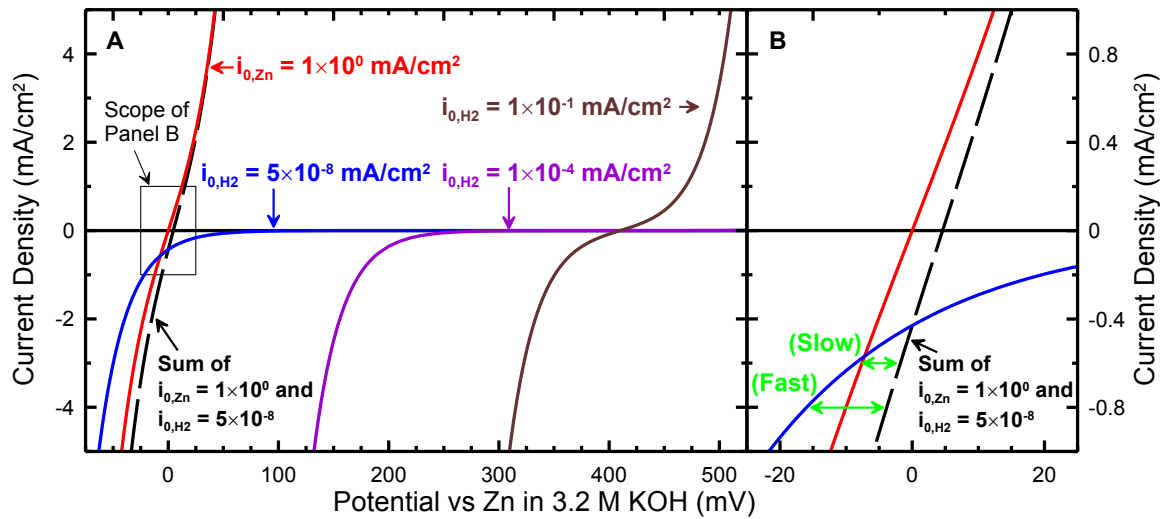


Figure 1-4: Example of Butler-Volmer curves. The brown, purple and blue curves in panel A use  $E_{eq,H_2}$  in 3.2 M KOH while the red curve uses  $E_{eq,Zn}$ . The dashed black line is the sum of the blue and red lines.

moles of electrons that are passed per mole of reaction,  $F$  is Faraday's constant (96,485 C/mol),  $R$  is the gas constant (8.31415 J/(K×mol reaction)) and  $T$  is the temperature (K). The  $\eta$  is the "overpotential", named as such because it is the difference between the potential of the electrode and the equilibrium potential for the reaction of interest:  $\eta = E - E_{eq}$ . The first exponent in the brackets represents the rate of oxidation, while the second exponent is the rate of reduction.

Figure 1-4 shows some example Butler-Volmer curves with different exchange current densities and two different equilibrium potentials: one at 410 mV vs Zn, which is  $E_{eq}$  for  $H_2$  evolution, and one at 0 mV vs Zn, which is  $E_{eq}$  for Zn. In this example, the equilibrium potentials are realistic, but the exchange current densities are not. Panel A shows three  $H_2$  curves that use  $E_{eq,H_2}$  and decreasing values of  $i_{0,H_2}$ , and one curve (red) for Zn with its own  $E_{eq,Zn}$  and  $i_{0,Zn}$ . If -2 mA/cm<sup>2</sup> were applied to the Zn electrode in this example, only  $H_2$  would be evolved unless  $i_{0,Zn} \lesssim 1 \times 10^{-7}$  mA/cm<sup>2</sup> since  $H_2$  evolution will provide all of the required current unless the potential of the electrode happens to be negative of  $E_{eq,Zn}$ . The smaller the  $i_0$ , the greater the  $\eta$  required to produce a specified current, and vice versa. Catalysts have high  $i_0$ 's while systems that want slow processes, like gas evolution in a battery, have low  $i_0$ 's.

The dashed, black line in panel A represents the current response of a hypothetical Zn electrode in a system where  $i_{0,H_2} = 5 \times 10^{-8}$  mA/cm<sup>2</sup> and  $i_{0,Zn} = 1$  mA/cm<sup>2</sup> (i.e. the sum of the red and blue curves):

$$i_{Total} = i_{0,Zn} \left( e^{(1-\beta)\left(\frac{nF}{RT}\right)\eta_{Zn}} - e^{-\beta\left(\frac{nF}{RT}\right)\eta_{Zn}} \right) - i_{0,H_2} e^{-\beta\left(\frac{nF}{RT}\right)\eta_{H_2}}. \quad (1-15)$$

Note that some  $H_2$  will always be produced while plating Zn in this system since some of the current is due to  $H_2$  evolution (the blue line). Panel B shows a close up of the region where these lines cross to demonstrate that if the Zn in solution were depleted (i.e. the red line disappeared) then the potential under a "slow" current of -0.6 mA/cm<sup>2</sup> would not fall as far

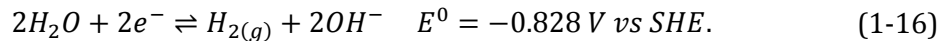
as it would if a “fast” current of  $-0.8 \text{ mA/cm}^2$  were used. This concept is important later and will be referenced throughout this thesis.

## 1.5 Overcharging Ni-Zn and Zn-air Cells

Unless the two electrodes in a cell have exactly the same capacity, one of those electrodes will reach the fully charged state before the other. If this happens and charging continues, that full electrode is said to be ‘overcharging’. Overcharging is generally bad for the cell, but why that is depends on the cell chemistry and design.

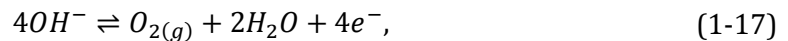
### 1.5.1 Electrolysis of the Electrolyte due to Overcharging

When a negative electrode is overcharged, the potential of that electrode drops until one or more other reactions occur at high enough rates to consume the overcharge. For an electrode submerged in water, this reaction is usually  $\text{H}_2$  evolution:<sup>62, 63</sup>



The potential at which  $\text{H}_2$  evolution occurs depends on the pH and the material of the surface on which the reaction is occurring.<sup>63, 64</sup> Recall that the higher the potential difference that can be achieved between the two electrodes, the higher the cell potential and energy density will be. Since the onset of  $\text{H}_2$  evolution limits how low the potential of the negative electrode can be without wasting current, materials with a high overpotential for  $\text{H}_2$  evolution are popular battery negative electrodes. For example, this is the case for Zn, Cd and Pb, all important negative electrode materials in aqueous cells.<sup>63, 65</sup>

Similarly, when the positive electrode in an aqueous system is overcharged,  $\text{O}_2$  evolution occurs:<sup>62, 66</sup>



which is Reaction (1-7) backward. Since this reaction syphons charge away from the active material, materials with a high overpotential for Reaction (1-17) are favoured as both active materials and cell components.<sup>66</sup> The exception to this is an air electrode since Reaction (1-17) is the reaction that is intended to occur. As such, air electrodes cannot be overcharged unless the electrolyte is gone, at which point there are larger problems to deal with.

If both the negative and positive electrodes are overcharged simultaneously, H<sub>2</sub> and O<sub>2</sub> evolution (Reactions (1-16) and (1-17)) combine to give the electrolysis of water:



The gases produced by overcharging can be reclaimed through the process known as “recombination”.<sup>44,67</sup> For instance, O<sub>2</sub> produced by Reaction (1-17) at the positive electrode can diffuse towards the negative electrode and recombine with Zn to form ZnO:<sup>44,</sup>

<sup>67</sup>



Similarly, H<sub>2</sub> can recombine at the positive electrode with NiOOH to form Ni(OH)<sub>2</sub>:



Unfortunately, Reaction (1-20) is so slow that it essentially does not occur in practice.<sup>44,67</sup>

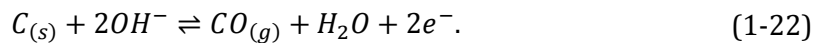
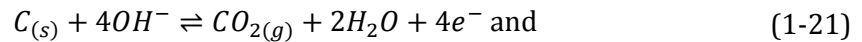
On the other hand, O<sub>2</sub> recombination (Reaction (1-19)) occurs at significant rates if the internal pressure in the cell rises above atmospheric pressure.<sup>44,67,68</sup> This process turns out to be quite useful for destroying Zn dendrites since the dendrite is the first Zn that the O<sub>2</sub> will encounter as it diffuses from the overcharging positive electrode toward the negative electrode.<sup>15</sup> Dendrites are covered in more detail in Section 1.8.1 (pg. 26).

Every commercial rechargeable cell strives to keep the state of charge of the electrodes matched due to the fact that repeatedly overcharging an electrode depletes either H<sub>2</sub>O or OH<sup>-</sup> from the electrolyte. However, a perfectly functioning Ni-Zn cell still

produces some O<sub>2</sub> during a normal charge half-cycle due to unavoidable O<sub>2</sub> evolution on the NiOOH active material, which can leave the Zn electrode at a higher state of charge.<sup>44</sup> To keep the state of charge of the electrodes in balance, ideal cell operation requires that the O<sub>2</sub> produced at the Ni electrode diffuses through the electrolyte to the Zn electrode to reduce an equivalent amount of Zn to ZnO (Reaction (1-19)). Microporous membranes usually have poor O<sub>2</sub> diffusion rates, which can limit this shuttling process.<sup>69</sup> As such, separators designed for Ni-Zn cells should have high O<sub>2</sub> diffusivity rates to promote this process, whereas separators designed for Zn-air cells should have low O<sub>2</sub> diffusivity rates to reduce the oxidation of the Zn electrode during charge.<sup>70</sup>

### 1.5.2 Other Consequences of Overcharging

Any material that is in contact with both the electrolyte and a polarized electrode could undergo a chemical reaction if the polarization is high enough. For instance, the acetylene black that is frequently used as a conductive additive in electrodes corrodes at high potentials in alkaline electrolyte via<sup>71</sup>



Both reactions occur resulting in a mass loss of about 0.01 wt%/hour at 550 mV vs Hg/HgO, or a Ni-Zn or Zn-air cell potential of about 1.95 V, in 30 wt% KOH (6.9 M) at 25°C.<sup>72</sup> <sup>73</sup> This rate seems small but all CO<sub>2</sub> produced becomes carbonate (CO<sub>3</sub><sup>2-</sup>) in concentrated KOH and eventually begins precipitating out as K<sub>2</sub>CO<sub>3</sub>, clogging the pores of the positive electrode.<sup>9,30</sup> Over many cycles this becomes a problem.<sup>21</sup> Additionally, catalyst particles can be lost due to their carbon support disappearing due to corrosion.<sup>74</sup>

At the negative electrode in Ni-Zn and Zn-air cells, Zn dendrites form whenever plating (charging) Zn becomes diffusion controlled, which happens when the charging

current density rises too high.<sup>14, 75, 76</sup> Overcharging plates any remaining dissolved  $\text{Zn(OH)}_4^{2-}$  from solution in a diffusion controlled manner while producing  $\text{H}_2$  via Reaction (1-16).

The buildup of gas in general is another consequence of overcharging both the positive and negative electrodes. Although this is not a problem for Zn-air cells since they are open to the atmosphere, sealed cells, like Ni-Zn cells, require a pressure release valve that is tuned to open at a particular internal pressure as a safety feature to allow any gases to escape without exploding the cell.

## **1.6 Overdischarging Ni-Zn and Zn-air Cells**

Similarly to overcharging, overdischarging occurs when one electrode finishes discharging before the device finishes drawing current. If the negative electrode finishes discharging (i.e. all Zn has been stripped from the current collector), the negative electrode potential will rise until another reaction begins that can provide the required current. Conversely, if the positive electrode finishes discharging first, the positive electrode potential will fall until a sustainable reaction is found. Overdischarging can also accidentally occur to an entire cell (both electrodes) in certain situations. For example, a battery pack without individually monitored cells will eventually have at least one cell that finishes discharging without triggering the low voltage alarm to stop the discharge. In this case, the battery pack continues discharging while the empty cell is forced into overdischarge. As a final note regarding air electrodes, an air electrode will never enter overdischarge unless  $\text{O}_2$  cannot reach it.

### 1.6.1 Electrolysis of the Electrolyte Due to Overdischarging

The most obvious reactions that occur during overdischarge are H<sub>2</sub> evolution (Reaction (1-16), pg. 19) on the positive electrode and O<sub>2</sub> evolution (Reaction (1-17)) on the negative electrode. As previously mentioned, if both electrodes are overdischarged simultaneously the result is the electrolysis of water as per Reaction (1-18).

### 1.6.2 Other Consequences of Overdischarging

Overdischarge generally involves a larger potential swing than overcharge. For example the positive electrode, Ni(OH)<sub>2</sub>, begins at a potential close to O<sub>2</sub> evolution while discharging, but then must descend about 1.3 V before reaching H<sub>2</sub> evolution during overdischarge. The chances that other reactions exist in a 1.3 V window are greater than they are in the 0.1 V window that separates charging Ni(OH)<sub>2</sub> from evolving O<sub>2</sub> during overcharge. During overdischarge, the Ni electrode first fills any remaining vacancies with H, triggering a structural change back to crystallized Ni(OH)<sub>2</sub>.<sup>50, 51</sup> Then any CoOOH additive present discharges to Co(OH)<sub>2</sub> and then possibly to Co.<sup>77</sup> Finally, H<sub>2</sub> evolution begins.<sup>78</sup>

The negative electrode, ZnO, also suffers serious consequences during overdischarge, but the damage is suffered by the current collector instead of the active material itself. ZnO is a semiconductor and essentially remains inert during overdischarge. If the current collector is copper (Cu), Zn that has alloyed with the Cu starts to be leached out; but this process is slow and likely cannot keep up with the current.<sup>79</sup> So the potential continues to rise until Cu is oxidized first to Cu<sub>2</sub>O, then to CuO and then Cu(OH)<sub>2</sub> before finally evolving O<sub>2</sub> gas.<sup>80</sup>

Tin (Sn) current collectors dissolve in alkaline electrolyte at about 0.3 V above the Zn electrode potential:<sup>64, 81</sup>





If the current collector were instead Sn plated onto Cu, the Cu core would remain after the dissolution of Sn; then during the subsequent charge half-cycle, the Sn would plate down on the Cu instead of Zn, effectively turning the cell into a Ni-Sn or Sn-air cell at a potential 0.3 V lower than a Zn cell. Although both Sn dissolution and Cu oxidation are reversible processes, both result in some changes and irreversibility in current collector structure, which are best avoided if long cycle life is desired.

## 1.7 Self-Discharge Reactions in Ni-Zn and Zn-Air Cells

In this thesis, self-discharge refers to the phenomenon where an electrode, left at open circuit, loses capacity over time despite not being connected to a load.

### 1.7.1 Zn Electrode Self-Discharge

Zn electrodes self-discharge through the Zn corrosion reaction,<sup>14</sup> which is a combination of Zn electrodisolution and ZnO precipitation (Reactions (1-2) and (1-1) backward) followed by H<sub>2</sub> evolution nearby (Reaction (1-16)), yielding



Any material that catalyzes H<sub>2</sub> evolution (Reaction (1-16)) increases the rate of Zn corrosion, which is unfortunate since most other metals have a lower overpotential for H<sub>2</sub> evolution than Zn. As such, battery-grade Zn must be as pure as possible to achieve the low self-discharge rates typical of primary alkaline batteries. To lower self-discharge rates further, primary battery Zn active materials are doped with indium and bismuth, since both of those metals have even higher H<sub>2</sub> evolution overpotentials than Zn.<sup>82</sup>

### 1.7.2 Air Electrode Self-Discharge

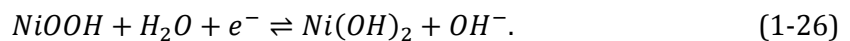
An air electrode cannot self-discharge since it does not hold energy in a chemical form. The O<sub>2</sub> and H<sub>2</sub>O that are the products of the charging process (Reaction (1-17), pg. 19) are stored in the environment and electrolyte, respectively. However, an air electrode made with carbon can corrode through carbon corrosion combined with O<sub>2</sub> reduction (Reaction (1-7)) to produce CO<sub>2</sub> gas:<sup>72</sup>



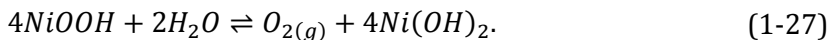
Carbon corrosion is discussed in Section 1.5.2 (pg. 21). Although this process does not reduce the capacity that could be delivered by the air electrode in the subsequent discharge half-cycle, carbon corrosion will slowly destroy the air electrode over time, which would reduce the discharge potential.

### 1.7.3 Ni Electrode Self-Discharge

A charged electrode left to sit in the electrolyte will undergo relatively slow reactions that discharge the electrode. To maintain charge neutrality, a simultaneous reaction must proceed to consume or produce the electrons required by the self-discharge reaction much like corrosion. NiOOH self-discharges by taking a H<sup>+</sup> from a H<sub>2</sub>O molecule:<sup>67</sup>



The e<sup>-</sup> is provided by O<sub>2</sub> evolution (Reaction (1-17)) or carbon corrosion (Reactions (1-21) or (1-22)). Combination with O<sub>2</sub> evolution makes the total reaction



The rate of this reaction is controlled by the rate of the reaction providing the electrons: O<sub>2</sub> evolution or carbon corrosion. As such, anything that catalyses these reactions will speed up the self-discharge of the Ni electrode.

## 1.8 Rechargeable Zn Electrode Challenges

### 1.8.1 Dendrites

Dendrites are the most troublesome challenge facing rechargeable Zn electrodes. They are needle-like protrusions that grow outward from Zn metal during Zn deposition, i.e. charging. These dendrites can grow long enough to penetrate porous separators and touch the other electrode, thereby causing a short circuit. Dendrites arise from the tips of Zn pyramids that themselves arise from the plating of Zn onto screw dislocations in the surface.<sup>83</sup> The needle begins growth once the tip of the pyramid has shrunk to a radius of curvature small enough (about  $< 2 \mu\text{m}$ ) to be subject to spherical diffusion rather than linear diffusion within the diffusion boundary layer. From that point on, dendrite growth is linear with time and subject to diffusion control.<sup>76</sup> If the overpotential is fixed (instead of the current), the total current increases quadratically with time ( $i = kt^2$ ) simply due to the increase in surface area that arises with dendrites.<sup>83</sup> Since dendrite initiation depends on temperature,  $\text{Zn}(\text{OH})_4^{2-}$  concentration, current density and/or overpotential, some circumstances will not give rise to dendrite growth. It is unfortunate that Zn electrodes with no inhibitors do have the right characteristics to grow dendrites; this has led to the search for additives and other tricks that shift these characteristics out of the optimum zone in order to prevent dendrite growth. One of the most common means of preventing dendrite growth on flat electrodes is by applying pressure onto a microporous separator that in turn presses against the current collector. This physically prevents Zn dendrites from growing. In sealed cells dendrites can be actively destroyed by slightly overcharging the positive electrode and creating  $\text{O}_2$  that devours Zn dendrites as mentioned in Section 1.5.1.<sup>15,44</sup> Unfortunately, this does not work in Zn-air cells since the internal pressure of  $\text{O}_2$

cannot rise above atmospheric pressure, although at least one author has noted that the presence of O<sub>2</sub> in a Zn-air cell might be high enough, in general, to consume dendrites.<sup>18</sup>

### 1.8.2 Passivation

Passivation of Zn occurs during discharge at all currents when a layer of zinc oxides and hydroxides forms that prevents further passage of Zn(OH)<sub>4</sub><sup>2-</sup> or Zn(OH)<sub>3</sub><sup>-</sup> ions.<sup>14,84</sup> The mechanism by which this occurs was described best by Cachet *et al.* who claimed that when the potential first became anodic during discharge, a partially conductive interphase consisting of zinc oxides and hydroxides grew to become a thick, porous layer on the Zn surface.<sup>39</sup> This layer shrank as the overpotential was increased, starting at about 14 μm at equilibrium and declining logarithmically to about 140 nm at 15 mV anodic overpotential, which is a typical discharging overpotential for a Zn electrode in a battery.<sup>39</sup> The pores had a radius of about 56 nm and the base of the pores in the layer were about 10 times as conductive as the walls, meaning that most Zn(OH)<sub>4</sub><sup>2-</sup> produced originated at the bottom of the pores and had to diffuse outward.<sup>39</sup> As time passes, the pores lengthen as ZnO precipitates onto the oxide surface, thickening it, and Zn at the bottom of the pores is preferentially dissolved. Eventually, either the pore gets long enough or the current density gets high enough that Zn(OH)<sub>4</sub><sup>2-</sup> ions cannot escape the pore fast enough to make room for more Zn(OH)<sub>4</sub><sup>2-</sup>. In this case, the electrolyte in the pore becomes supersaturated in Zn(OH)<sub>4</sub><sup>2-</sup> and precipitates ZnO fast enough to clog the pore and passivate the surface.

The severity of passivation in a particular system is measured by setting a current and measuring the time until the potential of the Zn electrode raises sharply, which signals either the onset of passivation or the complete dissolution of Zn off of the current collector.<sup>14</sup> The experimentalist can determine which event occurred by comparing the product of the current and time to the known capacity of the Zn electrode; if the product is

lower than the capacity, then passivation occurred. The relationship between the time to passivation and the current is derived from the rate of diffusion of  $\text{Zn}(\text{OH})_4^{2-}$  ions out of the pore:<sup>14, 84</sup>

$$i = -nFD \frac{(C_{\text{Bulk}} - C_{\text{crit}})}{\sqrt{\pi Dt_p}} \quad (1-28)$$

Here,  $i$  is the current,  $n$  is the number of electrons transferred per  $\text{Zn}(\text{OH})_4^{2-}$  ion (2),  $F$  is Faraday's constant (96,485 C/mol  $e^-$ ),  $D$  is the diffusion coefficient of  $\text{Zn}(\text{OH})_4^{2-}$  ( $7 \times 10^{-6}$   $\text{cm}^2/\text{s}$ <sup>14</sup>),  $C_{\text{Bulk}}$  is the concentration of  $\text{Zn}(\text{OH})_4^{2-}$  in the bulk electrolyte,  $C_{\text{crit}}$  is the critical concentration of  $\text{Zn}(\text{OH})_4^{2-}$  at the surface that triggers passivation and  $t_p$  is the time to passivation. Liu *et al.* shows the linear relationship between current density,  $i$ , and  $1/\sqrt{t_p}$  at various KOH concentrations, which demonstrates that likely only thick electrodes that are discharged at high rates need to be concerned with passivation.<sup>84</sup> For example, a flat Zn electrode discharged at 57 mA/cm<sup>2</sup> in 2.92 M KOH electrolyte passivated after 1.76 h, meaning that only an electrode that had a capacity of more than 100 mAh/cm<sup>2</sup> would have passivated before it was fully discharged.<sup>84</sup> For comparison with this thesis, the riskiest situations were a 0.5 mAh/cm<sup>2</sup> electrode discharged at 15 mA/cm<sup>2</sup> in Chapter 4 and an 11 mAh/cm<sup>2</sup> Zn electrode discharged at a rate of about 1 mA/cm<sup>2</sup> in Chapter 5. These rates and capacities were far from the danger zone presented by Liu *et al.*<sup>84</sup>

Evidently, the diffusion rate of  $\text{Zn}(\text{OH})_4^{2-}$  into and within the electrode bulk will determine the rate capability and perhaps longevity of the Zn electrode (see "densification" below). Passivation will occur sooner if  $\text{Zn}(\text{OH})_4^{2-}$  cannot diffuse fast enough from the pores on the Zn surface into the micro pores of the Zn electrode or from the micropores into the bulk electrolyte. This means that the porosity of the Zn electrode will determine the rate capability of the Zn electrode.<sup>18, 42, 85, 86</sup> Maintaining electrolyte flow through the electrode bulk prevents passivation by reducing the tortuosity of diffusion paths for

$\text{Zn(OH)}_4^{2-}$  ions.<sup>85, 86</sup> Consequently, three-dimensional current collectors with high surface areas, like Cu or Sn foam, help by maintaining good electrolyte flow paths and reducing the current density on any given patch of Zn. Non-electrochemically active fibers that act as wicks embedded in the electrode have also been used to promote electrolyte flow.<sup>15</sup>

Another cause of passivation after many cycles is sometimes referred to under the title “densification”. Since the entire Zn electrode dissolves and reforms itself twice each cycle, it should be unsurprising that any porosity that the electrode originally had can be ‘filled in’ over the course of many cycles, eventually reducing the charged Zn electrode to a solid block of Zn. As that porosity disappears over cycling, the current density increases, since the same amount of current is being forced through a smaller surface area, until it is high enough to trigger passivation and prevent Zn from discharging further.<sup>18</sup> Again, a 3-D current collector and/or electrolyte wicks embedded in the electrode can help mitigate this problem.<sup>15</sup>

### 1.8.3 Shape Change

Shape change refers to the movement of Zn active material from its location when the cell was fabricated, leaving behind a section of bare current collector.<sup>15, 43, 44, 87, 88</sup> As the Zn electrode cycles, Zn material tends to migrate either from the edges of the current collector into the middle or vice versa.<sup>43, 44, 87</sup> A simple explanation of shape change is that KOH and  $\text{K}_2\text{Zn(OH)}_4$  concentration gradients are set up across the separator and laterally along the electrode during cell operation, leading to the diffusion of  $\text{Zn(OH)}_4^{2-}$  ions.<sup>43, 89, 90</sup> Since the Zn spends some of its time in the electrolyte as  $\text{Zn(OH)}_4^{2-}$ , whether charging or discharging, this diffusion moves it a small distance before it attaches to the electrode as either Zn or ZnO, respectively. A more complex computer model and description of shape change was developed by Isaacson *et al.* and interested readers are directed there.<sup>43</sup> Of

particular note is Isaacson's conclusion that "a high value of the (ZnO) precipitation rate constant produces movement of ZnO toward the edge of the electrode, whereas a low value of the precipitation rate constant produces a movement of ZnO toward the center of the electrode."<sup>43</sup> It has also been observed that gravity has little to no effect on shape change.<sup>90</sup>

Shape change can be reduced by reducing the size or presence of electrolyte reservoirs at one side of the electrode<sup>43</sup>, using low  $\text{Zn(OH)}_4^{2-}$  solubility electrolyte additives like KF and  $\text{K}_2\text{CO}_3$ ,<sup>20, 44</sup> and by ensuring that the current collector promotes a uniform current density by choosing a uniformly shaped 3D material (like Cu foam) and attaching the tab to the opposite side of the Zn electrode from the tab position on the positive electrode.<sup>44</sup> It is also beneficial to use electro-osmosis inhibiting separators to reduce convection through the separators.<sup>89, 90</sup> However, electrolyte convection helps utilization and high rate discharge in Zn electrodes, so it is beneficial to prevent shape change without blocking all convective flow.<sup>90</sup> Reducing the solubility of ZnO in the electrolyte is the most popular strategy to battle shape change and thereby increase cycle life. This can be accomplished by reducing the KOH concentration, incorporating the ZnO into a structure that has an even smaller solubility, like calcium zincate ( $\text{Ca(OH)}_2 \cdot 2\text{Zn(OH)}_2 \cdot 2\text{H}_2\text{O}$ ), or filling the electrolyte with additives that reject  $\text{Zn(OH)}_4^{2-}$  ions.<sup>20, 44, 91</sup> Cairns' group developed a rather popular electrolyte using the last method that contains 3.2 M KOH, 1.8 M KF, 1.8 M  $\text{K}_2\text{CO}_3$  and is saturated with ZnO.<sup>92</sup>

## **1.9 Bi-functional (Rechargeable) Air Electrode Challenges**

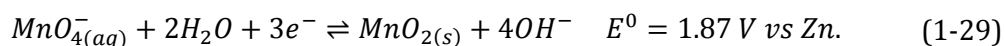
### *1.9.1 Destruction of the Support Structure*

As of the year 2000, it was the bi-functional air electrode that limited the cycle life of Zn-air cells; sadly, no cycle life experiments to cell failure of Zn-air cells using a bi-functional air electrode have been reported in the literature since the 1990s.<sup>18, 93, 94</sup> A key reason for

the destruction of the bi-functional air electrode structure during charge is the creation of O<sub>2</sub> bubbles within the structure.<sup>21</sup> The carbon structure is designed to provide a large surface area, and so it is rather delicate. As such, the rapid expansion of O<sub>2</sub> bubbles is enough to break the structure.<sup>21</sup> Toussaint *et al.* avoided this issue by splitting the positive electrode into two separate electrodes that were electronically disconnected from each other.<sup>21</sup> One of them was connected to the negative electrode, through the load, only during discharge. This electrode was the O<sub>2</sub> reduction electrode and was a typical, inexpensive air electrode utilizing a carbon structure with MnO<sub>2</sub> as the catalyst. The other electrode was only connected to the negative electrode during charge. This electrode was the O<sub>2</sub> evolution electrode and was made of an inert metal mesh: stainless steel in this case.<sup>21</sup> Alternatively, a more durable bi-functional air electrode could be made by growing a catalyst nanowire network directly onto a metal mesh without carbon or binder.<sup>95</sup> Lee *et al.* demonstrated that such an air electrode could survive at least 300 hours of charging at 50 mA with only about a 60 mV drop in discharge potential.<sup>95</sup> They did not specify the electrode area for this experiment, but from their plot of V vs current density for the air electrode alone the current density of the cycling experiment was likely about 20 mA/cm<sup>2</sup>.

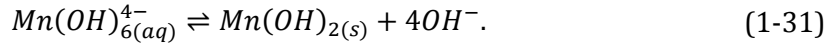
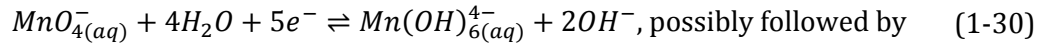
### 1.9.2 Manganese (Mn) Dissolution

MnO<sub>2</sub> is a common, cheap and effective O<sub>2</sub> reduction catalyst; but it can dissolve off of the air electrode if the potential rises above about 0.6 V vs SHE (about 1.9 V vs Zn during charging) or if the potential drops below about -0.1 V vs SHE (about 1.2 V vs Zn during discharge).<sup>64, 81, 96</sup> During charging, when the air electrode is raised to a potential of about 2 V vs Zn, MnO<sub>2(s)</sub> is oxidized to MnO<sub>4(aq)</sub><sup>-</sup> and dissolves:<sup>21, 64, 81</sup>

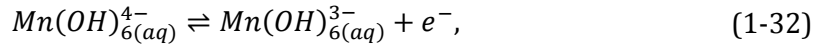




It can then diffuse to the Zn electrode where it will accept electrons and possibly precipitate as  $Mn(OH)_2$ .<sup>64, 96, 97</sup>

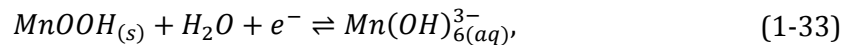


$Mn(OH)_6^{4-}(aq)$  that diffuses back to the air electrode can donate either one electron to become  $Mn(OH)_6^{3-}(aq)$ ,



or five electrons to once again become  $MnO_4^-(aq)$  via Equation (1-30).<sup>64, 96, 97</sup> Either way, this process of transferring electrons through ions in the electrolyte (as opposed to through the external circuit) is called 'shuttling' and steals electrons that would have otherwise gone towards plating Zn onto the negative electrode. This shuttling process was detected in Ni-MH cells, which also use KOH electrolyte and Mn in the metal hydride (MH) electrode, by Li *et al.*<sup>98</sup> This can be avoided by using a separate electrode to evolve  $O_2$  during charging or by not using  $MnO_2$  as the  $O_2$  reduction catalyst.

$MnO_2$  can also dissolve and bring about shuttling during discharge in alkaline electrolyte if the air electrode drops below -0.1 V vs SHE (1.2 V vs Zn).<sup>96</sup> Under these conditions  $MnOOH$  dissolves as  $Mn(OH)_6^{3-}(aq)$ ,



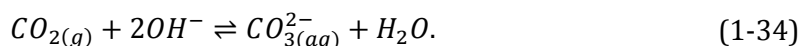
diffuses to the Zn electrode, accepts an  $e^-$  via Reaction (1-32) backward and finally diffuses back to the air electrode where it drops off the electron and repeats the shuttling process.<sup>97</sup>

<sup>98</sup> If  $MnO_2$  is to be used, this problem can be minimized by using low alkalinity electrolytes<sup>99</sup> (closer to 1 M KOH rather than 7 M KOH).

### 1.9.3 Carbon Corrosion

The corrosion of the carbon support during charging (discussed in Section 1.5.2) is also a concern. If the carbon around a particle of catalyst corrodes, the particle is set adrift in the electrolyte and no longer participates in the air electrode electrochemistry. To make matters worse, the catalyst itself can enhance corrosion of its own carbon support.<sup>74</sup>

Carbon corrosion in general is also problematic since CO<sub>2</sub> produced in alkaline electrolyte can be absorbed by the electrolyte to form carbonate:<sup>30</sup>



CO<sub>2</sub> drifting in from the atmosphere in air is also absorbed in this way, eventually precipitating out as K<sub>2</sub>CO<sub>3</sub>. This powder slowly clogs the pores of the air electrode, eventually reducing the effective surface area of the air electrode, thereby increasing current densities and overpotentials.<sup>30</sup> Recently, an interpenetrated polymer network of anionic polymer has been developed to provide OH<sup>-</sup> conductivity without allowing CO<sub>2</sub> access to the electrolyte, extending the lifetime of an aqueous Li-air cell air electrode one hundred-fold.<sup>100</sup> This semi-permeable membrane can be incorporated right into the air electrode.<sup>21</sup>

### 1.9.4 Water Management

Another challenge for small, electrically rechargeable Zn-air cells that do not have resealable air holes or their own humidity-control system is the simple evaporation or uptake of water through the holes in the canister. In commercial cells, a microporous PTFE (Teflon) layer is sealed over the holes (inside the cell) in an attempt to slow down the evaporation of water. As an example, a 4 cm<sup>3</sup> prismatic, primary, Energizer Zn-air cell lost 20% of its rated capacity in 21 days (52 days to 50%) due to evaporation, although the relative humidity was not mentioned.<sup>19</sup> The ratio of the partial pressure of H<sub>2</sub>O from the

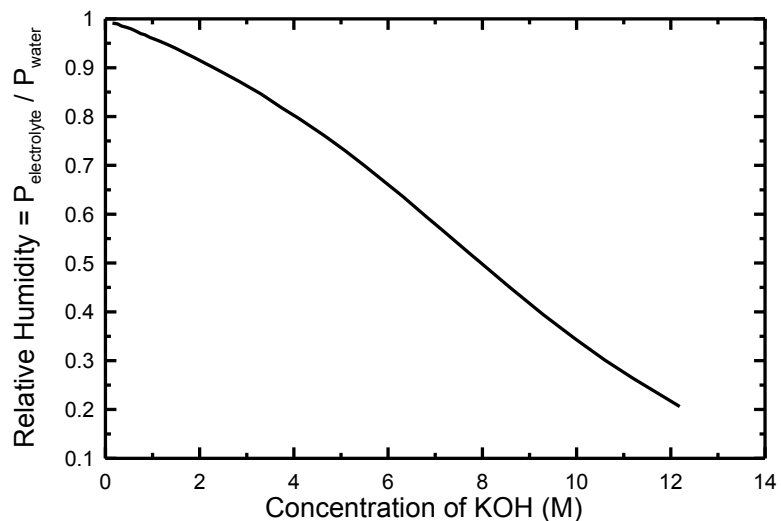


Figure 1-5: Vapour pressure of the electrolyte ( $P_{\text{electrolyte}}$ ) as a function of KOH concentration at room temperature. By dividing  $P_{\text{electrolyte}}$  by  $P_{\text{water}}$ , the relative humidity of the environment can be compared directly to the y-axis values to determine if water will diffuse into or out of the cell. For example, an 8 M KOH solution will lose water through evaporation if the relative humidity is < 50% and gain water if it is > 50%. This figure was created based on the data from reference 27.<sup>27</sup>

electrolyte to that of pure water compared to the relative humidity of the external environment determines if  $\text{H}_2\text{O}$  will leave or enter the cell. Figure 1-5 shows the relative humidity that a particular concentration of KOH will be in equilibrium with.<sup>27</sup> At relative humidity higher than the line, water will enter the cell, while at humidity below the line water will leave the cell. Since  $\text{H}_2\text{O}_{(\text{g})}$  is smaller than  $\text{O}_{2(\text{g})}$ , it is impossible to have a membrane that would allow  $\text{O}_{2(\text{g})}$  through at the required rates but not let  $\text{H}_2\text{O}_{(\text{g})}$  out. As such, a valve to seal the Zn-air cell when not in use and/or a means of manually adding or removing water to/from the cell are essential to extending the service-life of Zn-air cells.

## 1.10 Rechargeable Ni Electrode Challenges

### 1.10.1 Stack Pressure

Many of the early issues facing Ni electrodes have been solved in commercially made cells, but are still a challenge for researchers making electrodes for the first time. The first issue is maintaining contact between the active material and the conductive material or

current collector. As the  $\text{Ni}(\text{OH})_2$  is cycled, it shrinks and expands, and in the process breaks contact with its surroundings.<sup>60, 101</sup> The main solution to this problem is applying 50 – 100 kPa of stack pressure.<sup>101, 102</sup>

### 1.10.2 Conductivity

Another issue to beware of is maintaining conductivity within the Ni electrode. Historically in the literature this was done with carbon, like acetylene black or a mixture of acetylene black and graphite, which worked well, but corrosion prevented it from being a perfect solution.<sup>101-103</sup> Instead, the more permanent solution was to dope the active material with  $\text{Co}(\text{OH})_2$  and  $\text{Zn}(\text{OH})_2$  to improve conductivity within the  $\text{Ni}(\text{OH})_2$  particles and to coat the particles in  $\text{CoOOH}$  to improve conductivity between particles.<sup>48</sup>

Conductivity of  $\text{H}^+$  within the Ni active material is also important, and improves when the active material crystallites are smaller and less crystalline since defects in the crystal structure aid  $\text{H}^+$  diffusion.<sup>54, 104-107</sup> As cycling progresses, and the active material shrinks and expands, it slowly fixes the defects and recrystallizes.<sup>51, 60, 101, 108, 109</sup> As this happens, the resistance of the Ni active material increases, decreasing the cell potential and possibly the cell capacity if some  $\text{H}^+$  sites become unreachable.<sup>104, 105, 107</sup> This issue is once again mitigated by incorporating more permanent defects like Zn and Co into the crystal structure.<sup>48, 109, 110</sup> X-ray photoelectron spectroscopy (XPS) has suggested that recrystallization of the active material also makes it pull away from the conductive material, providing another explanation for the decrease in utilization;<sup>60</sup> however, this issue should be solved by applying stack pressure to the electrode.<sup>101, 102</sup>

### 1.10.3 Water Loss

An issue that still exists in commercial cells today is that of cell dry out.<sup>67</sup> Ni-Zn cells are frequently overcharged to achieve peak cell performance, but this practice slowly

consumes the  $\text{H}_2\text{O}$  of the electrolyte. Since the Ni-Zn cell reaction (Reaction (1-13) on page 15) consumes  $\text{H}_2\text{O}$  during discharge it will eventually dry out before it delivers all of its capacity.<sup>27</sup>

## 1.11 Construction of Typical Ni-Zn and Zn-Air Cells

### 1.11.1 Commercial Non-Rechargeable Zn-Air Coin Cell

The commercial Zn-air button cell currently dominates the hearing aid battery market due to it having the highest volumetric energy density of any cell on the market. A size 675 Duracell Zn-air cell was discharged in the lab and had volumetric and gravimetric energy densities of 1,800 Wh/L and 440 Wh/kg, respectively. A cut-away picture of a Zn-air button cell is shown in Figure 1-6. The cell is made by filling most of the anode cap with highly pure Zn mixed with 30 wt% KOH (6.8 M), leaving enough room for the Zn to expand into as it converts into ZnO during discharge. In contact with the Zn is a microporous separator. Pressed up against the microporous separator is the air electrode itself, which is made of carbon and usually  $\text{MnO}_2$  as the catalyst. The carbon and catalyst mixture is pressed onto a wire mesh or expanded metal layer that acts as the current collector. Pressed against the opposite side of the air electrode from the Zn is one or more layers of microporous and hydrophobic PTFE that is permeable to gases such as  $\text{O}_{2(g)}$  and  $\text{H}_2\text{O}_{(g)}$  but

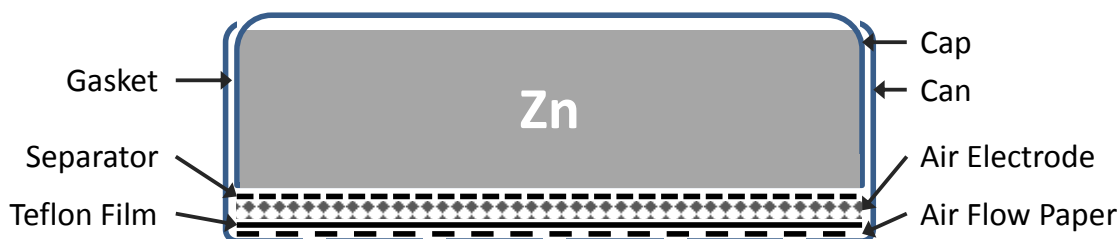


Figure 1-6: Cross section of a Zn-air button cell for a hearing aid. The Teflon film reduces water vapor exchange through the air holes. Note that there is some empty space above the zinc active material where the ZnO can expand into as it forms.

not to liquid water. The last layer in the stack is a gas diffusion membrane that allows O<sub>2</sub> to spread out over the surface of the air electrode once it has passed through the holes in the cell canister. The gasket that seals the cell and prevents electrolyte leakage is usually polyamide and is subjected to patented techniques to ensure electrolyte does not leak.<sup>27</sup>

### 1.11.2 Commercial Rechargeable Ni-Zn Cell

Commercial Ni-Zn cells are currently being produced by brands such as PowerGenix, PKCell, UltraCell and SCPS.<sup>111, 112</sup> Both prismatic and cylindrical designs are available;<sup>67, 111</sup> the cylindrical AA cells have a rated capacity of 2,500 mWh and an average discharge potential of 1.65 V. This makes their rated capacity about 1,500 mAh and their volumetric energy density about 325 Wh/L (a AA cell is about 1.4 cm diameter by 5 cm tall). Figure 1-7 shows two dismantled AA cells from PowerGenix and PKCell to demonstrate their construction and Table 1-2 lists the thicknesses of some of the components. A cylindrical cell is made by winding the stack, consisting of the electrodes and separators, into a cylinder (called a “jelly-roll” by the industry) and then inserting it into a cylindrical tin-plated iron cell casing (determined using EDS).<sup>67</sup> In the PowerGenix cell, the separator was left open at either end of the cylindrical winding (a noted difference from the prismatic design) so that the Zn electrode could be connected to the can through contact.<sup>67</sup> This was different from the PKCell design, which appeared to rely upon a metal sheath pressed up

Table 1-2: Thickness of various components in commercial, rechargeable AA Ni-Zn cells. The Zn current collector is included in the Zn electrode thickness measurement. The “Stack” is the sum of the Ni electrode, 2× non-woven separator, 2× microporous separator and Zn electrode.

<b>Component</b>	<b>PowerGenix AA</b>	<b>PKCell AA</b>
<b>Ni Electrode</b>	0.65 mm	0.82 mm
<b>Non-Woven Separator</b>	0.06 mm	0.08 mm
<b>Microporous Separator</b>	0.06 mm	0.07 mm
<b>Zn Electrode</b>	0.46 mm	0.43 mm
<b>Zn Current Collector</b>	0.10 mm	0.10 mm
<b>Stack (Zn+Ni+2×Sep.)</b>	1.35 mm	1.55 mm

against the cell casing to make electrical contact between the Zn electrode and the negative terminal. The current collector for the Zn electrode was an expanded metal foil that was determined to be Sn-plated Cu using Energy-Dispersive X-ray Spectroscopy (EDS).<sup>113</sup> The Ni electrodes used a fine Ni foam as the current collector, and were connected to the cap (below the pressure relieve valve) by a spot-welded Ni foil tab.<sup>67, 114</sup> To clarify, the pressure relief valve was only intended to open during abuse at 270 kPa in one case<sup>68</sup> and at 2,000 kPa in another,<sup>67</sup> but not under normal cell operation.

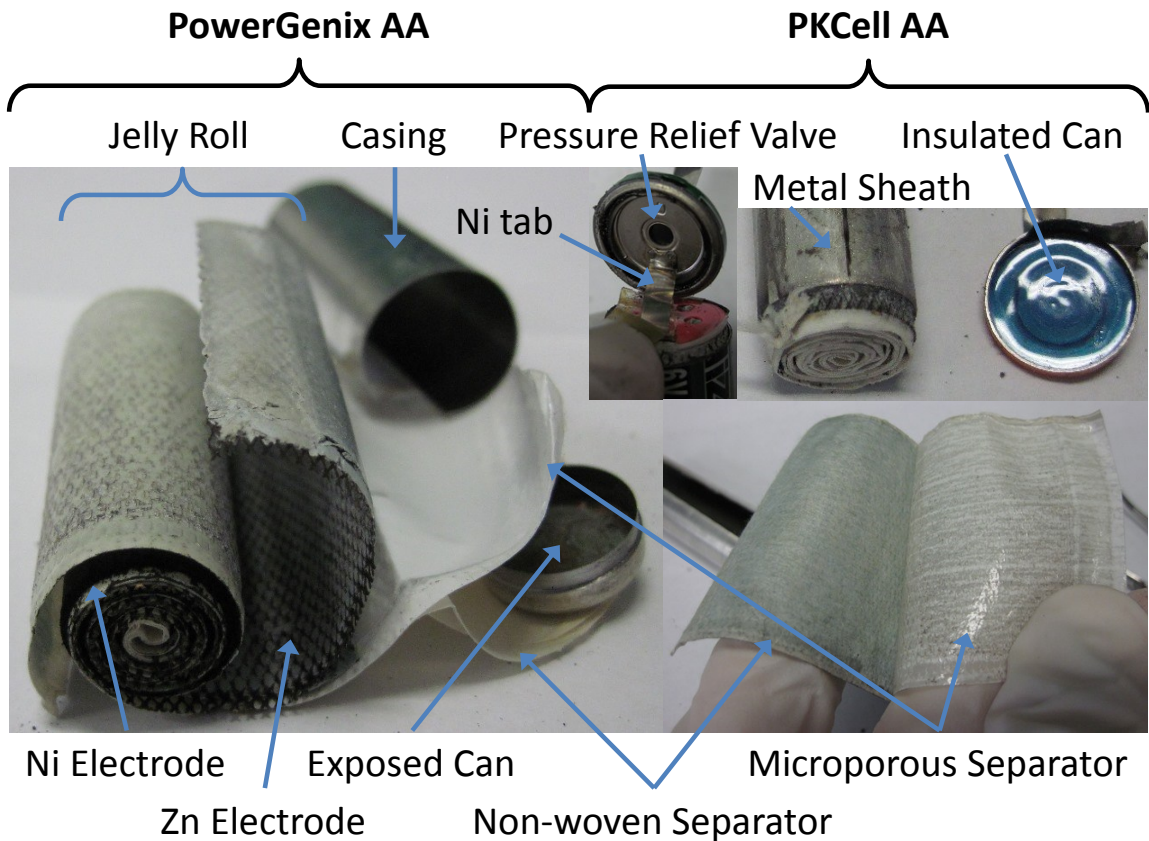


Figure 1-7: Dismantled PowerGenix and PKCell AA rechargeable Ni-Zn cells. The so-called “Jelly Roll” is the wound cylinder comprised of the Zn electrode, Ni electrode, 2× microporous separators and 2 × non-woven separators. The difference between the cells was the method of electrically connecting the Zn electrode to the negative terminal. The PowerGenix cell relied upon the contact of the edges of the tin-plated copper current collector to the tin-plated exposed can. The PKCell relied upon a tin-plated metal sheath that enwrapped the outer layer of the Zn electrode and pressed up against the tin-plated iron cell casing.

The following discussion about separators is paraphrased from Cook and Kritzer, which was a rare find in the literature in that no other author surveyed for this project had mentioned the importance of the separators.<sup>70</sup> The separator in an alkaline system is a key component in the system that influences many cell properties like capacity, cycle life, power output and charge retention. Both microporous and non-woven polyolefin or polyamide materials are important in cells incorporating Zn electrodes. A microporous membrane, like Celgard 3407 or 5550, is placed against the Zn electrode to prevent dendrite penetration of the separators by retarding dendrite growth through its small and tortuous pores. A non-woven material is placed against the positive electrode to act as an electrolyte reservoir, which is necessary for efficient cycling since the electrolyte itself is consumed and produced during cycling. It is worth noting that the fabrication method of the separator (wetlaid, drylaid, spun bound or meltblown) and the post treatment both determine the properties of the separator. Surfactant coating post treatments are the simplest and cheapest option to grant wettability to otherwise hydrophobic polyolefins, but surfactants leach into the electrolyte over time making this treatment unsuitable for long cycle life cells. If the separator loses its wettability, the cell will fail despite perfectly functioning electrodes and electrolyte. Acrylic acid grafting is the post treatment of choice for permanent and excellent separator performance. Wetlaid fabrication, using bi-component and single-component fibers, or meltblown fabrication is the best non-woven to use.<sup>70</sup> In prismatic cell designs separators are usually heat sealed tightly around the electrode, because reducing the free volume inside the separator bag reduces shape change over many cycles.<sup>91</sup>

### *1.11.3 Historical Laboratory Rechargeable Ni-Zn and Zn-Air Cells*

In 2009, a literature review in search of cell designs to gain insight from revealed a variety of designs suited to specific purposes.<sup>76, 86, 87, 90, 115-117</sup> But despite the importance of



measuring the effect of new discoveries on cycle life, only 18 of 84 papers read (on the topic of Zn electrodes) reported capacity vs cycle number data. Of those 18, only 6 reported the actual cycle life (i.e. cycled the cell to failure). Of those 6, two were from Lawrence Berkeley Laboratory and used the same Ni-Zn cell design;<sup>20, 91</sup> similarly, two were from the Paul Scherrer Institut and used the same Zn-air cell design;<sup>18, 118</sup> and the last two used commercial cells, which are prohibitively expensive to make in an academic research lab.<sup>68,</sup>  
<sup>119</sup> The other 12 papers that showed capacity vs cycle number data stopped cycling their cells after about 100 cycles when they felt that their point had been made.<sup>120-131</sup> This prevents any of the technologies being presented by these authors from being compared with each other since the technology that lasted the longest cannot be determined.

Furthermore, the design of the cell itself is usually, and frustratingly, partially responsible for the cycle life,<sup>20, 43, 87</sup> which suggests that the cell design must be taken into account when comparing results from different cell designs. Of course, this is difficult to do and has been avoided in the lithium ion research community by the widespread adoption of one of two standardized cell designs: the Swagelok cell and the coin cell. Having these two cells to choose from saves countless researchers from having to re-invent a cell for every experiment they want to run. Based on the success of choosing a standardized cell design in the lithium ion research community, it seems like it would be beneficial to adopt a standardized cell design in the Zn-air research community.

Ideally, every researcher would have access to commercial cells that they could modify as they pleased during the manufacturing process, but this is untenable because corporations are usually very secretive about their cell fabrication methods and materials, and because the equipment is costly. Instead, researchers must make do with an imitation of a commercial cell. These imitations usually do not reproduce the exact conditions that the electrode would be exposed to in a real cell. For instance, some experimental cells use

more electrolyte than a commercial cell would use (ex: mL vs  $\mu$ L).<sup>20, 86, 91, 115, 132</sup> The cycle life of alkaline rechargeable Zn electrodes is sensitive to the amount of electrolyte in the cell since excess electrolyte contributes to shape change.<sup>43, 87-90</sup> Having excess electrolyte is commonly referred to as having a “flooded” cell and means more electrolyte was used than the amount needed to soak the separators and electrodes, which is all that is typically used in commercial cells to keep cell weight low.<sup>20, 133, 134</sup> Most experimental cells seem to be flooded,<sup>20, 86, 91, 115, 122</sup> but since about the year 2000 many authors have not reported how much electrolyte they used.<sup>121, 123-131, 135</sup>

Many authors also do not mention stack pressure, despite the fact that the majority of papers on alkaline Zn electrodes use Ni(OH)<sub>2</sub> as the counter electrode, even if the purpose of the research was for Zn electrodes to be used in Zn-air systems.<sup>131</sup> Of the 84 papers mentioned at the beginning of this section, only two of them reported or mentioned stack pressure.<sup>20, 91</sup> Although, it is likely that many applied pressure to their electrodes without measuring it since stack pressure is important to the operation of Ni electrodes as discussed in Section 1.10.1 on page 34. As shown by the Ni electrode literature, stack pressure is an important parameter and should thus be reported.

Regrettably, as academic research on Ni-Zn and Zn-air systems shifted groups in the early 2000’s, many authors began omitting their cell designs from their publications. Instead, they began to limit their experimental discussion to the electrodes (and separator, but with no reasoning) and make no mention of stack pressure, electrolyte volumes, electrical connection method (to the electrodes), cell casing design, or whether the cell is sealed in the case of Ni-Zn cells.<sup>121, 123-131, 135</sup> Of the 14 articles (of the 84) that describe their cycle-life testing cell design in more detail, 3-electrode cell designs were the most popular since they allowed both electrodes to be monitored independently.<sup>18, 20, 42, 68, 87, 90, 91, 115, 118-120, 122, 136-138</sup> The 3<sup>rd</sup> electrode was usually Hg/HgO, but occasionally Zn metal was used.<sup>42</sup>

These cells were all greater than 5 cm in width with the earliest cells being generally larger (11 cm × 11 cm)<sup>115</sup> and trending towards smaller cells (5.64 cm diameter)<sup>18, 42</sup> as time went on. After about 2006, Zn electrodes seemed to regularly be 2 cm × 2 cm, albeit without many cell design details mentioned.<sup>124-130</sup> Large cells, and thus electrodes, are not ideal for laboratory use for two main reasons. First, large cells require more material: current collectors, separators, electrolyte and active material, any of which might be expensive or experimental and in short supply. Second, large cells occupy more space in the lab, which is also usually in short supply, especially when multiple cells of each design are required for statistical purposes. This is especially true when the researcher wants to fit as many cells as possible into a testing chamber that controls the temperature and/or humidity level at which the cell is cycled, both of which influence the discharge capacity and cycle life.<sup>30, 121</sup> Of the 18 papers mentioned above that reported cycle data, only three repeated a measurement, even once, to prove or suggest reproducibility.<sup>118, 119, 123</sup> Reproducibility is a vital parameter that should be reported more often in the literature.

Typical cell casings are acrylic since it is transparent and resistant to alkaline electrolyte, but any alkaline resistant plastic is sufficient. If heat dissipation is a concern, metal cell casings likely have higher heat dissipation rates since metal conducts heat better than plastics, but only the researchers using commercial cells have bothered to use metal cell casings.<sup>67, 119, 138</sup> Borosilicate glasses (Pyrex) have been used in some fundamental electrochemical experiments<sup>83</sup> on Zn electrodes, but since alkaline solutions are known to etch glass, caution should be exercised with experiments that might be sensitive to  $\text{SiO}_2(\text{OH})_2^{2-}$ .<sup>139</sup>

#### 1.11.4 Historical Laboratory Rechargeable Li-ion Coin Cell

From their introduction to the market in 1991 by Sony, Li-ion cells have grown from an R&D interest to sales in the billions of units per year.<sup>6</sup> One factor that contributed to widespread R&D on Li-ion technology was the laboratory coin cell. Lab-scale coin cells enabled researchers to more easily reproduce others' results and compare data sets since everyone was using the same generic hardware. No hardware that fulfils this role currently exists for aqueous cell designs in R&D labs.

Figure 1-8 shows the lab-scale Li-ion coin cell. The casing top (a.k.a. the cap), casing bottom (a.k.a. the can), spring and spacer are all made of stainless steel. When purchased in lots of 100,000 parts, the caps and cans cost \$0.20 each, the springs cost about \$1.00 each and the spacers cost \$0.05 each.<sup>140</sup> After use, the caps and cans are disposed of, but the springs and spacers are recovered and infinitely reusable. The gasket is polyamide and is

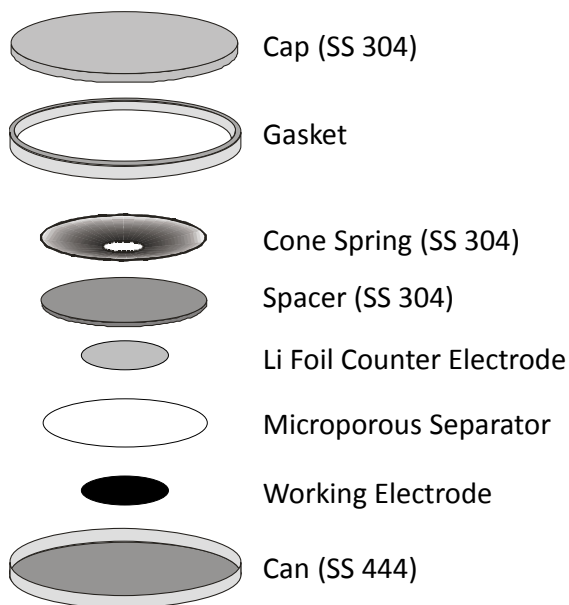


Figure 1-8: A Li-ion coin cell designed for laboratory R&D. The counter/reference electrode is usually pure Li foil but it can also be a negative electrode material spread, like carbon. The separator is usually microporous. The coin cell is constructed and crimped (sealed) in a glove box to avoid H<sub>2</sub>O and O<sub>2</sub> exposure.

squished between the cap and can during crimping (sealing). The counter/reference electrode is usually pure Li foil, but it can also be a negative electrode material spread, like carbon, on copper foil. The separator is a hydrophobic, microporous polyolefin material that, when combined with stack pressure, prevents Li dendrites from short circuiting the cell. The “working electrode” in Figure 1-8 is the positive electrode, which is a mixture comprised of positive electrode active material (usually a powder), conductive additive (carbon) and binder spread onto aluminum foil.

Coin cells have several benefits: Primarily, they are small. This means they use small amounts of active materials, current collector, separator and electrolyte. Small cells also occupy less space in the lab and allow multiple cells to be fit in reasonably sized boxes that allow other factors like temperature and humidity to be controlled.<sup>141</sup> Finally, the small electrode size and metal casing minimizes the heat buildup in the cell, increasing confidence that the electrodes are maintained at a constant temperature throughout the experiment. Another general benefit is the close reproduction of the environment experienced by a Li-ion electrode in a commercial cell. This means that with regard to a commercial Li-ion cell, the coin cell electrodes can be made with the same thickness, the stack pressure can be tuned to the same value and a minimal amount of electrolyte can be used.<sup>6</sup>

## Chapter 2: Laboratory Nickel-Zinc (Ni-Zn) Coin Cells

### 2.1 Motivation

When Li-ion research world-wide slows down, many Li-ion researchers will begin to look at alternative technologies, like Zn-air, to focus their attention on and may feel somewhat lost in the beginning as they struggle to learn the basics of this “new-to-them” system. This phenomenon is actually somewhat visible in the literature, where excellent papers on Ni-Zn and Zn-air from groups located in North America<sup>15, 20, 43, 91, 142</sup> and Europe<sup>18, 42, 94, 118, 143</sup> existed up until about 2000, at which point those groups changed topics. Subsequently, groups in Asia began Zn-air research in the early 2000's and produced several arguably low quality papers as they learned the system. For example, one group repeatedly examined a cyclic voltammogram (CV) of the Cu current collector, while thinking it was a CV of their Zn active material.<sup>144-146</sup> Other groups used Ni as their current collector for the Zn electrode, which is a poor choice as will be demonstrated in Chapter 4.<sup>124, 126, 127, 131</sup> When this project was started, the Dahn lab, a primarily Li-ion lab, had no experience with alkaline, aqueous systems and thus no basis to know which topics were important to search for in the literature or when to stop searching. In this situation, learning and failing experimentally, due to so-called common mistakes that seasoned aqueous electrochemists would not make, occurred in repetition as one might expect. This chapter is essentially a summary of those failures and lessons-learned so that other researchers will not have to repeat this arduous learning process when they begin work on alkaline, aqueous cells. As such, many of the topics covered in this chapter might not seem novel to readers who are versed in aqueous electrochemistry, but that is to be expected because this chapter was not written for them. Similarly, a reader might find topics presented here unsurprising because the topic was covered in Chapter 1. That chapter was intended to be an overview that

would stand alone, and so the reader should keep in mind that not all of the knowledge presented in Chapter 1 was known at the time that the research presented in Chapter 2 was performed.

Coin cells have been used for research on Li and Li-ion batteries for over 30 years and, along with the Swagelok cell, have become a recognized standard cell design. As such, when Li-ion researchers decide to try researching aqueous cell chemistries, like Zn-air, they will likely be tempted to use their existing coin cell infrastructure. However, aqueous, alkaline researchers never use coin cells for rechargeable Zn-based battery research, even though excellent aqueous, alkaline commercial cells like Ni-Cd coin cells, Ni-MH coin cells and Ni-Zn cylindrical cells exist. The reason why researchers do not use coin cells is unclear as it is not addressed in the literature. As such, the research of this chapter was undertaken to either create a potentially new standard cell design for aqueous, alkaline systems (i.e. a coin cell) to enhance the research efforts of the existing aqueous research community, or to explain why coin cells might be unsuitable as a test vehicle for aqueous cells for the benefit of new researchers entering the field who otherwise might waste time and money learning these same lessons.

Most of this chapter was published as a peer reviewed article: P. Bonnicksen and J. R. Dahn, *A Simple Coin Cell Design for Testing Rechargeable Zinc-Air or Alkaline Battery Systems*, *Journal of the Electrochemical Society*, **159**, 7, A981-A989 (2012).<sup>147</sup> Although, in this chapter most of the text has been rewritten and several figures are new or have been modified. The appreciation of such a simplistic “how to” paper is perhaps best demonstrated by the positive feedback from the peer reviewers, as follows. Reviewer 1: “The manuscript... is of good scientific quality... [and] of great significance”. Reviewer 2: “...It is thus refreshing to see a study on this underdeveloped system. This study focused on some fundamental issues involved in rechargeability and cycle life with a simple

experimental model. It has a clear thesis, an effective experimental approach and meaningful results.” Reviewer 3: “This is an excellent manuscript that provides a clear and valuable description of how to design coin cells for use in the development of rechargeable alkaline zinc cells... This has great significance, not only to developers of rechargeable alkaline zinc batteries, but also researchers who use coin cells to test and characterize any type of battery.”

## **2.2 Experimental Methods**

### *2.2.1 Electrode Manufacture*

Coin cell electrodes were formed by spreading a slurry of an active material, binder, liquid and additives onto a current collector (metal foil) using a notch bar (DPM Solutions, Hebbville, NS, Canada<sup>148</sup>) and then drying the spread. Optionally, the spreads can then be calendared (roll-pressed) before punching disk-shaped electrodes from them using a precision punch (DPM Solutions). All percentages listed here are by weight and further details, including pictures of various pieces of equipment, can be found in Marks *et al.*<sup>149</sup>

The solids in the Ni electrode consisted of 81 % Ni(OH)<sub>2</sub> active material (Shepherd Chemical Co., OH, USA), 6 % poly(vinylidene fluoride) (PVDF) binder (Kynar 301F), 8 % Super C45 carbon (TIMCAL) and 5 % CoO (Alfa Aesar). Both the carbon black and CoO are conductive additives to improve electrode behaviour. About 2 g of the solids and about 4 g of N-methylpyrrolidone (NMP, the liquid and binder’s solvent) were added to a 30 mL Nalgene bottle with 2 ZrO<sub>2</sub> pellets (9 mm diameter) and subsequently mixed in a planetary mixer (Mazerustar) for 10 min. Note that simply shaking the bottle or vial by hand in place of using a planetary mixer might be sufficient. The resulting slurry was spread on 25 µm thick Ni foil (McMaster Carr) using a 152 µm notch bar and dried in air at 120 °C for 2 hours before calendaring the spread at 100 MPa (actual pressure on spread<sup>149</sup>) with unheated



rollers. 1.27 cm diameter electrodes were then punched from the spread with a sacrificial, single layer of 22  $\mu\text{m}$  thick Al foil on top of the spread to prevent burrs on the disk edges.

The Zn electrode material (about 3 g) consisted of 93.5 % ZnO, 1.7 % carboxymethyl cellulose sodium salt (Aldrich, Typical MW 90,000), 2.8 % PTFE (Dupont, as a 60.4 % PTFE dispersion in water) and 2 % PbO (Aldrich). These were added to a stainless steel ball mill vial (DPM Solutions) with four 12 mm diameter hardened stainless steel balls and enough distilled water (about 6 g) to yield the desired final viscosity, which is thin enough to be spread uniformly but viscous enough to maintain its shape after spreading. The vial was shaken in a shaker for 20 min (at about 2 cycles/s) and then spread on 10  $\mu\text{m}$  thick Cu foil with a 216  $\mu\text{m}$  notch bar before the slurry had a chance to solidify. The spread was dried in air at 120  $^{\circ}\text{C}$  for 20 min and then left at room temperature overnight to finish drying. The shaking time and drying time are important in getting the material to stick to the Cu foil. The dried spread was calendared with unheated rollers under about 100 MPa and then 1.27 cm diameter electrodes were punched from it using a sacrificial layer of weigh paper to prevent burrs on the disk edges. The electrode material mass in each electrode was determined by weighing the electrode and subtracting the mass of the foil disk, as will be described in Section 2.3.1.

### 2.2.2 ZnO Purity

Impurities within the Zn active material can act as local cathodic sites for  $\text{H}_2$  evolution and increase the Zn corrosion rate.<sup>82</sup> Table 2-1 shows the purity of the ZnO materials that were used in this thesis and compares them to typical battery-grade Zn used in primary alkaline cells.<sup>82</sup> The reagent grade ZnO acquired from Anachemia (in 1988) was used for most of the research in this thesis (including this chapter), while the 99.999% pure Alfa Aesar ZnO was used in the 3-electrode foil experiments of Chapter 4. Both powders

appear to contain acceptable levels of impurities. According to Kita, the exchange current densities (equilibrium rate of reaction) of H<sub>2</sub> evolution in acid of Co, Fe and Ni are the largest of the elements in Table 2-1 and thus the quantity of those elements should be kept as low as possible.<sup>14, 65</sup>

Table 2-1: Elemental analysis of the two ZnO powders used in this thesis and the typical concentrations found in primary alkaline battery Zn active material. All concentrations are in ppm by mass. Note that the ICP-OES machine used to analyze the ZnO powders was not capable of measuring quantities below certain limits as noted and that the error of these measurements is about 5%.

<b>Element</b>	<b>Anachemia ZnO</b>	<b>Alfa Aesar ZnO</b>	<b>Battery Grade Zn</b>
<b>Ag</b>	0.6	< 0.1	1.56
<b>Al</b>	< 0.5	< 0.5	0.14
<b>As</b>	< 5	< 5	0.01
<b>Ca</b>	0.7	0.9	0.20
<b>Cd</b>	2	4	4.20
<b>Co</b>	< 1	< 1	0.05
<b>Cr</b>	< 0.5	< 0.5	0.10
<b>Cu</b>	< 0.5	< 0.5	1.50
<b>Fe</b>	< 0.5	< 0.5	4.00
<b>Mg</b>	0.1	< 0.1	0.03
<b>Mo</b>	< 1	< 1	0.04
<b>Ni</b>	< 1	< 1	0.20
<b>Sb</b>	< 25	< 25	0.09
<b>Sn</b>	< 25	< 25	0.10
<b>V</b>	< 1	< 1	0.001

### 2.2.3 Ni-Zn Coin Cell Design

Figure 2-1 shows the components and order of their assembly into a 2325 (23 mm diameter by 2.5 mm height) coin-type cell. The cap, can (304 and 444 stainless steel (SS) grades, respectively, from Kaga Steel, Japan), disc spring (17-4 SS, 18 mm O.D., 6.2 mm hole, 0.4 mm thickness, 0.6 mm dish, from Key Bellevilles, USA) and spacer (304 SS, 18 mm diameter, 0.81 mm thick, from Boker's, USA) were stainless steel parts that had been completely electroplated with Ni in the case of the cap, spring and spacer, or tin (Sn) in the

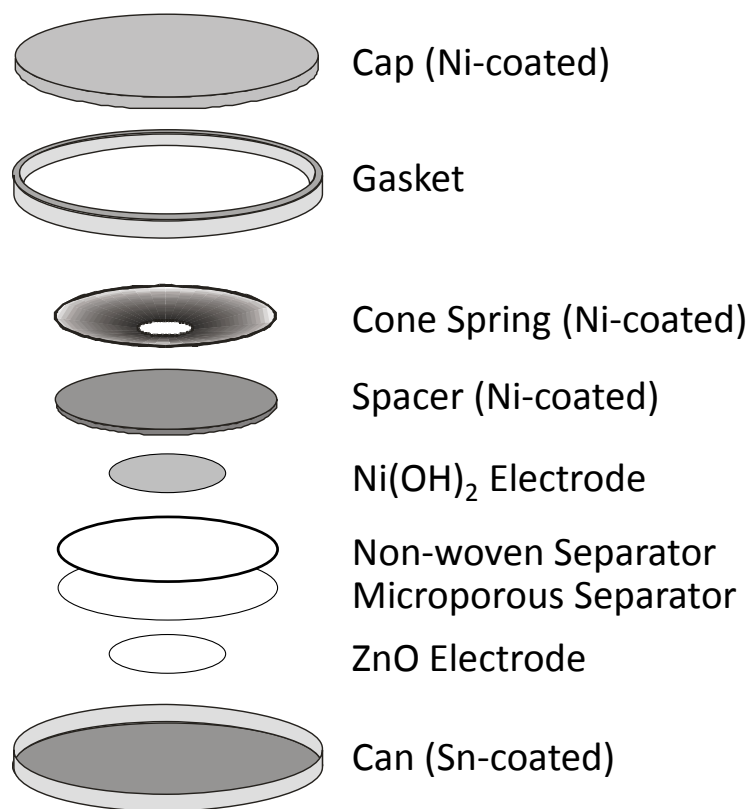


Figure 2-1: Coin cell components and their order of assembly. Coatings were electroplated. The electrodes consist of a thin layer of “electrode material” on a foil current collector (CC).

case of the can (Toronto Aerospace Finishing, Canada). The caps had a 1 mm diameter hole drilled through them that was covered with a piece of scotch tape to form a primitive pressure release valve. The spacers had a slight concavity due to the punching process used to make them and both the spring and spacer were oriented concave-side up in this figure. The concavity in the spacer is not crucial. The non-woven separator was a wet-laid, acrylic acid grafted polyolefin called 700/30K from Freudenberg. The microporous separator was a tri-layer polyolefin called Celgard 3407 from Celgard. The electrolyte was a low  $\text{Zn(OH)}_4^{2-}$  solubility electrolyte optimized by Cairns’ group<sup>20</sup> that consisted of 4 M KOH (Alfa Aesar, 85% min.), 2 M KF (Sigma-Aldrich) and 2 M  $\text{K}_2\text{CO}_3$  (Aldrich) in nanopure water (> 18 M $\Omega$ ) and then saturated with ZnO. About  $29 \mu\text{L} \pm 4 \mu\text{L}$  of electrolyte were dropped onto the

separators during cell assembly. The cells were constructed in open air and sealed with a cell crimper (DPM Solutions).

The above procedure describes the typical cell design, referred to hereafter as the “standard” coin cell design, to which other cell hardware options will be compared in this chapter. Other cell parts tested include: stainless steel parts (same sources as above), Sn electroplated caps, springs and spacers (Toronto Aerospace Finishing), Ti spacers (Boker’s, USA), thin, flat Ni spacers (NRC, Canada), brass cans (DPM Solutions), Cu sputter-coated stainless steel cans (coated in-house), Ni electroplated cans (Toronto Aerospace Finishing) and 25  $\mu\text{m}$  thick Sn foil current collectors (99.9% Alfa Aesar).

Commercial AA Ni-Zn cells by PowerGenix and PKCell were acquired from Amazon.com and eBay.ca, respectively. When asked, PowerGenix could not determine how old the cells were.

#### *2.2.4 Cell Cycling Procedure*

Cells were charged and discharged using a Maccor series 4000 battery tester with a time-limited charge and a lower voltage cut off of 1.4 V during discharge. The first 5 cycles were considered ‘formation’ cycles to activate the  $\text{Ni(OH)}_2$  active material in line with popular practices.<sup>142</sup> These cycles were performed at a C/1 rate and charged to 100% of their theoretical capacity ( $Q_T$ ). The “C” in “C/1” means  $Q_T$  and the denominator means “in 1 hour”; hence, a cell cycled at a “C/1 rate” should reach full charge in 1 hour, and then fully discharge in the next 1 hour. Cycles 6 – 20 were cycled at a C/2 rate and charged to 120%  $Q_T$  to finish activating the material. Cycles 21 – 50 were also cycled at C/2 but only charged to 105%  $Q_T$  since, according to the literature, oxygen evolution consumes about 2% of the total charge delivered to a Ni electrode depending on the charge rate.<sup>44</sup> Cells were cycled in

a temperature controlled box kept at  $20.0 \pm 0.5$  °C in a cap-side up orientation unless stated otherwise.

#### *2.2.5 Cyclic Voltammogram Measurement Procedure*

Cyclic voltammograms of stainless steel (SS) and Ni were measured in 3.2 M KOH using a Bio-logic VMP3 potentiostat with a 20 mV/s sweep rate on 1 cm × 2 cm SS or Ni foils (McMaster Carr) that were dipped 1 cm deep into the electrolyte. The reference electrode was a Hg/HgO electrode from Koslow Scientific with a 4.5 M KOH filling solution. The counter electrode was Ni foil with a large surface area ( $\sim 10$  cm<sup>2</sup>).

#### *2.2.6 Cell Thickness Measurement Procedure*

The cell thickness (or ballooning) measurement was done at room temperature with a standard cell using the Bio-logic VMP3 and a Durham Instruments DC-EC 500 AccuSens LVDT to measure the cell thickness. The cell was subjected to formation cycling for 10 cycles and then was cycled at a C/2 rate, charged to 120%  $Q_T$  and discharged to 1.4 V.

#### *2.2.7 Stack Pressure Measurement Procedure*

Stack pressure measurements were performed using Fujifilm Prescale ‘Super Low’ pressure film (Sensor Products, USA). Disks of the pressure film were punched using the same precision punch used to punch the electrodes, thereby making them the same area. During cell assembly, the pressure film was placed where the Ni electrode would be placed in an actual cell, followed by the two separators and finally the can. No Zn electrode, Ni electrode or electrolyte was used. The cell was crimped (sealed) and then dismantled carefully to retrieve the pressure film without applying any more pressure to it. The colour of the film was compared to the colour shade chart, provided with the pressure film, to give a rough pressure measurement. Since the pressure film was about 70  $\mu$ m thicker than the

combination of the Zn and Ni electrodes, the measured pressure was higher than what actual electrodes would experience.

## 2.3 Ni-Zn Coin Cell Results and Discussion

### 2.3.1 Electrode Capacity Determination

An electrode consists of a foil disk with a homogeneous, uniform layer of electrode material stuck to it. The mass of electrode material on an electrode can be calculated by subtracting the mass of the foil disk from the mass of the whole electrode; however, doing this assumes that the mass of every punched foil disk is the same. The theoretical capacity ( $Q_T$ ) of the electrode can then be calculated as follows,

$$Q_T = \frac{(m_{\text{Electrode}} - m_{\text{Foil}}) \cdot \text{wt}\%_{\text{AM}}}{MM_{\text{AM}}} \cdot \frac{nF}{3.6 \frac{\text{C}}{\text{mAh}}}, \quad (2-1)$$

where  $m$  = mass, AM = active material ( $\text{Ni}(\text{OH})_2$  or  $\text{ZnO}$  in this case), MM = molar mass,  $\text{wt}\%_{\text{AM}}$  = weight percent of the active material in the electrode material (81% or 93.5% in the case of Ni and Zn electrodes in this chapter),  $n$  = the number of electrons transferred in the relevant reaction (Reactions (1-2) and (1-11) in this case) and  $F$  = Faraday's constant.

Table 2-2 shows the error in  $Q_T$  associated with the variation in foil disk mass. Since the discharge capacities in this section were limited by the Ni electrode, the error in utilization that stems from the mass error is between 2.0% and 2.5% depending on the capacity of a given Ni electrode.  $Q_T$  for Ni electrodes in this work ranged from 1.2 to 1.5

Table 2-2: Error in  $Q_T$  associated with assuming all foil disks have equal mass. This error was calculated with 95% confidence and using either 234 mAh/g for Ni electrodes or 616 mAh/g for Zn electrodes.

Electrode	Foil Material	Sample Size	Mean Mass (mg)	Standard Dev. (mg)	Capacity Error (mAh)
Ni	Ni	9	26.71	0.064	0.030
Zn	Cu	52	11.13	0.038	0.047
Zn	Sn	8	24.03	0.071	0.088

mAh, which meant C/2 currents were from 600 to 750  $\mu\text{A}$ . In this chapter, cells had a Zn:Ni capacity ratio of 3.5:1 to 4.5:1, since the formation of the Ni electrode and the behaviour of the cell components was the focus of study.

### 2.3.2 Formation Cycling of Ni Electrodes

A unique feature of  $\text{Ni}(\text{OH})_2$  electrodes is their requirement of “formation” or “activation” cycles before the active material is fully utilized. Theoretically, these cycles *form* a conductive network within the initially non-conductive active material particles, allowing all of the active material to participate electrochemically via Reaction (1-11) (pg. 12).<sup>52, 60, 108</sup> For cells in this study, formation cycles were considered to be the first 5 cycles; however, it is evident from the increasing discharge capacities in the figures below that formation continues to occur incrementally if the Ni electrode is overcharged in subsequent cycles.

Figure 2-2 shows the formation cycles of a standard cell and a cell that is standard except for a Sn foil Zn electrode current collector (CC) instead of Cu foil. As will be seen later, the Sn foil CC promotes a longer cycle life than a Cu foil CC. Figure 2-2 also shows that Sn current collectors have a lower overpotential for Zn plating than Cu, which results in a

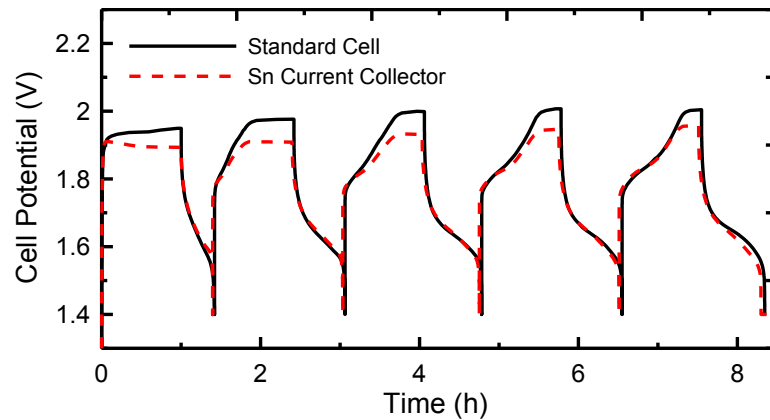


Figure 2-2: Formation cycles of Ni-Zn coin cells. These cells were cycled at a  $Q_T/1$  h rate, charged to 100%  $Q_T$  and discharged to 1.4 V. The flat plateaus at the top of charge are a combination of  $\text{O}_2$  evolution and “formation” reactions in the Ni electrode.

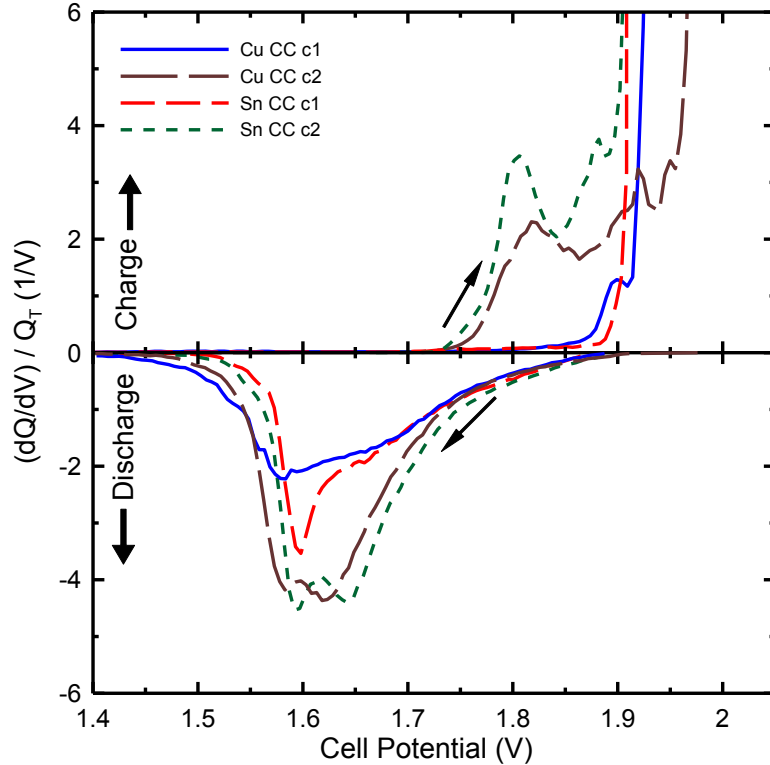


Figure 2-3: Differential capacity plots for the first 2 cycles of the two cells shown in Figure 2-2. For example, “Sn CC c2” means the 2<sup>nd</sup> cycle of a cell with standard components except tin foil has been used as the current collector instead of copper. The y-axis has been scaled to  $Q_T$  to allow peak intensity comparisons between the two cells.

lower charge and  $O_2$  evolution plateau near the end of charge.

Figure 2-3 and Figure 2-4 show differential capacity ( $dQ/dV$ ) versus cell voltage for selected cycles of the cells described in Figure 2-2, and depict a clearer picture of the processes occurring during the formation cycles. Note that the curves in Figure 2-3 and Figure 2-4 most likely arise solely from the Ni electrode since plating Zn requires no formation cycling and has a relatively flat potential profile during charge as will be shown later in Section 3.1.2 (pg. 94).<sup>15</sup> These Zn electrodes also had a capacity  $> 5\times$  that of the Ni electrode, ensuring that no change in the Zn electrode potential occurred as it would have if all the available Zn had been plated.

During the long flat plateau in the first cycle in Figure 2-2, which corresponds to the spike around 1.9 V in Figure 2-3, many reactions occur in the nickel electrode including



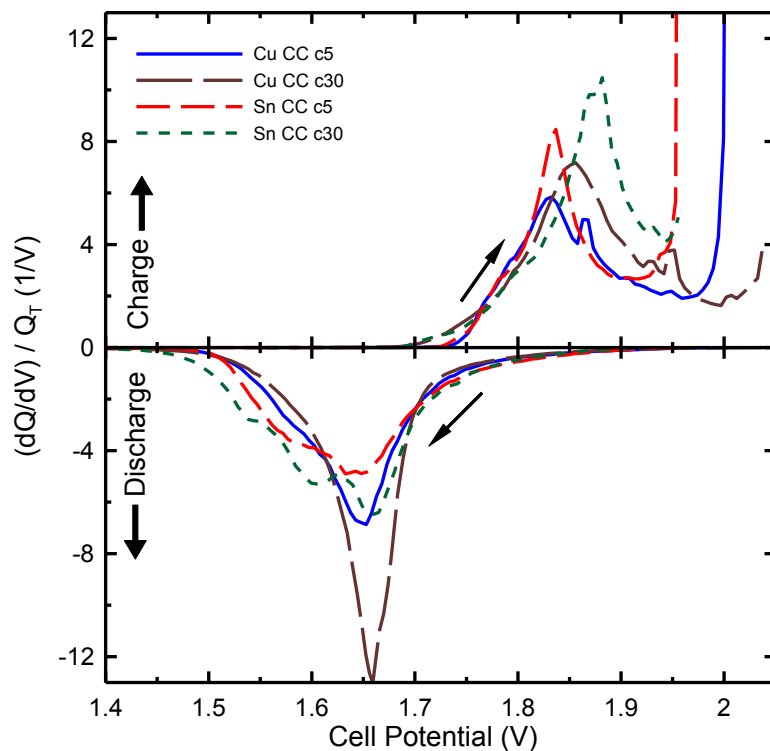


Figure 2-4: Differential capacity plots for the 5<sup>th</sup> and 30<sup>th</sup> cycle of the two cells shown in Figure 2-2. For example, “Sn CC c5” means the 5<sup>th</sup> cycle of a cell with standard components except tin foil has been used as the current collector instead of Cu. The y-axis has been scaled to  $Q_T$  to allow peak intensity comparisons between the two cells.

conversion of much of the active material to  $\gamma$ -NiOOH, the formation of a CoOOH conductive layer on the active material, the formation of NiOOH layers on the Ni cell parts, and  $O_2$  evolution. Tessier *et al.* describe in detail the processes that occur during the formation cycles and the later cycles of the  $Ni(OH)_2$  electrode, and interested readers are directed there.<sup>52</sup> Essentially, as Tessier *et al.* describe, the first charge converts much of the  $\beta$ - $Ni(OH)_2$  to  $\gamma$ -NiOOH, with no  $\beta$ -NiOOH being formed. This  $\gamma$ -NiOOH is discharged to poorly crystallized  $\beta$ - $Ni(OH)_2$  during the first discharge half-cycle (negative peak at about 1.6 V in Figure 2-3), but not all of it; some  $\gamma$ -NiOOH is electrically marooned before it can be discharged. The poorly crystallized  $\beta$ - $Ni(OH)_2$  created in cycle 1 is then available to be charged into a mixture of  $\beta$  and  $\gamma$ -NiOOH during the second cycle. In Figure 2-3 and Figure 2-4 the positive peaks close to 1.8 V are the  $\beta$ - $Ni(OH)_2$  to  $\beta$ -NiOOH conversion, while the negative peaks close to 1.65 V are  $\beta$ -NiOOH back to  $\beta$ - $Ni(OH)_2$ . As cycling progresses, the

amount of  $\gamma$ -NiOOH in the active material shrinks while the amount of  $\beta$ -NiOOH grows until the  $\beta$  form comprises most of the material, as made evident by the growth of the negative peak close to 1.65 V in Figure 2-4.

During cycle 1, irreversible reactions also occurred since only about 40% of the charge imparted to the electrode was retrieved during discharge. One such reaction was  $O_2$  evolution (Reaction (1-17) on page 19); however, without measuring the amount of  $O_2$  produced it is difficult to determine how much charge went to evolving  $O_2$  instead of forming  $\gamma$ -NiOOH.<sup>50,51</sup> A few other irreversible reactions also take place during the first charge, including CoOOH formation, which is widely regarded to be the reaction that forms the conductive network on the surface of the  $Ni(OH)_2$  particles.<sup>48,150</sup> It is implied in the literature that CoOOH does not discharge back to  $Co(OH)_2$  during regular cell operation.<sup>48,150</sup> Also,  $Ni(OH)_2$  layers must thicken on the Ni cell components, thereby consuming charge in going from  $Ni^{0+}$  to at least  $Ni^{2+}$ .<sup>78</sup> Although this thin surface layer (6 – 8 Å)<sup>78</sup> on the cell components cycled between  $Ni(OH)_2$  and NiOOH, the capacity provided by the cell components is negligibly small compared to that of the  $Ni(OH)_2$  within the electrode, as determined separately by cycling blank cells (not shown).

Figure 2-4 shows the cell behaviour at the end of the initial 5 formation cycles and during cycle 30, after formation was completed. Cycle 30 represents an ideal cycle where the Ni active material is fully activated and negligible capacity loss has occurred. By cycle 30, the average charge potential was 1.87 V for cells with either Cu or Sn current collectors (CC) and the average discharge potential was 1.64 V for a Cu CC and 1.63 V for a Sn CC cell.

Overall, plots of the potential curves of Ni electrodes during formation cycling are difficult to find in the literature, and so it was demonstrative to show them here. Since the  $dQ/dV$  plots are for the entire cell, instead of just the Ni electrode, cells with both Cu and Sn current collectors were included to show the relatively minor effect of the negative

electrode (Zn) on the signal. Recall that the intended purpose of the coin cell is to measure the discharge capacity of the Zn electrode for hundreds of cycles, which requires a counter electrode that outlasts the Zn electrode during each of those discharge half-cycles. Clearly, Figure 2-2 demonstrates that  $\text{Ni}(\text{OH})_2$  cannot fulfil that role during the formation cycles. This reduces its attractiveness as a potential counter electrode to Zn since any discharge half-cycles that are ended prematurely by the Ni electrode build up an undischarged reservoir of Zn on the Zn electrode. Once formed, the Ni electrode can be transplanted into a new cell with a fresh Zn electrode, but as demonstrated in Section 3.1.4 (pg. 97) the Ni electrode still finishes discharging first. Regardless, the Ni electrode is useful for demonstrating the effects of several other aspects of the coin cell design that affect cycle life.

### 2.3.3 *Reproducibility of the Coin Cells*

Throughout the next several sections, at least three copies of each coin cell design were tested. The reproducibility of the cycling behaviour generally increased with cell performance: the better a particular design, the more reproducible it was. With some designs, cell performance was erratic; in that one cell might behave well, while the rest would fail catastrophically. As such, it was deemed uninformative to show every data set due to space limitations, or to average the utilization ( $Q_{\text{Discharge}}$ ) vs cycle number data since the error bars would be ungainly large for the erratic data sets. Instead, the best cell data from each design was displayed in the figures in the following sections, except for the “standard” cell design described in Section 2.2.3 (pg. 49), which acted as a point of comparison throughout all the figures and was thus displayed with error bars representing one standard deviation. If the utilization ( $Q_{\text{Discharge}}/Q_{\text{Theory,Ni}}$ ) of a particular design was less than the standard cell design, then it was suboptimal and should be avoided in future research efforts.

In Figure 2-5, panel A shows the potential curves of the most successful cell design used in this chapter as an example of the spread in the potential curves over the first 50 cycles when an exemplary cell design is used. Panel B demonstrates potential curves from a cell with a suboptimal cell design, which grew dissimilar to one another sooner in the cycle life of the cell. Figure 2-6, panel A shows the utilization (i.e. normalized discharge capacity) vs cycle of all 3 cells of the Less Stack Pressure design shown in Figure 2-5B. Clearly, cell 2 yielded discharge capacities that were much lower than cells 1 and 3. Figure 2-6B shows the average utilization of the two designs shown in Figure 2-5 along with the “standard” Cu CC, Sn Can cell design. These data sets are represented by lines with error bars representing one standard deviation.<sup>151</sup> Since the discharge capacities of the cells using the

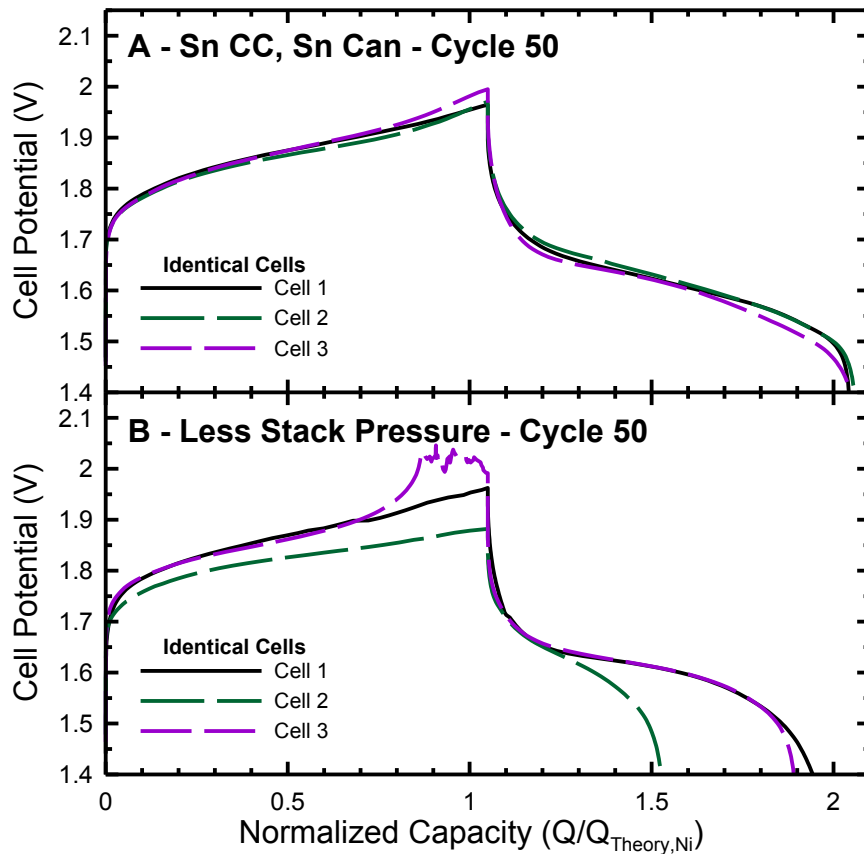


Figure 2-5: Demonstration of reproducibility in coin cells, part 1. The Sn CC, Sn Can coin cell design was the most successful. The Less Stack Pressure design demonstrates the erratic cell behaviour that results from poor cell designs.

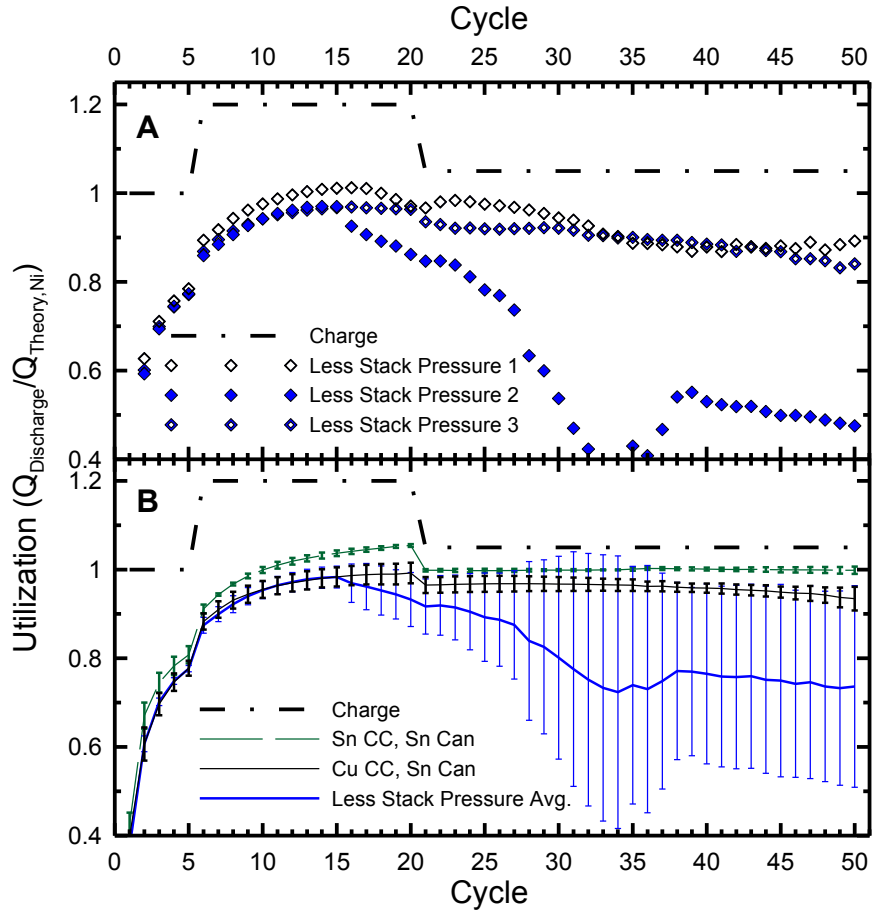


Figure 2-6: Demonstration of reproducibility in coin cells, part 2. The Sn CC, Sn Can coin cell design was the most successful. The Cu CC, Sn Can was the “standard” cell design. The Less Stack Pressure design demonstrates the erratic cell behaviour that can result from a poor cell design. For this design, the thick, solid, blue line in panel D is the average of the three diamond data sets in panel C, but the error bars include unrealistically high Utilization values due to data set 2 from panel C, which is much lower than the other two. All error bars represent one standard deviation.

Sn CC, Sn Can and Cu CC, Sn Can designs are clustered close together up to cycle 50, averaging the discharge capacities and reporting one standard deviation error bars made sense.<sup>151</sup> In this case, the Sn CC, Sn Can design was statistically superior to the Cu CC, Sn Can design from cycle 7 onward since the error bars did not overlap beyond that cycle. However, the error bars of the average data from the Less Stack Pressure design also overlapped with the Cu CC, Sn Can design even though the discharge capacities of cells 1 to 3 (see panel A) were clearly inferior to the Cu CC, Sn Can design. This occurred because the low discharge capacity of the Less Stack Pressure cell 2 (solid blue diamonds in panel C) artificially inflated the standard deviation of the set of three cells. As such, it did not make sense to report error bars on all data sets since only three or four cells of each design were tested and the spread of the data could lead to exaggerated error bars.

Another means of statistically measuring the cycle life is to average the cycle numbers at which the cells of a particular design deviated from optimal behaviour or descended (in discharge capacity) below some chosen value. A simplification of that method was used in this chapter where the best cell of a particular hardware-set was reported and compared to the average of the “standard” cell design. If the best cell of a particular design could not perform as well for as long as the “standard” cell, within error, then it was an inferior design. In panel A of Figure 2-6, the best Less Stack Pressure cell was Cell 1 (the fully hollow diamonds), which did not perform within error of the standard design, in panel B, beyond cycle 31, and so the Less Stack Pressure design was considered to be inferior.

#### 2.3.4 Effect of Stainless Steel Coin Cell Parts on Ni-Zn Cell Performance

Academic Ni-Zn and Zn-air authors that reveal their cell designs do not use metal cell casings that are at the potential of the electrodes, but most Li-ion laboratory cells do. The reasons for this are not immediately apparent since commercial, rechargeable Ni-Zn cells have metal cell casings and new researchers will want to understand how to adapt their metal casings for alkaline cell research. The coin cell springs, spacers and caps are made from stainless steel 304 (SS 304), while the coin cell cans were made of SS 444 and so it was prudent to test the behaviour of cells with SS components and compare them to coin cells using the Sn, Cu and Ni metal coatings that are found in commercial cells.

Table 2-3 defines the composition of a few SS grades. Figure 2-7A shows the cell

Table 2-3: The grades and composition of various types of stainless steel.<sup>152</sup> The “%” refer to weight percent. SAE = Society of Automotive Engineers and UNS = Unified Numbering System, and are both designation standards. The balance of percent in all cases is iron (Fe).

SAE	UNS	% Cr	% Ni	% C	% Mn	% Si	% P	% S	% N	% Mo
304	S30400	18 – 20	8 – 10.50	0.08	2	0.75	0.045	0.03	0.1	-
316	S31600	16 – 18	10 – 14	0.08	2	0.75	0.045	0.03	0.1	2 – 3
444	S44400	17.5 - 19.5	1	0.025	1	1	0.04	0.03	0.035	1.75 - 2.50

potential versus time during cycle 6 for Ni-Zn coin cells using various hardware sets, while

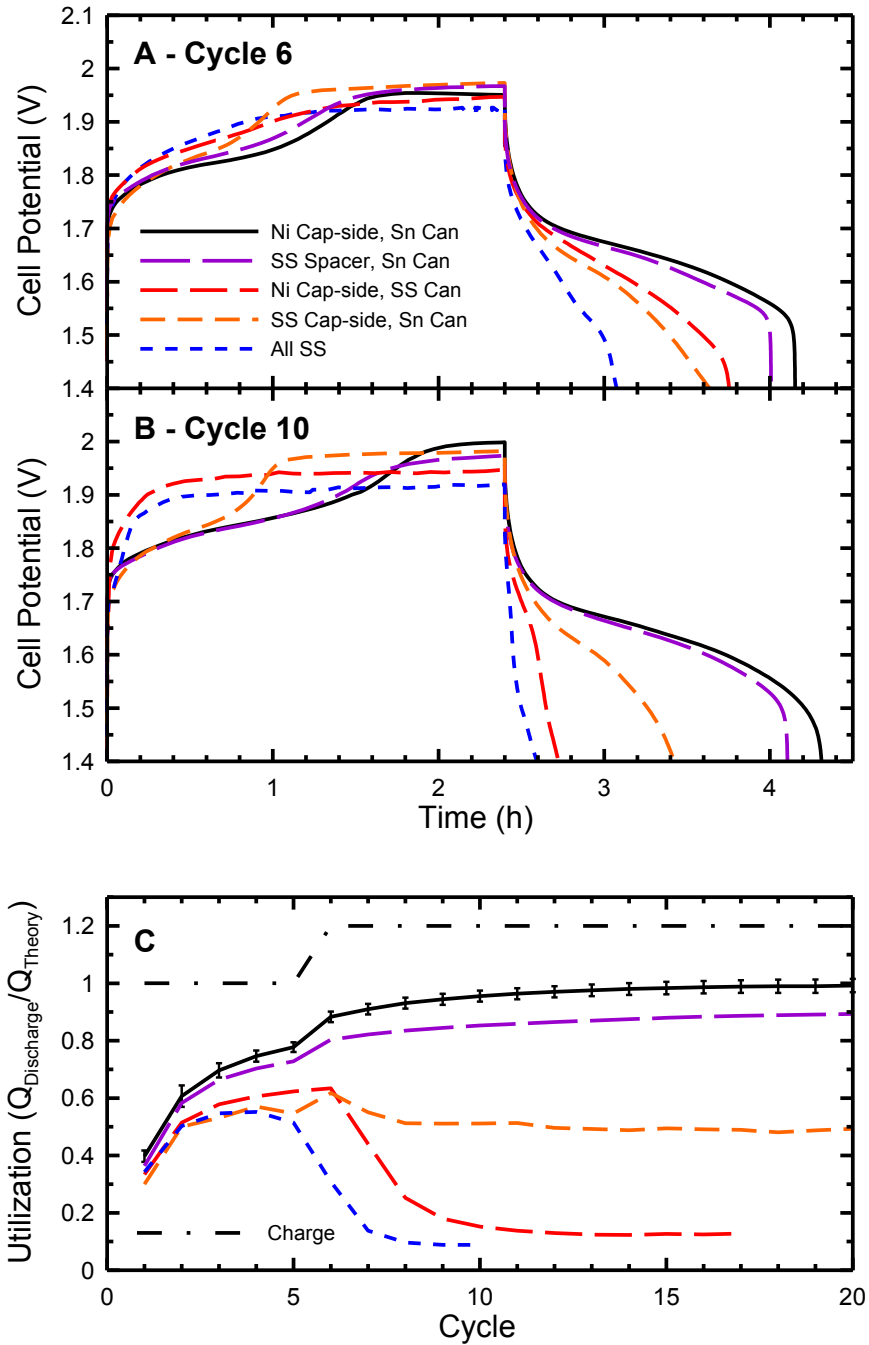


Figure 2-7: The effect of Stainless Steel (SS) coin cell components on cycling behaviour. Cap-side SS parts are SS 304, while the SS Can is SS 444. At least 3 cells of each hardware configuration were tested and the best cell of each configuration is shown here. Cycles 1-5 were formation cycles at a  $Q_T/1$  h rate (C rate) up to 100%  $Q_T$ . Cycles 6-20 were cycled at C/2 and charged to 120%  $Q_T$  (i.e. 2.4 h), so a discharge that terminated at 4.4 h would have delivered 100%  $Q_T$ . Discharge ended at 1.4 V. Panel C shows the fraction of expected capacity (Utilization) versus cycle number for the same cells shown in panels A and B, except for the standard “Ni Cap-side, Sn Can” for which the average of 3 cells is shown along with 1 standard deviation error bars.

Figure 2-7B shows analogous results for the same cells, except at cycle 10. Figure 2-7C shows the discharge capacity, normalized to the expected discharge capacity (a.k.a. utilization) of the Ni electrode versus cycle number for the same cells shown in panels A and B. Although only the best example cell of each hardware-set is shown, at least three cells of each set were made and tested. Overall, Figure 2-7 demonstrates the poor behaviour of SS components, and as a result SS components are unacceptable for use with alkaline electrolyte when charging at the potentials of Zn and Ni.

The root cause of the poor behaviour of cells with SS components was likely due to a combination of oxide growth and parasitic oxygen evolution on the cap-side components, and/or hydrogen evolution on the can-side components. Consider Figure 2-8, which shows

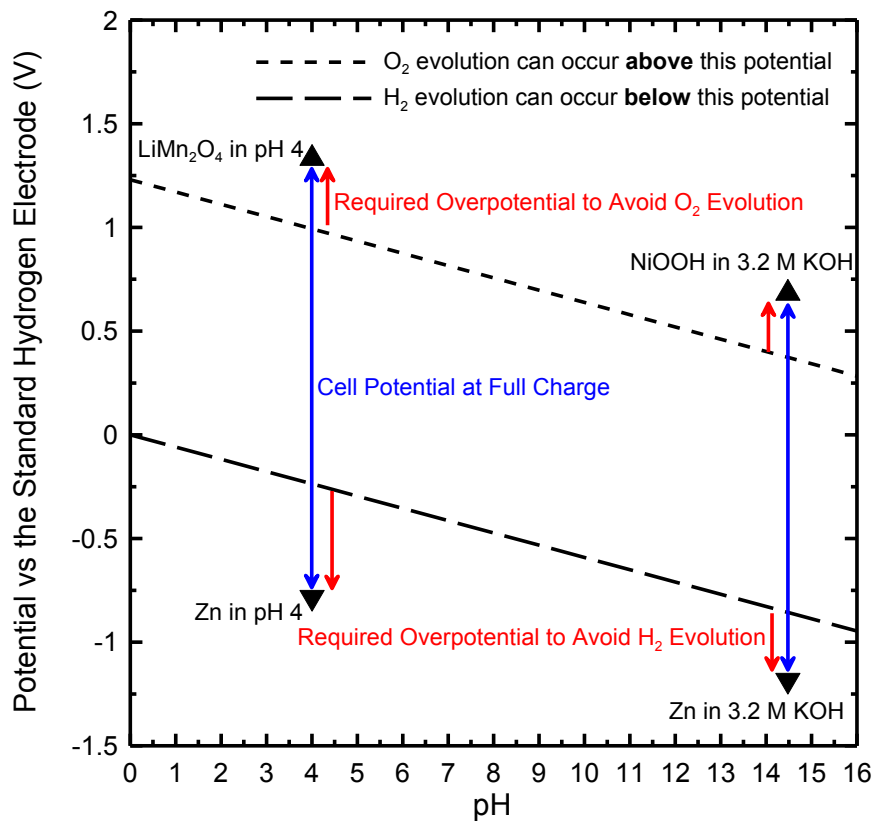


Figure 2-8: A simple Pourbaix diagram showing the potentials of fully charged Ni and Zn electrodes in 3.2 M KOH, and fully charged  $\text{LiMn}_2\text{O}_4$  and Zn electrodes in pH 4 electrolyte. The blue arrows between the electrode potentials represent the cell potentials. The dashed lines represent the stability of water. To avoid evolving either  $\text{H}_2$  or  $\text{O}_2$  gas, electrodes must have a minimum overpotential for the relevant gas evolution reaction as represented by the short, red arrows.



a simple Pourbaix diagram (potential vs pH) with the stability of water and the potentials of several fully charged electrodes relevant to this thesis marked. At any potential below the long dashed line, H<sub>2</sub> evolution via Reaction (1-16) on page 19 is energetically favoured; however, the nature of the substrate determines the kinetics of the reaction. In other words, different materials promote slower H<sub>2</sub> evolution rates, which is the primary topic of Section 2.3.5. At any potential above the short dashed line, O<sub>2</sub> evolution via Reaction (1-17) on page 19 is energetically favoured, but once again the material on which that reaction occurs can slow down the rate of O<sub>2</sub> evolution. Such materials are said to have a “high” overpotential for O<sub>2</sub> evolution. Indeed, the minimum overpotential required for a current collector material to be useful is the potential difference between the dashed line and the operating potential of the relevant electrode, as shown in Figure 2-8 by the short, red arrows. The LiMn<sub>2</sub>O<sub>4</sub> – Zn cell chemistry is discussed in Section A.5 (pg. 198), which highlights the fact that Zn plates and strips at a higher potential in acidic electrolytes. Some LiMn<sub>2</sub>O<sub>4</sub> – Zn cells are tested in Section 3.3 (pg. 109).

One of the reasons that Ni and Zn are good battery materials is their high overpotentials for O<sub>2</sub> and H<sub>2</sub> evolution, respectively, within the potential ranges of typical Ni-Zn electrode operation; this means that both produce some gas during charging, but not an excessive amount. The current collectors and cell casing are also at risk of producing gases during cell operation, which likely occurred in Figure 2-7. Before discussing how the curves of Figure 2-7 come about, it is informative to see a comparison of parasitic currents on SS and Ni in KOH.

Figure 2-9 shows the results of cyclic voltammogram (CV) potential sweep experiments performed on SS and Ni foils, dipped in 3.2 M KOH electrolyte at room temperature with a sweep rate of 20 mV/s. The positive peaks between 1.83 V and 1.87 V

in all 3 curves in Figure 2-9 are Reaction (1-11) on page 12 in the forward direction while the negative peaks between 1.77 and 1.75 V are Reaction (1-11) in the backward direction. These peaks are present because all three samples contain some Ni. The fact that the pure Ni foil displays a lower capacity of cyclable  $\text{Ni}(\text{OH})_2$  is interesting, but not investigated here. Of more importance is the potential at which  $\text{O}_2$  evolution accelerates. Figure 2-9 shows that the difference in the overpotential for  $\text{O}_2$  evolution between SS 304 and Ni is about 30 mV. This means that a Ni-Zn cell with SS components on the positive side that is being charged at  $1 \text{ mA}/\text{cm}^2$ , and has reached 1.93 V is likely producing nothing but  $\text{O}_2$  gas since SS 304 supports an  $\text{O}_2$  evolution current of about  $1 \text{ mA}/\text{cm}^2$  at 1.93 V. In contrast, a cell with Ni-coated components at 1.93 V is likely still charging the active material as desired, while

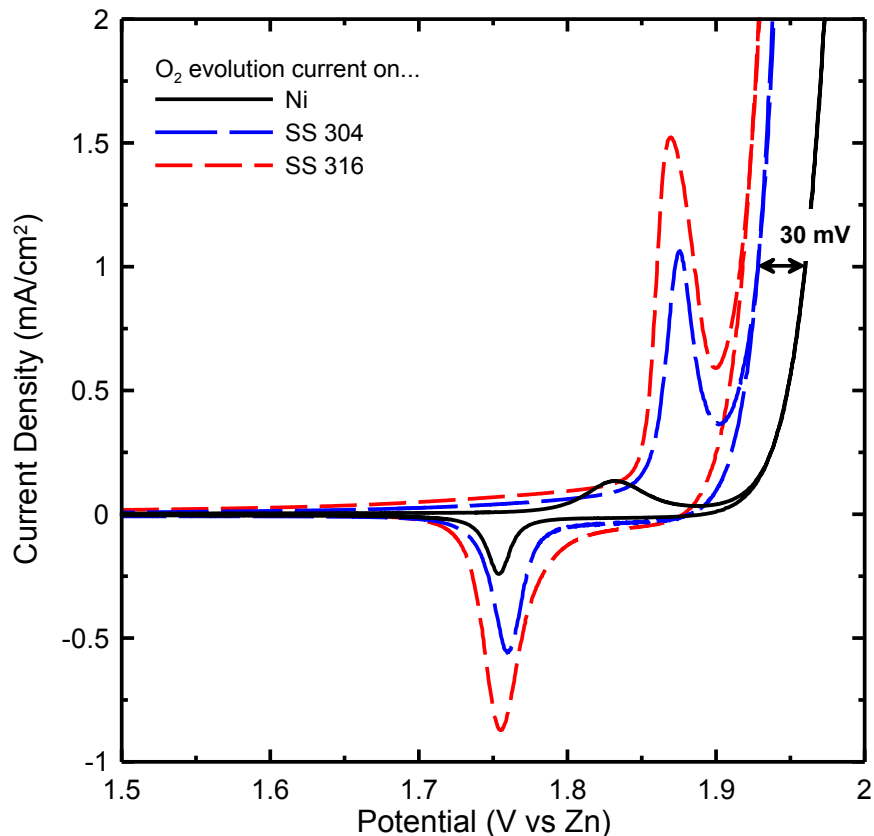


Figure 2-9: Cyclic voltammograms of nickel as well as stainless steel 304 and 316 in 3.2 M KOH. The sweep rate was 20 mV/s, from 0.55 V to 2.00 V vs Zn and started in the anodic direction. The cycles shown are the 3<sup>rd</sup> cycle, at which point the CVs were stable. The anodic spike in the potentials above 1.9 V signals an exponential increase in  $\text{O}_2$  evolution.

simultaneously producing about  $0.15 \text{ mA/cm}^2$  of  $\text{O}_2$  gas. Recall that Ni electrodes charge from about 1.75 to 1.95 V vs Zn.

Interestingly, the very first time that SS components are raised to a high potential in KOH (such as during the first charge half-cycle), an anodic reaction occurs on them that does not occur again unless the components are lowered to a potential below 0.55 V vs Zn. In Figure 2-9, this reaction had already occurred before the displayed data was recorded. Figure 2-10 demonstrates this phenomenon on SS 304 foil. The very first cycle is not shown, but the signal was essentially identical to the “0.05 V” data set. Before this experiment began, the electrode was exposed to potentials greater than 0.55 V vs Zn for

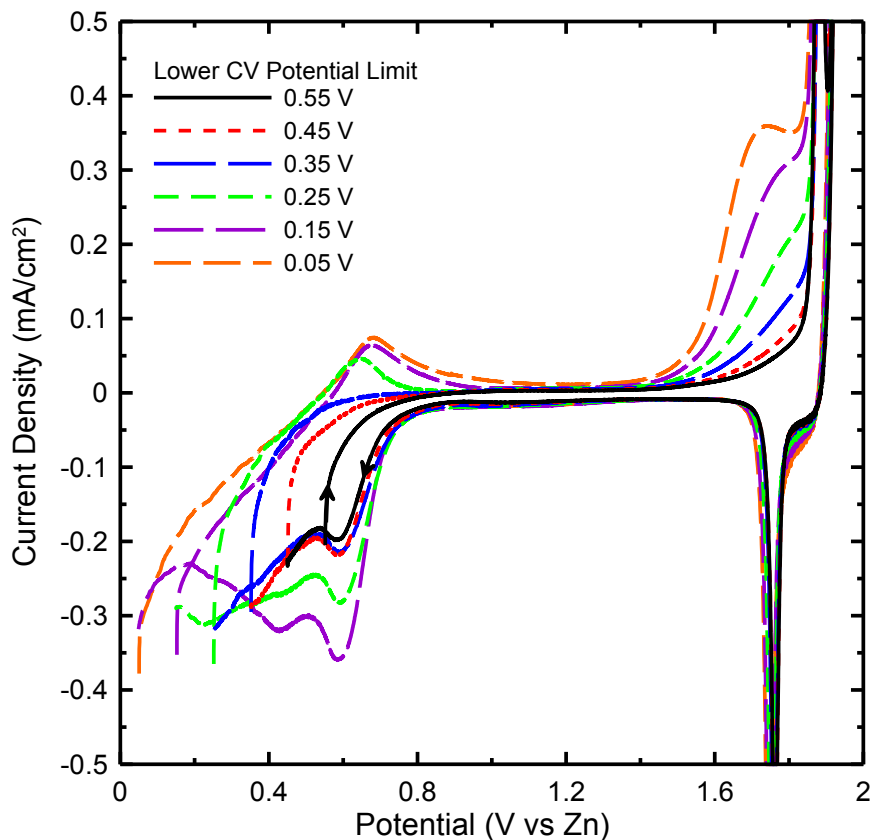


Figure 2-10: Cyclic voltammogram sweeps to progressively lower potentials on stainless steel 304 foil in 3.2 M KOH. The foil was held at potentials  $> 0.55 \text{ V}$  for about 10 min before this experiment began. The first sweep began at 0.55 V vs Zn, swept up to 1.95 V and then descended to the next lowest potential limit, 0.45 V, where the second sweep began. All potential sweeps had a maximum of 1.95 V and a rate of 20 mV/s. The anodic peak around 1.7 V only arises if the potential was previously lowered below 0.55 V.

about 10 min. As such, when this experiment began with the “0.55 V” data set, no anodic peak around 1.7 V existed. It is then evident as the experiment progresses that as the electrode either spends more time below 0.55 V or reaches lower potentials the anodic peak at 1.7 V grows. It is not clear what reaction this anodic peak reflects, but since it does not exist on pure Ni surfaces, it must be associated with Cr, Mn, Mo or Fe, and it is likely the formation of an oxide layer since the electrolyte is a strong base. If SS is used as the positive side components, then this oxide layer consumes some of the first charge and might lower the conductivity of the electrical connections within the coin cell, such as between the current collector and spacer. Conversely, these concerns can be ignored by using Ni, which maintains only a thin oxide layer at high potentials in alkaline electrolyte.<sup>78</sup>

It should now be evident that stainless steel components suffer larger parasitic currents than Ni when used as positive side components. Consequently, the cells with positive side SS components in Figure 2-7 had higher parasitic currents during charging, which caused the Ni electrodes in those cells to reach a lower state of charge than the Ni electrodes in cells without SS components. In fact, the more SS surface area a cell had, the less discharge capacity it returned. This is evident since the discharge capacities of the cells with varying positive side components descended like “Ni Cap-side, Sn Can” > “SS Spacer, Sn Can” > “SS Cap-side, Sn Can”.

Similarly, Zn plating (Reaction (1-2), pg. 6), H<sub>2</sub> evolution (Reaction (1-16), pg. 19) and possibly other reactions compete for current on the negative electrode current collector and cell casing. Figure 2-10 shows that SS 304 supports a few cathodic reactions (i.e. multiple cathodic peaks) on its surface as the potential is lowered towards 0 V, where Zn plates (charges). Also, H<sub>2</sub> evolution increases steadily below 0.05 V vs Zn, although only the beginning of this is visible at the beginning of the 0.05 V data set. It is unlikely that any of these parasitic, cathodic reactions will be beneficial to the operation of the Zn electrode, and

all of them consume charge that would otherwise plate Zn onto the current collector. In Figure 2-7, these higher parasitic currents that are supported on SS are likely what caused the Zn electrodes in coin cells with a SS can to reach a smaller state of charge during charge half-cycles, which translated into lower discharge capacities. Overall, the discharge capacities of cells with various negative casing materials descended as more SS was introduced into the cell: “Ni Cap-side, Sn Can” > “Ni Cap-side, SS Can” > “All SS”.

Avoiding parasitic currents, including O<sub>2</sub> and H<sub>2</sub> evolution, is important when considering materials for cell containers and current collectors, but several authors in recent years did not appear to be aware of this concern when they chose to use Ni foam as their Zn electrode current collector.<sup>124, 126, 127, 131</sup> Ni will act similarly to stainless steel and waste comparatively large amounts of current on H<sub>2</sub> evolution, as will be shown in Section 4.4.3 (pg. 133). As such, materials with low overpotentials for H<sub>2</sub> evolution should be avoided as a current collector material for the Zn electrode; further materials for the Zn current collector and can are explored in the next section. From this section the reader should note that a coating of Ni on the positive electrode components is superior to leaving the stainless steel bare due to the reduced rate of parasitic currents, including oxide layer growth and/or O<sub>2</sub> evolution, on Ni within the potential range experienced by the Ni(OH)<sub>2</sub> electrode during charge.

### *2.3.5 Zinc Electrode Current Collector and Cell Casing Materials*

Copper (Cu),<sup>121, 128, 130, 146, 153</sup> tin (Sn),<sup>113, 122</sup> nickel (Ni)<sup>124, 126, 127, 131</sup> and lead (Pb)<sup>68, 118</sup> have all been used as current collectors or coatings on current collectors in the past. It was prudent to determine which of these materials would be the most effective in coin cells as both the current collector and canister material. Ni was similar to stainless steel in terms of its low hydrogen evolution overpotential,<sup>154</sup> which did not work out well in the previous

section and so it was not tested in this section, but it will be revisited as a current collector material in Chapter 4. Pb is toxic and disfavoured in commercial alkaline cells for this reason, so it was also not tested in this section, but will be revisited in Chapter 4. A non-toxic and popular material for rechargeable Zn electrodes in the literature is Cu.<sup>121, 128, 130, 146, 153, 155</sup> However, dismantling a commercial rechargeable Ni-Zn cell (see Section 1.1.1.2, pg. 37) revealed that a Sn coating was used to coat all of the negative cell components.<sup>113</sup> As such, the coin cells of this section focused on the comparison of Cu to Sn current collectors and canisters. Brass was tested because it is an alloy of Cu and Zn, and has been used as a current collector at least once.<sup>123</sup>

Figure 2-11A shows the cell potential versus time during cycle 10 for Ni-Zn coin cells using various hardware sets. Figure 2-11B shows analogous results for the same cells, except at cycle 20. Figure 2-11C shows the utilization of the Ni electrode plotted versus cycle number for the same cells described by Figure 2-11A and B. Although only the best example cell of each hardware-set is shown, at least three cells of each set were made and tested.

Figure 2-11 shows the effect that current collector (CC) and canister (can) material can have on cell behaviour. This included the situation where the coin cell parts and electrodes were reversed: meaning the can was coated in Ni, the Ni electrode was in the can, the separators were reversed, the Zn electrode was on the cap side and the cap side components (cap, spring and spacer) were electroplated with Sn. This situation (“Cu CC, Sn Cap Side” in Figure 2-11) fails sooner than the standard cell configuration presumably because the electrolyte is drawn into the spring compartment and over all the exposed cap-side conducting surfaces via the electrolyte wicking phenomenon described later in Section 4.3 (pg. 126). Once there, the  $\text{Zn(OH)}_4^{2-}$  ions can continue to plate and strip during cycling, but they are more likely to become isolated from the electrolyte due to water evaporation

and because charge balancing ions have a more arduous diffusion path through the very

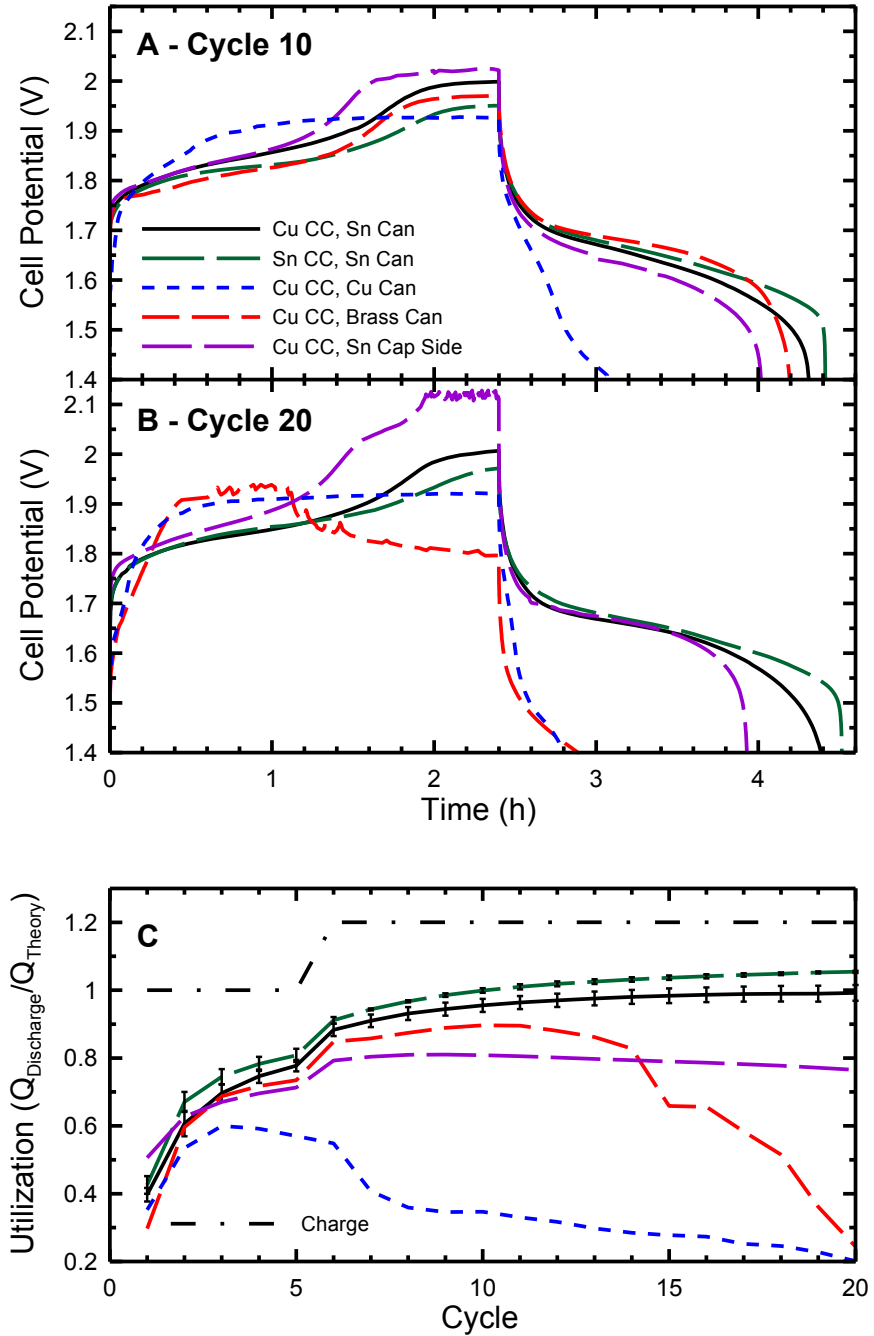


Figure 2-11: Effects of different can and current collector (CC) materials on cycle behaviour. At least 3 cells of each hardware configuration were tested and the best cell of each configuration is shown here. Cycles 1-5 were formation cycles at a  $Q_T/1$  h rate (C rate) up to 100%  $Q_T$ . Cycles 6-20 were cycled at  $C/2$  and charged to 120%  $Q_T$  (i.e. 2.4 h), so a discharge that terminated at 4.4 h would have delivered 100%  $Q_T$ . Discharge ended at 1.4 V. Panel C shows the fraction of expected capacity (Utilization) versus cycle number for the same cells shown in panels A and B, except for the standard “Cu CC, Sn Can” and “Sn CC, Sn Can” for which the average of their 3 cells are shown along with standard deviation error bars.

thin layer of electrolyte coating the cell components between where  $\text{Zn}(\text{OH})_4^{2-}$  plated and the bulk electrolyte. This leads to a loss of active material as  $\text{Zn}(\text{OH})_4^{2-}$  is marooned in the spring compartment or as the cell resistance increases due to the arduous ion diffusion path. Cycle 20 of the “Cu CC, Sn Cap Side” cell, in Figure 2-11B, exhibits a bump in the charging curve at 1.5 h, which was likely the Zn electrode reaching a full state of charge (see Section 3.1.3, pg. 96) and was expected if Zn active material was being marooned since less Zn was available to be plated. The subsequent plateau signaled when the Ni electrode had also entered into overcharge; the noisy data was attributed to either  $\text{O}_2$  or  $\text{H}_2$  bubbles evolved during overcharge. The theory that Zn migrated to the spacer compartment was corroborated when the cells were dismantled and ZnO deposits were observed on the spring and top side of the spacer.

It is also evident in Figure 2-11B that Cu and Brass undergo a detrimental reaction. Since cycle life decreases as Sn CC, Sn Can > Cu CC, Sn Can > Cu CC, Brass Can > Cu CC, Cu Can, it can be concluded that Cu is causing the problem and should be avoided in cell components. The reason why Cu was problematic as any of the negative electrode components was not obvious. One possibility for the root cause is the alloying of Zn into Cu, which has been shown to occur when Zn is electroplated onto Cu.<sup>79, 156</sup> In contrast, Sn does not alloy with Zn during deposition and instead likely stimulates epitaxial layer growth perpendicular to the basal plane.<sup>157</sup> Interestingly, both papers that discussed Cu/Zn alloy formation did so from the perspective of a battery researcher, but neither identified the alloying as a problem and Chu *et al.* even seemed to endorse Cu as a current collector due to the “growth of an active hexagonal deposit with many kink sites and edges”.<sup>79, 156</sup> They might have missed the drawback of using Cu because neither paper performed cycling experiments on cells that had alternative current collectors, the way this chapter has. In fact, no papers were found that compared the cycling behaviour of electrodes with different



current collector materials, and this research was likely the first academic publication to demonstrate that the current collector material is a critical factor in determining the cycle life.<sup>147</sup>

### 2.3.6 *Nickel-Side Component Materials, Cell Orientation and Separator Effects*

Figure 2-12A shows the cell potential versus time during cycle 10 for Ni-Zn coin cells using various hardware sets and with various cell orientations during cycling. Figure 2-12B shows analogous results for the same cells, except at cycle 20. Figure 2-12C shows the utilization of the Ni electrode plotted versus cycle number for the same cells described by Figure 2-12A and B as well as an additional cell containing only a non-woven separator. Although only the best example cell of each hardware-set is shown, at least three cells of each set were tested.

Figure 2-12 illustrates the crucial importance of having both a microporous and a non-woven separator in the Ni-Zn coin cells constructed here.<sup>70</sup> The microporous separator prevents dendrites from shorting the cell since dendrites cannot easily penetrate the sub-micrometer sized holes in the separator. So-called “soft” short circuits were observed in the “Only Non-woven” data set in panel C. A “soft short” is a relatively high resistance short circuit, where the potential of the cell remained at 1.87 V, for example, while allowing the charging current to by-pass the electrodes. Figure 2-12 also shows the effect of omitting the non-woven separator, as represented by the “Only Microporous” data set. The non-woven separator acts as an electrolyte reservoir for the Ni electrode, which can dry out if insufficient H<sub>2</sub>O is present during discharge. Omission of the non-woven separator resulted in shortened discharge half-cycles, where the gentle descent of the potential at the end of discharge suggests that the Zn electrode finished discharging first (see Section 3.1.2, pg. 94). The exact cause of this is unclear, but there are three plausible possibilities. (1) The

Ni electrode could have dried out during discharge, which would have changed the potential

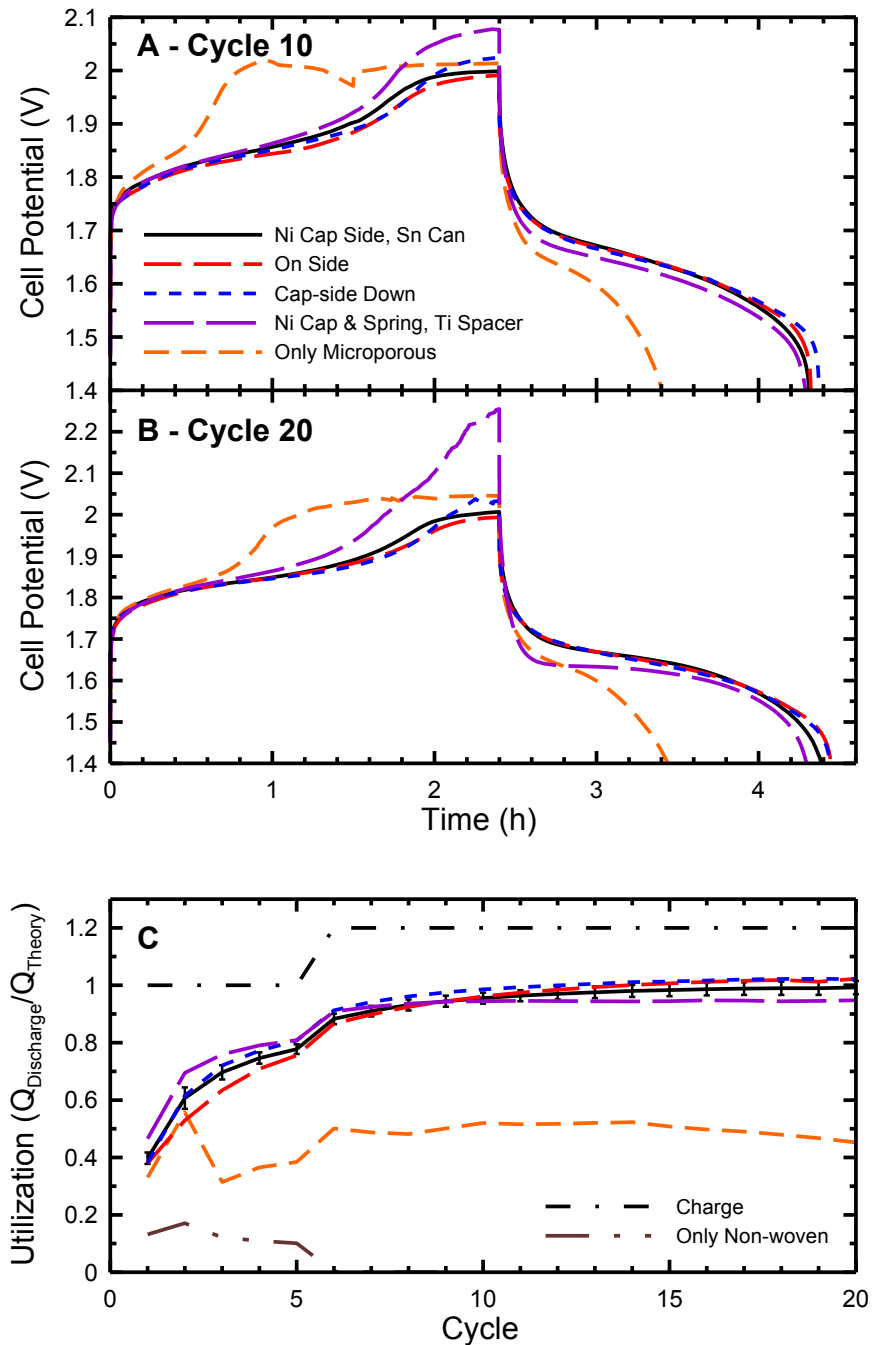


Figure 2-12: Effects of cell orientation, Ti and separators on cell behaviour. At least 3 cells of each hardware configuration were tested and the best cell of each configuration is shown here. Cycles 1-5 were formation cycles at a  $Q_T/1$  h rate (C rate) up to 100%  $Q_T$ . Cycles 6-20 were cycled at C/2 and charged to 120%  $Q_T$  (i.e. 2.4 h), so a discharge that terminated at 4.4 h would have delivered 100%  $Q_T$ . Discharge ended at 1.4 V. Panel C shows the fraction of expected capacity (Utilization) versus cycle number for the same cells shown in panels A and B, except for the standard “Ni Cap-side, Sn Can” for which the average of 3 cells is shown along with 1 standard deviation error bars.

curve. In this case, neither the Zn nor Ni electrode would have completely discharged by time the low voltage limit was triggered. (2) Soft short circuits could have syphoned some current. (3)  $O_2$  evolved at the Ni electrode during overcharge (a common occurrence during formation cycling) could have reduced Zn to ZnO, depriving the Zn electrode of some of its Zn deposit.

Figure 2-12 also shows the effect of using Ti, instead of Ni, as the spacer material (Ni Cap & Spring, Ti Spacer). Although the behaviour of cells with Ti spacers may look promising in Figure 2-12C, cells with Ti components developed a high charging potential near the end of charge (see Figure 2-12A and Figure 2-12B) and a depressed discharge potential, which decreased energy efficiency. The increased charging potential likely arose from the formation of a Ti oxide layer that thickened over time and increased the contact resistance between the Ti spacer and the Ni electrode. Upon dismantling the cells with Ti spacers, rainbow colouration on the Ti spacers was observed, which signified oxide layer growth. In the "Ti Spacer" potential curve in Figure 2-12B, the depression of the discharge potential at the beginning of charge was a feature that also arose occasionally in standard cells with Ni positive-side components, although later in cycle life (i.e. > cycle 50) and not as frequently as in cells with Ti parts. Hence, the discharge potential depression was not associated with Ti specifically, but was a sign of problems developing at one of the electrodes.

Figure 2-13A shows the cell potential versus time during cycle 30 for Ni-Zn coin cells using the most promising hardware sets and cell orientations, in terms of cycle life. Figure 2-13B shows analogous results for the same cells at cycle 50. Since the potential curves shown are for the singular best cell of each hardware-set, many of the curves lie nearly on top of one another with only a few notable features breaking away from the pack. For instance, Figure 2-13A and Figure 2-13B show that cells with Ti spacers continue to

reach a higher potential during charge and, on average, a lower potential during discharge

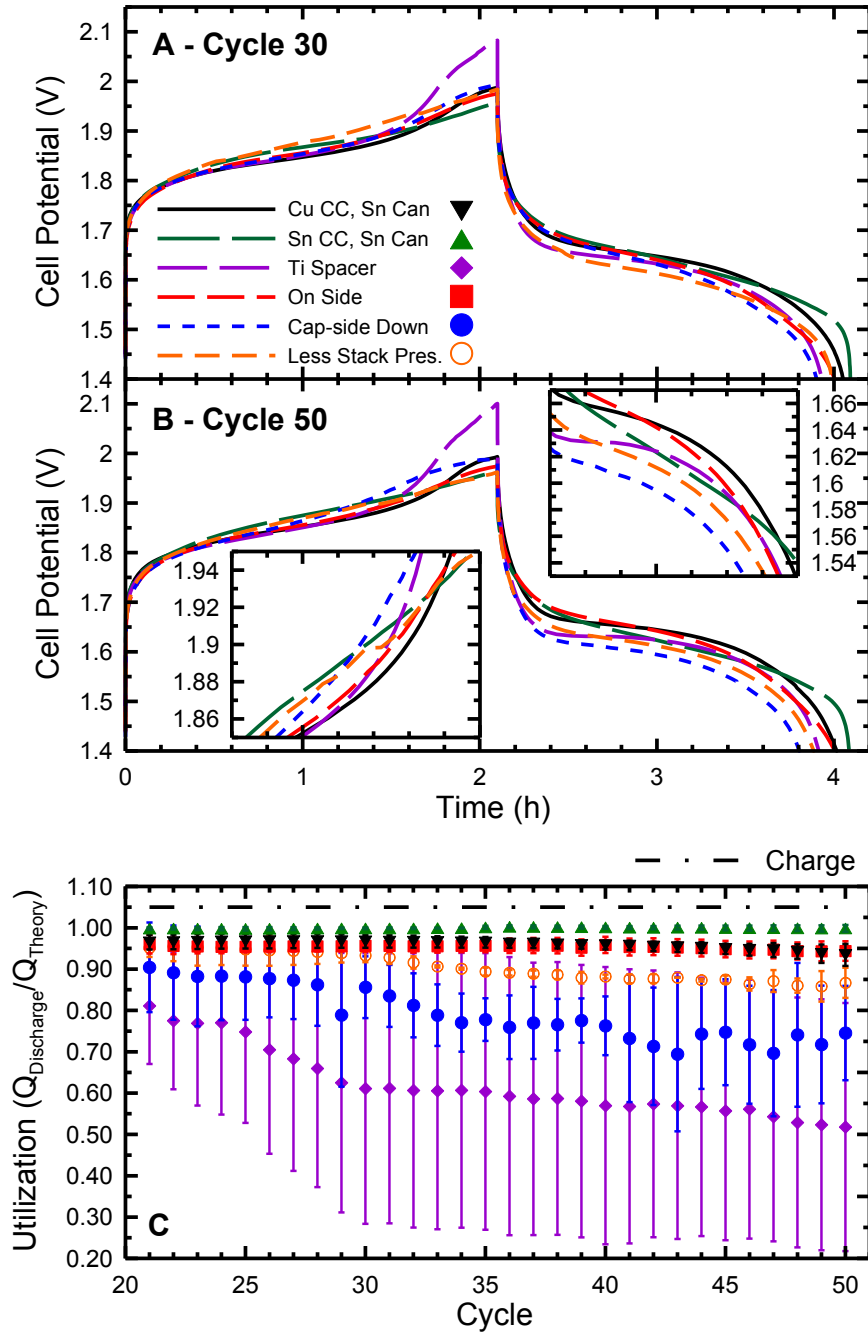


Figure 2-13: Extended cycling to cycle 50 of the best cell designs. At least 3 cells of each hardware configuration were tested and the best cell of each configuration is shown in panels A and B. Cycles 20-50 were cycled at  $C/2$  and charged to  $105\% Q_{\text{Theory,Ni}}$  (i.e. 2.1 h), so a discharge that terminated at 4.1 h would have delivered  $100\% Q_{\text{Theory,Ni}}$ . Discharge ended at 1.4 V. Panel C shows the average fraction of expected capacity (Utilization) versus cycle number for the batches of cells exemplified in panels A and B. Error bars are 1 standard deviation.

up to cycle 50. Another outlier is the potential curve of the “Cap-side Down” cell, which rose sooner during charge and dropped sooner during discharge. This is generally ascribed to electrolyte detaching from the “bulk” electrolyte in the separators and flowing down into the spring compartment due to gravity. Finally, the “Sn CC, Sn Can” cell consistently delivered more discharge capacity than the cell that had a Cu current collector. The steepness of the potential shoulder at the end of discharge also suggests that the Ni electrode reached the filled state (finished discharging) before the Zn electrode had all the Zn stripped from it (see Section 3.1.2, pg. 94).

In order to see the differences in behaviour between these hardware-sets, the average discharge capacities must be examined. Figure 2-13C shows the Ni electrode utilization versus cycle number for the average of 2 to 4 cells, depending on if any of the 4 cells made of each configuration suffered serious problems early on that would not be related to the variable being tested. For instance, on average, 1 cell in 16 would short circuit during assembly and 1 cell in 12 tended to short due to dendrites growing around the separator edges in a poorly assembled cell. Regardless, these averages give a more realistic and statistically accurate idea of coin cell behaviour.

The “Sn CC, Sn Can” data is an average of 3 cells that had nearly identical discharge capacities out to cycle 50, as evidenced by the error bars. In comparison with the standard hardware-set (Cu CC, Sn Can), the absence of overlap between the two data sets confirms that Sn current collectors promote higher discharge capacities. Note that Utilizations above 100% were assumed to be due to a combination of experimental error in calculating the theoretical capacity (see Table 2-2, pg. 53) and overcharging the  $\beta$ -NiOOH to form  $\gamma$ -NiOOH, which has a higher capacity than the  $\beta$ - form but is less stable over many cycles.<sup>48</sup>

The discharge capacity of “Cap-side Down” cells faded sooner than identical cells that were cycled cap-side up; however, cells cycled on their side (“On Side”) performed just

as well. This is likely because electrolyte that flowed into the spring area of the coin cell due to gravity became disconnected from the bulk electrolyte in the cap-side down cells. In the case of the cells on their sides, the wicking action of the non-woven and, to a lesser extent, microporous separators likely kept electrolyte in the lowest portion of the coin cell connected with the bulk electrolyte. Consequently, the “On Side” cell orientation was equal within experimental error to the standard hardware-set. Therefore, researchers need not fret about the performance of cells that are tilted up to 90°. Beyond that, error bar overlap was not significant for any other two data sets in Figure 2-13C, meaning that cells should not be tilted over 90°. In a commercial cell, the wicking action of the separators and tight fit of the electrodes within the canister make cell orientation unimportant, but clearly researchers using coin cells should be cautious.

Finally, the Ti and “Cap-Side Down” data sets had at least one cell that performed as well as the standard cell design in Figure 2-12C (pg. 73) up to only cycle 20, but when the data sets of all such cells were averaged up to cycle 50 and compared in Figure 2-13C there was a statistical difference from the standard. This illustrates the importance of reproducing one’s own work and reporting the results, which only a few authors seem to have done with respect to cycle life.<sup>118, 119, 123</sup> The difficulties of reporting reproducibility with respect to cycle life were touched on in Section 2.3.3 (pg. 58), which might explain why researchers tend to ignore reproducibility; however, they really should not continue to do so. Without averages and some statistical treatment of the data, authors are left with quite a bit of freedom to conclude what they want, as opposed to what is true.

### *2.3.7 Effect of Stack Pressure on Cell Performance*

Figure 2-13C also shows that applying insufficient stack pressure to the electrodes also reduces cycle life. “Stack pressure” is the pressure applied to the electrodes by the

spring and spacer. The “Less Stack Pressure” data set used flat, 0.77 mm thick spacers that only applied about 700 kPa as opposed to the 2,200 kPa that standard 0.88 mm thick, Ni coated spacers provided. Insufficient stack pressure might have brought about a decrease in discharge capacity due to the loss of good electrical contact with the Ni active material on the positive side or an increase in Zn shape change at the negative side. Note that the pressure film was 190  $\mu\text{m}$  thick, which was close to the combined thickness of the Ni and Zn electrodes (about 120  $\mu\text{m}$ ) but not close enough to conclude that the absolute pressure experienced by actual electrodes was exactly 700 kPa or 2,200 kPa. The value of these measurements was the determination of the distribution of pressure on the electrodes.

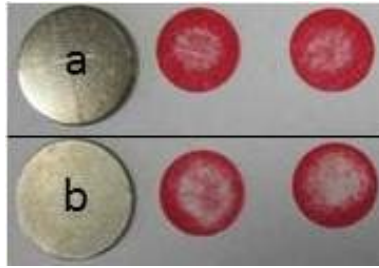


Figure 2-14: Example stack pressure distributions from the two shapes of spacers tested in this work. a – concave, 0.88 mm thick stainless steel spacer coated in Ni. The convex side was towards the electrodes in cell assembly. b – flat, 0.77 mm thick Ni 200 spacer. The two pressure distributions beside each spacer are examples. The darkest colour of red signifies  $> 3,000$  kPa while white signifies  $< 250$  kPa.

Figure 2-14 shows the pressure distribution on the electrodes with the two differently shaped spacers mentioned here. The thicker (0.88 mm) and slightly convex (toward the electrode) spacer applied noticeably more pressure in the center of the electrode than did the flat, thinner (0.77 mm) spacer. It was determined separately that the degree of concavity (within reason) had little to no influence on utilization, only the thickness, and thus the pressure, mattered. Note that it is likely that the Zn electrode experienced the same pressure distribution as the Ni electrode.

### 2.3.8 Effect of Gas Evolution in Coin Cells

Early in the research efforts presented in this chapter, it was discovered that the discharge capacity of fully sealed (non-vented) coin cells faded faster than cells with pressure-relief valves (i.e. a hole in the cap) and eventually the sealed cells burst open due to a build-up of gas pressure inside the cell. In order to gain some insight into when during the cycling process this gas was being created, the thickness of a cell, at the micrometer scale, was monitored during cycling. Figure 2-15 shows the potential versus time for a *sealed* Ni-Zn coin cell along with the cell thickness versus time. The cell was charged and discharged at room temperature at a C/2 rate. The charge half-cycles were terminated at 70%  $Q_{\text{Theory, Ni}}$  for the first 4 cycles, then at 100%  $Q_{\text{Theory, Ni}}$  for the next 6 cycles and finally at

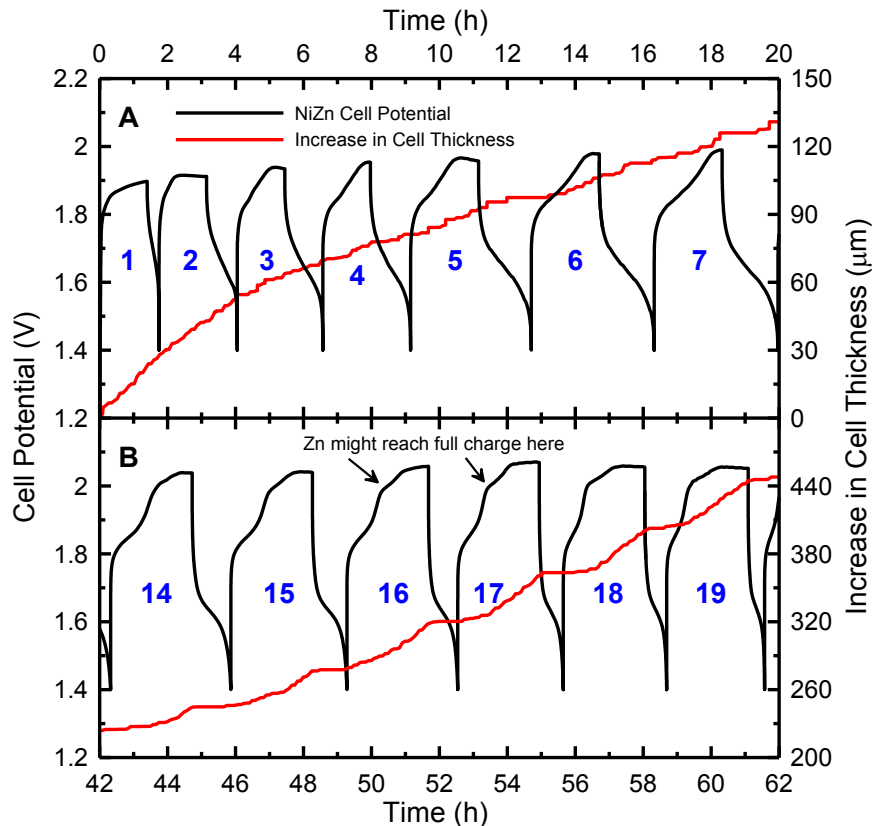


Figure 2-15: Ballooning of a sealed Ni-Zn coin cell during cycling. The cell was cycled at a C/2 rate, and was charged to 70%  $Q_T$  for the first 4 cycles, then 100%  $Q_T$  for the next 6, then 120%  $Q_T$  for the final 10 cycles. The cell was discharged to 1.4 V in all cycles. Panels A and B show the first 7 cycles and cycles 14 – 19, respectively, along with the corresponding increase in cell thickness from its initial value.



120%  $Q_{\text{Theory, Ni}}$  for the last 10 cycles. Discharge half-cycles were always terminated at 1.4 V. Cycles 1 to 7 are shown in panel A, while cycles 14 to 19 are shown in panel B. This coin cell “ballooned” when gas production inside increased the internal gas pressure.

Figure 2-15 shows that gas is evolved at a seemingly constant rate for the first five cycles, although that rate changes from cycle 2 to 3; “Seemingly” because the increase in cell thickness is not necessarily linearly related to the internal pressure in the cell. This was surprising since, until this experiment, it was assumed that gas was only significantly evolved on the Ni electrode (i.e.  $O_2$ ), during the high potential sections of the charge half-cycle. Indeed, evidence of  $O_2$  contributing to the ballooning of the cell was observed in cycle 6 when the thickness only resumed increasing midway through charge. But  $O_2$  evolution alone cannot describe the cell thickness increase during the formation cycles. If the formation charging of the Ni electrode were the only source of gas during cycles 1 to 5, then the cell thickness would be expected to stop increasing during discharge when no formation is taking place. Additionally, if all of the gas was  $O_2$  that recombined with Zn, the way it should ideally (see Section 1.5.1, pg. 19), then the ballooning would be expected to decrease during discharge when no more  $O_2$  would be produced but some would be consumed. Neither of these trends was observed.

The following discussion proposes a possible scenario to describe the observed behaviour of the sealed cell. A clue is present in panel B, which shows that eventually gas is only produced during the charge half-cycle and the rate of gas evolution increases as the potential increases. However, the bumps in the charge curves in panel B appear to be due to the Zn electrode overcharging (see Section 3.1.3, pg. 96), which would mean the gas being produced was  $H_2$ .  $H_2$  does not easily recombine at the Ni electrode, so if the majority of the gas was  $H_2$  it could explain why the pressure in the cell never decreased.<sup>67</sup>  $H_2$  can also be produced through the self-discharge (corrosion) of the Zn electrode.

Returning to panel A, the Zn electrode was not overcharged in at least the first 10 cycles since the Zn electrode had a theoretical capacity more than 3× larger than the Ni electrode. Therefore, the gas evolved in cycle 6 was likely O<sub>2</sub>, and so it appears that O<sub>2</sub> did not recombine well in this cell since the internal pressure never dropped. However, it cannot be concluded that no recombination occurred because the rate of H<sub>2</sub> gas evolution from self-discharge in this cell was unknown and it might have been faster than the O<sub>2</sub> recombination rate. As such, this experiment demonstrated that the self-discharge rate must be better understood before further coin cell experiments exploring gas evolution during formation cycling or O<sub>2</sub> recombination rates can be undertaken.

In the meantime, this experiment also demonstrated that O<sub>2</sub> recombination cannot be relied upon to prevent coin cells from ballooning and eventually bursting. The ballooning of the cell is detrimental because it decreases the stack pressure by releasing the spring. In Section 2.3.7, only a 110 μm difference in the spacer thickness created a noticeably detrimental trend in the discharge capacity of coin cells. That thickness does not directly translate to the thickness of the coin cell measured in this section since the thickness of the coin cell was measured at the center of the cap, whereas the spring pushes against the interior edges of the cap. Regardless, the increase in cell thickness cannot be good for cycle life. Consequently, researchers wanting to avoid cell ballooning or bursting should include a pressure release valve in their cells. In this thesis, that was achieved by drilling a 1 mm diameter hole in the cap (off-center) and applying a piece of scotch tape over the hole to reduce the evaporation of water from the electrolyte. To the author's knowledge, the only published data about gas evolution rates or internal pressure during the cycling of a Ni-Zn cell are plots disclosed from a commercial source (PowerGenix) in the Handbook of Batteries.<sup>67</sup> Since the plots in the Handbook of Batteries show only a single

charge half-cycle after the Ni electrode had been formed, the experiment shown in this section was potentially the first of its kind to be published in a journal.<sup>147</sup>

### 2.3.9 Comparison of Coin Cells with Commercial Ni-Zn AA Cells

Figure 2-16 shows a photograph of a commercial Ni-Zn AA-size cell produced by PowerGenix. To provide a comparison between the coin cells described here and commercial cells, several Ni-Zn PowerGenix AA cells were acquired and cycled under identical conditions to the coin cells in this study.

Figure 2-17 shows the utilization plotted versus cycle number for the PowerGenix cells cycled under a variety of conditions and a coin cell for comparison. The results shown are for the better cell of pairs of cells tested identically. PowerGenix AA cells are rated to have between 1350 and 1500 mAh of capacity, and no cycle life was specified on the manufacturer's website.<sup>158</sup> Only 2 of 8 cells (red and blue curves) demonstrated > 1350 mAh during the first discharge. The manufacturer's specified charging regime was to use a constant (2/3)C rate until the potential curve began to angle upward after the main charging plateau and then hold the potential at 1.9 V until the current decayed to below 90



Figure 2-16: PowerGenix AA cell tested in the same manner as the coin cells (also shown). These cells are rated to provide between 1350 and 1500 mAh. No expected cycle life is reported on the PowerGenix website.

mA or until 2.5 h had passed. Although there are clear differences in the results from the different charging regimes, all of the PowerGenix cells behaved surprisingly poorly compared to the coin cell. In the Li-ion research community, commercial cells nearly always perform better than lab-made, battery-like cells (like coin cells); however, this may not be the case for the commercial Ni-Zn cells tested here.

If the data in Figure 2-17 can be trusted, it shows that the coin cells used in this study are superior to commercial Ni-Zn AA cells. Unfortunately, the fact that each pair of commercial cells cycled under the same conditions gave dramatically different results from one another suggests a large variation in behaviour between commercial cells within the same batch, let alone between batches. Hence no conclusions can be drawn from this data about the effect of temperature or cycling rate. The fact that this can occur in commercial cells is worrisome with regards to scaling up Ni-Zn technology and demonstrates that a test system for research that can produce reproducible results is invaluable. The coin cell design described here is one such design that fulfills that need. Overall, the promising behaviour of the coin cells is not completely unexpected since coin cells have thin

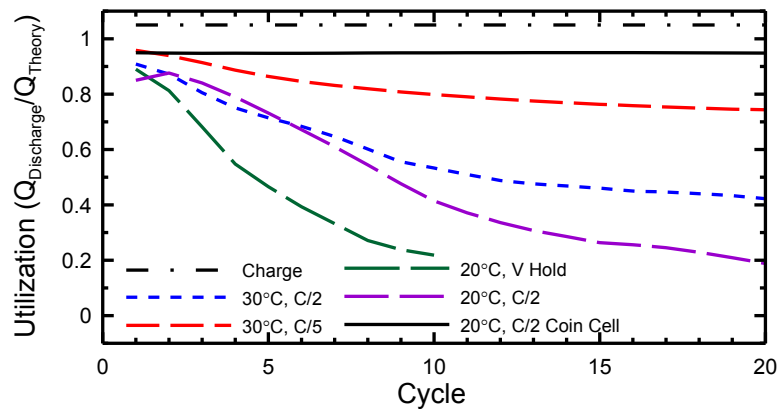


Figure 2-17: Cycling behaviour of PowerGenix AA cells using various charging regimes. All data sets are the best cell of a 2 cell batch.  $Q_T$  for PowerGenix cells was 1500 mAh. The low end of PowerGenix's acceptable range for capacity is 1350 mAh or a Utilization of 0.9. Only 2 cells of 8 (red and blue) achieved this minimum. All cells except the V Hold cells were charged to 105%  $Q_T$  at either a C/2 or C/5 rate. The V Hold cells were cycled according to PowerGenix's specified charging regime at a C/2 rate when under current control. The coin cell is a standard Cu CC coin cell for comparison. The cycles shown for the coin cell are the 20 cycles after the first 20 formation cycles (i.e. cycles 21-40).

electrodes, allowing the researcher to ignore  $\text{OH}^-$  concentration gradients,<sup>42</sup> macroscopic pore networks<sup>118</sup> or bulk electrode material conductivity issues within thick electrodes. This comparison between (poor) commercial cells and coin cells highlights the difference in cycling behaviour between thin and thick electrodes, and suggests that the thin electrodes used in this thesis could be useful for testing new active materials,<sup>124, 127, 131</sup> electrode additives<sup>15, 155, 159-161</sup> and electrolyte additives,<sup>145, 162-165</sup> but that they are probably not useful if the researcher is focussing on issues associated with thick electrodes.

Figure 2-18A shows the cell potential versus time, after formation, for the best Sn and Cu current collector (CC) Ni-Zn coin cells and the best commercial PowerGenix Ni-Zn AA cell. Figure 2-18 did not include the first 20 cycles for the two coin cell data sets, since formation ceased when the charge capacity was dropped to 105%  $Q_{\text{Theory, Ni}}$  at cycle 21. In effect, cycle 1 in Figure 2-18A and Figure 2-18C is in fact cycle 21 for the two coin cells. Figure 2-18B shows analogous results for the same cells, except at cycle 81. The PowerGenix cell was cycled at 30°C at a C/5 rate with charge up to 105%  $Q_{\text{Theory}}$  (also the red curve in Figure 2-17). The ‘hump’ in the PowerGenix voltage-time profile in panel B is unexplained in the literature, but it is likely the onset of  $\text{O}_2$  shuttling from the positive side to negative side and the drop in potential after the hump is likely due to an increase in cell temperature, which in turn speeds up the kinetics of the  $\text{O}_2$  evolution reaction.<sup>166</sup> This hump moves to the left with cycling, signifying that less and less Ni active material is available for charging as cycling continues. Figure 2-18B shows that the same sort of behaviour starts to appear in the standard “Cu CC, Sn Can” coin cell at cycle 81.

Figure 2-18C shows the utilization plotted versus cycle number for the same cells in Figure 2-18A and B as well as the average cycle life (to 50% Utilization) of all 3 cells of each type, although only utilizations of the best cell of each set are specifically shown. Panel C shows that the cycle life of coin cells was superior to that of the commercial cell, and that

coin cells with Sn CCs lasted longer than standard Ni-Zn coin cells with Cu CCs. The Cu CC cell was the longest lasting cell of a set of 3 identical coin cells and died abruptly at cycle

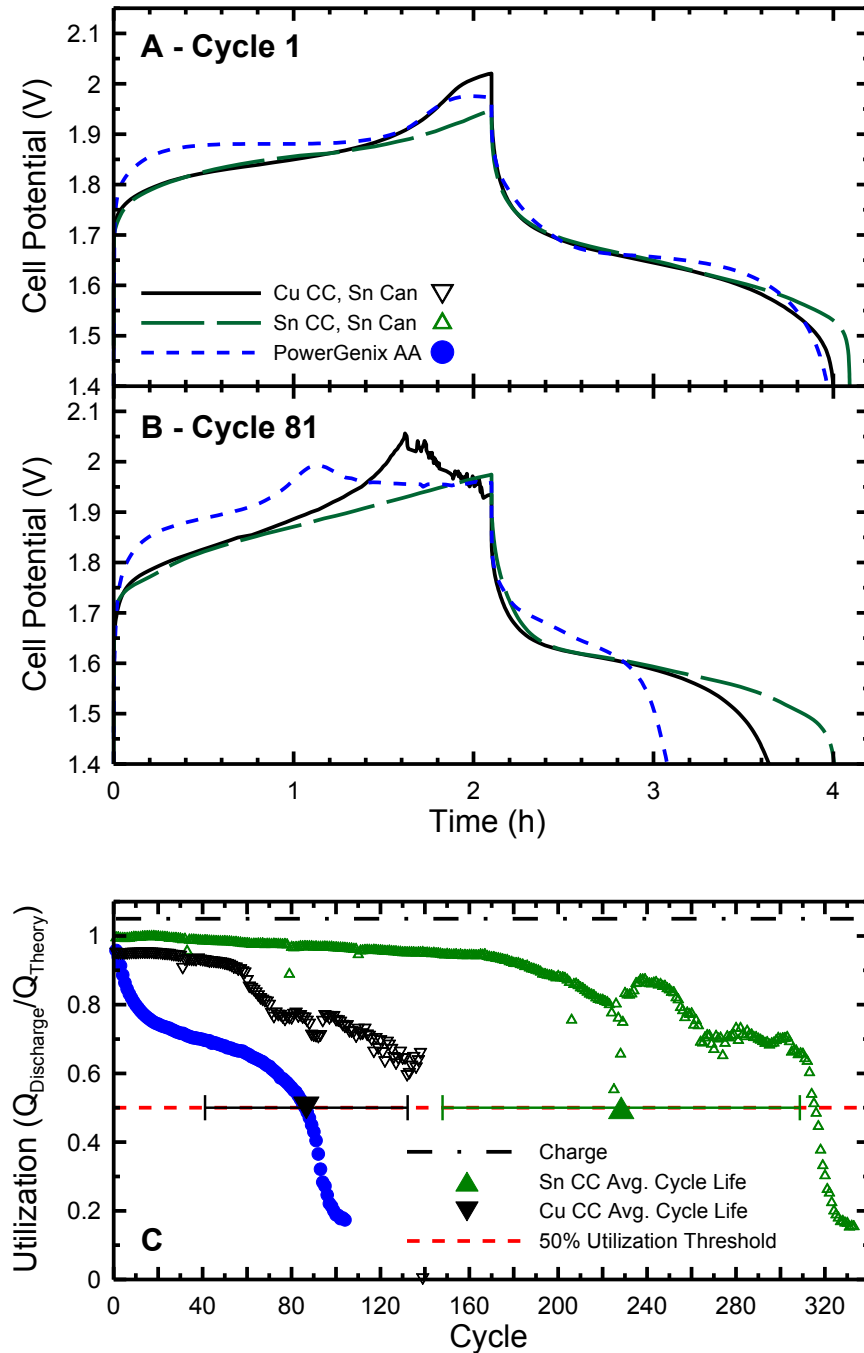


Figure 2-18: Comparison between the best PowerGenix AA cell and the best coin cells produced in this work. The PowerGenix AA cell was cycled at C/5 at 30°C, while the coin cells were cycled at C/2 at 20°C. All cells were charged galvanostatically to 105%  $Q_T$  each cycle. Panel C shows the cycle lives of the same cells shown in A and B. Also shown are the average cycle lives of the Sn CC and Cu CC coin cells with 1 standard deviation error bars.

140 (Figure 2-18C) when a dendrite formed. Meanwhile, the Sn CC cell survived a few

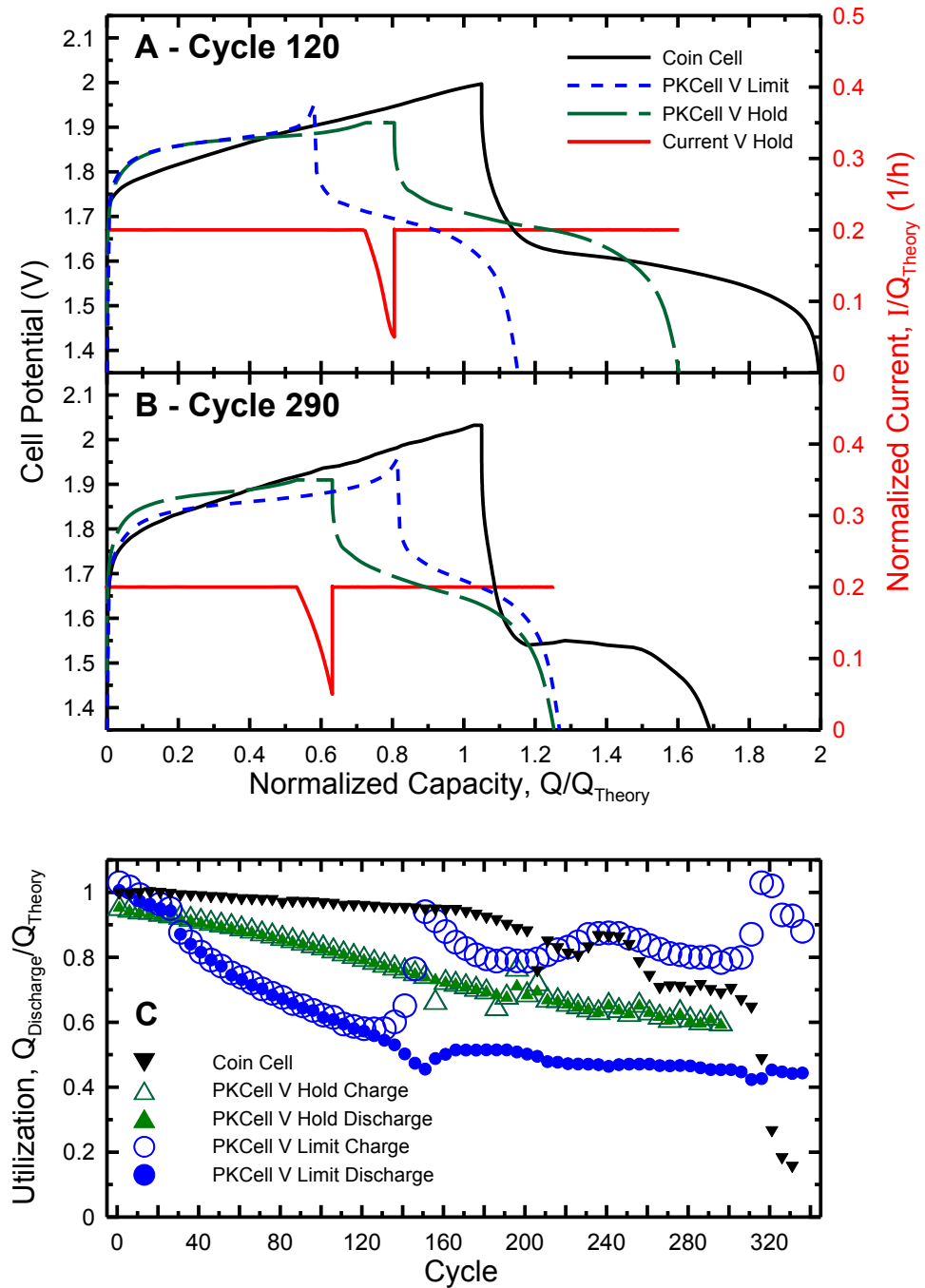


Figure 2-19: Comparison between PKCell AA cells cycled in two different ways and the best coin cell produced in this work. The experimental details are explained in the text. Panels A and B show the potential curves at cycle 120, when all 3 cells are operating well, and at cycle 290 when all 3 cells are nearing the end of their cycle life. Panel C shows every 5<sup>th</sup> cycle of the cycle lives of the same cells shown in A and B. The cycling current for the “V Hold” cell is shown in panels A and B to demonstrate the decay of the current when the potential is held at 1.91 V, and refers to the right side y-axis.  $Q_{\text{Theory}}$  for the PKCells was 1,500 mAh while that for the coin cell was 1.397 mAh.

dendrites around cycle 230 and failed (< 50% Utilization) at cycle 316.

A few years after testing the PowerGenix cells shown in Figure 2-17 and Figure 2-18, commercial Ni-Zn cells had evidently improved somewhat and so in 2014 a few AA cells of a new brand called PKCell were acquired. Figure 2-19 shows the cycling behaviour of these cells compared to the same Sn CC coin cell shown in Figure 2-18. To reiterate, it was charged galvanostatically at a C/2 rate at 20°C to 105% of  $Q_T$  each cycle and discharged down to 1.2 V. The PKCell AA cells were cycled at C/5 at 30°C. The “V Limit” cell was charged up to 2.00 V for the first 27 cycles and then only to 1.95 V for the remaining cycles, all of which were followed by a discharge down to 1.35 V. The “V Hold” cell was charged up to 1.91 V, and then held there until the current decayed down to C/20 (0.05 on the right y-axis) or until 103% of  $Q_T$  was reached. Then it was discharged down to 1.35 V.

The “V Hold” cycling procedure was the procedure favoured by Ni-Zn cell manufacturers, while the “V Limit” cycling procedure is closer to that used to cycle coin cells in this work. Panels A and B show example potential curves at various cycles for the reader’s interest, but the take-home message from panel C is that the coin cells developed in this work have cycle lives comparable to commercial Ni-Zn cells.

## **2.4 Coin Cell Design Conclusions**

Coin cells are easily fabricated in large quantities and have small space requirements that allow many cells to be tested simultaneously under controlled conditions, like inside a temperature or humidity controlled box. They can have good reproducibility once the researcher is skilled in their fabrication and if proper components are used. Additionally, coin cells only require small amounts of material, reducing the burden of electrode material fabrication on the researcher. If thin electrodes are used, concerns over bulk electrode issues are alleviated, making coin cells a good research tool



for testing new active materials, electrode material recipes, electrolytes and separators, but not a good system for research on features of thick electrodes, like densification or bulk electrode conductivity issues.

For both Ni-Zn and Zn-air cells, Ni was the material of choice for the positive-side components (cap, spring, spacer and current collector) since it supported low parasitic currents during charge. Stainless steels and titanium should be avoided due to their high parasitic currents within the operational potential window of the Ni electrode in alkaline electrolyte.

Selection of the negative-side components (the can and current collector) was more stringent due to the fact that Zn electroplates and strips repeatedly during cycling. As such, Sn was preferred since it had a high overpotential for H<sub>2</sub> evolution, was resistant to the alkaline electrolyte at the potentials of the Zn electrode and provided a favourable surface for Zn electroplating and stripping. Cu is widely used as a current collector for Zn electrodes, but the coin cells in this work that used Cu or brass performed poorly in comparison to Sn. The mechanism for why cells using Cu fail sooner was not determined, but the desire to study the difference between Cu and Sn current collectors did provide some of the motivation for the work of Chapter 4. Since no other studies have presented Zn cycling behaviour on different current collectors in alkaline electrolyte, it was assumed that other authors chose current collector materials due to ignorance or based on tradition. In the future, researchers should avoid Cu as a current collector or cell casing material. All coin cells from this point on in this thesis were constructed with Zn electrodes using Sn for the current collector and cell casing.

The stack pressure applied to the electrodes is also important for long cycle life. If stack pressure was too small, the discharge capacity faded noticeably sooner. This was thought to be due to a loss of electrical contact to the active materials as they cycled. To

prevent this, a spring to maintain pressure, a thick enough spacer and a pressure release valve to prevent ballooning were required.

The dual separator system evidently plays an important role in Ni-Zn cells as well. It was reasoned that the non-woven separator ensured adequate amounts of H<sub>2</sub>O were present next to the Ni electrode and the microporous separator prevented dendrites from growing on the Zn surface.<sup>70</sup> The necessity of these separators was previously known to experts in the field but had never before been demonstrated in the literature for the benefit of new researchers.<sup>70, 147</sup>

Reproducibility within individual bodies of work is poorly reported in the literature.<sup>118, 119, 123</sup> In the author's opinion, researchers should produce at least three identical cells and report the average and standard deviations of the discharge capacities vs cycle number and/or the cycle life, along with the criterion they used to determine cell failure (ex. 50% of the initial discharge capacity). Without such reporting, results can be selectively chosen to sway the conclusion in the direction the author wishes.

The ability to compare advancements across different bodies of work is also hindered by two factors in the current literature. First, authors have a poor habit of either not cycling their cells until they fail or not reporting the cycle life if they do.<sup>121-123, 126-131</sup> This prevents one author from determining if their advancement is any better than another without directly testing the other themselves. As demonstrated in Figure 2-18C (pg. 85), some comparisons, like that between the Cu and Sn current collector cells, cannot be made unless the cells are cycled to large enough cycle numbers. Second, the cell design might be a dominant factor in determining the cycle life of a particular researcher's experiment. Consequently, in the author's opinion researchers should divulge their entire cell design when reporting their results, including electrolyte volumes, separators, stack pressure, current collectors, methods of electrically connecting to the electrodes, cell casing materials,

temperature, and whether or not the cell was sealed, in addition to the details of electrode manufacture.

If the right components are used, coin cells can match or even outperform commercial Ni-Zn cells with regard to cycle life. Note that this benchmark was achieved with un-optimized electrode mixtures, which could no doubt be further improved by using more state of the art active materials and electrode material recipes.

## **2.5 Aspects of the Coin Cell Design to be Mindful of**

The drawbacks of the coin cell design are not debilitating to most experiments performed with coin cells, but might affect cycle life. Four aspects are presented here in order of decreasing importance in the author's opinion.

### *2.5.1 Primitive Pressure Release Valve*

The recombination of Zn and O<sub>2</sub> (Reaction (1-19)) to consume forming Zn dendrites requires an internal cell pressure greater than atmospheric pressure,<sup>67</sup> which the tape over the hole in the cap likely does not provide. Hence recombination of Zn and O<sub>2</sub> likely does not occur at significant rates in the coin cells presented here. In sealed commercial Ni-Zn cells the pressure release valve is tuned to allow recombination to occur before opening to relieve any excess pressure. Also, the tape could likely be replaced with something more effective at reducing H<sub>2</sub>O evaporation. With scotch tape over the hole, all of the cells in this chapter were cycled at 20°C and only lost  $4.0 \pm 1.1$  μL of water (out of  $29 \pm 4$  μL) over the course of their testing (about 8 days to cycle 50), so H<sub>2</sub>O evaporation was not an issue. However, in Chapter 5 coin cells held at 30°C and a relative humidity of about 50% lost about 1.5 μL/day out of about 36 μL. As such, researchers should be mindful of H<sub>2</sub>O evaporation.

### 2.5.2 *High Surface Area of Exposed Metal Surfaces*

Due to their design, coin cells have a high ratio of exposed metal surface area to electrode surface area. In particular, the positive side of the cell has exposed Ni surface area from the edges and back of the spacer, the spring and the cap, while the negative side has a Sn surface that extends beyond the edges of the negative electrode and separator. These metal surfaces can support parasitic gas evolution via Reactions (1-16) and (1-17). For example, at 2 V the current from these parasitic reactions in a fully charged Ni-Zn cell were observed to be about 100  $\mu\text{A}$ , although that current would be smaller at lower potentials when the cell is in the process of charging. The increased surface area of exposed metals reduces the coulombic efficiency (CE) of the relevant electrode due to this increased parasitic reaction rate. This did not affect any of the analysis in this chapter, but if the CE is an issue, then changing the cell design to reduce the amount of metal component exposure might help. Ideally, the only conducting surfaces that would be exposed to the electrolyte are the electrode materials themselves: active material, binder, conductive support and additives.

### 2.5.3 *Microporous Separator Encasement of the Zn Electrode*

Several successful cells reported in the literature fully encased the Zn electrode with microporous separator,<sup>15</sup> with the exception of a tab for electrical contact, to prevent dendrites from growing around the edge of the separator.<sup>91</sup> Dendrites were witnessed to form around the edges of the microporous separator in some coin cells to cause short circuits, but only seldomly. Dendrites occurred in about 10% of coin cells employing large capacity ( $\sim 8$  mAh) Zn electrodes. This might have occurred because the ZnO electrode material was smeared to the edges of the separator during cell construction. Since the Sn can extend past the edges of the separator and act as the current collector, it is also

possible that Zn simply plated beyond the separator, grew toward the Ni spacer and then short-circuited the cell. However, plating Zn beyond the edges of the separator is likely not favoured since Zn is more likely to plate directly across the separator from the Ni electrode where the path traversed by ions between the electrodes is shortest.

#### *2.5.4 Alignment of Cell Components*

Inexperience with cell construction can also lead to problems if the experimentalist is not careful to keep cell components aligned. Properly aligning the cell components was not difficult, and as long as the researcher pays attention to their work, the following issues should not be serious. Misalignment of either the spacer or Ni electrode with the other and with the plastic gasket can lead to an uneven, and possibly too light, stack pressure distribution. The ductility of the cell can is supposed to help alleviate this, but the effect has not been quantified to determine if it succeeds. Misalignment of the separators with the plastic gasket might allow Zn dendrites to form around the edges as discussed in Section 2.5.3 as well. Finally, misalignment of the Ni and Zn electrodes with each other means there will be overhang and thus some electrode material might be underutilized. This particular issue might resolve itself since Zn favourably plates directly across from the Ni electrode, which might result in the Zn electrode shifting over to re-align itself.

## Chapter 3: Further Applications of the Coin Cell Design

### 3.1 3-Electrode Ni-Zn Coin Cells

In an effort to better understand coin cell behaviour, 3-electrode coin cells using Zn foil as the reference electrode were created. A 3-electrode cell allows a researcher to monitor the potential of both the positive and negative electrodes separately, thereby allowing features in the potential curve of a 2-electrode cell to be unambiguously ascribed to one electrode or the other.

#### 3.1.1 3-Electrode Coin Cell Design

The 3-electrode coin cells were identical to standard Ni-Zn coin cells except for the addition of the reference electrode and a second layer of wetlaid separator. Figure 3-1 shows the cell design and a picture of an assembled cell. The reference electrode was made

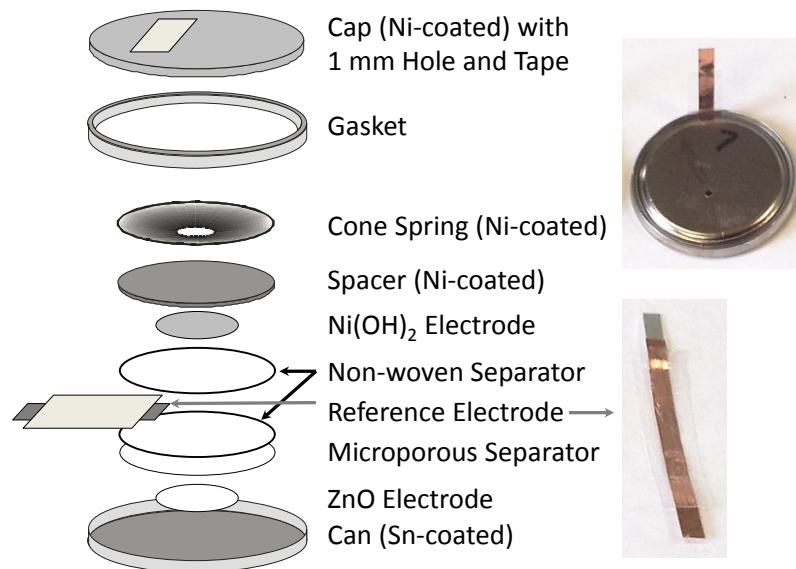


Figure 3-1: A schematic of a 3-electrode Ni-Zn coin cell. The reference electrode is Zn foil spot welded to Cu foil, and then heat-sealed into a plastic sheath, leaving the Zn end exposed to the electrolyte and the Cu end exposed to connect it to the potentiostat. Two non-woven separators provide the compressibility required to spread out the stack pressure around the reference electrode.

by spot welding a piece of 99.98% pure Zn foil (Alfa Aesar, 270  $\mu\text{m}$   $\times$  4 mm  $\times$  2 mm) to a thin strip of 99.99% pure Cu foil (27  $\mu\text{m}$   $\times$  2 cm  $\times$  2 mm). This strip was then sealed within low density polyethylene (plastic) using a TEW Impulse Sealer (heat sealer) such that only the Zn was exposed at one end and a short length of Cu at the other end. The Zn end of the reference electrode was inserted between the two layers of non-woven separator during cell assembly and the Cu end was folded over the cap during cell crimping so as to not interfere with the crimping process.

Ni electrodes were pre-formed in standard 2-electrode Ni-Zn coin cells. To accomplish this, a typical Ni capacity-limited Ni-Zn coin cell was created and cycled to achieve formation as discussed in Section 2.3.2 (pg. 54). Then this cell was carefully dismantled using a cell opener (DPM Solutions) so as not to harm the Ni electrode, which was then transplanted into a fresh 3-electrode coin cell as shown in Figure 3-1. The intention behind transplanting the Ni electrode was to have a 3-electrode coin cell with a previously uncycled Zn electrode that had a lower capacity than the Ni electrode.

### *3.1.2 Ideal Cycling of a Ni-Zn Coin Cell*

Figure 3-2 shows matched cycling behaviour in a Ni-Zn coin cell, where both electrodes finish charging and discharging at nearly the same time. Near the end of charge, the potential of the Ni electrode arched upwards toward  $\text{O}_2$  evolution and the potential of the Zn electrode arched downwards toward  $\text{H}_2$  evolution. This caused a steep rise in the total cell potential that triggered the end of the charge half-cycle. Discharge then commenced until the Ni electrode finished discharging after delivering 96% of its charged capacity. This happened just before the Zn electrode also finished discharging as evidenced by the upward arching of the potential curve of the Zn electrode.

The Zn potential curve is normally assumed to be flat, so it is illustrative to note that the potential range of the Zn electrode during discharge is about 100 mV, which is about half as much as the 200 mV potential range of the Ni electrode. Deiss *et al.* claim that this increase in potential is due to a decrease in conductivity of the Zn active material and, at the end of discharge, to passivation of the small amount of remaining Zn on the current collector.<sup>42</sup>

Of use to researchers working with standard, 2-electrode coin cells are the shapes of the potential curves of the individual electrodes. For example, the potential of the Ni electrode declines relatively sharply when it reaches the end of discharge, whereas the potential of the Zn electrode slopes more gradually towards the end of discharge. With a little practice, this allows a researcher to identify which electrode finishes discharging first by examining the total cell potential curve. If it drops off sharply, the Ni electrode filled with  $H^+$  first; whereas, if it declined gradually it was likely the Zn electrode that finished dissolving all of the Zn from the current collector first. Drawing similar conclusions from the charging portion of the potential curves is more difficult on account of the dependence

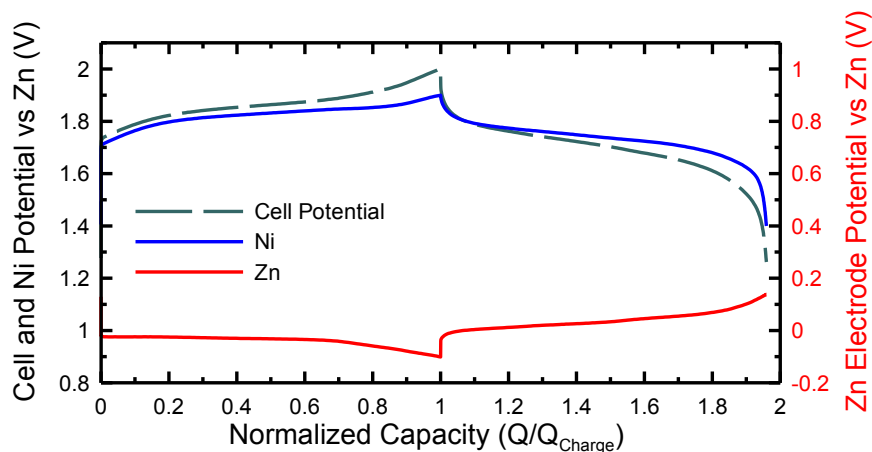


Figure 3-2: The typical charge and discharge curves of well-behaved Ni and Zn electrodes as well as the total cell potential ( $V_{Ni} - V_{Zn}$ ) in a 3-electrode Ni-Zn coin cell. The reference electrode was Zn foil. The right-side y-axis is used only by the red, Zn electrode curve. The x-axis was normalized to the charge capacity of this cycle.



of the shape of the Zn potential curve on the current, as will be shown next.

### 3.1.3 Overcharging a Ni-Zn Coin Cell

Although some published material shows the potential curve of a 2-electrode Ni-Zn cell during overcharge,<sup>67</sup> to the author's knowledge no demonstrations of overcharge have been shown with 3-electrodes. Figure 3-3 shows the overcharging behaviour of a 3-electrode Ni-Zn coin cell at a low current (136  $\mu\text{A}/\text{cm}^2$ ) and high current (634  $\mu\text{A}/\text{cm}^2$ ). This section draws heavily from the material covered in Section 1.4 (pg. 17). Recall that  $\text{H}_2$  and  $\text{O}_2$  evolution technically occur on the negative and positive electrodes, respectively, at nearly all times since the Zn electrode is always below 0.41 V vs Zn ( $E_{\text{eq,H}_2}$ ) and the Ni electrode is nearly always above 1.64 vs Zn ( $E_{\text{eq,O}_2}$ ); however, the corresponding currents are tiny in an ideal cell to allow the electrodes to charge and discharge without significant gas evolution. Gas evolution significantly increases when there is no more Zn to plate on

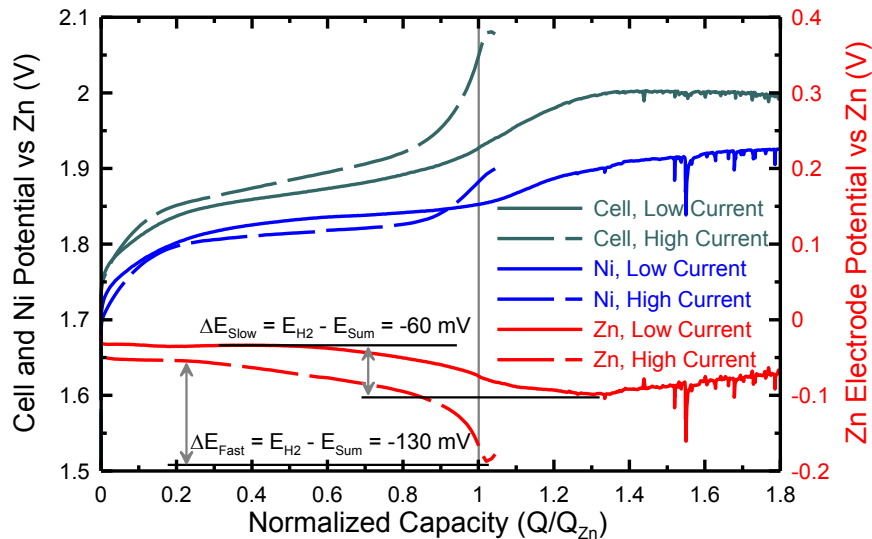


Figure 3-3: Overcharge behaviour of 3-electrode Ni-Zn coin cells. The two cycles shown come from different cells and different cycles so their history is different. The x-axis is arbitrarily scaled to the theoretical capacity of the corresponding Ni electrode. The Zn curves correspond to the right-side y-axis, while the other curves correspond to the left-side. “High” current is 634  $\mu\text{A}/\text{cm}^2$  ( $C_{\text{Zn}}/4$ ) and “low” current is 136  $\mu\text{A}/\text{cm}^2$  ( $C_{\text{Zn}}/6.75$ ). The coin cell design was the standard design discussed in Section 2.2 but with a 3<sup>rd</sup> Zn foil reference electrode.

the negative electrode or when no further  $H^+$  can be removed from the Ni; at that point, the current that is being forced through the cell by the charger causes only gas evolution.

As was briefly described in Section 1.4, the potential difference between charging an electrode and evolving gas depends on the current. At low currents, this difference is only about 60 mV, as evidenced by the “low” current Zn potential curve in Figure 3-3. Whereas at high currents, the potential change of the Zn electrode when the electrode goes from plating Zn to evolving  $H_2$  is more pronounced (about 130 mV) and thus noticeably different from the Ni electrode entering overcharge in the total cell potential curve. This means that a researcher working with a 2-electrode coin cell will not be able to easily determine when a cell begins overcharging the Zn electrode if they are using a low current. If knowing when the Zn electrode is finished charging is important, the researcher should take care to use a high enough current that they will be able to see a slight bump in the total cell potential charge curve (for an example, see Figure 5-7 on page 159).

#### *3.1.4 Overdischarging a Ni-Zn Coin Cell*

To the author’s knowledge, overdischarge is not demonstrated anywhere in the literature, even in 2-electrode cells. Figure 3-4 shows the first cycle of a fresh 3-electrode coin cell in which the Ni electrode is overdischarged. The shapes of these curves are indicative of several processes that are labelled alphabetically and described in the following paragraphs:

(A) The difference between these two curves shows the effect of allowing the Ni electrode to dry for about 1 minute as it was transplanted from the formation cell to the 3-electrode cell. When dismantling the formation cell, the non-woven separator, which is soaked in electrolyte, is normally removed and replaced with a fresh separator in the 3-electrode cell, which is then re-soaked with new electrolyte. The top inset in Figure 3-4

shows the potential curves of the Ni electrode when the separator was replaced (upper, blue) and when the old, wet separator was left attached to the Ni electrode (lower, orange). Evidently in a new cell where the Ni electrode was allowed a moment to dry, a higher Ni electrode potential is required at the beginning of the first charge until proper wetting has been re-established. This might be due solely to the use of a coating-style hydrophobic binder (PVDF binder and NMP solvent) in these Ni electrodes as opposed to the more usual spider web style hydrophobic binder (PTFE binder and shearing forces during slurry mixing). As a reminder, PVDF and NMP were used to make Ni electrodes in this thesis because they make electrode manufacture more facile by sticking to the Ni foil more easily.

(B) The small potential drop in the cell potential here is almost entirely due to the

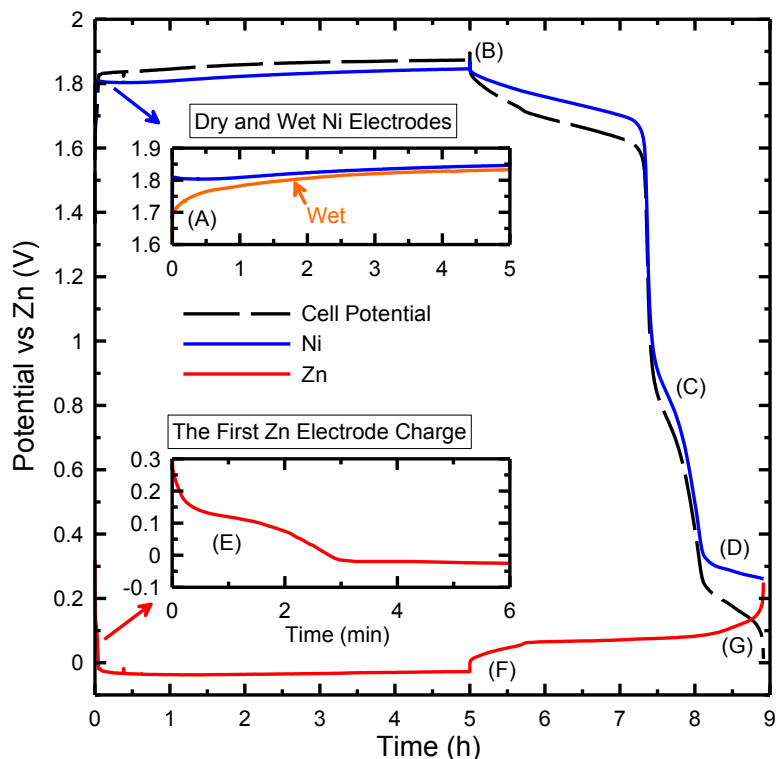


Figure 3-4: Demonstration of overdischarge of the Ni electrode in a 3-electrode Ni-Zn coin cell. These curves also demonstrate the shapes of Ni and Zn curves on the first cycle with a pre-formed Ni electrode. The insets have the same units for their axes as the larger graph except where noted. The top inset shows the Ni potential curves when the separator is (blue) and is not (orange) replaced during cell reconstruction. The bottom inset shows the potential curve during the first charge of a Zn electrode. Letters (A) through (G) are referred to in the text while discussing this data.

Zn electrode switching from plating to stripping Zn. The Ni electrode discharges nearly linearly until it is as filled with  $H^+$  ions, and corresponding  $e^-$ , as it can be without triggering a structural change.<sup>51</sup> Note that the coulombic efficiency (CE) of the 'dry' Ni electrode is 47% in this first cycle, while the pre-wetted Ni electrode delivers 59% in the first cycle (not shown). Evidently, dryer Ni electrodes waste more charge, but of more concern is the fact that even pre-formed Ni electrodes have a poor CE during the first cycle.

Of, perhaps understated, importance here is the fact that the pre-formed Ni electrode finished discharging before the Zn electrode. Further cycling was done to confirm that this is always the case. This means that experiments intending to measure the CE of the Zn electrode as a function of cycle number are not possible with Ni electrodes that are of a similar capacity to the Zn electrode or fully discharged when the first charge half-cycle is initiated.

To have the Zn electrode finish discharging first, the Ni electrode would have to begin in a partially charged state, and would ideally have a significantly larger capacity than the Zn electrode. The state of charge of the Ni electrode would drop each cycle, but until it reached the bottom, the Zn electrode would finish discharging first each cycle. The limits of the electrode construction techniques used in this thesis limited the largest possible Ni electrode to a theoretical capacity approximately twice that of the smallest Zn electrode. This capacity ratio was not enough to test the Zn discharge capacity for more than about 10 cycles given that the  $CE_{Ni}$  was about 96% for most cycles, but notably lower in cycle 1. Larger capacity Ni electrode spreads would not adhere well to the Ni foil current collector and thinner Zn electrodes than a 0.0015" coating did not spread uniformly.

(C) This short plateau is the intercalation of  $H^+$  and  $e^-$  into the small amount of  $\beta$ -NiOOH or  $\gamma$ -NiOOH ( $H_{0.5}K_{0.33}(H_2O)_{0.66}NiO_2$ )<sup>50</sup> that normally does not participate in the intercalation process to maintain conductivity in the  $Ni(OH)_2$  crystallites.<sup>51</sup> The capacity

locked away in this in-active material was 14%, which is in line with the 20% witnessed by Deabate *et al.*<sup>51</sup>

(D) This plateau is H<sub>2</sub> evolution on the Ni surface.<sup>78</sup> Note that Ni evolves H<sub>2</sub> at a potential about 400 mV higher than Zn would. Also note that Ni(OH)<sub>2</sub> does not convert back to Ni + 2OH<sup>-</sup> as would be suggested by Pourbaix,<sup>64</sup> but which is in agreement with what Hall *et al.* observed.<sup>78</sup> If Ni(OH)<sub>2</sub> has been charged to above 1.5 V, then it does not reduce to Ni again during subsequent cathodic polarizations. This was confirmed in cycle 2 (not shown) since no Ni + 2OH<sup>-</sup> → Ni(OH)<sub>2</sub> + 2e<sup>-</sup> reaction occurred, which would have appeared as a plateau around 400-500 mV vs Zn.<sup>78</sup>

(E) The shoulder here at 0.1 V is the plating of dissolved Sn in the electrolyte and/or the underpotential deposition of a monolayer of Zn on the Sn current collector surface.<sup>79</sup> This shoulder is present only in the first charge half-cycle of a new cell.

(F) The steeply sloped rise of the potential of the Zn electrode here is a mystery and its exact shape varied from cell to cell.

(G) As mentioned previously, this upward slope in the potential curve of the Zn electrode is thought to be an increase in electrode resistance as the conduction paths within

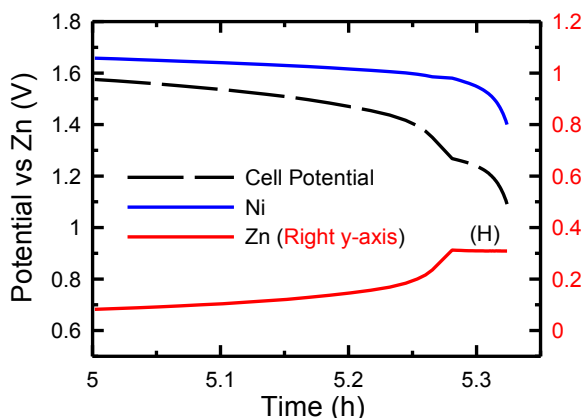


Figure 3-5: Demonstration of overdischarge of the Zn electrode in a 3-electrode Ni-Zn coin cell. The right-side y-axis is used by the Zn curve only and it has the same scale and units as the left-side. Only the end of a discharge half-cycle is shown in order to make the flat plateau obvious. The flat plateau in the Zn curve is Sn dissolution from the current collector and/or coin cell can.

the electrode become thin or disappear. The final upward spike in potential occurs when the active Zn surface area shrinks small enough to trigger passivation.<sup>42</sup>

(H) Figure 3-5 demonstrates the overdischarge of a Zn electrode and shows the resulting dissolution of the Sn current collector at about 0.3 V vs Zn.

### *3.1.5 Concerns with the 3-Electrode Coin Cell Design*

Unfortunately, the reference electrodes employed here sometimes seemed to contribute to cell failure and so should not be used in cycle life experiments intending to cycle more than about 100 cycles. Four factors are of note in this regard although only the last one was really suspected of causing cell failure. (1) The first is the fact that the Zn reference electrode maintains its potential by constantly corroding, albeit at a low rate (about 3  $\mu\text{A}/\text{cm}^2$ ). As such, Zn is constantly entering the electrolyte from the reference electrode, which would eventually contribute noticeably to the available capacity of the Zn electrode. (2) Second, it is difficult to seal the coin cell when there is a tab passing through the seal. Over time, water evaporates through the gaps on either side of the tab and the cell dries out, but this could be solved by sealing the gaps with epoxy. (3) The third issue is that of electrolyte wicking, discussed in detail in Section 4.3 (pg. 126). If the plastic heat seal around the Zn foil of the reference electrode is penetrated, then the electrolyte wicks up the copper foil until it eventually reaches the alligator clip attached to the other end. The copper corroded when this happened, but the corrosion did not seem to affect the reference potential since the reference potential itself is due to the corrosion of Zn. The Zn foil itself was thick enough to withstand corrosion for some time.

(4) Since the electrodes in these coin cells are relatively small and the space between them is thin, the relatively large size of the reference electrode can be an obstruction. Physically, it interrupts the current lines going between the two electrodes,

and the non-negligible thickness of the reference electrode results in a sub-section of the two electrodes that has a higher stack pressure. Surprisingly, this seemingly obvious problem did not seem to cause cell failure. Sometimes dendrites grew to contact the reference electrode, which shorted the potential measurements. However, if this was going to happen at all it seemed to happen during the first charge half-cycle, within the first 2-3 hours; three of the eight 3-electrode cells made shorted this way in the first charge half-cycle. One other cell shorted, but only after 85 hours of cycling (8 cycles). Two other cells failed due to unknown problems: one after 80 hours (13 cycles) and the other after 150 hours (56 cycles). Dismantling the cells did not reveal any obvious explanations. The final two cells did not fail, and finished their experiments: one after 160 hours (20 cycles) and the other after 100 hours (33 cycles). The number of cycles or time to cell failure is not specifically important since each cell was subjected to different tests; they are listed here for the reader's interest and to demonstrate that although some of these cells failed due to the inclusion of the reference electrode, most easily survived long enough to perform useful experiments with them.

### *3.1.6 3-Electrode Coin Cell Conclusions and Future Work*

The 3-electrode coin cell allowed 3-electrode experiments under nearly the same conditions that are experienced by commercial electrodes, which are cycled under stack pressure with a current collector and only a small amount of electrolyte. This section illustrated how a researcher can use a 3-electrode coin cell to explore how the electrodes perform under regular operation and abuse, the latter of which is rarely reported in the literature and usually has to be explored by the experimentalist. Here, it was shown that Zn electrode discharge potential curves are not perfectly flat, that Ni electrode potential curves drop off more steeply than Zn potential curves at the end of discharge, that Sn dissolution

can be identified by an additional plateau at the end of discharge of a 2-electrode cell, and that the onset of overcharging a Zn electrode can only be identified in the potential curve of a 2-electrode cell if the charging current is high enough (about  $C/2$ ). Even if some of these concepts have already been shown in the literature, it is often useful for an experimentalist to reproduce them in their own lab. If they are already using coin cells, then the 3-electrode coin cell design allows them to do so without changing their experimental test vehicle.

The most substantial realization that these 3-electrode experiments revealed was the significance of the low CE of the Ni electrode compared to the Zn electrode. The original purpose of creating a Ni-Zn coin cell was to create a test vehicle for testing the discharge capacity vs cycle number and overall cycle life of new Zn electrode active materials or additives for use in a Zn-air cell. The absence of an air electrode and, presumably, electrolyte evaporation issues was viewed as a simplification to the system that would make experimentation on new Zn electrodes easier. These experiments are not possible unless the electrode opposing the Zn electrode (i.e. Ni in this case) continually outlasts the Zn electrode during each discharge half-cycle. As an aside, in the Li-ion field, where the idea of the coin cell originated, Li metal fulfills the role of a counter electrode that outlasts the opposing electrode during each discharge for hundreds of cycles. As such, Ni-Zn cells are simply not sufficient for testing Zn electrode discharge capacities unless a significantly larger and pre-charged Ni electrode is used or a researcher inadvertently uses a poor Zn electrode that has a lower CE than the Ni electrode.

For future work, the reference electrode can enhance the analysis of a particular effect known to occur at one of the electrodes. For example, a 3-electrode cell could be used to form a Ni electrode, which would allow the acquisition of  $dQ/dV$  data free of negative electrode effects. This might provide a clearer picture than Figure 2-3 and Figure 2-4 of what occurs in the Ni active material during formation. Alternatively, if 3-electrode coin



cells that survived long enough to witness the failings of the electrodes were realized, then the origin of the potential depression at the beginning of discharge observed in cells with titanium (Ti) parts (Figure 2-12B, pg. 73) and at high cycle numbers (Figure 2-19B, pg. 86) could be better explored. The reference electrode itself could likely be improved by using a ring of Zn foil with a larger diameter and thinner thickness than the Zn electrode to avoid having the reference electrode interrupt the current lines between the electrodes or disturb the pressure distribution.

### **3.2 Zn-Air Coin Cells**

Since Ni electrodes were not capable of providing a sufficient counter electrode to Zn, an alternative needed to be found. An air electrode has an effectively infinite supply of O<sub>2</sub> from the environment, so it would not limit the discharge capacity of the cell the way Ni does. As such, efforts were made to obtain bi-functional air electrodes through fabrication or purchase. The task of fabricating durable bi-functional air electrodes was left to another graduate student. Commercial bi-functional air electrodes were hard to acquire and so only primary (i.e. discharge only) commercial air electrodes were successfully obtained. This section demonstrates that Zn-air coin cells can be made and how, but note that only air electrodes that were not designed to be charged were used since those were the only air electrodes on hand. Future research efforts can continue once true bi-functional air electrodes are fabricated or acquired.<sup>95</sup>

#### **3.2.1 Zn-air Coin Cell Design**

Figure 3-6 shows two designs for Zn-air coin cells; Figure 3-6A is the design used in experiments presented here, while Figure 3-6B shows an alternate coin cell design. Many components in Figure 3-6 are the same as those in Figure 2-1 (pg. 50) and have the same

roles. Beginning at the cap and working downward, cell design A includes a Ni-Cr wire mesh that acts as a simple air flow plate to promote an even distribution of oxygen over the air electrode surface. The non-rechargeable air electrode itself was made with a non-conductive Teflon coating, which was oriented towards the air hole, and necessitated a means of electrically connecting the electrode to the cap. This was achieved by using a “figure-8” shaped Ni foil cut-out that was wrapped around the air flow plate and electrode to make contact with the conductive bottom of the air electrode. Two non-woven separators were used to thicken the stack height and thereby increase the stack pressure to about 1,000 kPa using pressure film as described in Section 2.2.7 (pg. 52), except by placing the pressure film where the Zn electrode was normally located.

If a thicker coin cell canister with enough space inside is available, the alternate coin cell design B might work better. In this design, a Teflon microporous membrane would be sealed to the cap around the hole(s) to passively reduce the evaporation of H<sub>2</sub>O and a Ni wave spring would provide stack pressure. It would also include a machined air flow plate

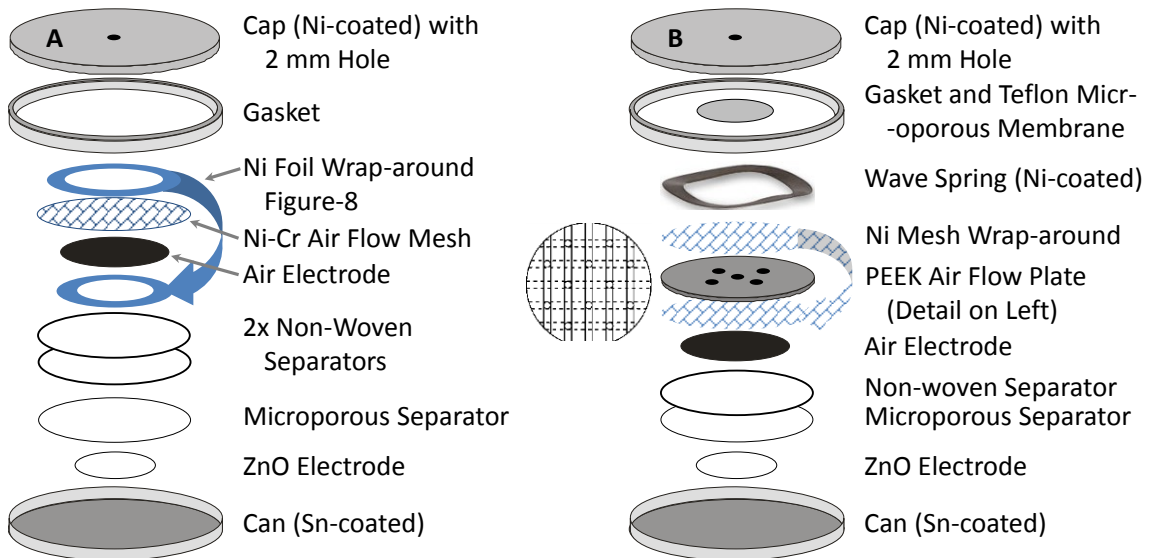


Figure 3-6: The Zn-air coin cell designs used for this thesis. The “Ni Mesh” and “Ni Foil” wrap-arounds were single pieces of material in the shape of a “figure-8”, or dumbbells, and folded to wrap around non-conductive components. The air flow plate is a plastic (PEEK) disk with 12 holes drilled in it, and 5 troughs dug into each side, as shown, to allow air to easily pass to any point of the air electrode.

made of PEEK plastic, which is strong, easily machinable and resistant to alkaline electrolyte. The wrap around Ni mesh provides electrical contact to the top side of the air electrode.

Design A was sufficient for a simple proof-of-concept demonstration and cells were constructed as shown in Figure 3-6. During cell fabrication, about 110  $\mu\text{L}$  of 6 M KOH, saturated with ZnO, electrolyte was used to soak the two non-woven separators. The cell was cycled at room temperature using a Bio-Logic VMP3 potentiostat.

### 3.2.2 Zn-air Coin Cell Cycling

Figure 3-7 shows the discharge capacity, in the form of the coulombic efficiency, as a function of cycle number for a Zn-air coin cell. The air electrode was kindly donated by Dr. Yi-Cheng Lee, a Taiwanese researcher, and was designed for non-rechargeable cells, but this does not mean it cannot be charged; it means that it will likely break down faster than a bi-functional air electrode during cycling. The catalyst was  $\text{MnO}_2$ , but Dr. Lee said that the manufacturer would not disclose the catalyst loading and current collector material. The Zn electrode of the cell depicted in Figure 3-7 had a capacity of 2.8 mAh. Along the lines of other researchers,<sup>118</sup> this cell was charged to 2 mAh (about  $2/3$  of its theoretical capacity,  $Q_T$ ), and then only 1 mAh was discharged ( $1/3 Q_T$ ), both at a rate of 1 mA (about  $C/3$ ). Discharge was also terminated at 1.0 V in case all of the Zn dissolved off of the current collector.

Since the potential drops to 1.0 V in the 4<sup>th</sup> discharge, it seems the extra 1 mAh of capacity that was charged in the first cycle was consumed within the first four discharge half-cycles. This is consistent with the observed coulombic efficiency (CE) decay evident in cycles 5 – 20 (see the linear equation in Figure 3-7). Extrapolating backwards, the CE in cycle 1 should have been 80%, decaying linearly to 76% in cycle 4. Based on this

extrapolation, the difference between the sum of what was likely charged in each of cycles 1 to 4 and the sum of what was actually discharged was 0.89 mAh, which is close to the 1 mAh of extra charge available from cycle 1. It is unlikely that the drop in potential to 1.0 V at the end of the 4<sup>th</sup> discharge was due to the air electrode drying out since the shape of the discharge curves match the shape of Zn electrodes approaching depletion as seen in the 3-

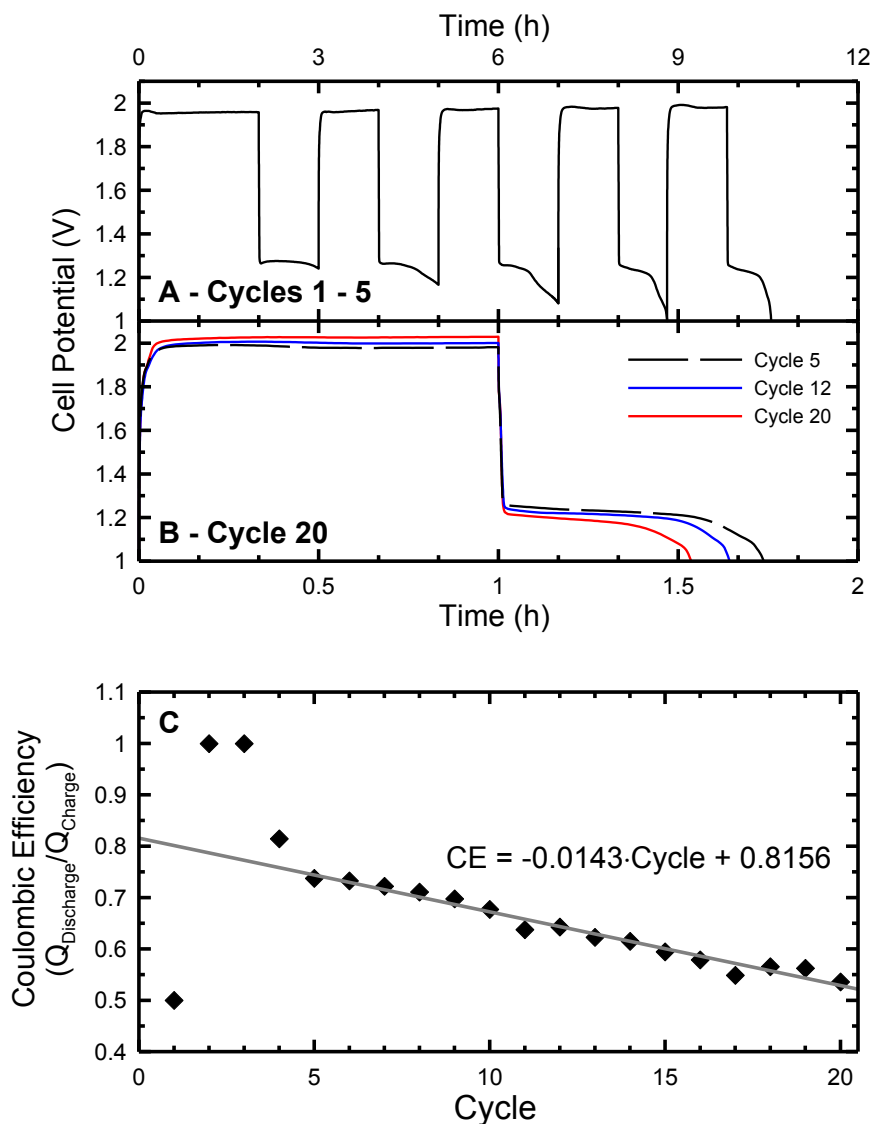


Figure 3-7: The cycling of a Zn-air coin cell. The constant current for both charge and discharge was 1 mA, while the theoretical capacity of the Zn electrode was 2.8 mAh. The first charge half-cycle was 2 mAh, while all other half-cycles were limited to either 1 mAh or reaching a lower potential of 1.0 V (as was the case in cycles 4 to 20). Panels A and B are example V vs t plots to demonstrate the decay of the cell's potential and capacity. Panel C shows the coulombic efficiency and a line of best fit to cycles 5 – 20 inclusive.

electrode cells of Section 3.1.4 (pg. 97).

The decay in CE of the Zn electrode is likely due to an increase in a combination of Mn(II)/Mn(III) shuttling between the electrodes as described in Section 1.9.2 (pg. 31) or an increase in the H<sub>2</sub> evolution rate on the zinc electrode due to the presence of Mn(OH)<sub>2</sub>.<sup>21, 97</sup> Increasing amounts of Mn likely dissolved off of the air electrode during each charge half-cycle since the potential during charge rose above the critical potential for MnO<sub>2</sub> dissolution (1.9 V vs Zn), and so the shuttling mechanism was likely the cause of the continuing decrease in the CE of the Zn electrode. Note that any Mn(OH)<sub>2</sub> that precipitated on the Zn electrode would not be further reduced to Mn because the potential of the Zn electrode did not reach the required ~ -0.26 V vs Zn during charge.<sup>81</sup> It is unclear how much MnO<sub>2</sub> would need to dissolve to significantly affect the parasitic H<sub>2</sub> evolution rate (*i*<sub>H2</sub>) and self-discharge rate (*i*<sub>SD</sub>) of the Zn electrode since it is unknown whether the Mn shuttling process occurs through a one- or five-electron process (see Section 1.9.2, pg. 31). Note that the small dips in the CE around cycles 11 and 17 were likely due to the daily temperature cycle of the lab since these cells were not cycled in a temperature-controlled box. The temperature was about 22 ± 4 °C.

Also of note is the small but steady increase in the cell resistance, evident by the increasing cell potential during charge and decreasing cell potential during discharge. Since the kinetics of the Zn electrode reactions are quite fast, this trend is likely due to a decreasing catalytic active surface area on the air electrode, which supports the dissolving MnO<sub>2</sub> theory, but it could also be due to the destruction of the support structure of the air electrode as described in Section 1.9.1 (pg. 30). Either way, to continue research on Zn-air coin cells, researchers should focus on acquiring or fabricating durable bi-functional air electrodes.

### 3.2.3 Zn-air Coin Cell Conclusions and Future Work

This section demonstrated how to make a functional Zn-air coin cell. The cycle life was short, but this was likely due to the air electrode, which was not designed to be charged. For continuing research efforts, using Zn-air cells instead of Ni-Zn cells to test Zn electrodes would be advantageous since the coulombic efficiency of the air electrode is not important. This is in contrast to the Ni electrodes used in this thesis that repeatedly showed inferior coulombic efficiencies to Zn electrodes, which made measuring Zn electrode discharge capacities difficult since the Ni electrode finished discharging before the Zn electrode. As such, future work should concentrate on acquiring or developing a durable bi-functional air electrode that survives many cycles (and thus does not use  $\text{MnO}_2$ ). For instance, Chen *et al.* have recently shown that a stainless steel mesh with a non-Mn catalyst grown directly onto the mesh, thereby avoiding corrodible binder materials, is quite durable.<sup>95</sup> Alternatively, future work could continue relatively quickly if a suitable air electrode were found commercially or through collaboration with another lab.

Also of note for future research is the looming issue of water management for (non-flooded) coin cells. The data in Figure 3-7 took about 36 hours to collect, so evaporation was not an issue in this case since the evaporation rate was about  $2 \mu\text{L}/\text{day} = 3 \mu\text{L}$  out of  $110 \mu\text{L}$ . However, any future work with long cycle life Zn-air coin cells will have to determine how to seal the Teflon microporous membrane to the cap and/or use a humidity-controlled chamber to house the coin cells in order to remove water management as a source of experimental error.

### 3.3 Aqueous Lithium Manganese Oxide Zinc ( $\text{LiMn}_2\text{O}_4$ -Zn) Coin Cells

Recently, Yan *et al.* demonstrated a cell using lithium manganese oxide ( $\text{LiMn}_2\text{O}_4$ ) as the positive electrode and Zn as the negative electrode that they claimed could last 4,000

cycles in a Swagelok style cell.<sup>167</sup> They did not mention the amount of metal in contact with the electrolyte nor the volume of electrolyte they used nor the amount of stack pressure, if any. In order to determine if the  $\text{LiMn}_2\text{O}_4$  – Zn cell chemistry worked as claimed,  $\text{LiMn}_2\text{O}_4$  – Zn coin cells were fabricated and cycled. The theoretical operation of these cells and a simple theoretical model of the volumetric energy density are presented in Appendix A, Section A.5 (pg. 198).

### 3.3.1 $\text{LiMn}_2\text{O}_4$ -Zn Coin Cell Design

The electrolyte was the same as that used by Yan *et al.*:<sup>167</sup> 3 M LiCl (Aldrich 99+%) and 4 M  $\text{ZnCl}_2$  (Sigma 98+%) with the pH adjusted upward to 4 using LiOH (Sigma-Aldrich 98+%). Yan *et al.* did not reveal what they used as the positive ( $\text{LiMn}_2\text{O}_4$ ) side component materials, but they used graphite foil for the positive current collector, and stainless steel (SS) 316 as the negative (Zn) side current collector. In order to determine which materials should be used for the positive and negative side components to avoid parasitic gas evolution, as was shown in Figure 2-8 (pg. 63), several coin cells were created with the

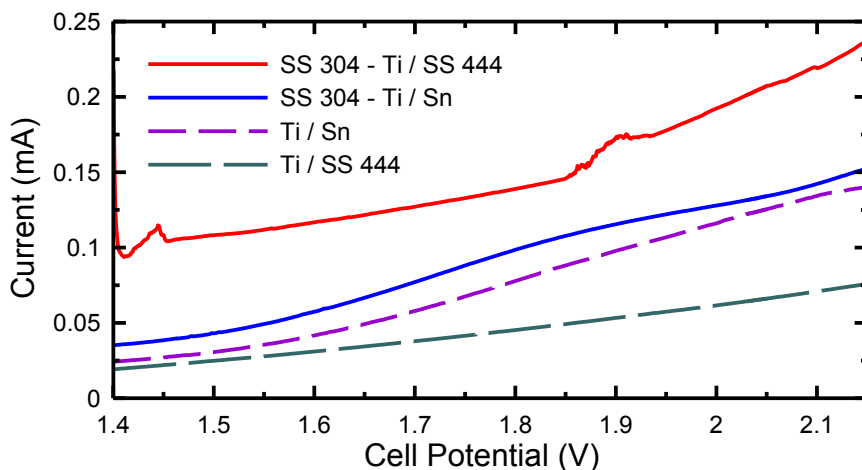


Figure 3-8: Current drawn by oxide layer formation and  $\text{O}_2$  evolution on coin cell components within the potential range of the  $\text{LiMn}_2\text{O}_4$  – Zn system. The electrolyte was 3 M LiCl, 4 M  $\text{ZnCl}_2$ , trace LiOH at pH 4. In the legend, the materials before the slash (/) are the positive side components and the material after the slash is the canister material. For example, “SS 304 – Ti / SS 444” means the cap and spring were SS 304, the spacer was Ti and the canister was SS 444.

electrolyte above and various materials on the positive and negative sides of the coin cell but with no  $\text{LiMn}_2\text{O}_4$  electrodes. Stainless steel (SS) 304 was tested as a positive side component material since the coin cell caps, springs and spacers on hand were made of that material. Ti was also tested because it is resistant to acid. The coin cell canisters were made of SS 444, so that material was tested as a negative side component material, along with tin (Sn) since it has a high overpotential for  $\text{H}_2$  evolution and should be stable in pH 4 electrolyte at the potential of the Zn electrode, according to Pourbaix.<sup>64</sup> These cells were subjected to a linear potential sweep up to 2.15 V and down to 1.4 V, several times, each at a sweep rate of 10 mV/s.

Figure 3-8 shows the results of these potential sweeps. Any detected current at a particular potential arose from parasitic reactions at the positive side components since Zn plating dominated at the negative electrode (which acted as the counter electrode and reference electrode in this situation). As such, the material combination that gave rise to the least current signal during the first sweep was qualitatively declared to be the best material to use. In decreasing order, the favoured material combinations were (positive side – negative side): (Ti / SS 444) > (Ti / Sn) > (SS 304 – Ti / Sn) > (SS 304 – Ti / SS). Here, SS is Stainless Steel, and SS 304 – Ti is a SS 304 cap and spring with a Ti spacer. As per these results, a Ti sputter-coated cap and spring, a pure Ti spacer and a stainless steel 444 canister were used in the fabrication of the  $\text{LiMn}_2\text{O}_4$  – Zn coin cells reported here.

$\text{LiMn}_2\text{O}_4$  electrodes were fabricated along the same lines as described in Section 2.2 (pg. 47). They consisted of 83 wt%  $\text{LiMn}_2\text{O}_4$ , 10wt% C45 carbon black conductive support, and 7 wt% PVDF binder. Double the powder mass (2g) of NMP solvent (4g) was added to dissolve the binder and form a slurry. The slurry was mixed in a Mazerustar planetary mixer for 10 min, then spread onto graphite foil using a 0.006 “ notch bar and finally dried in air in an oven at 80°C for 2 hours. 1.27 cm diameter disks were punched from the foil,



and used to make coin cells, along with one layer each of nonwoven (700/30K from Freudenberg) and microporous (3407 from Celgard) separators.

### 3.3.2 $\text{LiMn}_2\text{O}_4$ -Zn Coin Cell Cycling

$\text{LiMn}_2\text{O}_4$ -Zn coin cells were cycled at a 4C rate, the same as that used by Yan *et al.*, with charge ending at 2.15 V to avoid overcharging the  $\text{LiMn}_2\text{O}_4$  electrode and discharge ending at 1.4 V. Figure 3-9 shows a representative coin cell that had the same cycling behaviour as the other 3 identical cells used in this experiment. In cycle 0, the charged capacity is 0.445 mAh, which translates into 107 mAh/g  $\text{LiMn}_2\text{O}_4$  as expected for this material. The cell only returned 0.335 mAh during discharge though, since the Zn electrode finished discharging first, triggering the end of discharge at 1.4 V. The reason for this 75% CE in cycle 0 is unclear, but it does not persist in subsequent cycles when the CE of the Zn electrode increases to a more usual 98.9%. The 98.9% CE of the Zn electrode is directly observable in Figure 3-9C since the capacity of any given cycle was 98.9% of the previous cycle capacity up to around cycle 100. This is also evident in panel B, where it is apparent that as cycling continued the cell potential at the beginning of charge began higher up the  $\text{LiMn}_2\text{O}_4$  potential curve and the discharge potential curve dropped off sooner. This behaviour is proof that the  $\text{LiMn}_2\text{O}_4$  electrode was not fully discharged each cycle, and so its state of charge kept increasing, which in turn shortened the amount of time spent charging since the end of charge was triggered when the potential of the  $\text{LiMn}_2\text{O}_4$  electrode spiked upward to 2.15 V. In panel C, the bump around cycle 160 occurred when the initial cell potential surpassed the bump in panel B around 9 min (see the potential curves of cycles 120 vs 200). The bump in the potential curve occurred when half of the Li sites within the  $\text{LiMn}_2\text{O}_4$  had been vacated, and the repulsive force between the Li atoms in the two Li sublattices had disappeared.<sup>168</sup> The increase in discharge capacity around cycle 160 was due to

discharging the Zn electrode to a lower potential, which also increased the CE. After about cycle 180 in panel C, the CE of the Zn electrode had increased to 99.7%, but continued to limit the cell discharge since the  $\text{LiMn}_2\text{O}_4$  electrode continued to be pushed up its potential

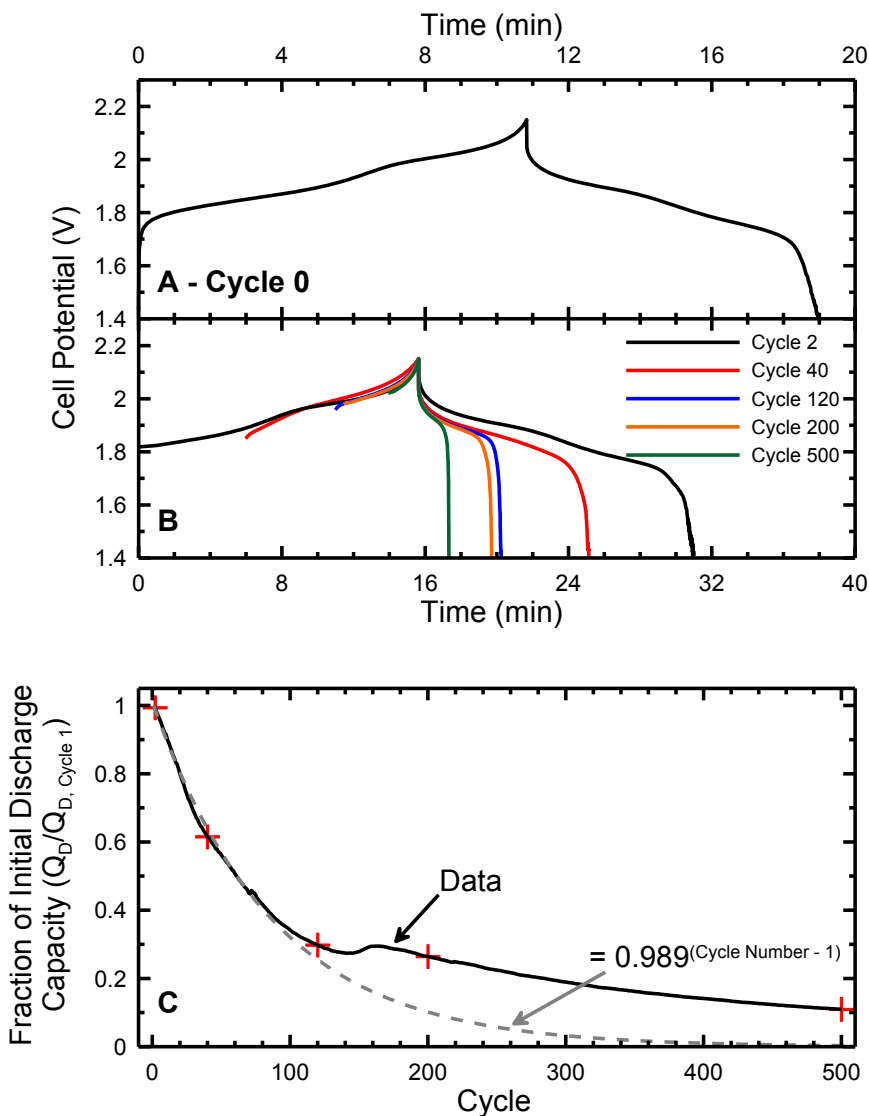


Figure 3-9: The cycling of an example  $\text{LiMn}_2\text{O}_4$  – Zn coin cell. The charge and discharge currents were  $4C$  for all cycles where  $C$  was the theoretical Li electrode capacity for Cycle 0 (panel A) and then  $C$  was readjusted to equal the discharge capacity of Cycle 0 (0.335 mAh) for cycles 1 - 1000. Panel B shows the potential curves of several cycles intentionally centered at the top of charge (2.15 V) to show that the potential curves are mostly co-linear. Each cycle was shifted along the time axis so that it finished charging at the same time as Cycle 2 did (15.64 min). Panel C shows the first 500 cycles of cycling, and an  $x^{\text{Cycle Number}-1}$  fit to the first 100 cycles. Although the cell was cycled 1000 times, the undisclosed cycles continue to decay in the same manner as cycles 200 – 500. The crosses indicate the positions of cycles 2, 40, 120, 200 and 500.

curve.

Closer inspection of Figure 2a in Yan *et al.*'s paper revealed that they overcharged their cell every cycle, but since they did not explain their cycling procedure, this was not obvious.<sup>167</sup> Because the coin cell cycled in Figure 3-9 had a CE that hovered around 99%, it is likely that if a cell was overcharged to 101% of its initial capacity every cycle, its discharge capacity would remain high throughout more cycles. Indeed, this might be exactly how Yan *et al.* kept their discharge capacity close to 100% for 1,000 cycles.

Figure 3-10 shows two LiMn<sub>2</sub>O<sub>4</sub>-Zn coin cells that were identical to the ones cycled in Figure 3-9 with the following differences: A pressure release valve (hole with tape) was added to the cap to allow excess O<sub>2</sub> to escape, the temperature was maintained at 30.±0.1°C, charge was limited by capacity (or time), and discharge was limited to 1.5 V. Until the cells shorted around cycle 30, it is evident that the LiMn<sub>2</sub>O<sub>4</sub> – Zn cell can indeed maintain its discharge capacity as Yan *et al.* claim, and there is effectively no difference between overcharging by 3% or by 10%.

However, overcharging the cell every cycle consumes the electrolyte and risks short circuiting due to dendrite growth. Hypothetically, if the hydrolysis of water is limited to the

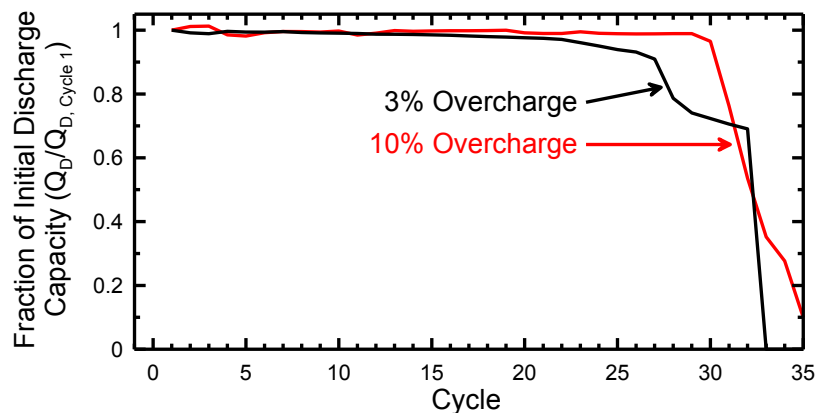


Figure 3-10: Discharge capacity of LiMn<sub>2</sub>O<sub>4</sub> – Zn coin cells that are overcharged each cycle to ensure that the Zn electrode has more capacity than the LiMn<sub>2</sub>O<sub>4</sub> electrode. These two cells had pressure release valves, and failed after cycle 30 from short circuits due to dendrites and/or electrolyte leakage. T = 30°C.

extra 1% mentioned above, and if a coin cell has 50  $\mu\text{L}$  of electrolyte but can only lose half of that (25  $\mu\text{L}$ ) before failing, then given that hydrolyzing water consumes 2,980 Ah/L, a coin cell could withstand 74 mAh of overcharge before failing. For a typical coin cell here with a realized maximum initial capacity of about 0.35 mAh and thus an overcharge of 0.0035 mAh per cycle, this would mean the electrolyte would not limit the cell's performance until after 21,000 cycles. In which case, hydrolyzing the electrolyte is likely not a threat to a coin cell or to the Swagelok-style cell used by Yan *et al.*, but it might be of concern in a commercial cell if the cell performance is sensitive to the concentrations of LiCl and  $\text{ZnCl}_2$  in the electrolyte. The dendrite threat could be mitigated by using a high pressure-release valve. This would allow the internal partial pressure of  $\text{O}_2$  to rise high enough to cause dendrite consumption via Reaction (1-19), but it must be noted that such consumption would eliminate capacity from the Zn electrode. If the purpose of overcharging is to increase the capacity stored in the Zn electrode then dendrite consumption negates the purpose of overcharging the cell in the first place.

### 3.3.3 $\text{LiMn}_2\text{O}_4$ -Zn Coin Cell Conclusions and Future Work

This section demonstrated that  $\text{LiMn}_2\text{O}_4$  – Zn cells in their current form require overcharging every cycle to deliver maximal discharge capacities over hundreds of cycles, which has not previously been demonstrated in the literature. This necessitates the use of a vented cell, since excess  $\text{O}_2$  produced in the cell would eventually negate the benefit of overcharging by consuming equal amounts of Zn. This concept of overcharging a vented cell to get one electrode to last longer than the other could be used in Ni-Zn cells to charge a Ni electrode more than the opposing Zn electrode, thereby allowing the Zn electrode to finish discharging first during the subsequent discharge half-cycle (as was done in Chapter 5).

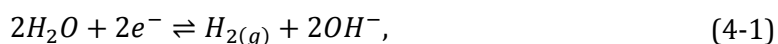
Any future work on  $\text{LiMn}_2\text{O}_4$ -Zn cells should focus on two main goals: First, the Zn electrode coulombic efficiency must be improved or a balance must be struck with a pressure-release valve to allow a small amount of overcharging to take place without oxidizing too much Zn. Second, as argued in Appendix A, Section A.6 (pg. 199), the LiCl concentration of the electrolyte limits the energy density of the cell, and so it must be increased for the energy density to become commercially competitive. The CE of the Zn electrode could likely be improved over the results presented here by using a negative electrode current collector with a higher overpotential for  $\text{H}_2$  evolution than SS 444 or possibly by using purer  $\text{ZnCl}_2$ .

## Chapter 4: Self-Discharge Experiments Using Metal Foil

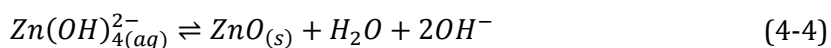
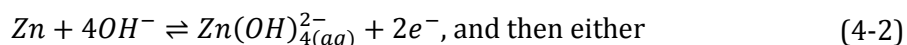
### 4.1 Motivation

One of the critical concerns for both research and commercial cells is self-discharge, which was described in Section 1.7 (pg. 24), but the reactions are reproduced in more detail below. No matter which system a researcher is working with, minimizing the self-discharge rate is important. Specifically, low self-discharge rates in commercial cells enhance marketability.<sup>169</sup> In research, the coulombic efficiency ( $Q_{\text{Discharge}}/Q_{\text{Charge}}$ ) is a commonly used measure of various phenomena in a cell.<sup>170</sup> It is affected by parasitic reactions, self-discharge and loss of active material. This means that a quantitative conclusion about the rate of loss of active material in a cell cannot be made using the CE unless the parasitic and self-discharge rates are known exactly, or known to be small in comparison to the phenomenon being measured. For example, the CE of a particular cycle of a Ni-Zn cell might be 95%, but it would be more useful to know how much of the lost 5% was due to self-discharge, parasitic currents or a loss of active material. This knowledge would help explain why cells fail.

Overall, the self-discharge mechanism involves

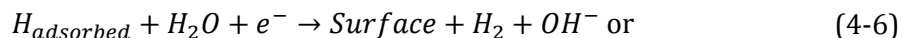
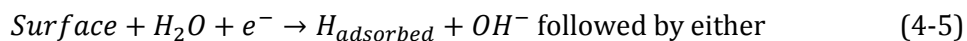


which occurs on either the Zn deposit or the current collector, while simultaneously



occur. Each of Reactions (4-1), (4-2) and (4-4) can be broken down into mechanistic steps.

Trasatti<sup>63</sup> explained the two possible mechanisms for H<sub>2</sub> evolution as



where Surface is a surface site that H can adsorb onto. Trasatti<sup>63</sup> summarizes that the rate determining step (rds) for H<sub>2</sub> evolution is Reaction (4-5) on “poorly active electrodes, for instance, lead and mercury”, while other authors have suggested that this is also the rds on Cu,<sup>171</sup> Ni<sup>172</sup> and Zn.<sup>65, 173</sup> Due to a lack of agreement in the literature (which will be discussed throughout the chapter) the rds of the entire self-discharge mechanism was unknown at the time this research was initiated. Throughout this chapter, the results obtained support the idea that, within the constraints of the present experiments, the rds for the entire self-discharge mechanism is Reaction (4-5) on the current collector (as opposed to on Zn). For this to be the case, the self-discharge rate should vary with the activity of water,  $a_{H_2O}$ :

$$rate = k \cdot a_{H_2O}, \quad (4-8)$$

where k is the rate constant, which increases with the surface area on which the reaction is occurring.

The self-discharge rate of Zn in alkaline electrolyte has historically been measured using the volume of H<sub>2</sub> evolved<sup>132, 174-176</sup> or using linear sweep voltammetry.<sup>145, 146, 165, 177-180</sup> Alas, measuring the volume of H<sub>2</sub> evolved is often done with Zn powder or pure pieces of Zn metal, which neglects the conditions in a battery-like cell (like a coin cell), in which the volume of electrolyte is small compared to the amount of Zn, a current collector is present, and ZnO powder might be present.<sup>14, 132, 164</sup> Furthermore, producing enough H<sub>2</sub> to make reliable measurements with simple equipment requires larger amounts of active material than the amount typically used in coin cells and other ~1 cm<sup>2</sup> scale experimental cells, since only about 1 μL H<sub>2(g)</sub> / (h×cm<sup>2</sup>) is produced by a self-discharge rate of 2.5 μA/cm<sup>2</sup> (i.e. 0.400

mL gas/mAh);<sup>14, 132, 164, 175, 179</sup> for comparison the reader will see later that the self-discharge rates reported here are around 3  $\mu\text{A}/\text{cm}^2$ .

With regard to linear sweep voltammetry, it seems that most authors using this technique since 2000 are not using it properly.<sup>145, 146, 165, 179, 180</sup> To be specific, Baugh *et al.* demonstrated that careful measurements of the Tafel slope of  $\text{H}_2$  evolution and Zn dissolution could be used to calculate the Zn corrosion current (and determined it was 5.8  $\mu\text{A}/\text{cm}^2$ ).<sup>178</sup> However, authors like Lee *et al.*, Kim *et al.* and Dobryzzycki *et al.* use linear potential sweeps but do not calculate Tafel slopes.<sup>145, 146, 165, 179</sup> Instead, they simply claim that since the additives they are testing alter the Tafel curve at currents far higher than the actual self-discharge current (ex. Lee used currents up to 400 mA (no area reported), Kim up to  $\sim 5 \text{ mA}/\text{cm}^2$  and Dobryzzycki up to  $2 \text{ mA}/\text{cm}^2$ ) that those additives will be equally effective at the corrosion potential where the current is orders of magnitude lower. What all three of those papers demonstrate is that the shape of the current vs potential curves does change with the addition of additives, which prevented the Tafel plot from being linear and thus likely prevented the calculation of Tafel slopes. Therefore, linear sweep voltammetry does not seem to be an appropriate method to determine the effectiveness of corrosion inhibiting additives.

As such, a new method was developed to measure the self-discharge rate of any electrode as a (coarse) function of time without the need to measure  $\text{H}_2$  volume. The method is powerful in its simplicity, in that it directly measures how much capacity has been lost as a function of the time that the electrode has been left to sit, and is described in the Experimental Methods section, below. This method is also better than the linear sweep voltammetry method since effects (like additives) that apparently de-linearize the Tafel slope do not interfere with it.



Many factors have been reported to affect the Zn corrosion rate, including the temperature, presence of ZnO, amount of Zn vs electrolyte, time, KOH concentration, active surface area, current collector and additives.<sup>14</sup> The effect of temperature was not explored here, but has been by others; for instance Snyder *et al.* found that the gassing rate increased by a factor of 4 – 7 when the temperature was increased from 25°C to 50°C.<sup>14, 132, 174, 175</sup>

Early on in this project it was discovered that keeping undissolved ZnO<sub>(s)</sub> powder in the electrolyte reduced the self-discharge rate significantly, presumably because it keeps the electrolyte saturated with Zn(OH)<sub>4</sub><sup>2-</sup>, and so this practice was adopted for all of the experiments presented here. In a battery-like cell, it is common to have some ZnO exposed to the electrolyte, even at “full” charge.<sup>15, 18, 44</sup>

The ratio of Zn to electrolyte was found to effect the self-discharge rate, with a higher mass ratio of Zn to electrolyte yielding a slower rate; for instance Meesus *et al.* noted a 3-fold decrease in H<sub>2</sub> evolution in going from 5 g Zn / 100 mL electrolyte to 100 g Zn / 100 mL electrolyte.<sup>176</sup> Consequently, battery-like cells should have lower self-discharge rates than flooded cells since battery-like cells usually have only enough electrolyte to soak the electrodes and separators.<sup>132</sup> Unfortunately, the low CE of the Ni electrode developed in Chapter 2 and the absence of a Mn-free air electrode prevented the experiments in this chapter from being performed with coin cells. So instead, a flooded cell was used to demonstrate the method and determine how the remaining five variables affected the self-discharge rate in that apparatus. Those five variables will be discussed in Sections 4.4.1 to 4.4.5.

## 4.2 Experimental Methods

### 4.2.1 3-Electrode Cell Design

A simple 3-electrode flooded cell was used, wherein metal foils were dipped into an electrolyte solution that sometimes contained additives, charged (Zn plated) and then left to sit for a period of time. Subsequently, the cells were discharged and the remaining capacity was recorded, thus determining how much capacity was lost to self-discharge or parasitic reactions.



Figure 4-1: Experimental apparatus for the foil experiments. The container is a 125 mL Nalgene bottle. The rods are brass and are soldered to Ni plated alligator clips (some with teeth, others flat). Foils of particular widths and heights are cut and partially covered in water resistant epoxy such that  $1.00 \pm 0.05$  cm remained uncovered from epoxy to bottom edge.

Figure 4-1 shows the experimental apparatus designed for these experiments. The container is a 100 mL Nalgene bottle, with three holes drilled in the lid that tightly allow three brass rods to be pushed through. Nickel-plated alligator clips (some with teeth, others without) were soldered to one end of the brass rods, while female banana connectors were soldered to the other end to allow facile connection with the VMP3 potentiostat (Bio-Logic). A lid with no air flow to the environment was used in order to avoid evaporation, which would increase the electrolyte concentration. Experiments were performed with air in the Nalgene bottle. A few experiments were performed with Ar gas instead, to determine if the reduction of Zn by  $O_2$  contributed to the self-discharge rate, and no difference in rate was found. Foils were used as electrodes since polishing soft metals like Sn and Pb is difficult and since real current collectors are not polished. The mid-sections of the foils were coated in Marine Epoxy (LePage) to prevent wicking of the electrolyte (electroosmosis) and keep the electroactive surface area constant. Electrodes were dipped into the electrolyte far enough to submerge the exposed foil bottom, but leave the upper exposed foil top above the surface. 40 mL of electrolyte was used in all experiments. The reference and counter electrodes were both Zn foil (0.27 mm thick, Alfa Aesar 99.98%) and the counter electrode had a surface area 20% larger than the working electrode. Any increase in the working electrode surface area through Zn dissolution and re-plating after the first charge/discharge cycle was likely matched by an increase in the counter electrode surface area. The working electrode foils were usually Cu (99.999%) or Sn (99.9%) from Alfa Aesar.

The electrolyte was created by making a concentrated KOH solution (usually about 5 M) using 45 wt% KOH solution from Alfa Aesar and nanopure water (18 M $\Omega$ ). An aliquot of this solution was then titrated with potassium hydrogen phthalate to determine its exact concentration using a Mettler DL-21 (auto-)titrator. The primary batch of KOH electrolyte

was then diluted to the desired concentration. ZnO powder (Anachemia, reagent grade) was then dissolved into solution using heat and stirring. Extra ZnO powder was intentionally left at the bottom of each solution bottle and experimental vessel to maintain the ZnO saturation concentration. If this was not done, then self-discharge rates were significantly higher than reported here. This mimics the situation in a cell where there would be some small amount of uncharged ZnO left in the electrode.<sup>15, 18, 44</sup> The working electrode was about 5 – 10 mm from either the counter electrode or ZnO reservoir and about 2 – 5 mm from the reference electrode.

#### 4.2.2 Cycling Method

Figure 4-2 shows an example of the “charge-wait-discharge” cycling procedure presented here. The working electrode was first charged by plating Zn onto it from solution at 3 mA/cm<sup>2</sup> for 10 min (green line) and then discharged at the same rate, which stripped the Zn off again until the potential rose to 0.25 V vs Zn (blue line). Unlike that shown in Figure 4-2, this was repeated about 10 times until the CE converged (see Figure 4-3). Then the electrode was charged once more and left to sit in the electrolyte for increasing amounts

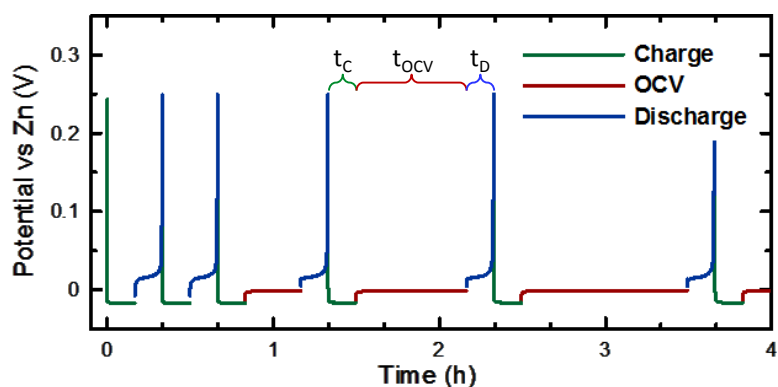


Figure 4-2: Demonstration of the typical OCV self-discharge experimental method. The foil is cycled a few times to prepare the surface, and then subjected to consecutively longer open circuit (OCV) steps between charge and discharge. Each subsequent discharge measures how much active material was left after the open circuit voltage step. The reference and counter electrodes were both Zn foil while the working electrode was Cu foil. The current was 3 mA/cm<sup>2</sup> and the electrolyte was 3.2 M KOH, saturated with ZnO.

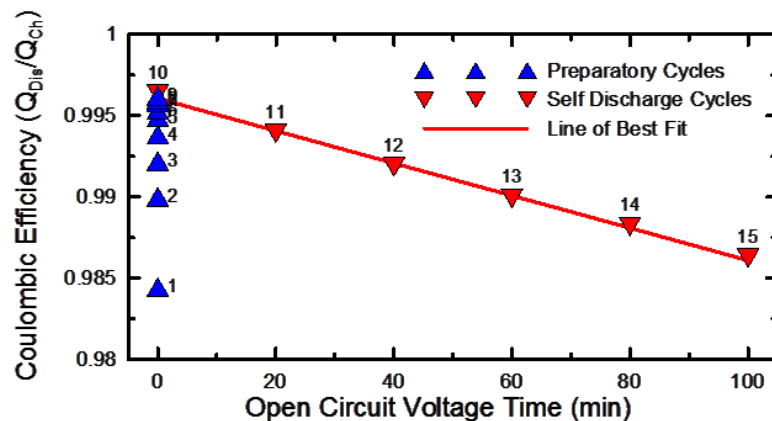


Figure 4-3: Example data extracted from OCV self-discharge experiments. The numbers next to data points are cycle numbers. The preparatory cycles ensure the system is in a form of dynamic equilibrium before starting the experiment. The fact that the experimental data points are linear means that the self-discharge rate is constant up to 100 min.

of time during successive cycles at its open circuit voltage (OCV) (red line). This “OCV time” was usually 20, 40, 60, 80 and 100 min. Upon completion of the OCV step, the electrode was discharged; the discharge capacity (or time) is the crucial variable in this experiment. The usual electrolyte was 3.2 M KOH that had been saturated with ZnO powder, which corresponded to a  $\text{Zn}(\text{OH})_4^{2-}$  concentration of about 0.2 M. In the experiments that follow, this method was changed as noted.

Figure 4-3 shows an example of a typical CE vs OCV time plot. The first 10 cycles (numbered in the figure) show the convergence of the CE to a value around 99.6% in this case. Cycles 10 – 15 demonstrate the remarkably linear relationship between the amount of time the electrode is left at open circuit in the electrolyte and the capacity lost to self-discharge, suggesting that the self-discharge current is constant in time (beyond the 1 to 2 minutes it takes for the potential to stabilize at about 0 V vs Zn).

#### 4.2.3 Calculation of the Self-Discharge and Parasitic Reaction Currents

Given that the self-discharge current ( $i_{SD}$ ) is constant in time, the following simple model describes the results quite succinctly: Assume that the only reactions happening during charging are Zn plating (Reaction (1-2) on page 6) and parasitic  $\text{H}_2$  evolution

(Reaction (1-16) on page 19). Then assume that only self-discharge occurs during the OCV step (Reactions (4-1) to (4-14) on page 117) and that only Zn stripping occurs during the discharge step (Reaction (1-2) backward). The charge balance equation equating the charge delivered to the electrode to the charge lost to discharge, self-discharge and parasitic H<sub>2</sub> evolution can then be written as follows and rearranged to isolate the CE:

$$\begin{aligned}
 Q_C &= Q_D + Q_{SD} + Q_{H_2} \\
 I_C t_C &= I_D t_D + I_{SD} t_{OCV} + I_{H_2} t_C \\
 I &= I \cdot CE + I_{SD} \left( \frac{t_{OCV}}{t_C} \right) + I_{H_2} \\
 CE &= -\frac{I_{SD}}{I} \left( \frac{t_{OCV}}{t_C} \right) + 1 - \frac{I_{H_2}}{I}
 \end{aligned} \tag{4-9}$$

where  $I_C = I_D = I$  and thus  $\frac{t_D}{t_C} = \frac{Q_D}{Q_C} = CE$ . Here, C = “Charge”, D = “Discharge”, SD = “Self-Discharge”, OCV = “Open Circuit Voltage” and H<sub>2</sub> = “H<sub>2</sub> evolution”. Note that this model treats H<sub>2</sub> evolved as part of the Zn corrosion reaction separately from the H<sub>2</sub> that is evolved during charge, which is not accompanied by Zn dissolution. The capacity consumed by parasitic H<sub>2</sub> evolution that only occurs during charge is  $Q_{H_2}$ , which can be expressed as the product of an average current,  $i_{H_2}$ , and the time spent charging,  $t_C$ . This model is linear and so the slope of a linear fit to the data, as shown in Figure 4-3, yields the self-discharge current ( $i_{SD}$ ), while the y-intercept yields the parasitic H<sub>2</sub> evolution current ( $i_{H_2}$ ). Software designed in-house was used to analyze the data sets and produce error estimates based on the linear fit (such as the values presented later in the caption of Figure 4-6). However, the error arising from variations between the results of identical runs proved significantly larger (at least 10x) than the errors generated by the linear fits. As such, the standard deviations gathered by performing at least four copies of each experiment are reported from here onward, instead.

It is important to note that a constant self-discharge rate makes the data analysis convenient, but is not necessary. The slope between any two points on the  $Q_D$  or CE vs  $t_{OCV}$  plot yields the average self-discharge current for the period of time between those two data points. So if the self-discharge current changed over time, the researcher would simply use the slope between adjacent points (i.e. the derivative,  $dQ_D/dt_{OCV}$ ) to determine  $i_{SD}$  as a (coarse) function of time.

#### 4.3 Electrolyte Wicking Along Conducting Surfaces

Early in this research effort, foils were lowered into the electrolyte without any sort of epoxy coating. It was observed that as these experiments progressed over hours, the electrolyte was drawn up along the foil surface until it reached the alligator clips. Once there, it initiated unwanted parasitic reactions, which polluted the CE data being collected.



Figure 4-4: Demonstration of electrolyte wicking up conducting surfaces. This is a long Zn foil electrode that was dipped in 3.2 M KOH, saturated with ZnO and cycled.

Furthermore as the electrolyte climbed the foil, the active surface area increased, throwing the legitimacy of the measured current density into question. An example of electrolyte wicking is shown in Figure 4-4 for a longer than usual Zn foil electrode. The spacing between the Zn ‘ridges’ is  $2.3 \pm 0.8$  mm, and each ridge was created during one cycle, which suggests that the electrolyte only moved up the foil during either plating or stripping.

The behaviour of this wicking phenomenon when the electrode is held at anodic potentials was explored by Baugh *et al.* quite well.<sup>181, 182</sup> Figure 4-5 shows a schematic of the basic premise that ions are drawn into the film of electrolyte rising out of the solution, dragging their hydration shells with them and thus “transferring their momentum to the film”.<sup>181, 182</sup> Today, this phenomenon is better known as electroosmosis instead of wicking.<sup>183</sup> Regardless, Baugh *et al.* demonstrated that the speed of the electrolyte propagation up the foil is

$$v_{electrolyte} = K \frac{i_{film} E \kappa \mu_+}{\eta \ell \sqrt{t}} \quad (4-10)$$

where  $i_{film}$  ( $\frac{A}{m^2}$ ) is the current passing through the film,  $E$  (V) is the potential of the electrode,  $\kappa$  ( $\frac{A}{V \cdot m}$ ) is the specific conductivity of the electrolyte,  $\mu_+$  ( $\frac{m^2}{V \cdot s}$ ) is the ionic mobility of the positive charge carrier ( $K^+$  in this case),  $\eta$  ( $\frac{kg}{s \cdot m}$ ) is the electrolyte viscosity,  $\ell$  (m) is the length of the film (distance traveled up the electrode),  $t$  (s) is time and  $K$  ( $\frac{V^2 s^{\frac{5}{2}}}{A}$ ) is a constant. Although their theory was consistent with all of their results, Baugh *et al.* noted that this model did not account for the negative ions, namely  $OH^-$  or  $Cl^-$ , that would be flowing *out* of the film and thus transferring water molecules the other way.<sup>181, 182</sup> Why this opposing flow did not affect their results remains a mystery. In the case of plating Zn during charge, both  $Zn(OH)_4^{2-}$  and  $K^+$  rush into the film, while  $OH^-$  rushes/hops out, as shown in Figure 4-5. This progression of an electrolyte film continually increases the



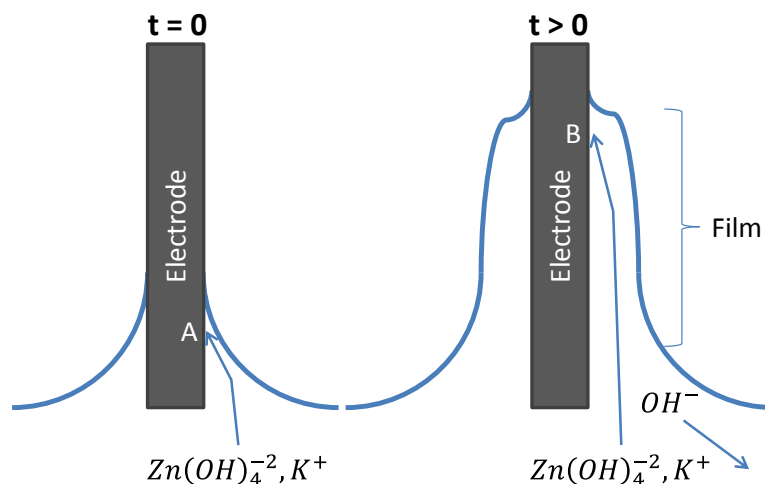


Figure 4-5: Schematic of the mechanism of electrolyte wicking (electroosmosis). At  $t = 0$ , Zn plates up to point A, which pushes the film up higher, exposing more area to plate onto. At  $t > 0$ , Zn plates all the way to point B (the edge of the film) and pushes the edge ever higher.

electrochemical surface area of the sample, which frustrates attempts to measure current densities with a constant, known area.

Electrolyte wicking is dependent on current flowing through the film though, which means encasing all of the non-experimental surfaces of a sample in an insulator will prevent it. Many aqueous electrochemistry researchers use various forms of epoxy to provide this coating, although it is not clear which type of epoxy, if any, is best for this purpose. Through trial and error, it was determined that hardware store Marine Epoxy (LePage) was passable in the current application. Unfortunately, even epoxies recommended by another alkaline researcher and curing the epoxy under a light vacuum were not sufficient to permanently or consistently prevent the electrolyte from detaching the epoxy from the foil surface and migrating up the narrow space between them.<sup>78</sup> Many experiments were repeated until at least four runs without epoxy-failure were obtained. Notably, few epoxy coatings would survive experiments longer than 20 hours, which limited what experiments were possible, such as preventing the determination of the linearity of self-discharge all the way to completion.

## 4.4 Results and Discussion

### 4.4.1 Time Dependence of Self-Discharge

Conflicting opinions of the time dependence of self-discharge exist in the literature with some researchers observing constant self-discharge rates,<sup>176</sup> some researchers reporting increasing self-discharge rates<sup>179</sup> and others reporting decreasing self-discharge rates.<sup>132, 175</sup> Zhang claimed in his literature review that self-discharge rates generally decreased with time until they reached a steady state,<sup>14</sup> while Gregory *et al.* explained the initial decrease as the time required to saturate the electrolyte with  $H_{2(aq)}$  and coat the Zn surface in ZnO or Zn(OH)<sub>2</sub>.<sup>175</sup>

To test whether the self-discharge rate remains constant with time throughout the

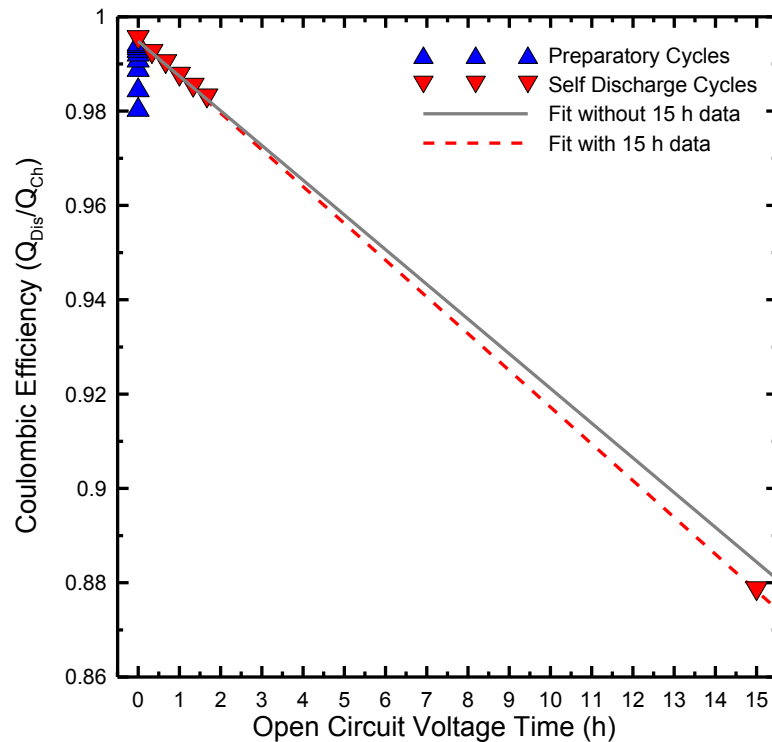


Figure 4-6: Example of self-discharge at long OCV times. This particular sample has 1 mM of CTAB additive in the 3.2 M KOH electrolyte. The solid fit is applied to only the first 6 data points of the self-discharge cycles, not including the 7<sup>th</sup> data point at 15 h. This fit yields a self-discharge rate of  $3.68 \pm 0.08 \mu A/cm^2$ . The dotted fit is applied to all 7 data points and yields a self-discharge rate of  $3.897 \pm 0.013 \mu A/cm^2$ .

self-discharge process in the experiments presented here, a few experiments were performed with a 15 hour OCV time. One such experiment is shown in Figure 4-6, which shows that the self-discharge rate is indeed constant with time, at least for the first 15 h. The solid, grey line represents a fit to only the first 6 data points, excluding the 15 h data point. This line produced effectively the same self-discharge rate as the dotted, red linear fit that incorporated all 7 data points, including the 15 h data point, which signifies that the rate did not change within the first 15 hours that the electrode was left at OCV. Unfortunately, longer durations could not realistically be attained due to problems with electrolyte wicking. Dobryszyci *et al.* observed an increase in the H<sub>2</sub> evolution rate after 4 days had passed, but it is shown in Chapter 5 that the self-discharge rates measured in this thesis are likely constant.<sup>179</sup>

Note that the electrolyte in these experiments was not bubbled with H<sub>2</sub> prior to the experiment to pre-saturate the solution with H<sub>2</sub> gas, but this was not an issue since the OCV periods did not begin until after the foils had spent 3 hours in the electrolyte. The amount of charge required to evolve enough H<sub>2</sub> gas to saturate the electrolyte was

$$Q_{H_2} = nFk_{Henry}^{\circ}x_{H_2}PV = 8.4 \times 10^{-7} \text{ mAh}, \quad (4-11)$$

which was vastly smaller than the 0.02 mAh that was lost to H<sub>2</sub> evolution in just the first preparatory cycle in Figure 4-6. As such, it seems unlikely that the concentration of H<sub>2</sub> gas in the electrolyte would speed up the self-discharge rate in the initial few days of the experiment as suggested by Gregory *et al.*<sup>175</sup> In Equation (4-11),  $n = 2 \frac{\text{mol } e^-}{\text{mol } H_2}$ ,  $F = 26,801 \frac{\text{mAh}}{\text{mol } e^-}$ ,  $k_{Henry}^{\circ} = 7.8 \times 10^{-4} \frac{\text{mol } H_2(\text{aq})}{\text{L} \cdot \text{Atm } H_2}$  is Henry's constant for H<sub>2</sub> in water,<sup>184</sup>  $x_{H_2} = 5.0 \times 10^{-7} \frac{\text{Atm } H_2}{\text{Atm } \text{Air}}$  is the mole fraction of H<sub>2</sub> in air,  $P = 1 \text{ Atm Air}$  and  $V = 40 \text{ mL}$  of electrolyte.

#### 4.4.2 KOH Concentration

Again, conflicting opinions on the effect of KOH concentration, in the range 3 to 7 M, on the self-discharge rate exist with some authors claiming the rate increases with KOH concentration,<sup>175</sup> some claiming it decreases,<sup>132</sup> and some claiming it does not change.<sup>174</sup> Zhang attempted to reconcile the differences in experimental technique between the three examples given, but failed to find a unifying explanation.<sup>14</sup>

To determine if the self-discharge current is dependent on the concentration of KOH in the electrolyte, within the experimental apparatus being used here, electrolytes of increasing KOH concentration were created, saturated with ZnO and then tested with Cu foil. Figure 4-7 shows the self-discharge current ( $i_{SD}$ ) and the H<sub>2</sub> evolution current ( $i_{H_2}$ ) as a function of KOH concentration. Since all  $i_{SD}$  and  $i_{H_2}$  values were equal within experimental error, neither was strongly dependent on the KOH concentration. A constant value for both  $i_{SD}$  and  $i_{H_2}$  can be calculated from the weighted average of the relevant data points:  $i_{SD}$  was  $2.94 \pm 0.18 \mu\text{A}/\text{cm}^2$  and  $i_{H_2}$  was  $10.8 \pm 1.1 \mu\text{A}/\text{cm}^2$ . This result agrees with the constant trend observed by Ruetschi *et al.*, although it should be noted that their result was obtained at 60°C and so an absolute comparison of rates was not possible.<sup>174</sup>

However, if the rate is instead dependent on the activity of water, as suggested by Equation (4-14) (pg. 132) and which does vary with the KOH concentration, as shown by Bro *et al.*,<sup>185</sup> then both  $i_{SD}$  and  $i_{H_2}$  should decrease slightly with KOH concentration as the average values in Figure 4-7 suggest. An interpolation of Bro *et al.*'s three data points from 3.08 M to 7.75 M KOH at 25°C yields a line:<sup>185</sup>

$$a_{H_2O} = -0.0657 \frac{1}{M_{KOH}} \cdot [KOH] + 1.0736. \quad (4-12)$$

When combined with Equation (4-8) (pg. 118), expressions for  $i_{SD}$  and  $i_{H_2}$  can be derived:

$$i_{SD} = nF \cdot Rate_{SD} = -0.0657 \frac{1}{M_{KOH}} \cdot nFk_{SD}[KOH] + 1.0736nFk_{SD}, \text{ and} \quad (4-13)$$

$$i_{H_2} = nF \cdot Rate_{H_2} = -0.0657 \frac{1}{M_{KOH}} \cdot nFk_{H_2}[KOH] + 1.0736nFk_{H_2}. \quad (4-14)$$

Here,  $n = 1$ ,  $F$  is Faraday's constant and both  $k_{SD}$  and  $k_{H_2}$  were determined by fitting Equations (4-13) and (4-14) to the data in Figure 4-7 using a least squares linear fit. The actual values of  $k_{SD}$  and  $k_{H_2}$  are not important since the surface area is unknown, but for the purposes of the fit  $k_{SD} = 3.91 \times 10^{-11} \text{ mol} \cdot \text{cm}^{-2} \cdot \text{s}^{-1}$  and  $k_{H_2} = 1.72 \times 10^{-10} \text{ mol} \cdot \text{cm}^{-2} \cdot \text{s}^{-1}$ . The blue (long dashed) lines in Figure 4-7 represent the model described by Equations (4-13) and (4-14) and fit the data quite well. These slight decreases in current are within experimental error of Snyder *et al.*'s  $i_{SD}$  dependence on KOH, which decreased by 25% in going from 3 to 7 M KOH.<sup>132</sup> However, the results of this section are notably different from Gregory *et al.*,

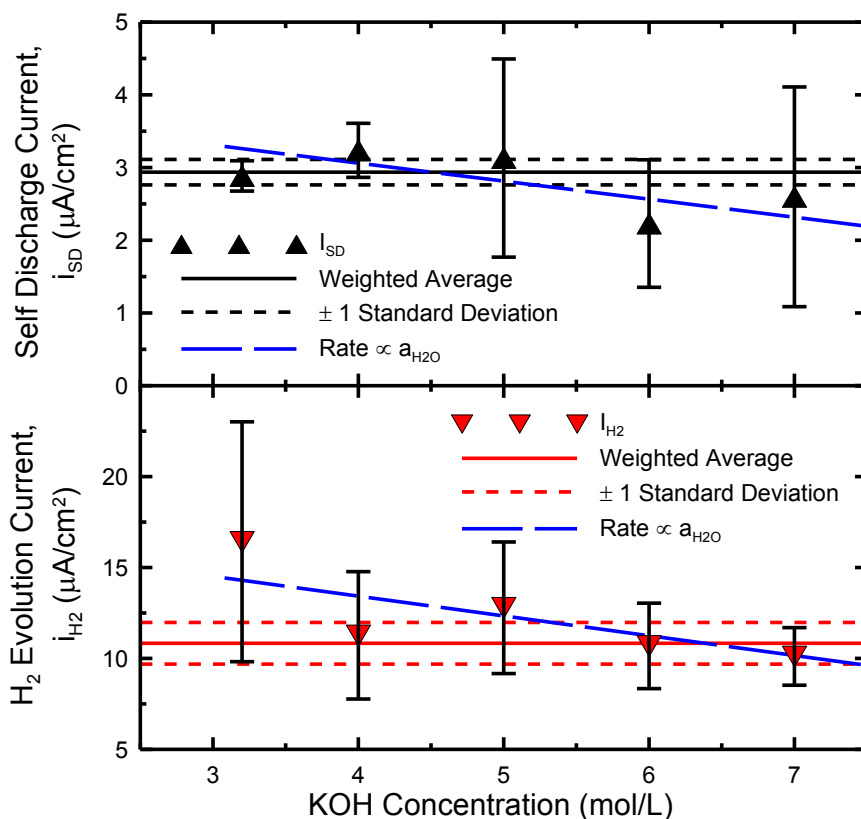


Figure 4-7: Self-discharge and hydrogen evolution rates in increasing concentrations of KOH. Both  $i_{SD}$  and  $i_{H_2}$  seemed either independent of the KOH concentration within experimental error (weighted averages of  $i_{SD} = 2.94 \pm 0.18 \mu\text{A}/\text{cm}^2$  and  $i_{H_2} = 10.8 \pm 1.1 \mu\text{A}/\text{cm}^2$ ) or dependent on the activity of water ( $a_{H_2O}$ ). The linear dependence on  $a_{H_2O}$  (blue, long dashed lines) was interpolated from Bro *et al.*'s data, which yielded  $i_{SD} = -0.248 \mu\text{A} \cdot \text{cm}^{-2} \cdot \text{M}^{-1} * [\text{KOH}] + 4.054 \mu\text{A}/\text{cm}^2$  and  $i_{H_2} = -1.088 \mu\text{A} \cdot \text{cm}^{-2} \cdot \text{M}^{-1} * [\text{KOH}] + 17.778 \mu\text{A}/\text{cm}^2$ .<sup>185</sup>

whose  $i_{SD}$  tripled in the KOH range from 3 to 7 M, suggesting a different rate determining step was in control in their work.<sup>175</sup>

The fact that the self-discharge rate did not increase with KOH concentration suggests that the rate determining step (rds) does not include the  $\text{OH}^-$  ion as a reactant, which eliminates all 4 of the mechanistic steps for Zn dissolution proposed by Bockris *et al.*<sup>29</sup> (Reactions (1-3) to (1-6) backward, pg. 6). Instead,  $i_{SD}$  either stayed constant or decreased slightly. A constant  $i_{SD}$  suggests that the rds could be the diffusion of  $\text{Zn}(\text{OH})_4^{2-}$  away from the Zn surface (Reaction (4-3), pg. 117), which has been suggested by Muralidharan *et al.*, but they did not use a current collector as would be the case in a rechargeable Zn electrode.<sup>177</sup> Alternatively, a slight decrease in  $i_{SD}$  with the concentration of KOH suggests the slow step of  $\text{H}_2$  evolution (Reaction (4-5), pg. 118) is the rds for the entire self-discharge process.

#### 4.4.3 Foil (Current Collector) Material

The material that the current collector is made of was noted by Gregory *et al.* to affect the self-discharge rate.<sup>175</sup> Chu, McBreen and Adzic also noted that the substrate determines the morphology of Zn deposits, which determines the surface area of the deposits and how much substrate is left exposed to the electrolyte.<sup>156, 157</sup> If the self-discharge rate is limited by  $\text{Zn}(\text{OH})_4^{2-}$  diffusion, then the substrate should have no effect on the self-discharge rate.

Foils of various materials that are commonly used in Zn electrodes were tested. Copper (Cu),<sup>121, 128, 130, 146, 153</sup> tin (Sn),<sup>113, 122</sup> nickel (Ni)<sup>124, 126, 127, 131</sup> and lead (Pb)<sup>68, 118</sup> have all been used as current collectors or coatings on current collectors. Indium (In) is commonly used as an additive in non-rechargeable battery Zn active material to reduce  $\text{H}_2$  evolution rates (along with bismuth (Bi)).<sup>186</sup> Several authors have also used graphite as a conductive

additive in rechargeable Zn electrodes so graphite foil was tested here as an approximation.<sup>123, 128, 187</sup> The metal foils were acquired from ESPI Metals and had the following purities: Cu (99.9%), In (99.9%), Sn (99.999%), Pb (99.9%) and Ni (99.9%). Graphite foil (graphoil) was acquired from Graphtek.

Figure 4-8 and Figure 4-9 show the self-discharge current ( $i_{SD}$ ) and the  $H_2$  evolution current ( $i_{H_2}$ ) as a function of foil material. Clearly, the Ni and graphite foils have high self-discharge and  $H_2$  evolution rates. The  $H_2$  evolution rate on Ni was so high, in fact, that no amount of Zn plated at a charging current of  $3 \text{ mA/cm}^2$ . At  $10 \text{ mA/cm}^2$ , Zn plating occurred faster than  $H_2$  evolution and so some Zn was plated, which subsequently reduced the  $H_2$  evolution rate on that patch of current collector as shown in Figure 4-9. The fact that the current collector has a strong effect on the self-discharge current proves that the diffusion of  $Zn(OH)_4^{2-}$  away from the Zn surface (Reaction (4-3), pg. 117) is not the rate determining

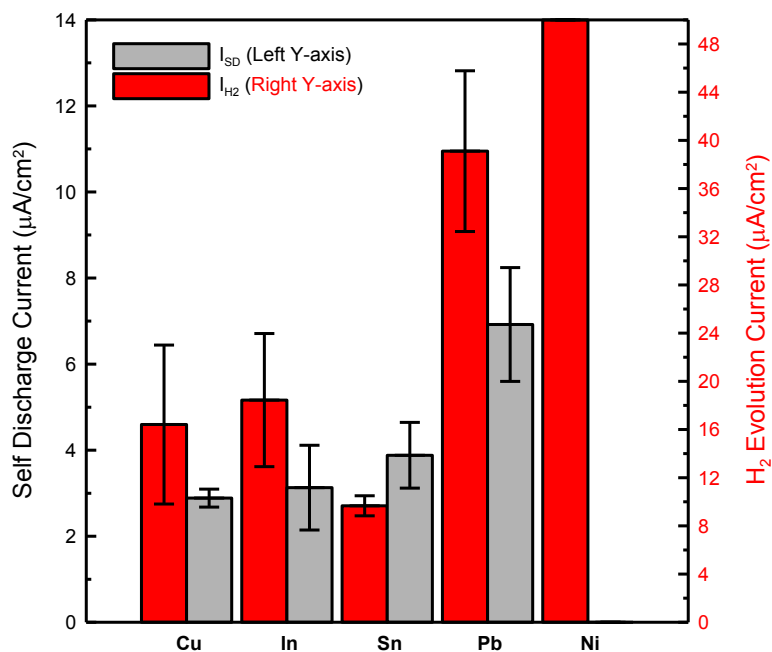


Figure 4-8: Self-discharge and hydrogen evolution rates on various current collector materials. Plating and stripping rates were  $3 \text{ mA/cm}^2$  for 10 min. OCV times increased in 20 min increments up to 100 min. The electrolyte was 3.2 M KOH, saturated with ZnO. The  $H_2$  evolution rate on Ni exceeds the maximum y-axis value and is actually  $3 \text{ mA/cm}^2$ , which is the charging current. Hence, Ni has no self-discharge current since no Zn was plated onto it.

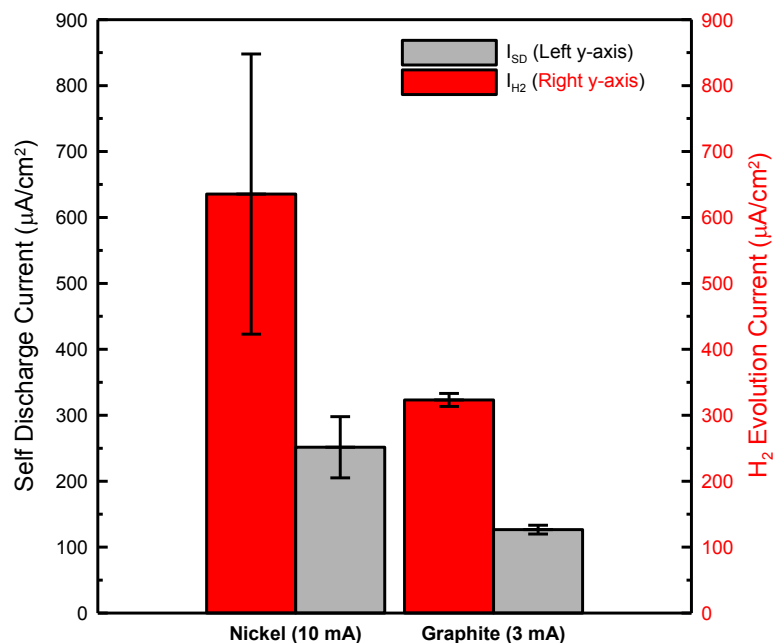


Figure 4-9: Self-discharge and  $H_2$  evolution rates of Ni and graphite current collectors. The plating and stripping current for graphite was the usual  $3 \text{ mA}/\text{cm}^2$  for 10 min while the current for Ni was  $10 \text{ mA}/\text{cm}^2$  for 3 min to plate some Zn despite the  $H_2$  evolution reaction consuming most of the current. The electrolyte was 3.2 M KOH, saturated with ZnO.

step since the current collector should not effect the diffusion rate.

An explanation for the currents seen in Figure 4-8 and Figure 4-9 can be qualitatively provided using Figure 4-10, which shows the surfaces of these materials after Zn has been plated on them. In, Sn and Cu exhibit small crystallite growth, with Zn covering the majority of the surface area. Bi, Pb and C (graphite) induce larger crystallite growth that leaves much of the surface exposed to electrolyte.<sup>156, 157</sup> Ni has no Zn on it. If the self-discharge rate is controlled by the surface area of non-Zn metals that are electrically connected to the Zn active material and exposed to the electrolyte, in addition to the overpotential for  $H_2$  evolution on that metal, then this could explain the results observed here. The larger area of exposed surface on Pb could have led to a higher  $H_2$  evolution and self-discharge current than the more uniformly coated Cu, even though Cu might have a lower overpotential for  $H_2$  evolution. This would signify that the exposed surface area of the current collector is about as important as the overpotential for  $H_2$  evolution when



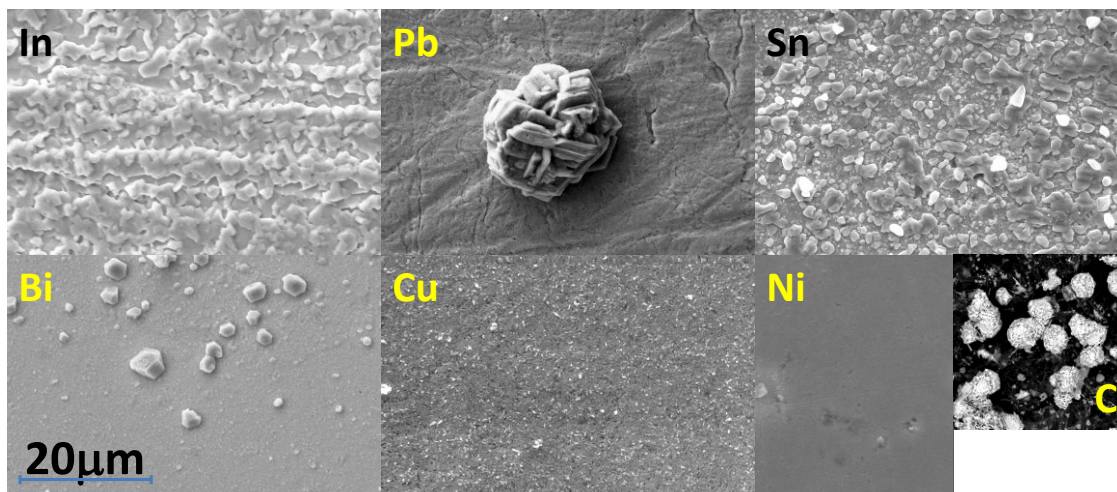


Figure 4-10: SEM pictures of Zn deposits on various current collector materials. The scale is the same in all of the pictures, except for Ni which has a scale 10x larger. Ni has no Zn on it.

selecting a current collector material for Zn. The  $i_{SD}$  values of Cu ( $2.9 \pm 0.2 \mu\text{A}/\text{cm}^2$ ), In ( $3.1 \pm 1.0 \mu\text{A}/\text{cm}^2$ ) and Sn ( $3.9 \pm 0.8 \mu\text{A}/\text{cm}^2$ ) were equal within experimental error, and so it was concluded that any of these three materials was suitable for further self-discharge experiments and current collectors in general.

It was hoped that these experiments would help explain the discrepancy between the cycle lifetimes of coin cells with Cu vs Sn current collectors, as shown in Figure 2-18 (pg. 85). The only notable difference between Cu and Sn current collectors here is the  $\text{H}_2$  evolution rate, which was  $16 \pm 7 \mu\text{A}/\text{cm}^2$  for Cu and  $9.7 \pm 0.8 \mu\text{A}/\text{cm}^2$  for Sn. Although they are technically equal within experimental error, a lower  $\text{H}_2$  evolution rate on Sn would favour Sn as a current collector material in a situation where the entire current collector is not covered in and protected by Zn. These foil experiments result in complete (macroscopic) coverage of the current collector, but the same is not true in coin cells. The Zn in coin cells tends to plate directly across from the Ni electrode, which would leave parts of the Zn current collector exposed to the electrolyte. Because of this, a Cu current collector in a coin cell would provide better local cathodic sites for  $\text{H}_2$  evolution than Sn and thereby increase the self-discharge current and reduce the coulombic efficiency in comparison to Sn.

When the entire coin cell canister was coated in Sn, and the current collector was also Sn, then the coin cell did not suffer from as high a self-discharge current since Sn has a lower H<sub>2</sub> evolution rate than Cu.

Mechanistically, the fact that different substrates change the self-discharge rate signifies that H<sub>2</sub> evolution on either the Zn deposit or the substrate itself is the rate determining step, and not the diffusion of Zn(OH)<sub>4</sub><sup>2-</sup>. This suggests that the rds for the self-discharge process is water giving up a proton at a surface site as part of H<sub>2</sub> evolution (Reaction (4-5), pg. 118). Furthermore, the results of this section suggest that the H<sub>2</sub> is created on the current collector since changing the current collector to Ni, for example, had such a dramatic impact, but changing the Zn morphology by using Cu instead of Sn did not affect the self-discharge current. Nevertheless, it would be reassuring to confirm that changing the surface area of Zn on the same current collector does not affect the self-discharge rate.

Gregory *et al.* and Snyder *et al.* also noted that changing the current collector (in their case by amalgamating copper grids with mercury) did reduce the self-discharge rate, but they did not identify the current collector as the determining factor for the self-discharge rate.<sup>132, 175</sup> Their studies were done with mercury additions to the electrode material, which coated their Zn and current collectors *in-situ* and reduced the self-discharge rate since mercury has an even lower H<sub>2</sub> evolution rate than Zn. Overall, to the author's knowledge no study to date has identified the current collector as the rate determining factor for self-discharge of rechargeable Zn electrodes.

#### 4.4.4 Electroplating (Charging) Current

The morphology of Zn deposits has been proven to vary with plating current density<sup>75, 76</sup> and so plating Zn at different current densities will change the surface area of

the Zn deposit.<sup>75</sup> If H<sub>2</sub> evolution is occurring on the Zn deposit itself, then performing the self-discharge experiment on higher surface area Zn deposits should yield a higher self-discharge rate.

Consecutive Sn foils were charged at different currents, but with a constant capacity density (i.e. Zn was plated for different times so that all deposits had 0.5 mAh/cm<sup>2</sup> of plated Zn) in case the thickness of the deposit affected the self-discharge rate. Figure 4-11 shows the self-discharge current ( $i_{SD}$ , panel A) and the H<sub>2</sub> evolution current ( $i_{H_2}$ , panel B) as a function of charging current. The 15 mA/cm<sup>2</sup> charging current experiment is shown for completeness; however, plating at this current was subject to diffusion control. As such, the 15 mA/cm<sup>2</sup> data point was ignored while drawing conclusions about this data since the exposed surface area of the current collector might have changed in this situation. Since all other  $i_{SD}$  values were equal within experimental error, it was determined that  $i_{SD}$  was independent of the plating current. For Sn foil, charged in 3.2 M KOH for 10 min at 3 mA/cm<sup>2</sup> (or to 0.5 mAh/cm<sup>2</sup>), the  $i_{SD}$  was  $3.6 \pm 0.5 \mu\text{A}/\text{cm}^2$ .

Since  $i_{SD}$  did not depend on the plating rate, this suggests that the rds, Reaction (4-5) (pg. 118), does not occur on Zn; however, scanning electron microscopy did not reveal an obvious difference in surface area between the samples (up to 12 mA/cm<sup>2</sup>), and so this conclusion is weak. Since the authors that described the deposit morphologies used generic “low” and “high” current density descriptors and a gel electrolyte, it is difficult to know which deposit would have been expected in the current experiment.<sup>75, 76</sup> If nothing else, demonstrating that the self-discharge current does not depend on plating rate below the diffusion control region and that the diffusion control region exists around 15 mA/cm<sup>2</sup> was comforting. As such, all other experiments in this chapter were performed at 3 mA/cm<sup>2</sup> to stay as far from the diffusion control region as possible without making the experiment too lengthy (to avoid electrolyte wicking problems).

Figure 4-11B shows that the parasitic H<sub>2</sub> evolution current increases logarithmically with the plating current, which is generally expected from the Butler-Volmer Equation (1-14) on page 17. Figure 4-11C shows a plot of  $\eta_{\text{H}_2}$  vs  $\log(i_{\text{H}_2})$ , which should only reflect

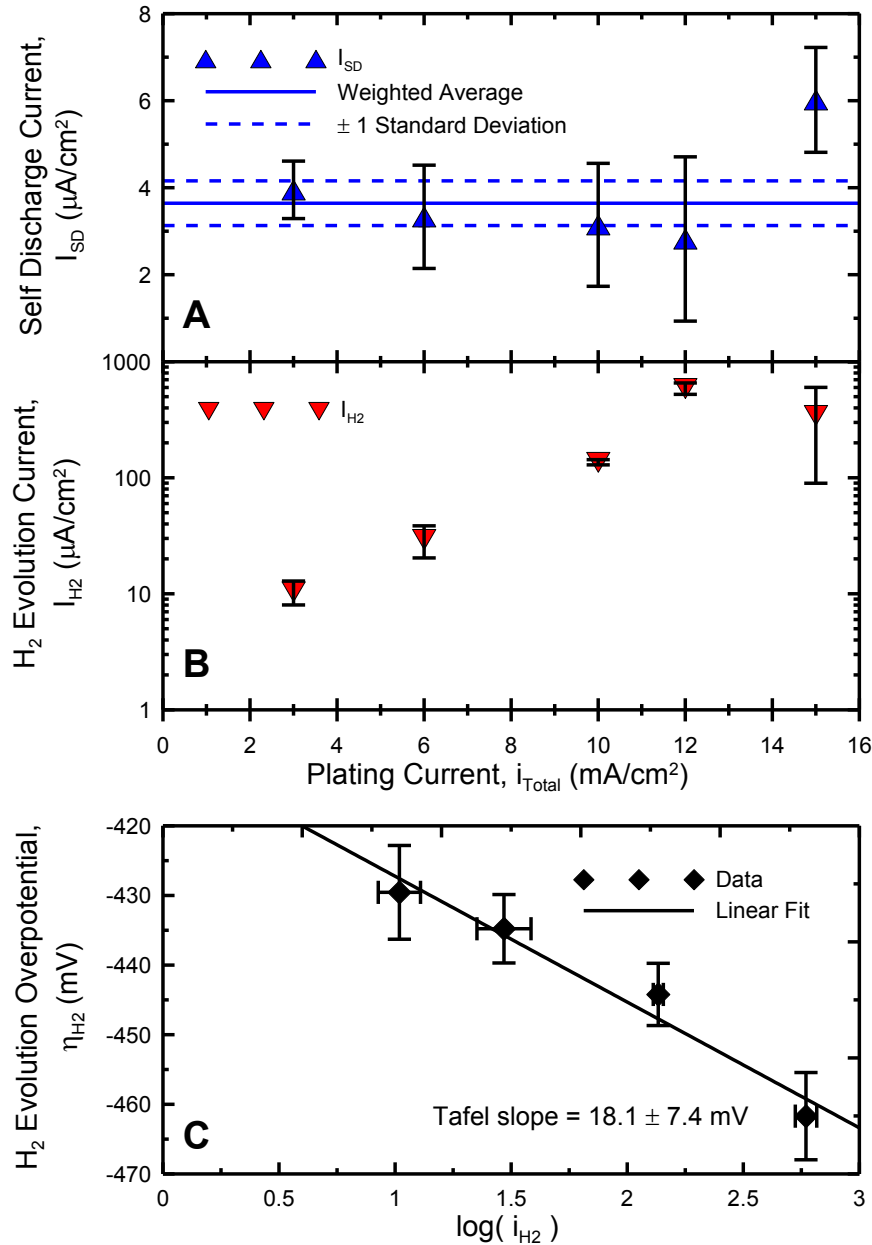


Figure 4-11: Self-discharge and hydrogen evolution rates with increasing plating current densities. Ignoring the  $15 \text{ mA}/\text{cm}^2$  data point,  $i_{\text{SD}}$  seems independent of plating current within experimental error and has a weighted average of  $3.6 \pm 0.5 \mu\text{A}/\text{cm}^2$ . Panel C shows the Tafel line for the H<sub>2</sub> evolution rates. The fit had a Tafel slope of  $18.1 \text{ mV}$ , which is unlikely to be real due to the variation in plating conditions and uncertainty in the assumed value of  $E_{\text{Eq,H}_2}$  ( $410 \text{ mV}$  vs Zn in  $3.2 \text{ M KOH}$ ).

the second term of Equation (1-14), since the first term will be negligibly small at  $\eta_{\text{H}_2} = -420$  mV. A line was fit to the data and the Tafel slope was calculated to be  $18.1 \pm 7.4$  mV. According to Trasatti, the Tafel slope for  $\text{H}_2$  evolution with Reaction (4-5) (pg. 118) as the rds should be 120 mV.<sup>63</sup> Considering the vertical error bars, the maximum value of the measured Tafel slope is lower than the lowest possible Tafel slope put forward by Trasatti<sup>63</sup> (30 mV) for the case when Reaction (4-7) is the rds, which makes the measured value determined here unlikely to be true. An inaccurate Tafel slope measurement is not entirely surprising for these experiments, since the surface area evolving  $\text{H}_2$  during the Zn plating process changes significantly, and not necessarily identically at different plating rates. Although, note that the constant  $i_{\text{SD}}$  as the plating current changed does suggest that the Zn-coated surface area reached approximately the same value after plating had finished.

#### 4.4.5 *Effect of Electrolyte Additives*

Historically, mercury (Hg) was used as the self-discharge suppressant of choice,<sup>14, 132, 174, 175</sup> but environmental and safety concerns resulted in the banning of Hg in batteries.<sup>186</sup> Since then, many researchers have sought out other additives to take the place of Hg and today indium (In) and bismuth (Bi) are alloyed with Zn in non-rechargeable cells in place of Hg.<sup>186</sup> Additives that are added to the electrode slurry (mixture) are referred to as “electrode additives”, while dissolved additives added to the electrolyte are referred to as “electrolyte additives”. In recent years the pursuit of electrolyte additives to reduce self-discharge rates,<sup>145, 146, 164, 165, 179, 180</sup> dendrite growth<sup>162</sup> or shape change<sup>20</sup> has progressed with several additives being claimed to be quite effective. However, the effects of these additives have not been compared to one another. This section compares the effect on self-discharge rate, if any, of several additives featured in the literature. Since the rate determining step of self-discharge with this apparatus appears to be Reaction (4-5) (pg.

118), any additive that occupies a surface site on the current collector or an impurity in the Zn, and does not yield it to the formation of  $H_{ad}$  could reduce the self-discharge rate. Additionally, any additive that improves the Zn coverage of the current collector would reduce the self-discharge rate.

In order to compare the effectiveness of these additives, electrolytes with the additives presented by other authors, at the ideal concentrations suggested by those authors, were created and tested.<sup>20, 145, 162, 164, 165, 179</sup> Testing was done with the most typical methodology: Cu foil was cycled at 3 mA/cm<sup>2</sup> for 10 min in 3.2 M KOH, saturated with ZnO (about 0.2 M) and left to sit at OCV for 20, 40, 60, 80 and 100 min. At least four successful runs of each additive were completed and the results from the linear fits were averaged. The additives used were PEG 400, PEG DiAcid 600 and L-Tartaric Acid (99%) from Aldrich,

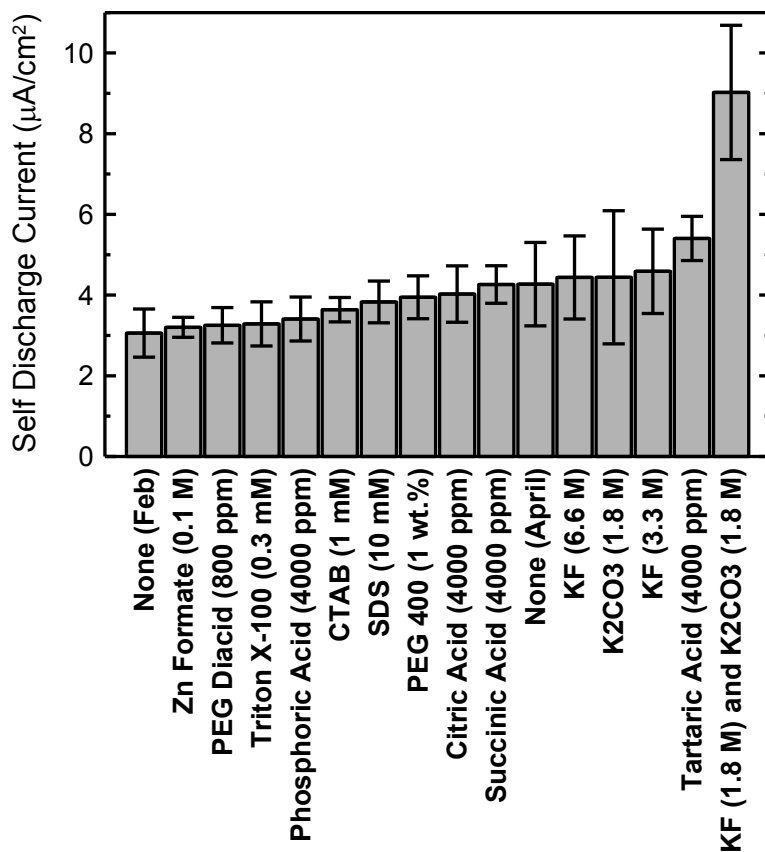


Figure 4-12: Self-discharge current in the presence of electrolyte additives. The plating and stripping current was 3 mA/cm<sup>2</sup> for 10 min in 3.2 M KOH, saturated with ZnO, onto Cu foil.

Succinic Acid (99.0+%), Citric Acid (99.5+%) and KF (99+%) from Sigma-Aldrich, Hexadecyltrimethylammonium bromide (CTAB, 98+%) from Sigma, Phosphoric Acid (35% HPO<sub>3</sub>, 60% NaPO<sub>3</sub>) and sodium dodecyl sulfate (SDS, 99+%) from Fisher, zinc formate (98%) from Alfa Aesar, and Triton X-100 (reagent grade) from Amresco.

The results are presented in Figure 4-12. Evidently, the absence of any additives yielded the lowest self-discharge rate (None(Feb)) but an unsettling variation was noticed between the same experiment in February and in April (None(April)) that might have been due to an increase in the lab temperature since these experiments were performed without temperature control. Regardless, the two experiments are equal within experimental error, and are also equal to all of the other additive experiments with the exception of the KF & K<sub>2</sub>CO<sub>3</sub> experiment and the possible exception of the Tartaric Acid experiment. Both of these experiments had a higher self-discharge current than if the additive had been absent, which suggests that they either increased the rate of Reaction (4-5) (pg. 118) or increased the surface area of exposed current collector.

Figure 4-13 shows Scanning Electron Microscopy (SEM) pictures of a few Zn deposits for demonstration purposes. Panel A shows a Sn foil that has been plated with Zn when no additive is present. Panel B shows a Zn deposit with 1 wt% PEG 400 electrolyte additive, which looks to have a higher surface area than the deposit without any additives. However, the PEG 400 additive did not result in an increase in the self-discharge rate, which supports the idea that the rate determining H<sub>2</sub> evolution step (Reaction (4-5) on page 118) does not occur on Zn. Panel C shows a Zn deposit with 3.3 M KF as an additive, which shows a more uniform deposit than the sample without any additive, but otherwise looks similar. Panel D shows a Zn deposit with 1.8 M KF & 1.8 M K<sub>2</sub>CO<sub>3</sub> additives, which looks like it might even have holes in the deposit surrounding tiny grains. If those features are holes, then

more electrolyte gained access to the current collector below the deposit. Considering the statistically higher self-discharge rate of this sample (Figure 4-12)

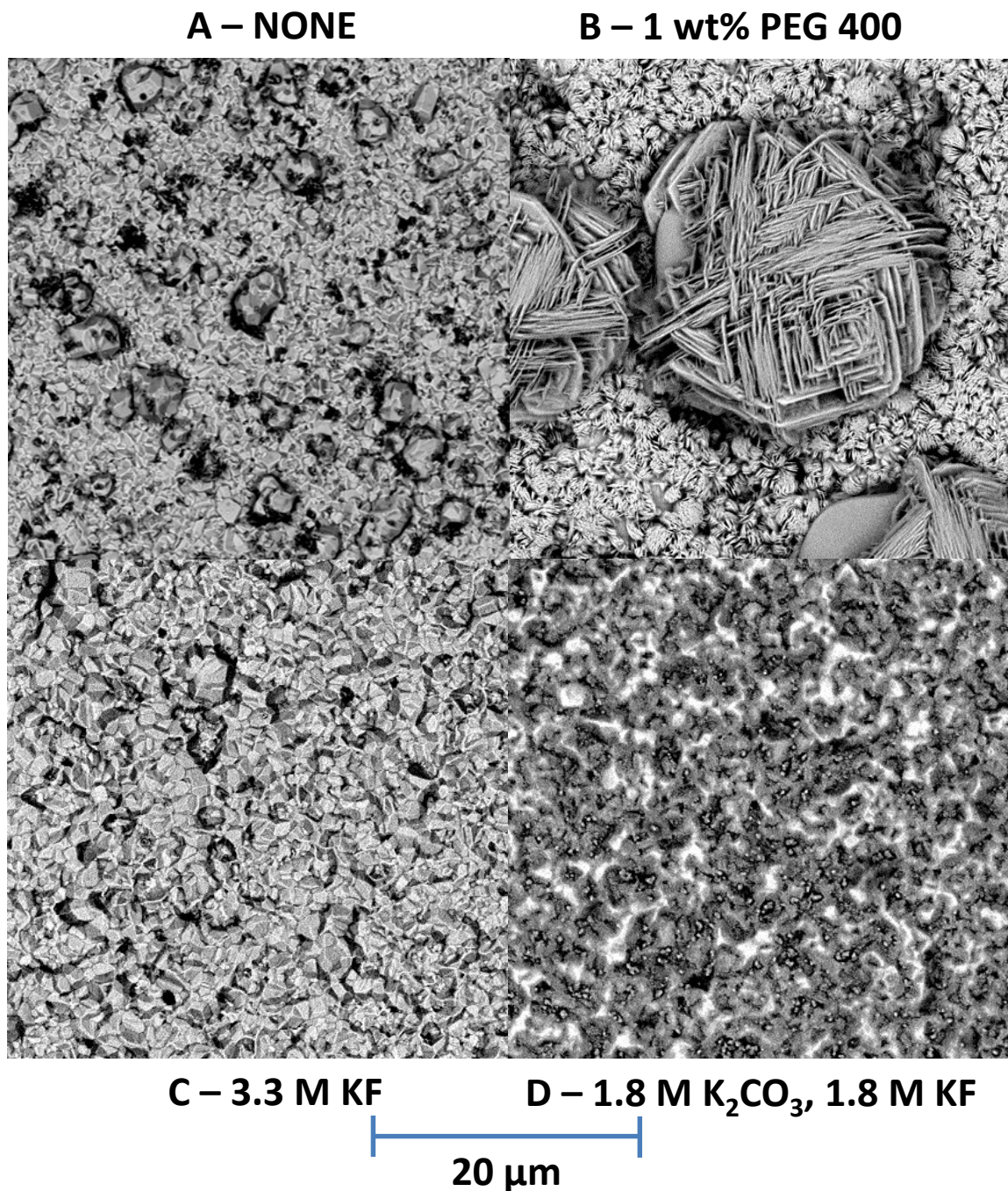


Figure 4-13: Scanning Electron Microscopy (SEM) pictures of Zn deposits on Sn foil from electrolytes with different additives. Zn plating was at a rate of  $3 \text{ mA/cm}^2$  for 10 min (i.e.  $0.5 \text{ mAh/cm}^2$ ). The electrolyte was 3.2 M KOH, saturated with ZnO, and contained various additives as labeled above.



than any other sample, this holey theory is compatible with the idea that the rate determining  $H_2$  evolution step occurs on the current collector.

Figure 4-14 shows the parasitic  $H_2$  evolution rates, which were similarly identical for most additives. The only additive that fared statistically better than None (April) was KF (3.3 M), although an increase in concentration seemed to negate the benefit. This is likely because 3.3 M KF acts as a simple supporting electrolyte and increases the conductivity of the electrolyte, whereas 6.6 M KF is such a high concentration that the electrolyte conductivity decreases again. This concept was supported by the fact that the overpotential to plate Zn in the 6.6 M KF electrolyte was about 5.5 mV higher than it was in 3.3 M KF electrolyte. According to the Tafel slope of 18.1 mV, derived in Section 4.4.4, this should result in an increase in the parasitic  $H_2$  evolution current from  $7 \mu A/cm^2$  for 3.3 M KF to 14

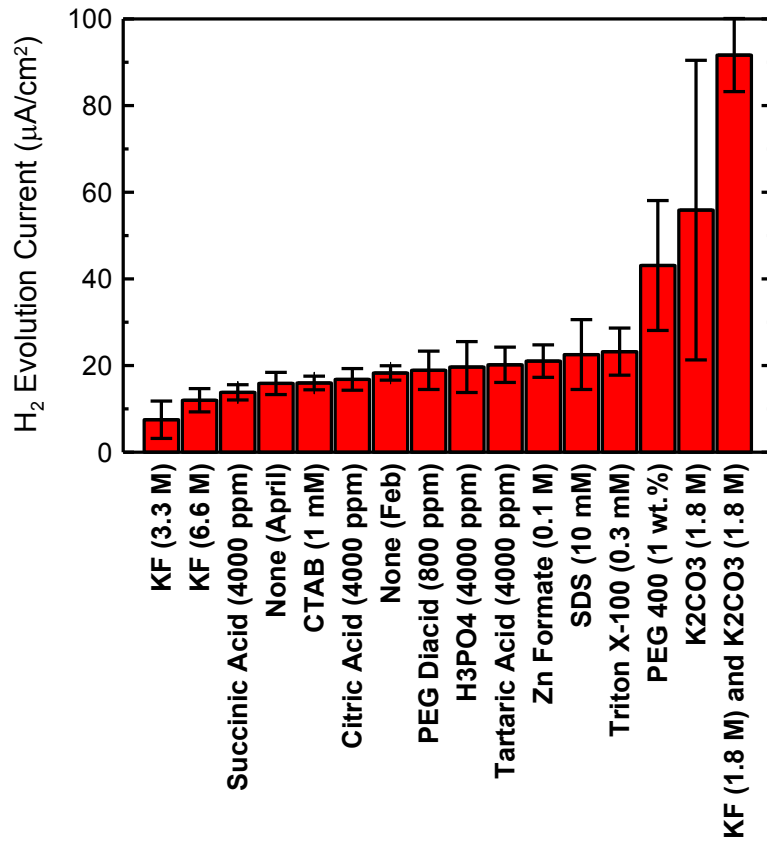


Figure 4-14: Parasitic  $H_2$  evolution current in the presence of electrolyte additives. The plating and stripping currents were  $3 \text{ mA}/\text{cm}^2$  for 10 min in 3.2 M KOH, saturated with ZnO, onto Cu foil.

$\mu\text{A}/\text{cm}^2$  for 6.6 M KF, which matches the data within experimental error. This result suggests that the reason 3.3 M KF produces statistically less parasitic  $\text{H}_2$  during charge is due to its increased electrolyte conductivity compared to the other additives, which are not concentrated enough to significantly enhance conductivity. The exception being the samples with  $\text{K}_2\text{CO}_3$ .

Conversely, the additives that appeared to increase the parasitic current were PEG 400,  $\text{K}_2\text{CO}_3$  and the combination of  $\text{K}_2\text{CO}_3$  & KF. As was mentioned above,  $\text{K}_2\text{CO}_3$  seems to promote larger holes in the Zn deposit, which would increase the surface area on which  $\text{H}_2$  evolution occurs during charge. Zn plating in the 1.8 M  $\text{K}_2\text{CO}_3$  & 1.8 M KF solution occurred at an overpotential about 10.8 mV higher than in the 3.3 M KF electrolyte, which would suggest an  $i_{\text{H}_2}$  of  $28 \mu\text{A}/\text{cm}^2$  in the 1.8 M  $\text{K}_2\text{CO}_3$  & 1.8 M KF electrolyte based on the measured value of  $7 \pm 4 \mu\text{A}/\text{cm}^2$  in the 3.3 M KF electrolyte. Since the theoretical  $28 \mu\text{A}/\text{cm}^2$  is significantly lower than the measured value of  $92 \pm 8 \mu\text{A}/\text{cm}^2$ , the increase in parasitic  $\text{H}_2$  evolution in baths containing  $\text{K}_2\text{CO}_3$  cannot be solely due to the increase in Zn plating overpotential, but could be explained by a combination of an increased Zn plating overpotential and a holey deposit. Adler *et al.* studied the effects of adding KF,  $\text{K}_2\text{CO}_3$  and LiOH to KOH electrolyte in Ni-Zn cells.<sup>92</sup> They determined that both [3.2 M KOH, 1.8 M KF, 1.8 M  $\text{K}_2\text{CO}_3$ ] and [3.5 M KOH, 3.3 M KF] electrolyte formulations were excellent at extending the cycle life of Ni-Zn cells by staving off shape change and generally reducing the capacity-loss per cycle. These formulations are thus important for rechargeable Ni-Zn cells and so it is interesting to observe that the KF &  $\text{K}_2\text{CO}_3$  formulation behaved so poorly here as it was the favoured formulation in the paper by Adler *et al.*<sup>20</sup> One possible explanation for the extension in cycle life would be that this formulation reduces the CE of the Zn electrode to be more in line with the Ni electrode CE, which would lead to less overcharging of the Zn electrode over many cycles. In effect, reducing the amount of Zn that is left

undischarged each cycle increases the number of cycles required to completely fill the available Zn capacity.

At first glance, it may seem surprising that none of the additives seemed to improve the self-discharge rate of the Zn electrode, considering that the papers from the literature that these additives and concentrations were taken from suggested that they do just that.<sup>20, 145, 162, 164, 165, 179</sup> However, a closer inspection of the experimental methods of these papers reveal several reasons why the results presented in this chapter have come about.

Lee *et al.*, who suggested Phosphoric, Succinic, Tartaric and Citric acids, used linear potential sweeps, reaching currents as high as 400 mA at potentials as low as -4.2 V vs Hg/HgO, to claim that these acids reduce self-discharge.<sup>145</sup> Without any data at the actual potential (about -1.4 V) and currents (about 3  $\mu\text{A}/\text{cm}^2$ ) where Zn corrosion occurs, nor any direct measurement of capacity lost or H<sub>2</sub> evolved, their results are questionable. Kim *et al.*, who suggested Zn Formate, also used high current density linear potential sweeps and cited the differences between the curves at high currents as their reasoning for believing their additives decrease self-discharge rates.<sup>165</sup> Finally, Dobryszycski *et al.*, who tested PEG 400, also used a linear potential sweep method and compared the changes in the curves at currents around 1 mA to make claims about the benefits of PEG 400.<sup>179</sup> Since none of these studies attempted to prove that their Tafel slopes extended to the corrosion potential or current, their conclusions are questionable. The experimental results of this section suggest that Phosphoric, Succinic, Tartaric and Citric acids, as well as Zn Formate and PEG 400 are not effective electrolyte additives within the parameters of this experimental method.

Cohen-Hyams *et al.*, who recommend PEG DiAcid 600, used a commercially made prismatic cell and a comparatively small amount of gel electrolyte.<sup>164</sup> They then heated the cell to 50°C in a sealed, stiff container and measured the volume of H<sub>2</sub> produced over 10 hours. Since they used a gel electrolyte, which slows diffusion rates, a larger active material

to electrolyte ratio and an increased temperature, it is not surprising that they came to a different conclusion. However, they also did not use a control, making a comparison between PEG DiAcid and the absence of it impossible. Regardless, PEG DiAcid 600 did not reduce the self-discharge rate within the parameters of the experimental method presented here.

Gomes *et al.*, who tested SDS, CTAB and Triton X-100, did not measure Zn corrosion at all.<sup>162</sup> They were more interested in the surface morphology of Zn plated with these different additives. These additives were tested here to see if they adjusted the coverage of the current collector (by Zn), which would bring about a change in the self-discharge rate. Evidently, the Zn coverage did not change significantly with any of these additives since the self-discharge rate did not change. Also, note that the addition of SDS, CTAB or Triton X-100, which were observed by Gomes *et al.* to change the Zn morphology,<sup>162</sup> did not change the self-discharge rate, similarly to PEG 400. This further confirms that the rate limiting H<sub>2</sub> evolution does not occur on the Zn deposit.

#### **4.5 Foil Experiment Conclusions**

The results of this chapter demonstrate that the self-discharge rate is controlled by the overpotential for H<sub>2</sub> evolution of the current collector material and the surface area of current collector that remains exposed to the electrolyte after Zn plating. Figure 4-15 shows a schematic of this mechanism, which is essentially the galvanic corrosion of Zn. Galvanic corrosion has not been formally recognized in the literature as the rate determining mechanism in the self-discharge of rechargeable Zn electrodes and has major ramifications for researchers who have been using Ni foam<sup>124, 126, 127, 131</sup> or even silver<sup>135, 175</sup> as a current collector, or graphite<sup>123, 128, 187</sup> as a conductive additive. Recall that Cu was shown to be a poor current collector material in Chapter 2, and should also be avoided. In

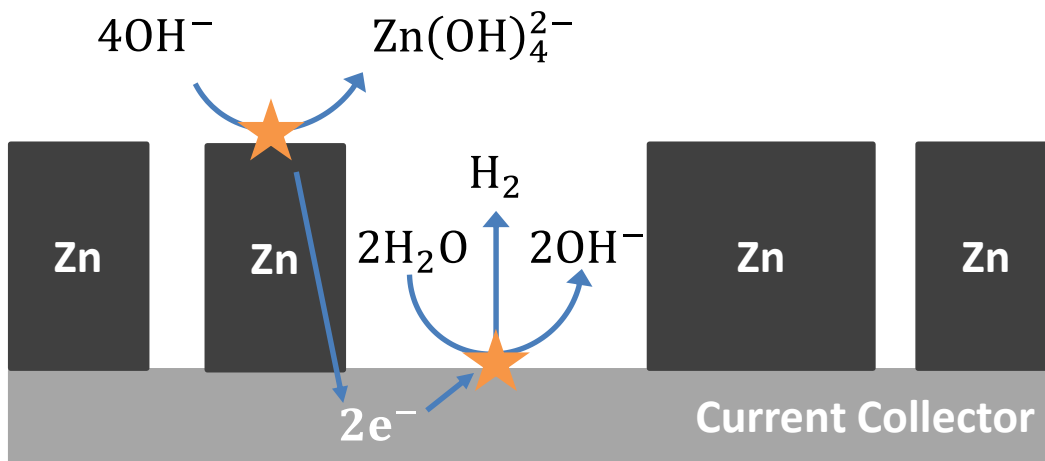


Figure 4-15: Schematic of the proposed mechanism for self-discharge in rechargeable Zn electrodes. The mechanism is the galvanic corrosion of Zn. The self-discharge rate is controlled by the rate of  $H_2$  production on the current collector.

the coin cells, more current collector surface area was left exposed than in the foil experiments of this chapter, which could explain the difference between the results in Figure 2-18C (pg. 85) and Figure 4-8 (pg. 134). Indium (In) would be a good current collector material, but it is rare and expensive (~700 US\$/kg In vs 24 US\$/kg Sn). Researchers should instead use Sn electroplated current collectors. An ideal Zn electrode current collector might well be Sn electroplated Cu foam. Commercial battery manufacturers might already be aware of this since at least one rechargeable Ni-Zn manufacturer (PowerGenix) uses a Sn-coated Cu expanded mesh as the Zn electrode current collector.<sup>113</sup> This also helps explain how non-rechargeable alkaline batteries can have a shelf-life of 8 years. The current collector in “alkaline batteries” is a low surface area nail in the center of the cell or coin cell cap surface that has been electroplated with Sn, In, Bi and/or Zn (with proprietary techniques that produce a hole-free coating).<sup>188, 189</sup> Overall, self-discharge rates are kept low in alkaline batteries by using Zn alloyed with indium and/or bismuth, keeping the current collector surface area small (compared to a rechargeable cell) and using a gel electrolyte, which slows diffusion and further reduces the activity of water.<sup>82, 188, 189</sup>

Section 4.4.5 demonstrated that many additives, such as Phosphoric, Succinic, Tartaric and Citric acids, as well as Zn Formate, PEG 400 and PEG DiAcid 600 are not effective as self-discharge inhibitors when using a rechargeable Zn electrode with a current collector, contrary to the claims of several authors.<sup>145, 146, 164, 165, 179, 180</sup> Recently, rechargeable Zn electrodes made entirely of Zn (i.e. Zn plated onto a Zn foam current collector) have been proposed, and these additives might behave differently in that case;<sup>190, 191</sup> however, a current collector made of Zn runs the risk of dissolving every cycle and therefore might be a foolish idea for long cycle life cells. A few Zn plating additives including SDS, CTAB and Triton X-100 were also shown to have no significant effect on self-discharge rates. Finally,  $K_2CO_3$ , which is an electrolyte additive intended to extend cycle life,<sup>20</sup> was shown to accelerate self-discharge.

The “charge-wait-discharge” method of measuring the self-discharge rate of rechargeable electrodes demonstrated in this chapter is also new and should make measurements of the self-discharge rate easier in that a battery researcher does not have to come up with a means of collecting and measuring  $H_2$  gas evolution. In particular, this method should work quite well on rechargeable Zn-air cells where the CE of the positive electrode will not limit the discharge capacity of the Zn electrode and the Zn electrode will be exposed to the conditions of a battery-like cell instead of the more usual  $H_2$  evolution experiment where some form of Zn is placed in a vial full of electrolyte.<sup>174, 175, 179</sup> Additionally, the charge-wait-discharge method can produce time dependent rates of self-discharge by taking the derivative of the resulting  $Q_D$  vs  $t_{ocv}$  data, if applicable.

The primary lingering concern with the experiments presented here was the inability to measure self-discharge rates over long periods of time (i.e. > 15 hours) due to electrolyte wicking and the failure of the marine epoxy to prevent it. As was mentioned in Section 4.4.1, researchers have observed different trends in the self-discharge rate with

respect to time.<sup>175, 176, 179</sup> The cause of these varied results has not been elucidated;<sup>14</sup> but clearly, further experiments with the charge-wait-discharge method in an apparatus that is not at risk of breaking down and that last at least 10 days<sup>175</sup> should be performed to determine if self-discharge rates remain constant or increase with time. This was the goal of Chapter 5.

## Chapter 5: Self-Discharge Experiments Using Coin Cells

### 5.1 Motivation

As was discussed in Section 4.4.1 (pg. 129), controversy exists in the literature about the time dependence of the self-discharge rate ( $i_{SD}$ ) of Zn electrodes.<sup>14, 132, 174-176, 179</sup> In Chapter 4, self-discharge rates appeared to be constant with time, and this fact was exploited in the data analysis by fitting a line to the discharge capacity (or CE) vs OCV time data. However, those experiments only probed the first 2 hours of OCV time (a.k.a. self-discharge time) due to problems with electrolyte wicking. Additionally, those experiments were conducted in flooded cells, without separators or stack pressure, and without ZnO necessarily building up on the current collector (due to gravity since the foils were vertical). The rate determining step determined in Chapter 4 suggests that these factors should not affect the self-discharge rate, but it was prudent to confirm that. Along those lines, the experiments in this chapter establish three things about Zn electrodes: (1) They suggest that the  $i_{SD}$  of Zn in a coin cell is the same as that measured in a flooded cell. (2) They also suggest that the  $i_{SD}$  of Zn in a coin cell is constant in time, just like the flooded cells of Chapter 4. (3) They demonstrate that additives can behave differently in a battery-like cell than in a flooded cell.

The coin cells developed in Chapter 2 can be charged and left to sit for days without worrying about electrolyte wicking issues, and they are a battery-like system with separators, stack pressure, small amounts of electrolyte, current collectors and ZnO that builds up directly on the current collector. A 'storage system' already existed in-house that was designed to monitor the shelf-life of a cell by measuring the potential over time. Monitoring the potential of the cell revealed the self-discharge rate of the Ni electrode, the potential of which is dependent on the state of charge, but the state of charge of the Zn



electrode did not bring about a change in potential until it had finished discharging, due to its flat potential curve at slow discharge rates. As such, the storage system could be used to measure the length of time until all of the Zn had dissolved off of the current collector and to determine the self-discharge rate of the Ni electrode. The ability to measure the length of time until the Zn electrode finished discharging was enough to determine the average self-discharge current by dividing the capacity stored by the Zn electrode (mAh) by the time to complete self-discharge (h). However, this technique did not work when the Ni electrode finished self-discharging first and so the first challenge was to measure the self-discharge rate of the Ni electrode.

## 5.2 Self-Discharge of Ni Electrodes in Coin Cells and Commercial Ni-Zn Cells

To measure the self-discharge rate of the Ni electrode and compare this rate to that of a commercial Ni electrode for the sake of interest, a coin cell and a commercial cell were charged and then their potentials were monitored over time as they self-discharged, as shown in Figure 5-1. The ‘storage system’ used to monitor the cells was a Keithley 2750 potentiometer, programmed to only connect to the cell once per hour to record the cell

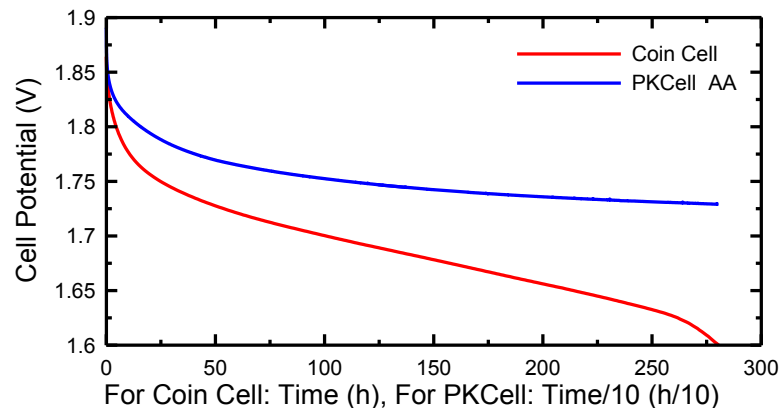


Figure 5-1: Self discharge of a Ni-Zn coin cell and commercial AA cell (PKCell). The terminals of the cells were only connected to the potentiometer long enough to collect a measurement once per hour, thereby leaving the cell truly disconnected the majority of the time. The commercial PKCell Ni-Zn AA cell was still discharging at the time of writing after 2,800 h.

potential. As such, the cells were left disconnected from the measuring device the majority of the time. In the figure it appears that the commercial cell, with a capacity of 1530 mAh, self-discharges more slowly than does the coin cell, with a capacity of 3.69 mAh. But since this data does not contain direct information about the current, more information is needed together with Figure 5-1 to determine the actual self-discharge current. It is important to note that the Zn electrode potential is flat during the majority of self-discharge, and so the entire potential drop until 1.63 V (about 260 h) observed in Figure 5-1 is due solely to the Ni electrode losing charge and intercalating  $H^+$  ions and corresponding  $e^-$ . A self-discharge current acquired using Figure 5-1 will therefore only represent the self-discharge rate of the Ni electrode. The steeper potential drop below 1.63 V is due to the Zn electrode approaching the end of its state of charge, as was demonstrated in Figure 3-4 (pg. 98).

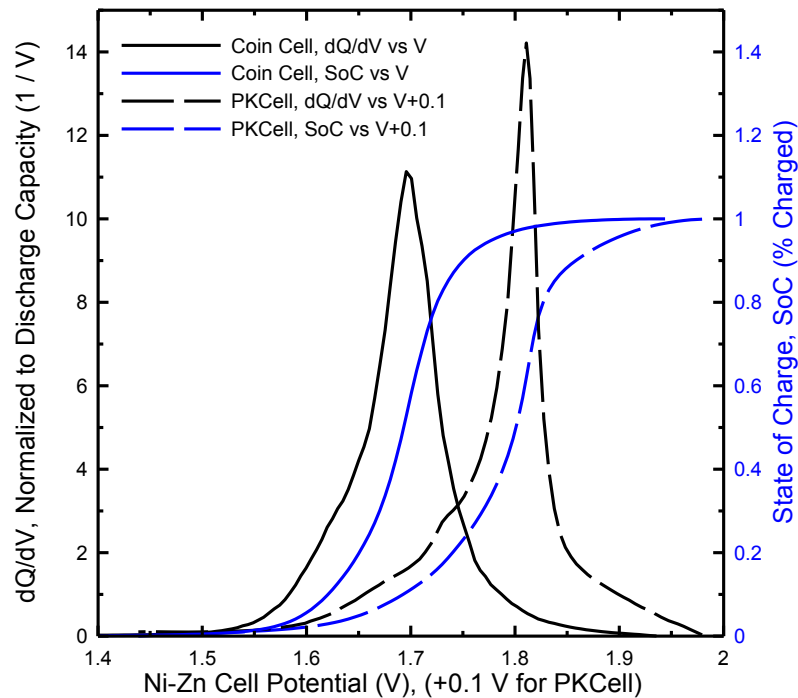


Figure 5-2:  $dQ/dV$  curves for a typical Ni-Zn coin cell and commercial AA cell (PKCell). The coin cell was discharged at a C/5 rate while the PKCell was discharged at a C/20 rate, yielding discharge capacities of 3.691 mAh and 1,532 mAh, respectively. Both cells were held at  $30. \pm 0.1^\circ C$ . The SoC vs V lines (blue) correspond to the right-side y-axis. The PKCell data was intentionally offset by +0.1 V to separate the two data sets for easier examination.

To determine the self-discharge current, a reference curve for the potential must first be obtained to specify the link between potential and state of charge. Then, the derivative of both the self-discharge curve and the reference curve are multiplied together to acquire the current as a function of potential:

$$\frac{dQ(V)}{dV} \cdot \frac{dV}{dt} = \frac{dQ(V)}{dt} = I_{SD,Ni}(V). \quad (5-1)$$

Figure 5-2 shows the reference potential curve (in blue) and the derivative of it (in black) for the V vs Q curves of the two cells shown in Figure 5-1, acquired in a separate experiment. The dQ/dV data was normalized to account for the larger capacity of the commercial cell by dividing the data by the capacity of the relevant cell. Because of this, the area under both dQ/dV curves is equal to 1.

Figure 5-3 shows the dV/dt curves for the same two cells, acquired directly from Figure 5-1. A fit was applied to both data sets here (not shown) to allow for interpolation to generate data points at the same potentials as the data points in Figure 5-2. The data from Figure 5-2 is then multiplied by the fit from Figure 5-3 to generate the Ni electrode self-discharge current as a function of potential, which is shown in Figure 5-4. Again, the data has been normalized to the discharge capacity of the two cells to allow them to be compared to each other. The “1/year” unit effectively means “how many times would this Ni electrode

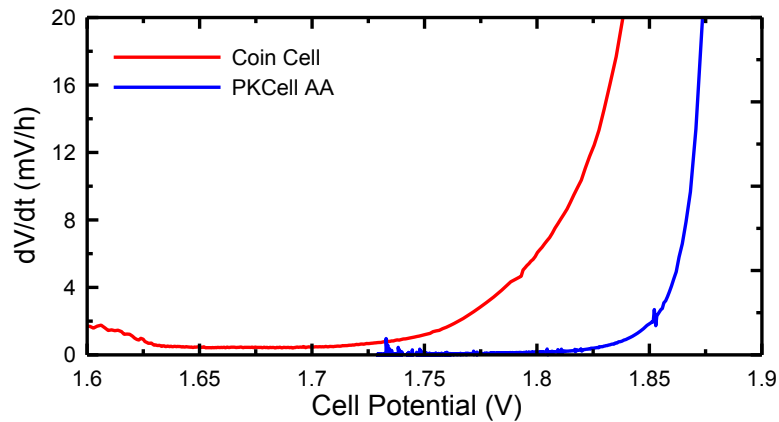


Figure 5-3: dV/dt curves calculated from the V vs t data in Figure 3-1.

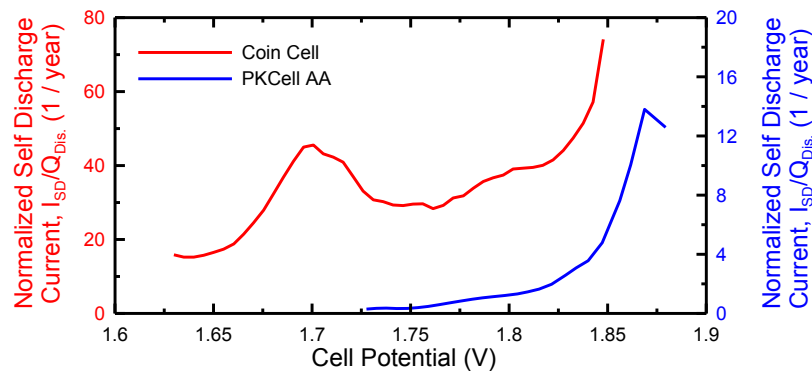


Figure 5-4: Normalized self-discharge current of the Ni electrodes of a coin cell and a commercial AA cell (PKCell). Normalization was achieved by dividing the currents by the discharge capacity of the respective cell. The PKCell cell uses the right-side y-axis, which is 4x lower in scale than the left-side y-axis.

discharge in one year". Evidently, the commercial Ni-Zn cell had a Ni electrode that self-discharged via Reaction (1-26) (pg. 25) more than four times slower than the Ni electrode in the coin cell. This was likely due to proprietary techniques and materials used by commercial cell manufacturers.<sup>114</sup> The coin cell Ni electrode here displayed an average self-discharge current of 14.4  $\mu\text{A}$ , or 8.14  $\mu\text{A}/\text{cm}^2$ , down to 1.63 V. The self-discharge current likely stayed low below 1.63 V, so this averaged rate would be lower still if the data in Figure 5-1 was complete. Regardless, knowing the relative scale of the self-discharge current of the Ni electrode is important because if the Ni electrode reaches the end of charge before the Zn electrode does, then a measurement of the Zn electrode self-discharge rate cannot be made. Since the self-discharge rate of a coin cell Ni electrode demonstrated here was on the same scale, and greater than, the Zn self-discharge currents measured by the foil experiments, the Ni electrode of a coin cell left at open circuit might finish discharging first.

### 5.3 Experimental Methods

#### 5.3.1 The "Race to the Bottom" Between Self-Discharging Ni and Zn Electrodes

The most confounding problem with using Ni-Zn coin cells to measure the self-discharge rate of Zn electrodes is the fact that the Ni electrodes have a lower coulombic efficiency ( $CE = Q_{\text{Dis.}}/Q_{\text{Charge}}$ ) than the Zn electrodes and a similar self-discharge rate. This means that if the cell is charged to a fixed potential limit, the Ni electrode will always contain less charge than the Zn electrode and will thus finish discharging before the Zn electrode. Figure 5-5 demonstrates what the potential curves look like when either a Ni electrode or a Zn electrode finish discharging first. The simplest way to tell whether the Zn or Ni electrode finished discharging first is the presence or absence of the Sn dissolution plateau, respectively. The Sn dissolution process was described in Section 1.6.2 (pg. 23).

In order to measure Zn electrode self-discharge rates, the goal must be to measure the relative shelf-life (i.e. time) of Zn electrodes in coin cells under different conditions. The potential-monitoring storage system allowed the determination of the time at which the Zn

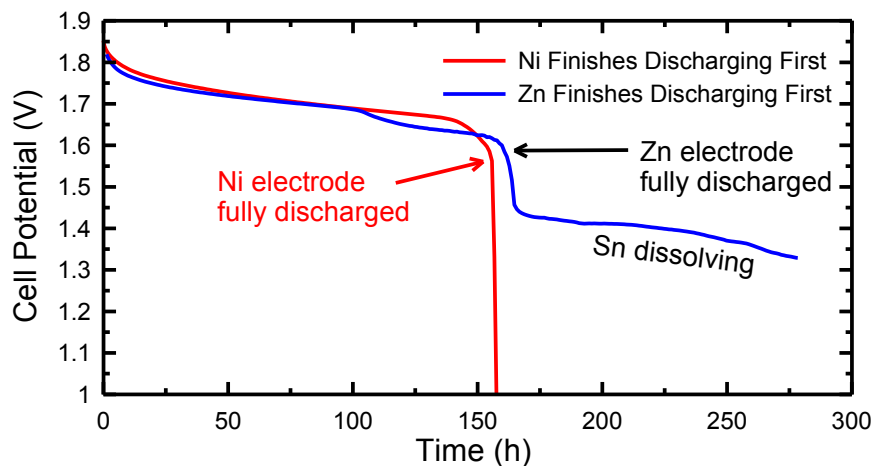


Figure 5-5: Example self-discharge data for coin cells. The completion of discharge by the Zn electrode can be identified by the presence of the Sn dissolution plateau. The self-discharge current is determined by dividing the theoretical capacity of the Zn electrode by the time the cell took to fully discharge the Zn electrode. If the Ni electrode instead finished discharging first, then the potential dropped to about 0.9 V vs Zn, where it finished intercalating  $H^+$  and  $e^-$  as shown in Figure 3-4.

electrode finished discharging; however, to ensure the Zn electrode discharged first, special precautions during the preparation of these cells had to be taken.

### *5.3.2 Preparation Procedure for the Ni-Zn Coin Cells*

Typical coin cells were fabricated as described in Section 2.2 (pg. 47), with the following changes: 1.5 cm diameter electrodes of both Ni and Zn were used instead of 1.27 cm diameter electrodes. They were punched out of the foil using a knife punch acquired from DPM Solutions without using any sacrificial layers to aid the punching process. Zn electrodes used 0.001" thick Sn foil instead of Cu foil. PbO was not added to the Zn electrodes, since no additives other than the ones intended to be tested were desired; the ZnO electrodes were thus 95.5 wt% ZnO. The ZnO electrode slurries were mixed using the Mazerustar in the same way that the Ni electrode slurries were mixed since it was easier than using the ball mill and just as effective. Finally, different sized notch bars were used to make electrodes of different capacities for reasons that will be described momentarily.

As was described in Section 2.3.2 (pg. 54), Ni electrodes must be 'formed' before they can be used. In this work, that process is always completed with a larger capacity Zn electrode before moving the formed Ni electrode to a new cell with a smaller capacity Zn electrode. A large capacity Zn electrode was used during formation cycling to avoid excessive overcharging of the Zn electrode and the associated risk of dendrite-induced short circuits. Large capacity Ni electrodes (ex. 3.6 mAh) were created with an 0.011" notch bar. These electrodes were formed in a cell with a large capacity Zn electrode (ex. 20 mAh) created with a 0.006" notch bar. Figure 5-6 shows the formation cycling of the Ni electrodes before they were transplanted into the storage cells with additives. The formation procedure included 4 cycles at a C/2 rate with charge terminating at 100% of the theoretical capacity of the Ni electrode, and a discharge ending at 1.4 V. The 5<sup>th</sup> cycle was at

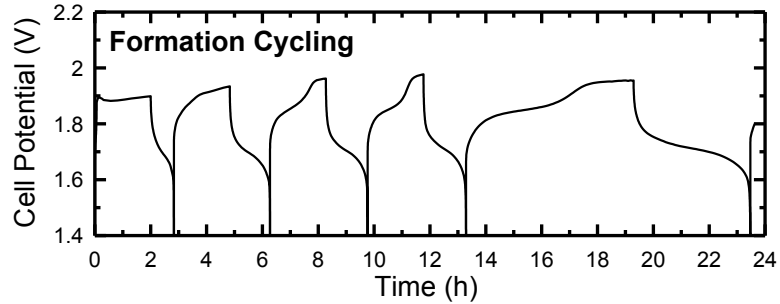


Figure 5-6: Formation of Ni electrodes for storage experiments. Ni electrodes were formed in coin cells with larger capacity Zn electrodes, as shown here, and then transferred to new cells with smaller capacity Zn electrodes to be prepared for storage.

a C/5 rate with charge terminating at 120% of the theoretical capacity and the 6<sup>th</sup> charge half-cycle ended at 1.8 V. The last short charge half-cycle was intended to leave the electrode in a slightly charged state to prevent it from entering into overdischarge due to self-discharge before the next procedural step could be completed.

Once formation was finished, the cell was carefully dismantled using a Cell Opener (DPM Solutions), which avoids short circuiting the cell and does not destroy the cell components, and the Ni electrode was removed. It was moved to a new cell with new separators, new electrolyte and a fresh, smaller capacity Zn electrode (ex. 1.6 mAh) created with a 0.0015" notch bar. This new cell was put back on the Maccor charger and cycled in such a way as to leave the Zn electrode fully charged and the Ni electrode significantly more

Table 5-1: Summary of storage preparation procedures. These procedures all begin in a constant current mode, but shift to constant voltage if the voltage limit is reached during charge. "C" refers to the theoretical capacity of the Zn electrode.  $0.5 C = C_{\text{Theoretical}}/2$  h. A limitation of 1.5 C means the Zn electrode was overcharged by 50%. The discharge procedure was the same for all cycles.

Procedure	Half-cycle	Current	Limitations	Repeat n Times
<b>A</b>	Charge	0.5 C	1.5 C 2.06 V	3
<b>B</b>	Charge	0.5 C	1.2 C 2.06 V	1
	Charge	0.5 C	1.4 C	1
<b>C</b>	Charge	0.5 C	1.5 C 2 V, 150 $\mu$ A	3
<b>All</b>	Discharge	0.5 C	1.4 V	Varied

charged than the Zn electrode.

Achieving the state where the Ni electrode was holding more charge than the Zn electrode was tricky, and three procedures for accomplishing this were used in this work. These three procedures are shown in Figure 5-7 and defined in Table 5-1. Some cells from all three procedures “failed” in that the Ni electrode finished self-discharging first, but the proportion of cells that failed this way was reduced with each new preparation procedure. Only data from cells where the Zn electrode finished discharging first was used to draw conclusions, which included cells from all three procedures. The first procedure (A) was quite aggressive, overcharging the cell by 50% for three cycles in a row. This increased the

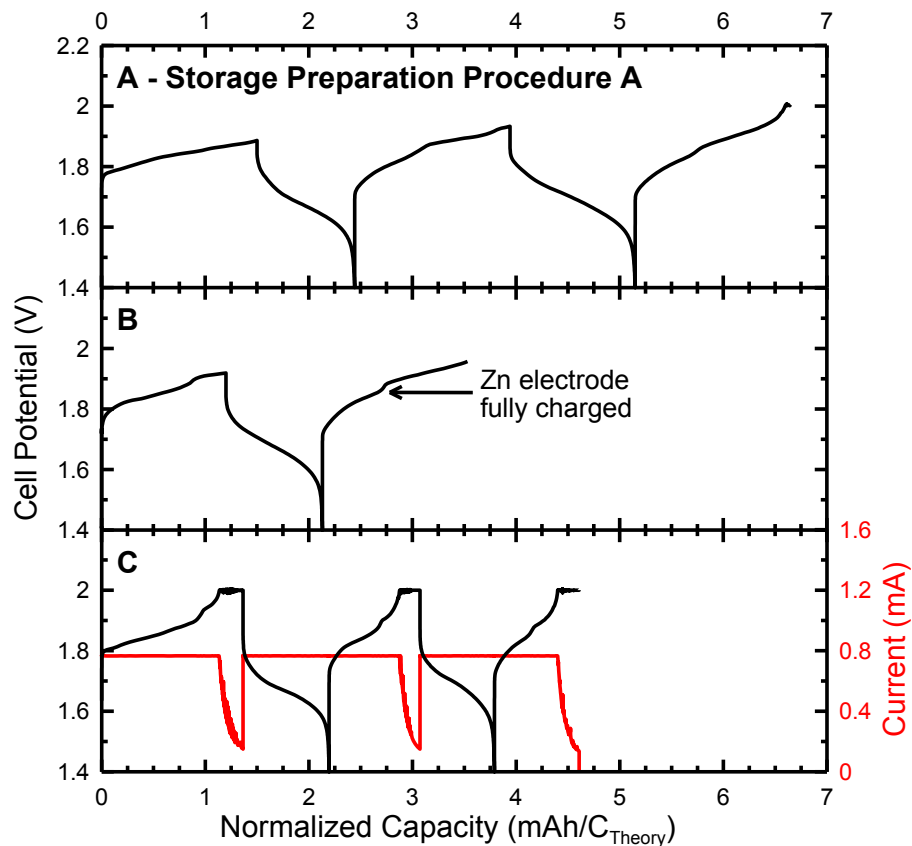


Figure 5-7: Preparation cycling of a pre-formed Ni electrode and a small capacity Zn electrode in a Ni-Zn coin cell before placing the cell on the long term storage system. The x-axis is normalized to the theoretical capacity of the Zn electrode. The current in all of these procedures was  $Q_{\text{Theoretical, Zn}}/2$  h except where the potential was limited to 2 V in panel C. These three example cells contained no electrolyte additives.



risk and rate of Zn dendrite formation and subsequent cell failure. In order to reduce the risk of short circuiting, procedure B only had one conditioning cycle and the overcharge of the first and second cycles was limited to 20% and 40%, respectively, as listed in Table 5-1. 20% overcharge was chosen because the typical Ni electrode coulombic efficiency witnessed during this work was greater than 80% so it was thought that 20% overcharge would leave the Ni electrode at a higher state of charge than the Zn electrode by the end of the charge half-cycle. This was found to be overly optimistic since the discharge capacities of cycle 1 in procedure B varied wildly between 61% and 103% of the theoretical capacity of the Zn electrode, ostensibly because the Ni electrode had a lower CE than 80% in some cells during cycle 1. Note that the point where the Zn electrode becomes fully charged is marked in panel B. The slight step in potential was identifiable because the current was high enough to make the transition from Zn plating to H<sub>2</sub> evolution noticeable as was described in Section 3.1.3 (pg. 96).

For the final procedure, it was discovered that holding the Ni electrode at 2.00 V during charge and letting the current decay resulted in cells that were more reliably Zn capacity limited. Figure 5-7C shows this procedure C, while Table 5-1 lists the relevant parameters it used. It was decided that at least two conditioning cycles were required: The first cycle was to re-wet or re-form the Ni electrode to return it to proper working order and the second was to measure the accessible Zn capacity. Current was included on the right-side y-axis in panel C of Figure 5-7 to illustrate how the current decayed when the cell reached 2.00 V and was held there until the current decayed to 150  $\mu$ A.

Throughout these experiments, it was assumed that any H<sub>2</sub> produced on the negative electrode successfully escaped the vicinity of its production since the diffusion constant of H<sub>2</sub> in water is quite large ( $D = 45 \times 10^{-6} \text{ cm}^2/\text{s}$ ).<sup>192</sup> A rough estimate of the time

required for a H<sub>2</sub> molecule to diffuse from the center of the electrode to the edge (d = 0.75 cm) can be calculated from

$$t = \frac{d^2}{\pi D} = 1.1 \text{ hours.} \quad (5-2)$$

Since the experiments lasted about 300 hours, H<sub>2</sub> had plenty of time to diffuse out of the electrolyte. Any H<sub>2</sub> that then escaped into the cell would have then escaped the cell altogether since the pressure release valve was weak (i.e. scotch tape), thereby keeping the internal pressure in the coin cells used here at 1 atm.

Recall that the purpose of overcharging the Zn electrode while further charging the Ni electrode was so that the capacity that self-discharged during storage would be equal to the theoretical capacity of the Zn electrode. After the storage preparation procedure, the cell was immediately moved to the storage system where its potential was measured once per hour for several hundred hours. Two example data sets have already been shown in Figure 5-5. Both the preparatory cycling and storage were carried out at  $30.0 \pm 0.1$  °C. The average self-discharge current was determined by taking the theoretical Zn electrode capacity and dividing it by the time to Zn electrode failure measured by the storage system.

#### **5.4 Effect of Time and Electrolyte Additives on the Self-Discharge of Ni-Zn Coin Cells**

Coin cells with pre-formed Ni electrodes and the same additives used in Section 4.4.5 were created, prepared and placed on the storage system. As reasoned in Chapter 4, the rate determining step of self-discharge is Reaction (4-5) (pg. 118) on the current collector. If the additive effectively reduces H<sub>2</sub> evolution on Sn by occupying surface sites on the current collector, then it will reduce the self-discharge rate of the Zn electrode.

Figure 5-8 shows the results of these experiments. Unfortunately, the difficulty of the cell preparation procedure and time limitations led to the large error bars shown in the figure. From the “None” data of Figure 5-8, the self-discharge current of Zn electrodes in Ni-Zn coin cells was equal, within experimental error, to the rate measured using the flooded cells of Chapter 4 (about  $3.5 \mu\text{A}/\text{cm}^2$ ). The fact that the self-discharge rate was the same suggests that the same rate determining step is in control in a battery-like system.

Of particular importance is the fact that the average self-discharge currents ( $i_{SD}$ ) in Figure 5-8 were all under  $3.5 \mu\text{A}/\text{cm}^2$ , which is close to the initial rates measured with the foil experiments of  $3.1 \mu\text{A}/\text{cm}^2$ . If the Zn corrosion current increased markedly by a factor of about 10 as observed by Dobryzskyi *et al.*,<sup>179</sup> then a higher average would be expected

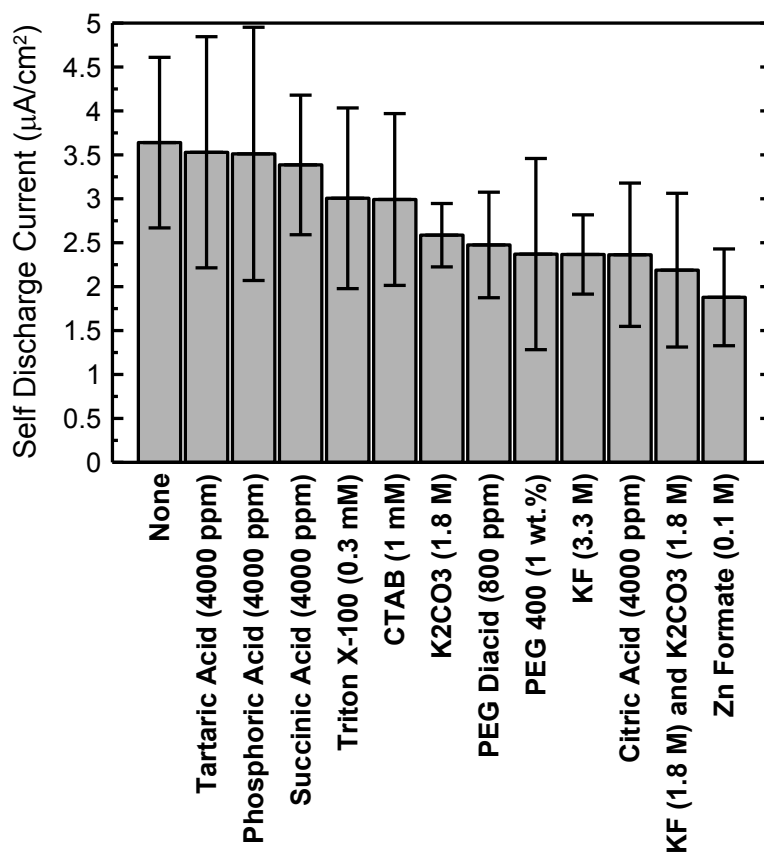


Figure 5-8: Self-discharge rates of Ni-Zn coin cells with various electrolyte additives. The bar heights and error bars represent the average and standard deviation of 4 cells, except for K<sub>2</sub>CO<sub>3</sub>, KF and K<sub>2</sub>CO<sub>3</sub> and PEG DiAcid which all had only 3 cells. The base electrolyte to which all the additives were added was 3.2 M KOH, saturated with ZnO.

from the coin cell experiments after about 10 days. Similarly, if  $i_{SD}$  had decreased by a factor of about 4 over the first 10 days as observed by Gregory *et al.*, then a lower average would be expected.<sup>175</sup> However, a change in  $i_{SD}$  was not observed, which suggests that the  $i_{SD}$  is constant in time as observed in the charge-wait-discharge experiments of Chapter 4 and by Meesus *et al.* and Ruetschi *et al.*<sup>174, 176</sup>

For the additives, four successful experiments with each additive were completed, except for  $K_2CO_3$ , KF &  $K_2CO_3$ , and PEG Diacid which all had only 3 experiments. In comparison with the blank ( $3.6 \pm 1.0 \mu A/cm^2$ ), the only additive that is statistically lower (i.e. not equal within experimental error) is Zn formate ( $1.9 \pm 0.6 \mu A/cm^2$ ). Researchers hypothesize that additives, such as Zn formate, adsorb onto the electrode surface and reduce the rate of water electrolysis (i.e. Reaction (4-5) on page 118).<sup>165</sup> Determining whether or not Zn formate adsorbs onto the current collector surface more strongly or weakly than the other additives tested here could be pursued as future work.

The fact that KF &  $K_2CO_3$  do not increase the self-discharge rate in full coin cells, but do increase it in a flooded 3-electrode experiment like the foil experiments is difficult to reconcile. The presence of a Ni electrode, separators and stack pressure can change the interactions of electrolyte additives from what they were in a flooded 3-electrode foil experimental set up. To be specific, Ni electrodes operate at potentials up to 2 V vs Zn, so if an additive reacts at any potential up to 2 V, it will react on the Ni electrode. Furthermore, microporous separators, along with stack pressure, can influence the morphology of the Zn deposit. What factors are important in the present situation requires further research to explain. Again, the purpose of this research was to develop a method of measuring the self-discharge rate of battery-like rechargeable cells in order to compare the effectiveness of these additives to one another.

An important observation during these coin cell self-discharge experiments was that mass was lost over the course of the experiments. The low humidity in the lab during winter, when these experiments were run, at 30°C coupled with the pressure relief valve being a simple cellophane tape-covered hole resulted in a water loss rate of about 1 to 3  $\mu\text{L}/\text{day}$  when there was only 30 to 40  $\mu\text{L}$  of electrolyte in each cell to begin with. This water loss should not have affected the self-discharge rate until the electrodes themselves started drying out, at which point the surface area would have shrank and so too would the self-discharge current. The critical volume of electrolyte at which the self-discharge rate was affected was not easily determined, since the self-discharge rate of the Zn electrode at a given point in time could not be determined using the storage system. In the future, this added complication could be avoided by storing the cells in a humidity controlled box. If the humidity is kept at the proper level with respect to the KOH concentration in the electrolyte, as determined by Figure 1-5, then evaporation from the electrolyte will effectively be eliminated.

## **5.5 Coin Cell Self-Discharge Conclusions and Future Work**

This chapter demonstrated four things. (1) The procedure for measuring the self-discharge rate of an intercalation electrode (like Ni) was demonstrated. By measuring the potential of the Ni electrode at open circuit over time and comparing the rate of potential loss to a calibration curve from a slowly discharged Ni electrode, the self-discharge rate as a function of time or potential can be determined. In this chapter, Ni electrodes made for coin cells were measured to have an average self-discharge current of about 8.1  $\mu\text{A}/\text{cm}^2$ . This rate was over 4x faster than the  $i_{\text{SD}}$  of a Ni electrode in a commercial AA Ni-Zn cell, but this was expected since manufacturers use proprietary techniques and materials to reduce self-discharge.<sup>114</sup> Of more immediate importance was the fact that this rate outstripped the  $i_{\text{SD}}$

of the Zn electrodes of Chapter 4. If both electrodes were charged to the same state of charge in a cell and then left to self-discharge, the faster  $i_{SD}$  of the Ni electrode would result in the Ni electrode reaching the end of discharge before the Zn electrode. As such, one way to use Ni-Zn cells to determine if the self-discharge rate of Zn electrodes increased over time was to overcharge the Zn electrode to leave the Ni electrode at a higher state of charge so that the Zn electrode would finish discharging first during a self-discharge measurement.

(2) The potential monitoring of the overcharged Ni-Zn cells yielded the amount of time until the Zn electrode had fully self-discharged, which in turn yielded the average self-discharge rate of the Zn electrode. Since this rate was equal, within experimental error, to the rate measured in Chapter 4, it was concluded that the  $i_{SD}$  in coin cells was the same as in the flooded cells of Chapter 4 and that the  $i_{SD}$  remained constant throughout the first 10 days, in agreement with some authors,<sup>176</sup> but at odds with others.<sup>132, 175, 179</sup> This result is important because it confirms that short term experiments, like the charge-wait-discharge method of Chapter 4, can provide meaningful mechanistic conclusions. If the self-discharge current had changed, then the results of Chapter 4 would require further proof that the rate determining step (rds) observed at short times continued to be the rds into the long term. A constant  $i_{SD}$  also suggests that the surface area of the current collector that is exposed to the electrolyte does not increase with time, since the self-discharge current is controlled by  $H_2$  evolution on the current collector (Reaction (4-5) on page 118). This means that the Zn that dissolves cannot originate from the edges of the base of the pores in the Zn deposit (see Figure 4-15) since this would increase the surface area of exposed current collector.

(3) The results of the additives suggest that the other cell components, like the separator and positive electrode, can affect additives to either enhance or reduce their effects on the Zn electrode. For instance, the presence of  $K_2CO_3$  was notably detrimental in the flooded cells of Chapter 4, but did not significantly affect the  $i_{SD}$  of the coin cells. Why

$K_2CO_3$  behaves differently in coin cells than in the flooded cell was not determined in this work but would be a valuable endeavor for researchers interested in Ni-Zn cells. Conversely, Zn formate did not significantly enhance  $i_{SD}$  in Chapter 4, but it did have a noticeably beneficial effect in the coin cells. Of all the additives studied in this thesis, Zn formate was the only one to statistically reduce the self-discharge rate, and so it warrants further research to determine how it achieved this. Overall, the fact that the self-discharge current of Zn electrodes exposed to additives in battery-like cells was different than that in flooded cells suggests that further research on additives should be performed, or at least confirmed, in battery-like cells before an additive is declared effective. This is currently not the practice in the literature,<sup>145, 146, 165, 179, 180</sup> and would improve the quality of research on self-discharge inhibitors.

(4) The difficulty of making and overcharging, without shorting, the Ni-Zn cells of this chapter demonstrates the importance of finding an alternative positive electrode to Ni to act as the counter electrode to Zn in future research efforts. A positive electrode with a higher coulombic efficiency (CE) and lower self-discharge current than Zn would allow the relatively easy charge-wait-discharge procedure of Chapter 4 to be used with a battery-like cell in place of waiting for the cell to completely self-discharge or trying to collect  $H_2$  gas from the cell. A durable bi-functional air electrode would satisfy both requirements (higher CE and lower  $i_{SD}$  than Zn) since the capacity of the air electrode, which is stored in the electrolyte and air, is larger than that stored in Zn, no matter whether the cell is being charged or discharged. Furthermore, a bi-functional air electrode used in a battery-like cell would ensure that additives being tested are properly evaluated in the intended system (assuming the additive is intended to be used in Zn-air cells). Consequently, developing or acquiring a durable bi-functional air electrode should be the first priority in continuing the research efforts discussed in this thesis.

## Chapter 6: Conclusions

### 6.1 Regarding Coin Cells

#### 6.1.1 Chapter 2 Conclusions

The purpose of the research in Chapter 2 was to convert the ubiquitous Li-ion lab-scale coin cell into a test vehicle for rechargeable Zn electrodes to facilitate and encourage more research into Zn-air and other alkaline metal-air technologies. The importance of several aspects of Ni-Zn cell design was demonstrated. This should help inform researchers who have been trying to enter into the research area of Ni-Zn and Zn-air cells while seemingly oblivious to the importance of these aspects, as evidenced by a lack of consideration for or reporting of those aspects:<sup>123, 124, 126-128, 130, 131</sup>

(1) The quantity of electrolyte in relation to the amount that can be held by the electrodes and separators has been shown to affect the shape-change phenomenon of the Zn electrode.<sup>43, 87, 88</sup> Consequently, it is important to make experimental cells that can operate with minimal amounts of electrolyte so that pools of electrolyte are avoided. The coin cell is one example of these so-called “battery-like” cells. Many authors do not report how much electrolyte they used, or even whether or not it was more than the amount required to soak the electrodes and separators.<sup>123-131</sup>

(2) Separators must be chosen properly, both in terms of number and type. The importance of the separators has been understated in the literature;<sup>70, 193</sup> therefore, it was enlightening to demonstrate the cycle life of cells with incorrectly chosen combinations of separators. In the literature, authors tend to report which separators they used, but no one has published a comparison of the cycle life of Ni-Zn cells built with different separators before.



(3) The research presented in Chapter 2 demonstrated the importance of stack pressure in determining cycle life. As such, the presence or absence of stack pressure should be reported in the literature. Although actual stack pressure measurements would be ideal, authors should at least state whether there was any kind of stack pressure applied to the electrodes or if the electrodes were simply dangled in the electrolyte. This is especially true for Ni-Zn cells since the importance of stack pressure for proper Ni electrode operation has been demonstrated in the past.<sup>101, 102</sup>

(4) Chapter 2 also demonstrated that the orientation of the coin cell can affect the cycle life. This concept is fairly specific to the coin cell design since it has an air pocket. Consequently, the Ni-Zn coin cells developed here should not be rotated more than 90° to keep the electrolyte from flowing into empty internal space.

(5) The stability and parasitic gas evolution propensity of all materials that are exposed to the electrolyte at the potentials of the corresponding electrode seem to have been overlooked by several authors.<sup>124, 126, 127, 131</sup> Chapter 2 demonstrated that materials like stainless steel are unsuitable as casing components or current collectors since they support high parasitic currents, which hinders cycle life. Ni metal should be used for positive-side components and current collectors. Cu was also shown to be unsuitable as a current collector for Zn in that it reduced the cycle life of coin cells in comparison with Sn. For the first time, Sn (tin) was demonstrated to enhance the cycle life of Zn electrodes, and researchers should consider coating their Zn current collectors with Sn in the future.

The advantage of having a low H<sub>2</sub> evolving current collector that also promotes a flat Zn deposit and does not alloy with Zn is particularly notable because it might explain the results of a few authors who claim that a metallic oxide additive to the electrode is beneficial.<sup>15, 115, 127, 159, 160, 194-196</sup> These additions might operate simply by coating the current

collector; in which case, it would likely be more efficient to simply use a different current collector in the first place.

(6) As discussed at the end of Section 2.3.6 (pg. 72), reproducibility has historically been poorly reported in the literature with few authors reporting it at all.<sup>118, 119, 123</sup> This could be due to a lack of space, materials or time, but frighteningly it could also be due to the erratic behaviour of cells and the authors' apprehension to report anything other than their best data. The consequence of erratic discharge capacity vs cycle data on standard deviations was touched on in Section 2.3.3 (pg. 58). In the author's opinion, researchers should produce at least three identical cells and report the average and standard deviations of the discharge capacities vs cycle number and/or the cycle life. Otherwise, the results are not as powerful as they could have been, and are more difficult to compare to the results of other authors. The ability to compare different advancements across research papers is also limited by the fact that authors have adopted the poor habit of not reporting their cell designs. As Chapter 2 showed, the cell design can affect the cycle life, and so comparisons of cycle life between bodies of research requires detailed cell designs to be reported.

### *6.1.2 Chapter 3 Conclusions*

Section 3.1 demonstrated some fundamental features of the 2-electrode Ni-Zn cell potential curves by conducting experiments with 3-electrode coin cells. It was demonstrated that during charging, the potential of the Zn electrode only reveals when it has finished charging if the current is high enough to create a noticeable potential difference between Zn plating and H<sub>2</sub> evolution. It was also demonstrated that a Ni electrode has a more abrupt drop in potential when it finishes discharging as compared to the Zn electrode. This had not been drawn attention to in the literature and was a useful tool in some circumstances to determine whether the Ni or Zn electrode had finished discharging first.

Most importantly though, it was also demonstrated that Ni electrodes commonly finish discharging before the Zn electrodes with Sn current collectors used in coin cells in this thesis. That is to say, the Ni electrodes had a lower coulombic efficiency (CE). This meant that Ni electrodes were insufficient as a counter electrode to Zn in a 2-electrode system where the purpose was to measure the discharge capacity of the Zn electrode. Conversely, this also meant that Zn was a fine counter electrode to Ni if the purpose of the research was to measure the discharge capacity of the Ni electrode. This revelation weakens the results of several studies that use 2-electrode Ni-Zn cells and claim that it was the discharge capacity of a modified Zn electrode that was measured.<sup>126-128, 130, 131</sup> A lower CE than Zn does not discount their results, but it does complicate them since a direct measurement of the intended variable might not have been achieved. For instance, the cycle life measurements made in Chapter 2 were carried out in intentionally Ni electrode limited coin cells, but the difference in cycle life between cells containing a Cu or Sn current collector was so dramatic that Sn can still be concluded to be superior to Cu. The trouble comes when a researcher wants to demonstrate *why*. If a counter electrode with a superior CE to Zn were present in the coin cell, then every cycle the discharge capacity would reflect only the behaviour of the Zn electrode instead of, for example, reflecting one electrode in early cycles and then the other in later cycles. Consequently, Ni electrodes should not be used in 2-electrode cell research intended to improve the Zn electrode unless they are pre-charged and have a large-enough capacity compared to the Zn electrode to reach the end of the Zn electrode cycle life before themselves becoming fully discharged. Alternatively, if a Ni electrode that had a higher CE than the Zn electrode were developed, this would also work. Either a reference electrode should be used or a new counter electrode should be found.

A bi-functional air electrode has a higher CE than the Zn electrode, suggesting that it should be used instead of Ni as the counter electrode. If a researcher can acquire or make an air electrode that outlives the Zn electrode then air electrodes should be used in future research efforts. Section 3.2 demonstrated how to adapt a coin cell to work with Zn and air electrodes for researchers who have durable, bi-functional air electrodes.

Coin cells can also be adapted to work with acidic aqueous cell chemistries, like  $\text{LiMn}_2\text{O}_4 - \text{Zn}$  as demonstrated in Section 3.3. These cells demonstrated that a counter electrode to Zn with a higher CE than Zn would not necessarily be advantageous if the counter electrode has a limited capacity available to be charged. Effectively, the  $\text{LiMn}_2\text{O}_4$  limited the charging half-cycles, while Zn limited the discharging half-cycles, leading to a short cycle life. In combatting this issue, it was realized that overcharging one electrode ( $\text{LiMn}_2\text{O}_4$  in this case) could cause that electrode to finish discharging first, even if the other electrode (Zn in this case) had a lower CE. Using this concept, the Zn electrodes in Chapter 5 were overcharged so that they would be first to finish discharging despite the lower CE of the Ni electrode. In general, this trick of overcharging an electrode essentially trades electrolyte (which is consumed during overcharging) to increase cycle life. As such, researchers should state whether they are intentionally overcharging as part of their cycling regime or not, since it affects the cycle life. In situations where overcharging is present, it is even more important to include the amount of electrolyte used in the cell as part of the experimental procedure since a particular cycling regime might overcharge a cell so much that the electrolyte is significantly changed (i.e. pH) or consumed before the electrodes themselves fail.

## 6.2 Coin Cell Future Work

Any future 2-electrode, battery-like cell research on Zn electrodes should begin with acquiring or fabricating durable bi-functional air electrodes and making Zn-air cells, since air electrodes effectively have infinite capacity. Provided the air electrode functioned as designed, this would guarantee that the Zn electrode would finish discharging first in every discharge half-cycle, thereby allowing accurate CE and self-discharge measurements of the Zn electrode to be made.

In order to eliminate H<sub>2</sub>O evaporation as a concern from future efforts, humidity (and temperature) controlled test chambers should also be developed. Then, the best practices outlined in this thesis regarding cell design, reproducibility, and reporting should generate high quality research on the cycle life of Zn electrodes for rechargeable alkaline Zn cells.

These Zn-air cells could also be used with the charge-wait-discharge method described in Chapter 4 to measure the self-discharge rate of Zn electrodes as a function of time. This would be particularly useful because the effect of any sort of cell modification on the self-discharge and H<sub>2</sub> evolution currents, such as electrode additives, different active materials, new separators or non-liquid electrolytes, could be tested instead of limiting the scope to electrolyte additives.

If the goal of a research project is instead to work with thick electrodes like those used in commercial cells, then a new current collector structure (other than Sn foil) with a larger surface area should be developed first. Cu foam has a 3D structure and high surface area, but it should be electroplated with Sn first since Sn improves the cycle life. These thicker Zn electrodes could either be used in thicker format coin cells or in the same thinner coin cells used in this thesis with a smaller spring (like a wave-spring) as long as enough current collector was left exposed to make contact with the Sn-plated canister.

Alternatively, an entirely new cell could be designed that uses transparent, alkaline-resistant plastic, has the ability to adjust the stack pressure, can be used with minimal amounts of electrolyte, allows current collector tabs to extend out of the cell without leakage, and has the option to include a reference electrode (like Zn foil). However, such a cell should be designed to maintain the small size, cost and manufacturing time of coin cells. If such a design were realized, it would be a contender for the recognized standard cell design for Zn-air cell research, which the Zn-air field seems to need.

Finally, if the gas outlets of a Zn-air cell were connected directly to a differential electrochemical mass spectrometer (DEMS) then not only could H<sub>2</sub> evolution rates be measured, but carbon corrosion at the positive electrode could also be analyzed.<sup>197, 198</sup> DEMS is a powerful technique for studying metal-air systems since it allows the researcher to monitor the gasses produced by the cell as a function of time or state of charge.

### **6.3 Regarding Self-Discharge Measurements**

#### *6.3.1 Chapter 4 Conclusions*

The new charge-wait-discharge method of measuring the self-discharge rate of charged Zn electrodes was introduced in Chapter 4 and demonstrated using foil electrodes. It revealed that the self-discharge rate of a charged Zn electrode was not dependent on time, KOH concentration, or plating rate. The only factor that did change the self-discharge rate was the current collector, leading to the conclusion that the mechanism controlling the rate of self-discharge was galvanic corrosion, where H<sub>2</sub> was evolved on the current collector while Zn dissolved to provide the electrons.

Therein, it was demonstrated that nickel (Ni) and graphite (C) have self-discharge rates over 30× higher than copper (Cu), indium (In) or tin (Sn), damning the use of Ni and C as current collector material and/or conductive electrode additive, respectively. Lead (Pb)

also had a poor self-discharge rate of 2× higher than Cu, which was surprising considering that Cu has a higher exchange current density than Pb for H<sub>2</sub> evolution.<sup>65</sup> This was explained through reasoning that the Zn deposit might leave more current collector surface area exposed on the Pb surface than on the Cu surface. The sensitivity of the self-discharge rate on exposed current collector surface area could also explain the difference between using Cu and Sn current collectors in the coin cells; if it is assumed that the entire current collector was not covered with Zn (unlike the charge-wait-discharge foil experiments), then the Cu current collector could have promoted a higher self-discharge rate than the Sn. This was the first time that the current collector has been identified as the primary factor affecting the self-discharge rate of rechargeable Zn electrodes.

Several electrolyte additives that have been claimed to serve various purposes for rechargeable Zn electrodes were then tested using the charge-wait-discharge method. Only one of them significantly affected the self-discharge rate. That additive was the combination of 1.8 M K<sub>2</sub>CO<sub>3</sub> & 1.8 M KF, which appeared to promote a holey Zn deposit that potentially exposed more current collector to the electrolyte and significantly increased the self-discharge rate. Therefore, none of the additives tested were deemed to be useful in reducing the self-discharge rate, suggesting that the charge-wait-discharge method might be a more effective self-discharge measurement technique than linear sweep voltammetry or H<sub>2</sub> gas collection.<sup>145, 146, 164, 165, 179</sup>

### 6.3.2 Chapter 5 Conclusions

The coin cell self-discharge experiments of Chapter 5 were primarily concerned with determining whether the self-discharge rate increased, decreased or stayed constant over a several day time period. It was determined that the self-discharge rate remained constant over time since Zn electrodes displayed average self-discharge rates that nearly

matched the measurements of the foil charge-wait-discharge experiments of Chapter 4. The nearly equal values obtained from both experiments also suggested that the foil experiments were accurate in reproducing the situation in a battery-like cell such as the coin cell.

In the process of determining the above, a new method of measuring the self-discharge rate of a Ni electrode was demonstrated. That method yielded the self-discharge rate as a function of time or state of charge. The average discharge rate of the Ni electrode in the coin cells was determined to be on the same order of magnitude as that of the Zn electrode. This meant that the Zn electrode had to be overcharged to leave the Ni electrode with more charged capacity than the Zn electrode so that the Zn electrode would finish discharging first. This method worked as predicted, and allowed the average self-discharge rate of the Zn electrode to be determined.

Finally, this method was used to determine whether any of the additives tested in the flooded foil experiments of Chapter 4 behaved differently in Ni-Zn coin cells. A few of them did. Of note was Zn formate, which was the only additive to statistically reduce the self-discharge rate, and the combination of 1.8 M  $K_2CO_3$  and 1.8 M KF, which did not increase the self-discharge rate as it had in the flooded foil experiments. The reasons for these discrepancies were not elucidated at the time of writing, but the fact that they occurred demonstrates that electrolyte additives can behave differently in a battery-like cell that has separators, stack pressure, a small amount of electrolyte and a positive electrode. As such, future efforts to determine the effectiveness of additives should be confirmed in battery-like cells, and not simply tested in a flooded cell and assumed that the result will apply equally well in both cases.



#### **6.4 Self-Discharge Measurement Future Work**

The primary goal for moving forward with the charge-wait-discharge self-discharge measurements is the same as future work for coin cells: acquire a durable bi-functional air electrode. Once a rechargeable Zn-air cell that maintains a relatively constant discharge capacity over at least about 10 cycles has been developed, then the charge-wait-discharge method can be used directly on a battery-like cell. For completeness, the results of Chapter 4 should be repeated in the Zn-air cell to confirm that the mechanism of self-discharge is the same. Then, the researcher is free to measure the self-discharge rate of Zn with any number of potential electrolyte additives, electrode additives, electrode coatings, new active materials, etc. The ones that cause a noticeable change in the self-discharge rate can then be further studied by other experiments to attempt to learn how they function.

Another interesting challenge would be to determine whether electrochemical impedance spectroscopy (EIS) can be used to determine the self-discharge rate of rechargeable Zn electrodes. Cachet and Wiart published several interesting papers on analyzing the processes occurring on a Zn electrode in alkaline electrolyte using EIS.<sup>38, 39, 199-203</sup> However, the same sort of work has not been done on a Zn electrode that has been plated onto a current collector.

#### **6.5 A Note on World Resources**

Astute readers might have noticed that “sustainable” was not one of the qualities associated with Zn in the introduction to this thesis. An interesting story lies behind this: One of the reasons for initiating research on Zn-air batteries in 2007 was the fear of world Li supplies being insufficient to provide enough batteries to replace the cars in the world with electric vehicles. However, that idea was convincingly argued to be false in 2008 by Keith Evans, although the author did not find this article until 2011.<sup>204</sup> To double check the

claim that Li was not in short supply, the method pioneered by M. King Hubbert<sup>205</sup> and explained by McFarland *et al.*<sup>206</sup> was used to generate predictions of the year of peak material production for zinc<sup>207</sup> (Zn), nickel<sup>208</sup> (Ni), cobalt<sup>209</sup> (Co), manganese<sup>210</sup> (Mn) and lithium<sup>211</sup> (Li). Figure 6-1 shows the resulting Gaussian fits to the historical data acquired from the US Geological Survey (USGS) website.<sup>212</sup> The fits were confined to have an area under the curve equal to the estimated amount of a particular resource (ex. Zn) that ever existed on Earth, which was also acquired from the USGS. The production rates of some resources, such as Zn, vastly dwarf the production rates of other resources, such as Li, so the data in Figure 6-1 was normalized to the peak production rate of that resource so that the year at which the peaks occur could more easily be compared. In order to understand the significance of the data, a short discussion of the error is necessary.

The fits are quasi-single point fits, so the peak year is dependent on which year's production rate the Gaussian is fit to. To generate a standard deviation, the fit was applied to the production rates of each year from 2000 to 2014 and the average peak year was determined. An example of this data is shown in Figure 6-2. These peak years and their

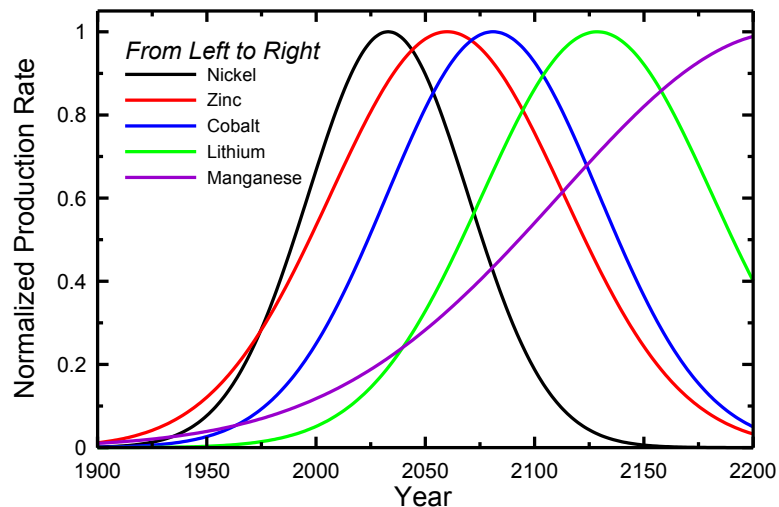


Figure 6-1: The predicted world production rates of five metals that are important to battery technologies. Predictions were calculated using Hubbert's model, which is a Gaussian fit to the historical production rates with the area under the curve set to equal the estimated amount of resource on Earth.

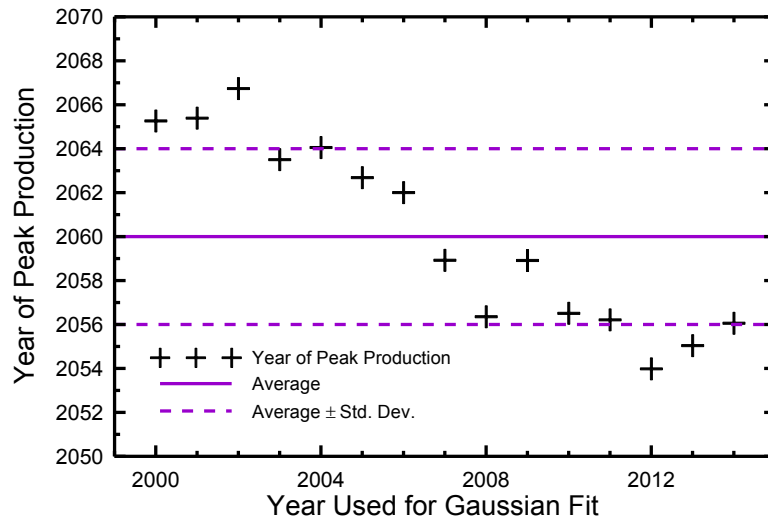


Figure 6-2: Year of peak production of Zn as a function of the year used to generate the Gaussian fit. For instance, the cumulative production of Zn up to the year 2000 was 327,396,000 tonnes, which generated a peak production year of 2065, while that up to the year 2014 was 484,206,000 tonnes, which generated a peak production year of 2056.

standard deviations are shown in Table 6-1, along with the peak production rates. It should be noted that the peak years determined this way were not randomly distributed about the mean but instead trended towards a nearer date, as shown in Figure 6-2, and so these predicted years of peak production might be further away than in reality. The production rates are a good reminder that although the amount of Zn on Earth is vastly larger than the amount of Co, Zn is predicted to run out before Co because humans consume vastly larger quantities of Zn each year.

Also of importance is the accuracy of the estimate of resource remaining on Earth.

Table 6-1: Calculated years of peak resource production for five metals that are important to cell technologies. The peak year was calculated using the Hubbert method and data from the US Geological Survey. The peak year was an average calculated from 15 fits to data ending in the year 2000 to 2014.

Metal	Peak Year (yr)	Standard Deviation (yr)	Estimated Total Resource on Earth (tonnes)	Peak Production (tonnes/yr)	Standard Deviation (tonnes/yr)
Nickel	2033	3	190,297,690	2,100,000	400,000
Zinc	2060	4	2,384,206,000	17,500,000	1,400,000
Cobalt	2081	16	27,501,330	230,000	40,000
Lithium	2129	21	40,166,036	310,000	50,000
Manganese	2216	48	20,614,729,000	81,000,000	17,000,000

When discussing the topic of peak oil, uninformed people state that new oil is always being found and so the model must just be unrealistic, without realizing that resource discovery is implicitly included in Hubbert's peak model. New resource discoveries do increase the estimate of total resources remaining on Earth, but not by enough to significantly move the year of the peak. For example, in the highly unlikely event that an incredible amount of previously undiscovered Zn was found that doubled the amount of Zn currently estimated to be on Earth, the peak calculated here would shift from the year  $2060 \pm 4$  to  $2100 \pm 6$ . Although 40 years might seem like a lot, it is in fact tiny since the discussion at hand is concerned with the amount of Zn available for all humanity for all time.

Clearly then, the impending end of cheap raw ore of many important metals within the next century is sobering and indicative of the coming end of the consumer era along with a dramatic increase in the importance of recycling and products made from plentiful or cheaply recycled materials. Ironically, Figure 6-1 and Table 6-1 show that Zn will run out before Co; however, Zn is more easily recycled from spent cells than Ni and Co are, suggesting that Zn might still be the better option. Whatever cell chemistry holds the highest market share in the future, its continued dominance will depend on its sustainability.

## References

1. N. Ramez, <http://rameznaam.com/2015/04/14/energy-storage-about-to-get-big-and-cheap/>, Accessed: April 17 2015 (Last updated: 2015).
2. P. Mock and S. A. Schmid, in *Encyclopedia of Electrochemical Power Sources* Editor: J. Garche, p. 566, Elsevier, Amsterdam (2009).
3. C. J. Boreiko, in *Encyclopedia of Electrochemical Power Sources* Editor: J. Garche, p. 233, Elsevier, Amsterdam (2009).
4. Y. Guo, in *Encyclopedia of Electrochemical Power Sources* Editor: J. Garche, p. 241, Elsevier, Amsterdam (2009).
5. C. D. Parker, in *Encyclopedia of Electrochemical Power Sources* Editor: J. Garche, p. 225, Elsevier, Amsterdam (2009).
6. J. R. Dahn and G. M. Ehrlich, in *Linden's Handbook of Batteries*, 4th ed., Editors: T. B. Reddy and D. Linden, p. 26.1, McGraw-Hill, Toronto (2010).
7. G. Girishkumar, B. McCloskey, A. C. Luntz, S. Swanson and W. Wilcke, *J. Phys. Chem. Lett.*, **1**, 14 (2010).
8. S. A. Freunberger, Y. Chen, Z. Peng, J. M. Griffin, L. J. Hardwick, F. Barde, P. Novak and P. G. Bruce, *J. Am. Chem. Soc.*, **133**, 20 (2011).
9. M. Xu, D. G. Ivey, Z. Xie and W. Qu, *J. Power Sources*, **283** (2015).
10. A. C. Luntz and B. D. McCloskey, *Chem. Rev.*, **114**, 23 (2014).
11. O. Haas and J. V. Wesemael, in *Encyclopedia of Electrochemical Power Sources*, 1st ed., Editor: J. Garche, p. 384, Elsevier, Amsterdam (2009).
12. T. B. Atwater and A. Doble, in *Linden's Handbook of Batteries*, 4th ed., Editors: T. B. Reddy and D. Linden, p. 33.1, McGraw-Hill, Toronto (2010).
13. O. Haas, F. Holzer, K. Muller and S. Muller, in *Handbook of fuel cells: fundamentals, technology, applications. Fundamentals and survey of systems*, 1st ed., Editors: H. Gasteiger, A. Lamm and W. Vielstich, p. 382, Wiley, Milan (2003).
14. X. G. Zhang, *Corrosion and Electrochemistry of Zinc*, 1st ed., Plenum Press, New York (1996).
15. F. R. McLarnon and E. J. Cairns, *J. Electrochem. Soc.*, **138**, 2 (1991).
16. K. Kotaich and S. E. Sloop, in *Encyclopedia of Electrochemical Power Sources*, 1st ed., Editor: J. Garche, p. 188, Elsevier, Amsterdam (2009).

17. S. Kursunoglu and M. Kaya, *Fizykochemiczne Problemy Mineralurgii*, **50**, 1 (2014).
18. S. Muller, F. Holzer, O. Haas, C. Schlatter and C. Comninellis, *Chimia*, **49**, 1-2 (1995).
19. Energizer, <http://data.energizer.com/pdfs/zincairprismatichandbook.pdf>, Accessed: March 10 2015 (Last updated: 2014).
20. T. C. Adler, F. R. McLarnon and E. J. Cairns, *J. Electrochem. Soc.*, **140**, 2 (1993).
21. G. Toussaint, P. Stevens, L. Akrou, R. Rouget and F. Fourgeot, *ECS Transactions*, **28**, 32 (2010).
22. G. Toussaint, P. Stevens, R. Rouget and F. Fourgeot, *ECS Meeting Abstracts*, **MA2012-02**, 11 (2012).
23. G. Dalin and A. Charkey, *Mech. Eng.*, **90**, 6 (1968).
24. [Anonymous], *Metallurgia*, **77**, 460 (1968).
25. [Anonymous], *Industrial Electronics*, **6**, 1 (1968).
26. A. M. Moos, *Chemical & Engineering News*, **46**, 40 (1968).
27. J. Passaniti, D. Carpenter and R. McKenzie, in *Linden's Handbook of Batteries*, 4th ed., Editors: T. B. Reddy and D. Linden, p. 13.16, McGraw-Hill, Toronto (2010).
28. H. Arai and M. Hayashi, in *Encyclopedia of Electrochemical Power Sources*, 1st ed., Editor: J. Garche, p. 55, Elsevier, Amsterdam (2009).
29. J. O. Bockris, Z. Nagy and A. Damjanov, *J. Electrochem. Soc.*, **119**, 3 (1972).
30. L. A. Tinker and K. A. Striebel, in *Energy Storage Systems in Electronics*, 1st ed., Editors: T. Osaka and M. Datta, p. 409, Taylor & Francis (2000).
31. V. Neburchilov, H. Wang, J. J. Martin and W. Qu, *J. Power Sources*, **195**, 5 (2010).
32. L. Jöerissen, in *Encyclopedia of Electrochemical Power Sources*, 1st ed., Editor: J. Garche, p. 356, Elsevier, Amsterdam (2009).
33. J. Y. Huot, in *Encyclopedia of Electrochemical Power Sources*, 1st ed., Editor: J. Garche, p. 883, Elsevier, Amsterdam (2009).
34. Olin Corporation, <https://koh.olinchloralkali.com/TechnicalInformation/PhaseDiagram.aspx>, Accessed: March 9 2015 (Last updated: 2015).
35. E. Samson, J. Marchand and K. A. Snyder, *Mater. Struct.*, **36**, 257 (2003).

36. W. H. Dyson, L. A. Schreier, W. P. Sholette and A. J. Salkind, *J. Electrochem. Soc.*, **115**, 6 (1968).
37. M. Liu, B. R. Faulds, G. M. Cook and N. P. Yao, *J. Electrochem. Soc.*, **128**, 10 (1981).
38. C. Cachet, B. Saidani and R. Wiart, *J. Electrochem. Soc.*, **138**, 3 (1991).
39. C. Cachet, B. Saidani and R. Wiart, *J. Electrochem. Soc.*, **139**, 3 (1992).
40. J. T. Nichols, F. R. McLarnon and E. J. Cairns, *Chem. Eng. Commun.*, **37**, 1-6 (1985).
41. K. J. Cain, C. A. Melendres and V. A. Maroni, *J. Electrochem. Soc.*, **134**, 3 (1987).
42. E. Deiss, F. Holzer and O. Haas, *Electrochim. Acta*, **47**, 25 (2002).
43. M. J. Isaacson, F. R. McLarnon and E. J. Cairns, *J. Electrochem. Soc.*, **137**, 7 (1990).
44. E. J. Cairns, in *Encyclopedia of Electrochemical Power Sources*, 1st ed., Editor: J. Garche, p. 528, Elsevier, Amsterdam (2009).
45. D. Yunchang, Y. Jiongliang and C. Zhaorong, *J. Power Sources*, **69**, 1-2 (1997).
46. D. Yunchang, Y. Jiongliang, W. Zeyun, D. Yong and G. B. Sheng, *J. Power Sources*, **66**, 1-2 (1997).
47. Z. Chang, G. Li, Y. Zhao, Y. Ding and J. Chen, *J. Power Sources*, **74**, 2 (1998).
48. S. Ochiai, M. Kodama, K. Furukawa, T. Tanaka, M. Kuzuhara, M. Watada and M. Oshitani, *US Patent*, **10/486,906**, 7,635,512 (2009).
49. D. Singh, *J. Electrochem. Soc.*, **145**, 1 (1998).
50. A. Van der Ven, D. Morgan, Y. S. Meng and G. Ceder, *J. Electrochem. Soc.*, **153**, 2 (2006).
51. S. Deabate and F. Henn, *Electrochim. Acta*, **50**, 14 (2005).
52. C. Tessier, C. Faure, L. Guerlou-Demourgues, C. Denage, G. Nabias and C. Delmas, *J. Electrochem. Soc.*, **149**, 9 (2002).
53. C. Faure, C. Delmas and P. Willmann, *J. Power Sources*, **36**, 4 (1991).
54. Q. Song, Z. Tang, H. Guo and S. L. I. Chan, *J. Power Sources*, **112**, 2 (2002).
55. C. Faure, C. Delmas, M. Fouassier and P. Willmann, *J. Power Sources*, **35**, 3 (1991).
56. C. Faure, C. Delmas and P. Willmann, *J. Power Sources*, **35**, 3 (1991).
57. C. Faure, C. Delmas and M. Fouassier, *J. Power Sources*, **35**, 3 (1991).

58. C. Faure, Y. Borthomieu, C. Delmas and M. Fouassier, *J. Power Sources*, **36**, 2 (1991).
59. J. Mrha, I. Krejčí, Z. Zábranský, V. Koudelka and J. Malík, *J. Power Sources*, **4**, 3 (1979).
60. J. Jindra, I. Krejčí, J. Mrha, B. Folkesson, L. Y. Johansson and R. Larsson, *J. Power Sources*, **13**, 2 (1984).
61. Wikipedia, [http://en.wikipedia.org/wiki/Electrochemical\\_cell](http://en.wikipedia.org/wiki/Electrochemical_cell), Accessed: June 2 2015 (Last updated: 2015).
62. V. Svoboda, in *Encyclopedia of Electrochemical Power Sources* Editor: J. Garche, p. 424, Elsevier, Amsterdam (2009).
63. S. Trasatti, in *Encyclopedia of Electrochemical Power Sources* Editor: J. Garche, p. 41, Elsevier, Amsterdam (2009).
64. M. Pourbaix, *Atlas of Electrochemical Equilibria in Aqueous Solutions*, National Association of Corrosion Engineers, (1974).
65. H. Kita, *J. Electrochem. Soc.*, **113**, 11 (1966).
66. S. Trasatti, in *Encyclopedia of Electrochemical Power Sources* Editor: J. Garche, p. 49, Elsevier, Amsterdam (2009).
67. J. Phillips and S. Mohanta, in *Linden's Handbook of Batteries*, 4th ed., Editors: T. B. Reddy and D. Linden, p. 23.1, McGraw-Hill, Toronto (2010).
68. D. Coates, E. Ferreira and A. Charkey, *J. Power Sources*, **65**, 1–2 (1997).
69. J. Jindra, *J. Power Sources*, **37**, 3 (1992).
70. J. Cook and P. Kritzer, in *Encyclopedia of Electrochemical Power Sources*, 1st ed., Editor: J. Garche, p. 424, Elsevier, Amsterdam (2009).
71. A. P. Young, V. Colbow, D. Harvey, E. Rogers and S. Wessel, *J. Electrochem. Soc.*, **160**, 4 (2013).
72. P. N. Ross and H. Sokol, *J. Electrochem. Soc.*, **131**, 8 (1984).
73. P. N. Ross and M. Sattler, *J. Electrochem. Soc.*, **135**, 6 (1988).
74. N. Staud and P. N. Ross, *J. Electrochem. Soc.*, **133**, 6 (1986).
75. X. G. Zhang, in *Encyclopedia of Electrochemical Power Sources*, 1st ed., Editor: J. Garche, p. 454, Elsevier, Amsterdam (2009).
76. R. Y. Wang, D. W. Kirk and G. X. Zhang, *J. Electrochem. Soc.*, **153**, 5 (2006).
77. Q. Zhu, D. S. Lu, J. J. Lin and L. Du, *J. Electroanal. Chem.*, **722-723**, 0 (2014).



78. D. S. Hall, C. Bock and B. R. MacDougall, *J. Electrochem. Soc.*, **160**, 3 (2013).
79. I. T. Bae, *J. Electrochem. Soc.*, **155**, 5 (2008).
80. S. T. Mayer and R. H. Muller, *J. Electrochem. Soc.*, **139**, 2 (1992).
81. P. Vanysek, in *CRC Handbook of Chemistry and Physics*, 79th ed., Editor: D. R. Lide, p. 8-21, CRC Press, Boca Raton (1998).
82. J. C. Nardi and R. J. Brodd, in *Linden's Handbook of Batteries*, 4th ed., Editors: T. B. Reddy and D. Linden, p. 11.1, McGraw-Hill, Toronto (2010).
83. J. W. Diggle, A. R. Despic and J. O. Bockris, *J. Electrochem. Soc.*, **116**, 11 (1969).
84. M. Liu, G. M. Cook and N. P. Yao, *J. Electrochem. Soc.*, **128**, 8 (1981).
85. W. G. Sunu and D. N. Bennion, *J. Electrochem. Soc.*, **127**, 9 (1980).
86. W. G. Sunu and D. N. Bennion, *J. Electrochem. Soc.*, **127**, 9 (1980).
87. J. McBreen, *J. Electrochem. Soc.*, **119**, 12 (1972).
88. J. Jorné, T. C. Adler and E. J. Cairns, *J. Electrochem. Soc.*, **142**, 3 (1995).
89. K. W. Choi, D. N. Bennion and J. Newman, *J. Electrochem. Soc.*, **123**, 11 (1976).
90. K. W. Choi, D. Hamby, D. N. Bennion and J. Newman, *J. Electrochem. Soc.*, **123**, 11 (1976).
91. R. Jain, T. C. Adler, F. R. McLarnon and E. J. Cairns, *J. Appl. Electrochem.*, **22**, 11 (1992).
92. T. C. Adler, F. R. McLarnon and E. J. Cairns, *J. Electrochem. Soc.*, **140**, 2 (1993).
93. P. Pei, K. Wang and Z. Ma, *Appl. Energy*, **128** (2014).
94. S. Muller, F. Holzer, H. Arai and O. Haas, *J. New Mat. Electrochem. Systems*, **2**, 4 (1999).
95. D. U. Lee, J. Choi, K. Feng, H. W. Park and Z. Chen, *Advanced Energy Materials*, **4**, 6 (2014).
96. S. W. Donne, G. A. Lawrance and D. A. J. Swinkels, *J. Electrochem. Soc.*, **144**, 9 (1997).
97. M. R. Bailey and S. W. Donne, *J. Electrochem. Soc.*, **159**, 12 (2012).
98. X. Li, Y. Song, L. Wang, T. Xia and S. Li, *Int. J. Hydrogen Energ.*, **35**, 8 (2010).
99. Y. Ratiouville, W. L. Wu, D. Lincot, J. Vedel and L. T. Yu, *J. Electrochem. Soc.*, **146**, 9 (1999).
100. P. Stevens, G. Toussaint, G. Caillon, P. Viaud, P. Vinatier, C. Cantau, O. Fichet, C. Sarrazin and M. Mallouki, *ECS Transactions*, **28**, 32 (2010).

101. K. Micka, J. Mrha and B. Klapste, *J. Power Sources*, **5**, 2 (1980).
102. V. Koudelka, J. Malík, J. Mrha, I. Krejčí and M. Špinka, *J. Power Sources*, **6**, 2 (1981).
103. D. Yunchang, Y. Jiongliang, L. Hui, C. Zhaorong and W. Zeyun, *J. Power Sources*, **56**, 2 (1995).
104. K. Watanabe, T. Kikuoka and N. Kumagai, *J. Appl. Electrochem.*, **25**, 3 (1995).
105. C. Delmas and C. Tessier, *J. Mater. Chem.*, **7**, 8 (1997).
106. M. C. Bernard, R. Cortes, M. Keddam, H. Takenouti, P. Bernard and S. Senyarich, *J. Power Sources*, **63**, 2 (1996).
107. R. S. Jayashree, P. V. Kamath and G. N. Subbanna, *J. Electrochem. Soc.*, **147**, 6 (2000).
108. C. Greaves, M. A. Thomas and M. Turner, *J. Power Sources*, **12**, 3-4 (1984).
109. S. Deabate, F. Fourgeot and F. Henn, *Electrochim. Acta*, **51**, 25 (2006).
110. C. Tessier, L. Guerlou-Demourgues, C. Faure, C. Denage, B. Delatouche and C. Delmas, *J. Power Sources*, **102**, 1-2 (2001).
111. PowerGenix, <http://powergenix.com/cells/>, Accessed: May 29 2015 (Last updated: 2014).
112. PKCell, <http://www.pkcell.net/?cat=28>, Accessed: May 29 2015 (Last updated: 2015).
113. F. Feng, J. Phillips, S. Mohanta, J. Barton and Z. M. Muntasser, *US Patent*, **13/452,629**, US 2012/0205248 A1 (2012).
114. M. Geng, S. Mohanta, J. Phillips, Z. M. Muntasser and J. Barton, *US Patent*, **13/250,217**, US 2012/0018669 A1 (2012).
115. J. McBreen and E. Gannon, *J. Electrochem. Soc.*, **130**, 10 (1983).
116. J. K. Weaver, F. R. McLarnon and E. J. Cairns, *J. Electrochem. Soc.*, **138**, 9 (1991).
117. R. Jiang and D. Chu, *Rev. Sci. Instrum.*, **76**, 6 (2005).
118. S. Muller, F. Holzer and O. Haas, *J. Appl. Electrochem.*, **28**, 9 (1998).
119. Y. Shen and K. Kordesch, *J. Power Sources*, **87**, 1-2 (2000).
120. S. Muller, F. Holzer and O. Haas, in *Batteries for the 21st Century*, 1st ed., Editors: W. R. Cieslak and K. M. Abraham, p. 101, Electrochemical Society (1999).
121. J. X. Yu, H. X. Yang, X. P. Ai and X. M. Zhu, *J. Power Sources*, **103**, 1 (2001).
122. C. Zhang, J. M. Wang, L. Zhang, J. Q. Zhang and C. N. Cao, *J. Appl. Electrochem.*, **31**, 9 (2001).

123. H. Yang, H. Zhang, X. Wang, J. Wang, X. Meng and Z. Zhou, *J. Electrochem. Soc.*, **151**, 12 (2004).
124. Y. F. Yuan, J. P. Tu, H. M. Wu, Y. Z. Yang, D. Q. Shi and X. B. Zhao, *Electrochim. Acta*, **51**, 18 (2006).
125. Y. F. Yuan, J. P. Tu, H. M. Wu, B. Zhang, X. H. Huang and X. B. Zhao, *J. Electrochem. Soc.*, **153**, 9 (2006).
126. C. J. Lan, C. Y. Lee and T. S. Chin, *Electrochim. Acta*, **52**, 17 (2007).
127. Y. F. Yuan, J. P. Tu, H. M. Wu, C. Q. Zhang, S. F. Wang and X. B. Zhao, *J. Power Sources*, **165**, 2 (2007).
128. S. Wang, Z. Yang and L. Zeng, *Mater. Chem. Phys.*, **112**, 2 (2008).
129. C. Yang, J. M. Yang and C. Wu, *J. Power Sources*, **191**, 2 (2009).
130. S. Wang, Z. Yang, J. Hu, J. Liao and W. Chi, *J. New Mat. Electrochem. Systems*, **12**, 4 (2009).
131. C. Yang, W. Chien, P. Chen and C. Wu, *J. Appl. Electrochem.*, **39**, 1 (2009).
132. R. N. Snyder and J. J. Lander, *Electrochem. Technol.*, **3**, 5-6 (1965).
133. J. Jindra and D. Becker-Roes, *J. Power Sources*, **45**, 1 (1993).
134. H. Wenzl, in *Encyclopedia of Electrochemical Power Sources* Editor: J. Garche, p. 401, Elsevier, Amsterdam (2009).
135. J. Zhu and Y. Zhou, *J. Power Sources*, **73**, 2 (1998).
136. J. O. M. Bockris, A. K. N. Reddy and M. E. Gamboa-Aldeco, *Modern Electrochemistry 2A: Fundamentals of Electrodics*, 2nd ed., Springer US, (2007).
137. J. McBreen, E. Gannon, D. - Chin and R. Sethi, *J. Electrochem. Soc.*, **130**, 8 (1983).
138. Y. Sharma, M. Aziz, J. Yusof and K. Kordesch, *J. Power Sources*, **94**, 1 (2001).
139. H. Seidel, L. Csepregi, A. Heuberger and H. Baumgärtel, *J. Electrochem. Soc.*, **137**, 11 (1990).
140. Jeff R. Dahn. Topic: The cost of coin cell components, E-mail, 2015.
141. A. J. Smith, J. C. Burns and J. R. Dahn, *Electrochem. Solid-State Lett.*, **13**, 12 (2010).
142. R. F. Plivelich, F. R. McLarnon and E. J. Cairns, *J. Appl. Electrochem.*, **25**, 5 (1995).
143. J. F. Drillet, F. Holzer, T. Kallis, S. Muller and V. M. Schmidt, *Physical Chemistry Chemical Physics*, **3**, 3 (2001).

144. C. W. Lee, K. Sathiyarayanan, S. W. Eom and M. S. Yun, *J. Power Sources*, **160**, 2 (2006).
145. C. W. Lee, K. Sathiyarayanan, S. W. Eom, H. S. Kim and M. S. Yun, *J. Power Sources*, **159**, 2 (2006).
146. C. W. Lee, S. W. Eom, K. Sathiyarayanan and M. S. Yun, *Electrochim. Acta*, **52**, 4 (2006).
147. P. Bonnicksen and J. R. Dahn, *J. Electrochem. Soc.*, **159**, 7 (2012).
148. S. Trussler, DPM Solutions, <http://www.design-prove-machine-solutions.ca/>, Accessed: April 29 2015 (Last updated: 2014).
149. T. Marks, S. Trussler, A. J. Smith, D. Xiong and J. R. Dahn, *J. Electrochem. Soc.*, **158**, 1 (2011).
150. M. Oshitani, H. Yufu, K. Takashima, S. Tsuji and Y. Matsumaru, *J. Electrochem. Soc.*, **136**, 6 (1989).
151. J. R. Taylor, *An Introduction to Error Analysis: The Study of Uncertainties in Physical Measurements*, 2nd ed., University Science Books, (1997).
152. Wikipedia, The Free Encyclopedia, [https://en.wikipedia.org/w/index.php?title=SAE\\_steel\\_grades&oldid=666724815](https://en.wikipedia.org/w/index.php?title=SAE_steel_grades&oldid=666724815), Accessed: June 26 2015 (Last updated: 2015).
153. Y. Cho and G. T. Fey, *J. Power Sources*, **184**, 2 (2008).
154. D. S. Hall, D. J. Lockwood, C. Bock and B. R. MacDougall, *Proc. R. Soc. A*, **471**, 2174 (2014).
155. Z. Luo, S. Sang, Q. Wu and S. Liu, *ECS Electrochemistry Letters*, **2**, 2 (2013).
156. M. G. Chu, J. McBreen and G. Adzic, *J. Electrochem. Soc.*, **128**, 11 (1981).
157. J. McBreen, M. G. Chu and G. Adzic, *J. Electrochem. Soc.*, **128**, 11 (1981).
158. PowerGenix, <http://www.powergenix.com/files/powergenix/docs/powergenix-specs-aa.pdf>, Accessed: January 4 2012 (Last updated: 2009).
159. L. Zhu, H. Zhang, W. Li and H. Liu, *J. Phys. Chem. Solids*, **70**, 1 (2009).
160. Zhang Hui, Zhu Liquan, Li Weiping and Liu Huicong, *J. Rare Earths*, **27**, 6 (2009).
161. J. Zhu, Y. Zhou and H. Yang, *J. Power Sources*, **69**, 1-2 (1997).
162. A. Gomes and M. I. D. Pereira, *Electrochim. Acta*, **51**, 7 (2006).
163. R. K. Ghavami and Z. Rafiei, *J. Power Sources*, **162**, 2 (2006).
164. T. Cohen-Hyams, Y. Ziengerman and Y. Ein-Eli, *J. Power Sources*, **157**, 1 (2006).

165. K. Kim, Y. Cho, S. W. Eom, H. Kim and J. H. Yeum, *Mater. Res. Bull.*, **45**, 3 (2010).
166. M. Fetcenko and J. Koch, in *Linden's Handbook of Batteries*, 4th ed., Editors: T. B. Reddy and D. Linden, p. 22.1, McGraw-Hill, Toronto (2010).
167. J. Yan, J. Wang, H. Liu, Z. Bakenov, D. Gosselink and P. Chen, *J. Power Sources*, **216** (2012).
168. T. Zheng and J. R. Dahn, *Phys. Rev. B*, **56**, 7 (1997).
169. H. Wenzl, in *Encyclopedia of Electrochemical Power Sources* Editor: J. Garche, p. 407, Elsevier, Amsterdam (2009).
170. A. J. Smith, J. C. Burns, D. Xiong and J. R. Dahn, *J. Electrochem. Soc.*, **158**, 10 (2011).
171. S. Sharifi-Asl and D. D. Macdonald, *J. Electrochem. Soc.*, **160**, 6 (2013).
172. P. C. Andricacos and H. Y. Cheh, *J. Electrochem. Soc.*, **128**, 4 (1981).
173. S. Stankovic, B. Grgur, N. Krstajic and M. Vojnovic, *J. Electroanal. Chem.*, **549** (2003).
174. P. Rüetschi, *J. Electrochem. Soc.*, **114**, 4 (1967).
175. D. P. Gregory, P. C. Jones and D. P. Redfearn, *J. Electrochem. Soc.*, **119**, 10 (1972).
176. M. Meesus, Y. Strauven and L. Groothaert, *Power Sources*, **11** (1987).
177. V. S. Muralidharan and K. S. Rajagopalan, *Journal of Electroanalytical Chemistry and Interfacial Electrochemistry*, **94**, 1 (1978).
178. L. M. Baugh, F. L. Tye and N. C. White, *J. Appl. Electrochem.*, **13**, 5 (1983).
179. J. Dobryszycski and S. Biallozor, *Corros. Sci.*, **43**, 7 (2001).
180. Y. Ein-Eli, *Electrochem. Solid-State Lett.*, **7**, 1 (2004).
181. L. M. Baugh, F. L. Tye and N. C. White, *J. Electroanal. Chem.*, **183**, 1-2 (1985).
182. L. M. Baugh, F. L. Tye and N. C. White, *J. Electroanal. Chem.*, **183**, 1-2 (1985).
183. B. J. Kirby, *Micro- and Nanoscale Fluid Mechanics: Transport in Microfluidic Devices*, 1st ed., Cambridge University Press, (2010).
184. R. Sander, Max-Planck Institute of Chemistry, <http://www.mpch-mainz.mpg.de/~sander/res/henry.html>, Accessed: June 15 2015 (Last updated: 1999).
185. P. Bro and H. Y. Kang, *J. Electrochem. Soc.*, **118**, 9 (1971).

186. T. Takamura, in *Encyclopedia of Electrochemical Power Sources* Editor: J. Garche, p. 28, Elsevier, Amsterdam (2009).
187. R. Othman, A. H. Yahaya and A. K. Arof, *J. Appl. Electrochem.*, **32**, 12 (2002).
188. K. Mori, T. Ohhara and K. Sato, *US Patent*, **US 09/947,978**, US6794082 B2 (2004).
189. J. L. Stimits, *US Patent*, **US 13/288,102**, US8318340 B2 (2012).
190. J. F. Parker, C. N. Chervin, E. S. Nelson, D. R. Rolison and J. W. Long, *Energy Environ. Sci.*, **7**, 3 (2014).
191. J. F. Parker, E. S. Nelson, M. D. Wattendorf, C. N. Chervin, J. W. Long and D. R. Rolison, *ACS Appl. Mater. Inter.*, **6**, 22 (2014).
192. E. L. Cussler, *Diffusion: Mass Transfer in Fluid Systems*, 2nd ed., Cambridge University Press, (2009).
193. P. Kritzer and J. A. Cook, *J. Electrochem. Soc.*, **154**, 5 (2007).
194. J. Mcbreen and E. Gannon, *J. Power Sources*, **15**, 2-3 (1985).
195. S. Wang, Z. Yang and L. Zeng, *J. Electrochem. Soc.*, **156**, 1 (2009).
196. Y. F. Yuan, Y. Li, S. Tao, F. C. Ye, J. L. Yang, S. Y. Guo and J. P. Tu, *Electrochim. Acta*, **54**, 26 (2009).
197. B. D. McCloskey, D. S. Bethune, R. M. Shelby, G. Girishkumar and A. C. Luntz, *J. Phys. Chem. Lett.*, **2**, 10 (2011).
198. H. Baltruschat, *J. Am. Soc. Mass Spectrom.*, **15**, 12 (2004).
199. C. Cachet, U. Stroder and R. Wiart, *J. Appl. Electrochem.*, **11**, 5 (1981).
200. C. Cachet, U. Stroder and R. Wiart, *Electrochim. Acta*, **27**, 7 (1982).
201. C. Cachet, Z. Chami and R. Wiart, *Electrochim. Acta*, **32**, 3 (1987).
202. C. Cachet, B. Saidani and R. Wiart, *Electrochim. Acta*, **33**, 3 (1988).
203. C. Cachet, B. Saidani and R. Wiart, *Electrochim. Acta*, **34**, 8 (1989).
204. R. K. Evans, <http://lithiumabundance.blogspot.ca/>, Accessed: April 15 2015 (Last updated: 2008).
205. M. K. Hubbert, *Science*, **109**, 2823 (1949).

206. E. L. McFarland, J. L. Hunt and J. L. Campbell, *Energy, Physics and the Environment*, 3rd ed., Thomson, Toronto (2006).
207. A. C. Tolcin, US Geological Survey,  
<http://minerals.usgs.gov/minerals/pubs/commodity/zinc/index.html>, Accessed: February 10 2015 (Last updated: 2015).
208. P. H. Kuck, US Geological Survey,  
<http://minerals.usgs.gov/minerals/pubs/commodity/nickel/index.html>, Accessed: February 10 2015 (Last updated: 2015).
209. K. B. Shedd, US Geological Survey,  
<http://minerals.usgs.gov/minerals/pubs/commodity/cobalt/index.html>, Accessed: February 10 2015 (Last updated: 2015).
210. L. A. Corathers, US Geological Survey,  
<http://minerals.usgs.gov/minerals/pubs/commodity/manganese/index.html>, Accessed: February 10 2015 (Last updated: 2015).
211. B. W. Jaskula, US Geological Survey,  
<http://minerals.usgs.gov/minerals/pubs/commodity/lithium/index.html>, Accessed: February 10 2015 (Last updated: 2015).
212. T. D. Kelly and G. R. Matos, US Geological Survey,  
<http://minerals.usgs.gov/minerals/pubs/historical-statistics/>, Accessed: February 10 2015 (Last updated: 2014).

## Appendix A: Simple and Intermediate Modeling of a Cell

### A.1 Simple Zn-Air Cell

When people pitch new battery chemistries to investors, or anyone else that they want to impress, they tend to quote the “theoretical” energy density of a given chemistry. To calculate this, they conveniently ignore the cell casing, current collectors (metal foil that the electrodes are stuck to), separators, electrolyte, electrode porosity, reaction products and, thus, reality. Figure A-1 shows two such theoretical Zn-air cells, where Figure A-1B is slightly more realistic than Figure A-1A in that it accounts for the expanded volume of the reaction product (ZnO).

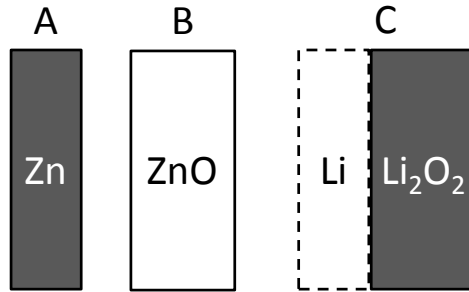


Figure A-1: Example of three different simple cell models. Both models A and B represent a Zn-air cell. Model A consists of only a piece of pure Zn metal, while model B consists of a solid block of pure ZnO, the discharge product of model A, which is larger. ZnO occupies the same space in a cell that was occupied by Zn, but this is not the case for Li in a Li-air cell as shown in model C. Model C shows the space where the Li was before discharge and where the  $\text{Li}_2\text{O}_2$  is formed after discharge in a non-aqueous Li-air cell.

If Figure A-1A were a functional cell, it would have a gravimetric capacity density (GCD) of

$$\text{Gravimetric Capacity Density (GCD)} = \frac{nF}{MM} \cdot \frac{1}{3.6 \frac{\text{C}}{\text{mAh}}} = \frac{2 \cdot 96485}{65.38 \cdot 3.6} = 820 \frac{\text{Ah}}{\text{kg}}. \quad (\text{A-1})$$

Here, MM is the molar mass and n is the moles of  $e^-$  per mole of active material. To get the volumetric capacity density, simply multiply by the density of the material ( $\rho$ ):

$$\text{Volumetric Cap. Den. (VCD)} = \text{GCD} \times \rho_{\text{Zn}} = 820 \frac{\text{Ah}}{\text{kg}} \times 7.14 \frac{\text{kg}}{\text{L}} = 5,850 \frac{\text{Ah}}{\text{L}}. \quad (\text{A-2})$$



Finally, both of these values can be converted into energy densities by multiplying them by the average cell potential ( $V_{avg}$ ) for this chemistry, which in the case of Zn-air is 1.2 V:

$$\text{Gravimetric Energy Density (GED)} = \text{GCD} \times V_{avg} = 984 \frac{\text{Wh}}{\text{kg}} \text{ and} \quad (\text{A-3})$$

$$\text{Volumetric Energy Density (VED)} = \text{VCD} \times V_{avg} = 7,025 \frac{\text{Wh}}{\text{L}}. \quad (\text{A-4})$$

In comparison to the ubiquitous  $\text{LiCoO}_2$  – Carbon, Li-ion battery that has a theoretical GED of about 370 Wh/kg and a VED of about 1,370 Wh/L, these numbers for Zn-air are huge and get bigger if one assumes they can coax the  $V_{avg}$  higher with additives or other tricks.

A slightly better approach to calculating a theoretical cell energy density is to take reaction products into account. Often, active materials will change size when they are cycled and space for them in the cell must be factored in to the model. ZnO is about 55% larger than Zn, for example. The reaction products are also sometimes located in entirely different areas of the cell.  $\text{Li}_2\text{O}_2$  in a Li-air battery is actually formed *inside* the air electrode, while the Li originates at the negative electrode as shown in Figure A-1C. Dealing with a different material (ZnO, say) means the MM and  $\rho$  will change, which in turn changes the

Table A-1: Theoretical capacity and energy densities of various cell chemistries mentioned in this thesis. Since active materials change volume during cycling, each cell chemistry has two entries to better determine realistic values. The Li-ion cell ‘ $\text{LiCoO}_2$  – C’ is present for comparison to the current most important rechargeable technology in the world. The simple model ignores cell casing, current collectors, separators, electrolyte and electrode porosity. The intermediate model includes all of these things, but is still an ideal.

Charge State	Positive – Negative Materials	Average Discharge Potential	Simple Model				Intermediate Model
			$\text{GCD}_{\text{Cell}}$	$\text{GED}_{\text{Cell}}$	$\text{VCD}_{\text{Cell}}$	$\text{VED}_{\text{Cell}}$	$\text{VED}_{\text{Cell}}$
	<i>Units:</i>	V	Ah/kg	Wh/kg	Ah/L	Wh/L	Wh/L
Charged	Air - Zn	1.2	820	984	5,854	7,025	900 to 1,400
Discharged	Air - ZnO		658	790	3,694	4,433	
Charged	NiOOH - Zn	1.65	215	356	1,137	1,877	500 to 600
Discharged	Ni(OH) <sub>2</sub> - ZnO		201	331	872	1,439	
Charged	2MnO <sub>2</sub> /LiCl - Zn	1.85	108	199	409	756	250 to 350
Discharged	LiMn <sub>2</sub> O <sub>4</sub> – ZnCl <sub>2</sub>		108	199	449	831	
Charged	Air - Li	2.7	3,862	10,427	2,062	5,568	1,000 to 1,400
Discharged	Air/Li <sub>2</sub> O <sub>2</sub> – (Li)		1,168	3,154	1,169	3,156	
Discharged	LiCoO <sub>2</sub> - C	3.65	100	365	375	1,368	600 to 700

GCD, VCD, GED and VED. This still constitutes a “simple” model, but the difference between considering a charged state of the cell and a discharged state is notable. Table A-1 shows the theoretical capacity and energy quantities for several cell chemistries mentioned in this thesis, as well as how performing the calculations with the discharged state of the active materials changes the values. Table A-1 will be referred back to several times throughout this text as the relevant section is covered.

## A.2 Intermediate Zn-Air Cell

The best compromise between a theoretical cell capacity and reality is an intermediate cell model that takes into account the cell casing, current collectors, separators, electrolyte, electrode porosity and reaction products, which can be made in Excel. In the case of Zn-air, the current collector could be a Sn-coated Cu foam with 97% porosity, the separator could be something like Celgard 5550, which is 100  $\mu\text{m}$  thick, the electrolyte is assumed to occupy the pores of the electrodes and the thick separator, and the Zn electrode porosity is about 50% to allow for expansion of the Zn into ZnO. In order to compare this cell with common Li-ion cells, it is assumed that this Zn-air cell is being rolled (wound) and inserted into an 18650 cell, which is 1.8 cm in diameter and 6.50 cm tall. In the case of an 18650 cell, the jelly-roll to cell casing volume ratio is about 70.0 v%. Figure

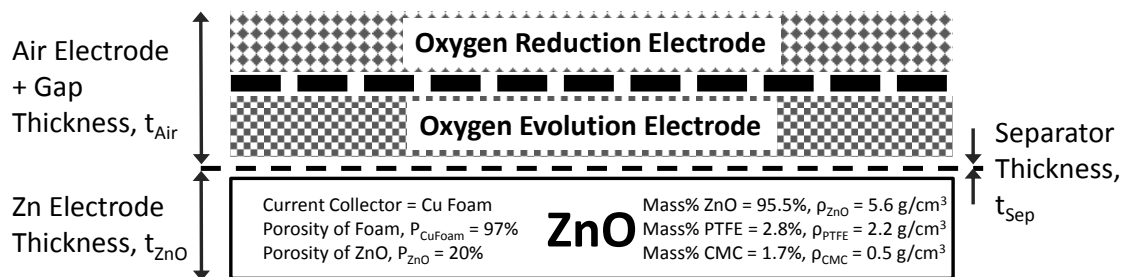


Figure A-2: Schematic of the stack for the intermediate model of a Zn-air battery. The thick dashed line is the gap added to prevent evolved  $\text{O}_2$  bubbles from disturbing the  $\text{O}_2$  reduction electrode. In reality, the entire stack would be mirrored before being rolled into a jelly-roll.

A-2 shows the electrodes laid out flat before being rolled up, which is known as the “stack”.

Recently, Toussaint *et al.* have taken to using a separate electrode for the O<sub>2</sub> reduction (Reaction (1-7)) and oxygen evolution (Reaction (1-17)) reactions to extend cycle life.<sup>21</sup> This works by avoiding support structure destruction and MnO<sub>2</sub> dissolution as discussed in Sections 1.9.1 (pg. 30) and 1.9.2 (pg. 31). They use a simple stainless steel mesh as the O<sub>2</sub> evolution electrode. Unfortunately, the O<sub>2</sub> reduction electrode still suffers support destruction if it is too close to the O<sub>2</sub> evolution electrode so a gap is left between the two, as shown in Figure A-2. That gap could be filled with a low weight structurally rigid material that repels O<sub>2</sub> bubbles but has holes large enough to allow the electrolyte to easily flow through it, like PTFE. This is easily included in the model being explored here, as shown in Figure A-2.

To mathematically determine the VED<sub>cell</sub> within the intermediate model, the VCD'<sub>ZnO</sub> of a ZnO electrode that is porous and contains binder is first calculated using

$$VCD'_{ZnO} = \frac{(P_{CuFoam} - P_{ZnO}) \cdot m\%_{ZnO} \cdot GCD_{ZnO}}{\left(\frac{m\%}{\rho}\right)_{ZnO} + \left(\frac{m\%}{\rho}\right)_{CMC} + \left(\frac{m\%}{\rho}\right)_{PTFE}} \quad (A-5)$$

where P is porosity, wt% is the weight percent of the electrode material and ρ is the density. This accounts for the fact that the volume of any electrode is not all active material. Note that when the cell is charged, the ZnO will shrink as it becomes Zn and thus the porosity of the negative electrode will increase to about 48% at full charge. To continue the model, the VCD'<sub>ZnO</sub> is multiplied by the average discharge potential, fraction of cell canister volume occupied by the jelly-roll, and then by the fraction of the thickness that is capacity-holding ZnO:

$$VED_{cell} = VCD'_{ZnO} (V_{Avg}) \left(\frac{V_{J-roll}}{V_{Can}}\right) \left(\frac{t_{ZnO}}{t_{ZnO} + t_{Air} + t_{Sep}}\right). \quad (A-6)$$

Here, V<sub>Avg</sub> is the average discharge potential, V<sub>J-roll</sub> is the volume of the jelly-roll, V<sub>Can</sub> is the volume of the outside dimensions of the cell canister and the t's are all thicknesses. Figure

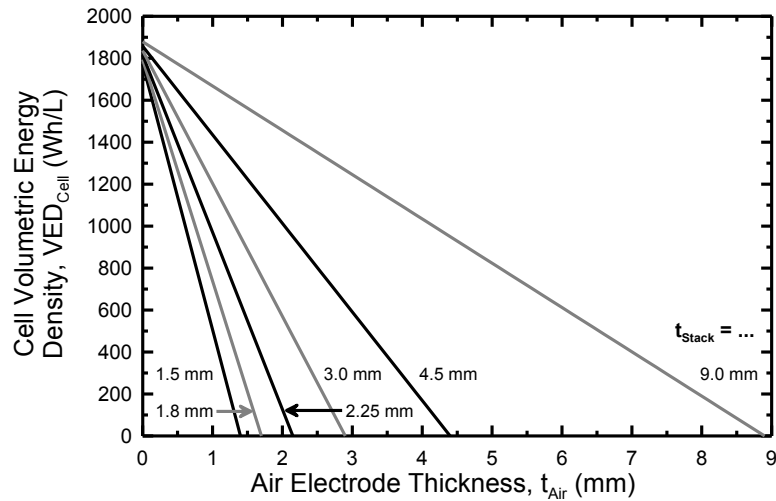


Figure A-3: Volumetric energy density of a Ni-Zn 18650 cell using the intermediate model. Each successive line represents an increasing thickness of the ZnO electrode. The x-axis reflects an increasing air electrode thickness, which includes the space meant to allow air bubbles to escape. The separator thickness was assumed to be 0.1 mm. Since an 18650 cell has a diameter of 18 mm, the maximum stack thickness is the radius, 9 mm.

A-3 shows the results of this model if the thickness of the stack is decreased in steps from the maximum of 9 mm, and as the thickness of the air electrode is linearly increased (the x-axis). Since only a whole number of stacks can fit in the 9 mm radius of the 18650, the thickest electrodes would be 9 mm/1, 9 mm/2, 9 mm/3 and so on. A thicker stack effectively represents a thicker ZnO electrode. Figure A-3 demonstrates that Zn-air cells could, in theory, achieve large VEDs if the air electrode (and space) is kept thin. For example, Zn-air button cells have Zn electrodes that are about 4 mm thick, so a stack of 4.5 mm with a 3.4 mm ZnO electrode and 1.0 mm air electrode would yield over 1,400 Wh/L. However, even if the air electrode is granted a thickness approaching that of the ZnO electrode the Zn-air cell could still deliver an impressive 1,000 Wh/L.

### A.3 Simple Ni-Zn Cell

Ni-Zn cells are a little more challenging to model with the simple model. This is due to the presence of the positive electrode, which was conveniently ignorable in the case of

the Zn-air cell. The GCDs and VCDs of the positive (+) and negative (-) electrodes are determined by Equations (A-1) and (A-2). Then the individual electrodes' GCD and VCD values are combined via

$$GCD_{Cell} = \frac{nF}{M_{Cell}} = \frac{1}{\left(\frac{1}{GCD_{+}} + \frac{1}{GCD_{-}}\right)} \quad (A-7)$$

and

$$VCD_{Cell} = \frac{nF}{V_{Cell}} = \frac{1}{\left(\frac{1}{VCD_{+}} + \frac{1}{VCD_{-}}\right)} \quad (A-8)$$

to generate values for the cell as a whole:  $GCD_{Cell}$  and  $VCD_{Cell}$ . Here,  $n$  is the number of moles of electrons stored in either of the two electrodes,  $F$  is Faraday's constant,  $M_{Cell}$  is the mass of the entire cell, and  $V_{Cell}$  is the volume of the entire cell, although these variables are only shown for clarification purposes; only the right hand side of the equations were used to generate the values in Table A-1. The GED and VED were then calculated by multiplying by  $V_{avg}$  using Equations (A-3) and (A-4).

#### A.4 Intermediate Ni-Zn Cell

The intermediate model of a Ni-Zn cell is similar to that of the Zn-air cell. The main difference is the fact that the thickness of the Ni electrode is determined by the thickness of the zinc electrode since the two electrodes must hold a particular ratio of capacities. Several cells in the literature use an abundance of Zn active material in case some Zn drifts away and becomes electronically insulated from the current collector, although ideally, the ratio of Zn to Ni active material capacity would be 1:1 in order to maximize the energy density of the cell by avoiding the excess volume and weight of a Zn reservoir. In any case, the thickness of the Ni electrode is

$$t_{Ni} = \frac{VCD'_{ZnO} \cdot t_{Zn}}{VCD'_{Ni} \cdot R} \quad (A-9)$$

where the  $t$ 's are thicknesses, the  $VCD'_{XX}$ s are volumetric capacity densities that were calculated taking into account the electrode material recipe as in Equation (A-5), and  $R$  is the Zn to Ni capacity ratio. A schematic of the stack is shown in Figure A-4.

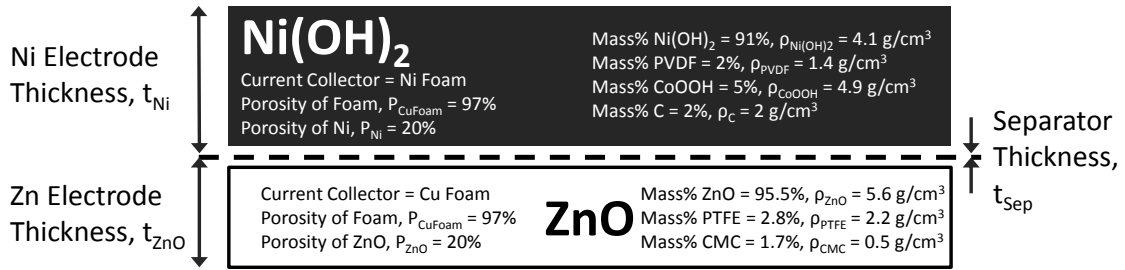


Figure A-4: Schematic of the stack for the intermediate model of a Ni-Zn battery. The current collectors for both electrodes are metal foams that permeate the electrodes and are assumed to have a 97 v% porosity. The separator was assumed to be 100  $\mu\text{m}$  thick.

Since researchers have historically added more Zn active material than necessary, the intermediate model of the Ni-Zn 18650 cell was performed for a varying ratio,  $R$ , of Zn to Ni capacities. The results are shown in Figure A-5. From the model it is evident that Ni-Zn cells have the potential to achieve about half of the VED of a Zn-air cell (550 Wh/L). The

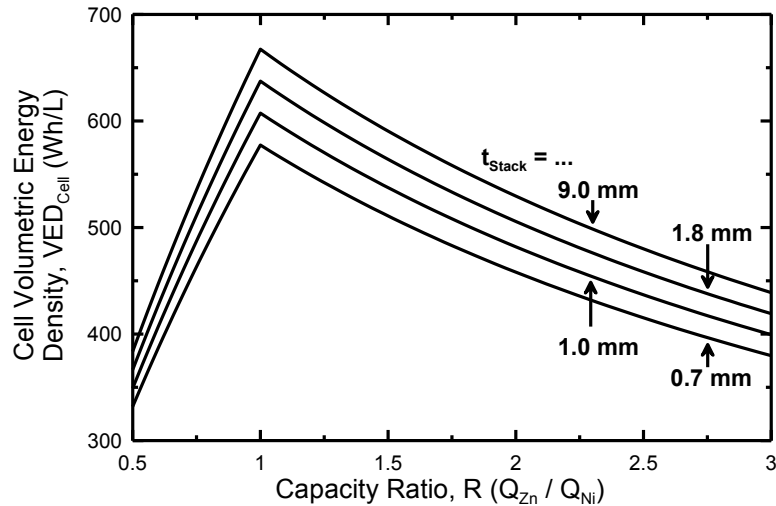
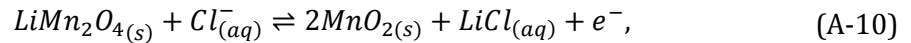


Figure A-5: Volumetric energy density of a Ni-Zn 18650 cell using the intermediate model. The successive data sets are for decreasing stack thicknesses of 9 mm divided by 1, 5, 9 and 13. The capacity limiting electrode is ZnO below  $R = 1$ , and  $Ni(OH)_2$  above  $R = 1$ .

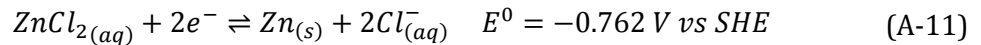
main benefit of Ni-Zn cells over Zn-air is the absence of air holes and, thus, water management issues as discussed in Section 1.9.4 (pg. 33).

### A.5 Simple Aqueous Lithium Manganese Oxide Zinc (LiMn<sub>2</sub>O<sub>4</sub>-Zn) Cell

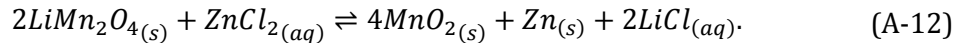
Yan *et al.* published a paper touting the feasibility of an aqueous LiMn<sub>2</sub>O<sub>4</sub> – Zn cell.<sup>167</sup> Their experimental (and unrevealed) cation-doped LiMn<sub>2</sub>O<sub>4</sub> performed exceptionally well, with the cell maintaining 95% of its capacity after 4,000 cycles.<sup>167</sup> They estimate an energy density for this battery of 50-80 Wh/kg and claim it is superior to commercial non-lithium ion rechargeable batteries. A simple and intermediate model of their proposed battery is presented here to determine if this battery technology is indeed competitive. The positive electrode charging reaction in this cell is



while the negative electrode charging reaction is



and the total cell charging reaction is



The LiCl and ZnCl<sub>2</sub> are intended to be dissolved in the electrolyte, but for the purposes of the simple model, where the goal is to obtain the highest energy densities possible, it will be assumed that LiCl and ZnCl<sub>2</sub> precipitate out as solids upon formation. As such, the capacity densities of the positive (+) electrode in the charged state, where it is assumed the LiCl precipitates out during charging, becomes a combination of both MnO<sub>2</sub> and LiCl, and can be calculated using

$$GCD_+ = \frac{nF}{M_+} = \frac{F}{(N \cdot MM)_{MnO_2} + (N \cdot MM)_{LiCl}} \text{ and} \quad (A-13)$$

$$VCD_+ = \frac{nF}{V_+} = \frac{F}{\left(\frac{N \cdot MM}{\rho}\right)_{MnO_2} + \left(\frac{N \cdot MM}{\rho}\right)_{LiCl}}, \quad (A-14)$$

where  $F$  is Faraday's constant,  $n$  is the number of moles of  $e^-$  stored in the electrode,  $MM$  is the molar mass and  $N$  is the number of moles of substance per mole of electrons. For instance,  $N_{MnO_2} = 2 \frac{\text{mol MnO}_2}{\text{mol } e^-}$ .  $GCD_-$  and  $VCD_-$  were calculated using Equations (A-1) and (A-2), while  $GCD_{\text{Cell}}$  and  $VCD_{\text{Cell}}$  were calculated using Equations (A-7) and (A-8), and finally,  $GED_{\text{Cell}}$  and  $VED_{\text{Cell}}$  were calculated via Equations (A-3) and (A-4). The results are listed in Table A-1. It is clear from the table that the  $\text{LiMn}_2\text{O}_4 - \text{Zn}$  cell has the lowest energy densities of all the cell chemistries considered here. The advantage of this particular cell chemistry would be a large cycle life, safety and low price, but whether or not its energy density can realistically be high enough to be useful in things like cell phones depends on how much volume the electrolyte requires since it must contain the dissolved  $\text{LiCl}$  and  $\text{ZnCl}_2$ . This can be explored using the intermediate model.

## A.6 Intermediate $\text{LiMn}_2\text{O}_4$ -Zn Cell

A schematic of the intermediate model stack for a  $\text{LiMn}_2\text{O}_4$ -Zn cell is shown in Figure A-6. The electrolyte used by Yan *et al.* was made by dissolving in water: 3 M  $\text{LiCl}$  and 4 M  $\text{ZnCl}_2$ , and then adjusting the pH upward to pH 4 using  $\text{LiOH}$ .<sup>167</sup> This means that adding

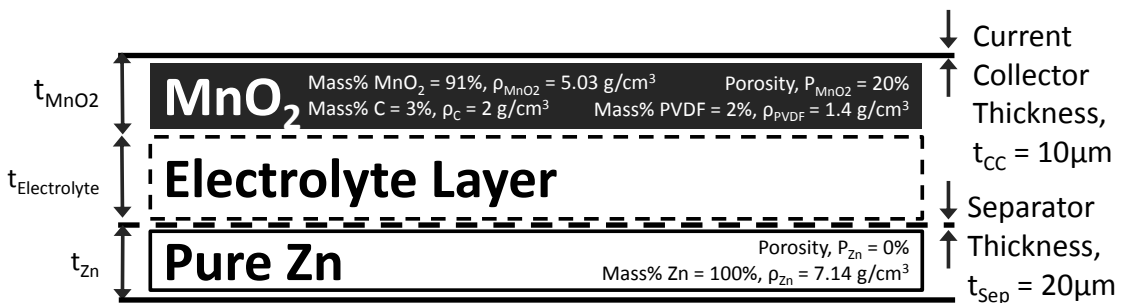


Figure A-6: Schematic of the stack for the intermediate model of a  $\text{LiMn}_2\text{O}_4$ -Zn cell. Although two current collectors are in the figure, mirroring the stack before rolling it means only one  $t_{\text{CC}}$  need be considered.



more capacity to the cell requires adding more electrolyte or increasing the concentration of the electrolyte. Since the maximum concentration of  $\text{ZnCl}_2$  and  $\text{LiCl}$  in water at  $25^\circ\text{C}$  is 31.7 M and 19.9 M, respectively, and since this cell requires 2 moles of  $\text{LiCl}$  for every mole of  $\text{ZnCl}_2$ , it is safe to assume that the  $\text{LiCl}$  concentration when the cell is in the charged state will be the limiting factor if precipitation is to be avoided. The VCD of the electrolyte is

$$VCD_{\text{Electrolyte}} = \frac{nFC}{1000 \frac{\text{mL}}{\text{L}}} \quad (\text{A-15})$$

where  $F$  is Faraday's constant,  $C$  is the concentration of the pertinent species ( $\text{LiCl}$  in this case) and  $n$  is the number of moles of electrons per mole of species (1 in this case). The rest of the calculations were done as in previous sections: Equations (A-1) and (A-5) were used to calculate the VCD of  $\text{Zn}$  and  $\text{MnO}_2$  respectively. Given a fixed stack thickness, Equation (A-9) ( $R = 1$ ) was then used to calculate the thickness of the electrolyte,  $\text{Zn}$  and  $\text{MnO}_2$  layers. Finally, the total  $\text{VED}_{\text{Cell}}$  was calculated using Equation (A-6). The results of this intermediate model are shown in Figure A-7 for an increasing concentration of  $\text{LiCl}$  and at incremental stack thicknesses corresponding to the maximum, 9 mm, divided by 1, 5, 9 and 13.

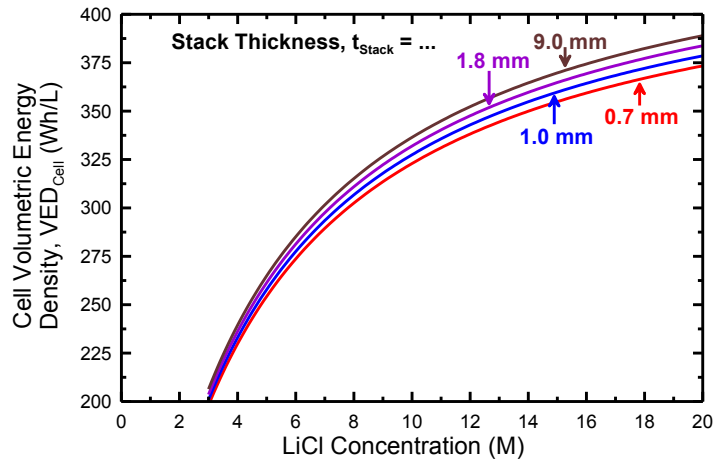


Figure A-7: Volumetric energy density of a  $\text{LiMn}_2\text{O}_4 - \text{Zn}$  cell in the charged state using an intermediate model. The successive data sets are for decreasing stack thicknesses of 9 mm divided by 1, 5, 9 and 13. The maximum concentration of  $\text{LiCl}$  in pure water at  $25^\circ\text{C}$  is about 20 M. Note that  $t_{\text{Stack}} = t_{\text{electrolyte}} + t_{\text{Zn}} + t_{\text{MnO}_2} + t_{\text{Sep}} + t_{\text{CC}}$  where  $t_{\text{Sep}} = 0.01$  mm and  $t_{\text{CC}} = 0.02$  mm.

Since the thicknesses of the separator ( $t_{sep}$ ) and current collector ( $t_{cc}$ ) are so thin, the stack thickness does not strongly affect the volumetric energy density. Evidently, the  $\text{LiMn}_2\text{O}_4$ -Zn cell modeled here could realistically obtain a maximum of about 375 Wh/L before LiCl would start precipitating out, regardless of the electrode thicknesses. Instead, the concentration of the electrolyte is far more important for this cell. No consideration for issues with conductivity or freezing point associated with high concentrations has been included in this model. In the unlikely case that high LiCl concentrations are not a problem, particles precipitating out of electrolytes tend to clog vital pore volume in separators and electrodes; thereby increasing the tortuosity of the path that must be taken by travelling ions, which leads to an increase in cell impedance and a reduction in discharge potential and rate capability. Hence, precipitation of LiCl (or  $\text{ZnCl}_2$ ) is best avoided if possible. If precipitation is avoided, this technology could achieve about half the VED of a Li-ion cell ( $\text{LiCoO}_2 - \text{C}$ ). This would limit the success of  $\text{LiMn}_2\text{O}_4$ -Zn cells in mobile devices, like cell phones, where energy density is the more important than cycle life. However, the  $\text{LiMn}_2\text{O}_4$ -Zn cell could excel in electric vehicles or grid energy storage where cycle life and cost/kWh are the most important factors.

#### **A.7 Simple Non-Aqueous Lithium Air (Li-Air) Cell**

Currently, non-aqueous Li-air cells are attracting a lot of research money because the GED of a Li-air cell calculated using the simple model of the charged state is nearly as high as gasoline (10,400 Wh/kg), and stakeholders are led to believe that achieving an energy density surpassing that of any other cell is likely. To clarify, the “Charged” entry in Table A-1 treats both the air and Li electrodes as if they were in the charged state, in which case the air electrode is empty and assumed to occupy no volume. The improved simple cell model for a discharged Li-air cell calculated here demonstrates that expectations of energy

densities higher than gasoline are unfounded because the  $\text{Li}_2\text{O}_2$  that precipitates during discharge does so within the air electrode on the opposite side of the separator from whence it came. Recall Figure A-1C. This means that volume within the air electrode must be left vacant for when the  $\text{Li}_2\text{O}_2$  precipitates. The “Discharged” entry in Table A-1 treats the air electrode as if it is in the *discharged* state to account for the  $\text{Li}_2\text{O}_2$  and the Li electrode as if it is in the *charged* state to account for Li for the purposes of calculating  $\text{VCD}_{\text{Cell}}$  and  $\text{VED}_{\text{Cell}}$ . To make this calculation simpler, the air electrode in the discharged state is assumed to be a solid block of  $\text{Li}_2\text{O}_2$ . Since the Li metal is not actually present in the discharged state, the mass of the cell is determined solely by the  $\text{Li}_2\text{O}_2$  and so the  $\text{GCD}_{\text{Cell}}$  and  $\text{GED}_{\text{Cell}}$  calculations for the discharged state are unmodified from the method used to calculate the charged state of the Li-air cell. The equations used to calculate these simple models have already been covered and include Equations (A-1) and (A-2) for each electrode, and then (A-7), (A-8), (A-3), and (A-4) in that order. The results are listed in Table A-1. It is apparent from this consideration of the discharged state of the Li-air cell that energy densities approaching that of gasoline are pure fantasy.

### **A.8 Intermediate Non-Aqueous Li-Air Cell**

Considering an intermediate model of the Li-air cell that includes the carbon structure of the air electrode, porosity within the air electrode and diffusion limitations of organic electrolyte are even more sobering. A schematic of the intermediate model stack is shown in Figure A-8.

As an example of air electrode porosity, Xiao *et al.* claimed to have obtained the highest capacity air electrode reported up until 2011 with a carbon structure that had a porosity of 63%. Their air electrode would have to have either expanded when  $\text{Li}_2\text{O}_2$  precipitated out inside the air electrode, or the  $\text{Li}_2\text{O}_2$  ended up on the outside of the air

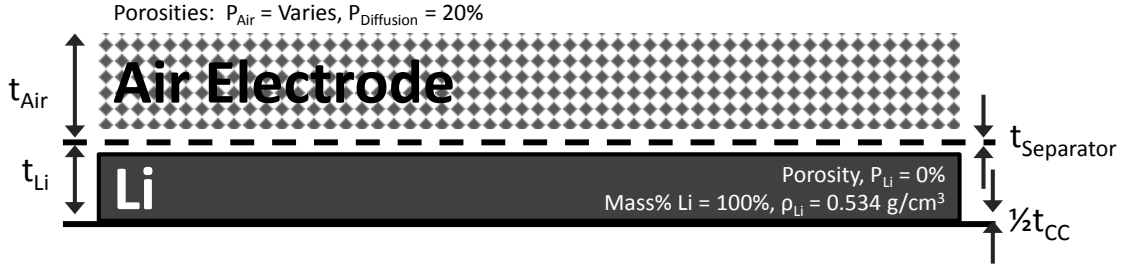


Figure A-8: Schematic of the stack for the intermediate model of a Li-air cell.  $P_{Air}$  refers to the overall porosity of the air electrode carbon structure while  $P_{Diffusion}$  is the porosity that must be left empty in order for ions to diffuse freely through the electrode. Mirroring the stack before rolling it means only half of a current collector ( $\frac{1}{2}t_{CC}$ ) need be considered.  $t_{CC}$  and  $t_{Separator}$  were assumed to be 10  $\mu\text{m}$  and 100  $\mu\text{m}$  respectively.

electrode in order for it to attain the claimed 15,000 mAh/g C. If the electrode expanded, then after expansion the air electrode had a porosity of about 90%, assuming no volume was left over for electrolyte and thus diffusion. Assuming an electrode needs a porosity of about 20% for ions to diffuse through it, the volume left over for  $\text{Li}_2\text{O}_2$  is about 70% of the total volume of the electrode, which is likely a best case scenario. As such, the modified

$$VCD'_{Li_2O_2} = (P_{Air} - P_{Diff})VCD_{Li_2O_2}, \quad (\text{A-16})$$

where  $VCD_{Li_2O_2}$  is calculated using Equation (A-2),  $P_{Air}$  is the porosity of the air electrode itself and  $P_{Diffusion}$  is the porosity that must remain after discharge for ions to diffuse through the electrode and thereby allow the electrode to be charged again in the next cycle. The stack thickness was calculated using Equation (A-9) given a particular Li negative electrode thickness and that  $R = 1$ . The stack thickness was then used with Equation (A-6) to calculate  $VED_{Cell}$ . The results of this model for several porosities are shown in Figure A-9.

As Figure A-9 shows, even with the inclusion of the air electrode and  $\text{Li}_2\text{O}_2$  reaction products, Li-air cells appear to be able to deliver quite high volumetric energy densities. However, one more consideration should be taken into account. Non-aqueous cells have the weakness of having a low diffusivity for the primary charge carrier,  $\text{Li}^+$ . The diffusion constant,  $D$ , of  $\text{Li}^+$  in a typical non-aqueous electrolyte is about  $10^{-6} \text{ cm}^2/\text{s}$  as compared to that of  $\text{OH}^-$  in water which is about  $5.27 \times 10^{-5} \text{ cm}^2/\text{s}$ .<sup>35</sup> As such, non-aqueous Li-ion

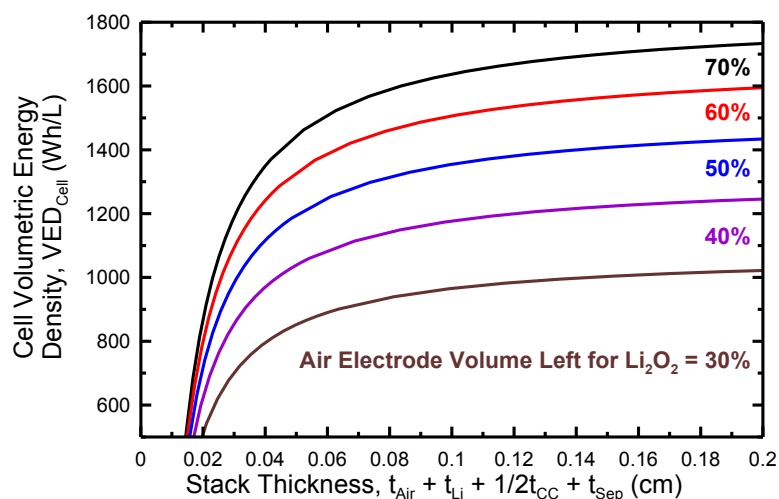


Figure A-9:  $VED_{\text{Cell}}$  of a non-aqueous Li-air cell as the thickness of the Li electrode ( $t_{\text{Li}}$ ) is increased. This dependence has been calculated for increasing amounts of volume available within the air electrode for  $\text{Li}_2\text{O}_2$  to precipitate out.  $t_{\text{CC}}$  and  $t_{\text{sep}}$  were assumed to be  $10\ \mu\text{m}$  and  $100\ \mu\text{m}$  respectively. Although the stack shown here is up to  $0.2\ \text{cm}$  thick, the maximum stack thickness for a non-aqueous Li-ion battery is actually about  $0.05\ \text{cm}$  due to diffusion rate limitations.

batteries have to keep their stack thicknesses below about  $500\ \mu\text{m}$  in order to keep currents at useful rates whereas an aqueous cell using  $\text{OH}^-$  can have a stack thickness as high as  $2.5\ \text{cm}$  and still achieve the same rate. This is why the x-axis in Figure A-9 only extends to  $2,000\ \mu\text{m}$ , whereas Figure A-3, Figure A-5 and Figure A-7 all have their x-axes extended to the thickest stack thickness possible,  $9,000\ \mu\text{m}$ . Under the limitation of a  $500\ \mu\text{m}$  stack thickness, Li-air can only achieve between about  $1,000$  and  $1,400\ \text{Wh/L}$  according to this ideal model, which is essentially the same range possible with Zn-air.

It should be noted that the barriers to developing a long cycle life and safe Li-air battery are still significant and include increasing the coulombic efficiency of the pure Li metal along with preventing all of the following: electrolyte decomposition during charging, Li dendrite growth,  $\text{H}_2\text{O}$  or  $\text{O}_2$  from getting at the Li electrode,  $\text{CO}_2$  from poisoning the air electrode,  $\text{O}_2$  bubbles from destroying the air electrode during charging, precipitated  $\text{Li}_2\text{O}_2$  particles from losing contact with the OER catalyst, electrolyte evaporation, and Li from being a safety hazard. This list is not exhaustive. These issues are instead mentioned for context; compared to these, the issues facing Zn-air batteries are minor or the same in some

cases. Given these results, it seems unwise to invest capital in Li-air research in comparison to Zn-air.

## Appendix B: Permissions to Reprint Material from the Literature

*The following e-mail was received in response to a permission request to reproduce the work from P. Bonnicks and J. R. Dahn, A Simple Coin Cell Design for Testing Rechargeable Zinc-Air or Alkaline Battery Systems, Journal of the Electrochemical Society, 159, 7, A981-A989 (2012).*<sup>147</sup>

Dear Patrick Bonnicks,

Thank you for your permission request. Since you are the author of the article, as per the ECS Transfer of Copyright Agreement, you have the right to reproduce your own work. Please see part "C" of the "Rights of Authors" section on the agreement:

<http://www.electrochem.org/dl/support/assets/crtf.pdf>

Please let me know if you have any questions, or if there is anything additional I can do to assist.

-Logan Streu

Logan Streu | Content Associate & Assistant to the CCO  
ECS – The Electrochemical Society  
Pennington, NJ USA  
609.737.1902 x116 | [Logan.Streu@electrochem.org](mailto:Logan.Streu@electrochem.org)  
[electrochem.org](http://electrochem.org) | [ECSBlog.org](http://ECSBlog.org) | [@ECSorg](https://twitter.com/ECSorg)

The following is the permission form to reproduce Figure 1-3 (pg. 13) from A. Van der Ven, D. Morgan, Y.S. Meng and G. Ceder, *Phase Stability of Nickel Hydroxides and Oxyhydroxides*, JES 153, A210 (2006).

### Request for Permission to Reproduce or Re-Publish ECS Material

Please fax this form to: The Electrochemical Society (ECS), Attn: Permissions Requests, 1.609.730.0629. You may also e-mail your request to: [copyright@electrochem.org](mailto:copyright@electrochem.org). Include all the information as required on this form. Please allow 3-7 days for your request to be processed.

I am preparing a (choose one):  paper  chapter  book  thesis

entitled: Development of a Lab-Scale, Rechargeable Alkaline Cell for Laboratory R&D Applications

to be published by: Patrick Bonnick

in an upcoming publication entitled: N/A (This is my PhD thesis)

I request permission to use the following material in the publication noted above, and request nonexclusive rights for all subsequent editions and in all foreign language translations for distribution throughout the world.

**Description of material to be used**—Indicate what material you wish to use (figures, tables, text, etc.) and give the full bibliographic reference for the source publication. You may attach a separate list, organized by ECS title.

Figure 1 from the paper: A. Van der Ven, D. Morgan, Y. S. Meng and G. Ceder, Stability of Nickel Hydroxides and Oxyhydroxides, JES 153, A210 (2006).

Signature: \_\_\_\_\_ Date: March 22, 2015

Name: Patrick Bonnick

Address: 22B Titus Street, Halifax, Nova Scotia, CANADA, B3M 2N4

Telephone: 902-789-6266 Fax: \_\_\_\_\_

E-mail: pbonnick@gmail.com

Permission is granted to reproduce the above-referenced material. Please acknowledge the author(s) and publication data of the original material, and include the words: "Reproduced by permission of The Electrochemical Society."

March 23, 2015  
Date

  
Ann F. Goedkoop, Publications Production Director